VOLUME 78 MAY 23, 1974 NUMBER 11

JPCHAx

THE JOURNAL OF PHYSICAL CHEMISTRY

PUBLISHED BIWEEKLY BY THE AMERICAN CHEMICAL SOCIETY

THE JOURNAL OF

PHYSICAL CHEMISTRY

AMERICAN CHEMICAL SOCIETY, *1155 Sixteenth St., N.W., Washington, D. C. 20036*

Books and Journals Division

JOHN K CRUM *Director*
RUTH REYNARD *Assistant to the Director*

CHARLES R. BERTSCH *Head, Editorial Processing Department*
D. H. MICHAEL BOWEN *Head, Journals Department*
BACIL GUILEY *Head, Graphics and Production Department*
SELDON W. TERRANT *Head, Research and Development Department*

 Published biweekly by the American Chemical Society at 20th and Northampton Sts., Easton, Pa. 18042. Second-class postage paid at Washington, D. C., and at additional mailing offices.

All manuscripts should be sent to *The Journal of Physical Chemistry*, Department of Chemistry, University of Minnesota, Minneapolis, Minn. 55455.

Additions and Corrections are published once yearly in the final issue. See Volume 77, Number 26 for the proper form.

Extensive or unusual alterations in an article after it has been set in type are made at the author's expense, and it is understood that by requesting such alterations the author agrees to defray the cost thereof.

The American Chemical Society and the Editor of *The Journal of Physical Chemistry* assume no responsibility for the statements and opinions advanced by contributors.

Correspondence regarding accepted copy, proofs, and reprints should be directed to Editorial Processing Department, American Chemical Society, 20th and Northampton Sts., Easton, Pa. 18042. Head: CHARLES R. BERTSCH. Editorial Assistant: JOSEPH E. YURVATI.

Advertising Office: Centcom, Ltd., 50 W. State St., Westport, Conn. 06880.

Business and Subscription Information

Send all new and renewal subscriptions *with payment* to: Office of the Controller, 1155 16th Street, N.W., Washington, D. C. 20036. Subscriptions should be renewed promptly to avoid a break in your series. All correspondence and telephone calls regarding changes of address, claims for missing issues, subscription service, the status of records, and accounts should be directed to Manager, Membership and Subscription Services, American Chemical Society, P.O. Box 3337, Columbus, Ohio 43210. Telephone (614) 421-7230.

On changes of address, include both old and new addresses with ZIP code numbers, accompanied by mailing label from a recent issue. Allow four weeks for change to become effective.

Claims for missing numbers will not be allowed (1) if loss was due to failure of notice of change in address to be received before the date specified, (2) if received more than sixty days from date of issue plus time normally required for postal delivery of journal and claim, or (3) if the reason for the claim is "issue missing from files."

Subscription rates (1974): members of the American Chemical Society, $20.00 for 1 year; to nonmembers, $60.00 for 1 year. Those interested in becoming members should write to the Admissions Department, American Chemical Society, 1155 Sixteenth St., N.W., Washington, D. C. 20036. Postage to Canada and countries in the Pan-American Union, $5.00; all other countries, $6.00. Air freight rates available on request. Single copies for current year: $3.00. Rates for back issues from Volume 56 to date are available from the Special Issues Sales Department, 1155 Sixteenth St., N.W., Washington, D. C. 20036.

Subscriptions to this and the other ACS periodical publications are available on microfilm. Supplementary material not printed in this journal is now available in microfiche form on a current subscription basis. For information on microfilm or microfiche subscriptions, write Special Issues Sales Department at the address above.

Notice to Authors last printed in the issue of December 6, 1973

THE JOURNAL OF

PHYSICAL CHEMISTRY

Volume 78, Number 11 May 23, 1974

JPCHAx 78 (11) 1043-1136 (1974)

ISSN 0022-3654

COMMUNICATIONS TO THE EDITOR

■ Supplementary material for this paper is available separately, in photocopy or microfiche form. Ordering information is given in the paper.

* In papers with more than one author, the asterisk indicates the name of the author to whom inquiries about the paper should be addressed.

AUTHOR INDEX

THE JOURNAL OF
PHYSICAL CHEMISTRY

VOLUME 78, NUMBER 11 MAY 23, 1974

On the Stereochemistry of the Decay-Induced Gas-Phase Halogen Exchange in Diastereomeric 2,3-Dichlorobutanes[1]

Samuel H. Daniel, Hans J. Ache,*

Department of Chemistry, Virginia Polytechnic Institute and State University, Blacksburg, Virginia 24061

and Gerhard Stocklin

Institut fur Nuklearchemie, Kernforschungsanlage Julich, Julich, West Germany (Received January 18, 1974)

The stereochemistry of halogen-for-halogen substitution at asymmetric carbon atoms by decay-produced bromine and iodine species was studied in diastereomeric alkyl halide molecules such as *d,l*- and *meso*-2,3-dichlorobutane. Energetic ^{80}Br ions were generated *via* the $^{80m}Br(IT)^{80}Br$ nuclear process using $CF_3{}^{80m}Br$ as source and allowed to react with the substrate molecules while still possessing excess kinetic energy or after having become thermalized in collisions with argon atoms. ^{125}I ions were produced *via* the EC decay of ^{125}Xe. In unmoderated systems a predominance of retention of configuration is generally observed. In the presence of excess argon, however, the degree of stereospecificity of the reaction varies with the type of diastereomer used as substrate. In the case of the thermodynamically less stable *d,l* system the stereospecificity decreases from about 2.5 (as expressed by the ratio of retention to inversion) in the absence of Ar moderator to 0.4 at high Ar concentrations whereas, under the same conditions, only small changes in the stereospecificity are observed if the meso diastereomer is the substrate. The results are explained on the basis of an electrophilic substitution involving a front-side attack of a positive halogen ion. In the case of the *d,l* system the initially formed halocarbocation can then undergo two competing processes: excitation racemization or Cl^- transfer, which, depending on the environment, can be kinetically or thermodynamically controlled.

Introduction

Previous work by several investigators has suggested that a considerable fraction of the halogen species generated by nuclear processes involving inner shell vacancies such as $^{80m}Br(IT)^{80}Br$ or $^{125}Xe(EC)^{125}I$ reacts as thermal ionic species with organic substrate molecules in the gas phase.[2-14]

The isomeric transition (IT) of ^{80m}Br incorporated in alkyl bromides gives rise to vacancy cascades following internal conversion and eventually to a substantial fragmentation of the molecule *via* Coulomb explosion leading to ^{80}Br ions with multiple positive charges.[15] Similarly, the electron capture decay (EC) of ^{125}Xe results in the formation of multiply charged positive ^{125}I ions.

If these processes occur in the presence of a large excess of a rare gas having an ionization potential intermediate between the first and second ionization potential of Br or I the charge of the ^{80}Br or ^{125}I ions will be rapidly reduced to unity by charge transfer processes,[15] while the excess kinetic energy of some electron volts resulting from the Coulomb explosion or neutrino emission, respectively, is removed from the ions in unreactive collisions. The resulting thermal $^{80}Br^-$ or $^{125}I^-$ ions can subsequently undergo electrophilic reactions with organic substrate molecules.

This is quite different from the hot homolytic substitution reactions of nucleogenic tritium and halogen atoms resulting from neutron-induced nuclear reactions, where the recoil species have very high initial kinetic energies and lose their possible charge very quickly while slowing down to the chemical energy range where they react predominantly as neutral atoms.[16] Thus, it seems that the study of the reactions of *decay-induced* halogen species could significantly contribute to our knowledge of the detailed reaction mechanisms and parameters involved in electrophilic substitution reactions of simple hydrocarbons in the gas phase. It appears that this technique can be of

special importance in cases where other methods such as ion cyclotron resonance or high-pressure mass spectrometry cannot provide the necessary information, *i.e.*, in cases where one wishes to study the stereochemistry of the reaction or where several isomers may result from the substitution. An interesting application of this technique is the recent investigation by Cacace and Stocklin[7] in which they studied the isomer distribution following the electrophilic attack of halogen in various benzene derivatives.

In the present study we tried to assess the stereochemical course of the decay-induced halogen for halogen substitution following $^{80m}Br(IT)^{80}Br$ and $^{125}Xe(EC)^{125}I$ in *meso*- and *d,l*-2,3-dichlorobutane in the gas phase under various experimental conditions. An attempt will be made to explain the observed results in terms of a mechanism which involves an electrophilic (front side) attack of the halogen ion at the asymmetric carbon atom leading to the formation of a relatively long-lived complex which may undergo subsequently racemization. This mechanism is similar to the mechanism recently proposed by Cacace[17] for the gas-phase electrophilic attack of gaseous Brønsted acids such as $^3HeT^+$ at asymmetric carbon atoms.

Experimental Section

Materials. CF_3Br, $CH_2{=}CH{-}CH{=}CH_2$, Cl_2, and O_2 were obtained from Matheson Chemical Co. with a stated purity level greater than 99.0%. Argon and xenon with a stated purity level of 99.999% were purchased from Air Reduction Co. and used without further purification. The meso and *d,l* forms of 2,3-dichlorobutane were prepared by stereospecific addition of Cl_2 to *trans*- and *cis*-2-butene, respectively.[18]

The products were purified by gas chromatography, using 4-m glass columns (5 mm i.d.) with 20% DEGS on Chromosorb W, 60–80 mesh at 80° and 100 cc of He/min. Similarly, the diastereomers of 1-bromo-2,3-dichlorobutanes and the diastereomers of 2-bromo-2,3-dichlorobutanes were obtained by stereospecific addition of Cl_2 to *cis*- and *trans*-1- and -2-bromo-2-butene (purchased from K & K), respectively. Purification was achieved by gas chromatography on the columns described above at 110°.

erythro- and *threo*-2-bromo-3-chlorobutane and 2-iodo-3-chlorobutane which were used in small amounts as carriers were prepared following procedures described in the literature[19-21] and subsequently gas chromatographically purified.[22]

Preparation of ^{80}Br Source. CF_3Br was preferentially used as the ^{80}Br source because of its ionization potential of 12.3 eV, which lies above that of Br^+ and thus would not interfere with the Br^+ reaction by charge transfer.

A few milligrams of CF_3Br were sealed in a quartz capillary and irradiated in the VPI and SU nuclear reactor at a neutron flux density of about 10^{12}n cm^{-2} sec^{-1} for 30 min at 40°. After the reactor irradiation the contents of the quartz ampoule were subjected to gas chromatographic purification on a 2-m Poropak Q column. The CF_3Br fraction, containing ^{80m}Br-, ^{80}Br-, and ^{82}Br-labeled CF_3Br formed during the irradiation, was trapped and transferred to the reaction vessel.[23] The other radioisotopes of bromine produced do not impose any problems, since they lead to stable daughters not giving rise to any relevant products.

Preparation of ^{125}Xe. About 15 ml of Xe at 5 atm were sealed in quartz ampoules and neutron irradiated in the FRJ-1 nuclear reactor of the Nuclear Research Center Juelich at neutron flux density of 8×10^{12} cm^{-2} sec^{-1} for a period of 75 min. Aliquots of about 2 ml (STP) were subsequently transferred into the reaction vessel. The other radioisotopes of Xe produced during neutron irradiation do not interfere since the EC decay of ^{127}Xe leads to the stable (nondetectable) ^{127}I and the neutron rich isotopes of Xe decay by β^- emission to Cs isotopes.

Preparation of Reaction Mixture. The reaction was carried out in a spherical, specifically designed, Pyrex glass vessel with a total volume of 500 ml. In- and outlet valves were Kontes' greaseless high vacuum values. The vessel was filled by standard vacuum line technique with the desired amounts of reactants and additives.

In the case of the Br^+ investigation the reaction mixture was allowed to stand (in the dark, at room temperature) for 100 min to permit the ^{80}Br to attain equilibrium with the ^{80m}Br while in the reaction vessel.

In the case of the $^{125}I^+$ experiments the exposure time was 70 min at room temperature.

Sample Analysis. At the end of the reaction the ^{80}Br or ^{125}I labeled products were collected in traps at liquid nitrogen temperature and appropriate amount of carriers dissolved in CH_2Cl_2 added. The resulting solution was washed first with aqueous (dilute) Na_2SO_3 solution then with distilled water and dried. The analysis of the ^{80}Br or ^{125}I labeled products was accomplished by a discontinuous radio-gas chromatographic technique.[23,24]

Columns used were either a 4-m glass column (5 mm i.d.) with 20% DEGS on Chromosorb W 60–80 mesh, temperature programmed, or a 8-m glass column (5 mm i.d.) 15% SF-96 on Chromosorb W, 60–80 mesh operated at 80°. The latter column was used for the separation of the diastereomeric 2-iodo-3-chlorobutanes.

Radioactivity Assay. The separated radioactive products were directly trapped from the effluent gas stream by bubbling the effluent gas from the gas chromatograph through toluene solutions containing liquid scintillation fluors. More than 99% of all the reaction products identified in this investigation were retained in the solution, with the exception of CF_3Br, for which calibration runs were carried out and appropriate corrections made.[23]

The ^{80}Br-counting was done by liquid scintillation spectrometry applying appropriate energy discrimination.

Alternatively the ^{125}I labeled fractions were adsorbed on charcoal tubes[24] and counted in a well type scintillation counter. Radionuclidic purity was checked by γ spectrometry in the case of ^{80}Br by using the 665-keV line.[25]

The radiochemical yields of the products, *i.e.*, the ratio of the ^{80}Br activity present at the end of the reaction in each individual product to the total ^{80}Br activity (at end of the reaction) were computed by using the well-known equations for radioactive decay and growth. In the case of ^{125}I ($t_{1/2}$ = 60 days) decay corrections were not necessary due to the long half-life and the radiochemical yields were obtained by comparing the activity of the individual fractions with that of the total activity directly measured on an aliquot.

Results and Discussion

Several series of experiments were carried out to identify the products resulting from the reaction of ^{80}Br and ^{125}I species generated in the nuclear decay of ^{80m}Br or ^{125}Xe with *meso*- and *d,l*-2,3-dichlorobutane as substrate in the gas phase and to determine their relative radiochemical yields.

Of particular interest for this study were the ^{80}Br or ^{125}I substitution products derived from the two diastereomers

of the 2,3-dichlorobutane substrate molecules, which include in the case of *meso*-2,3-dichlorobutane the following products as shown schematically

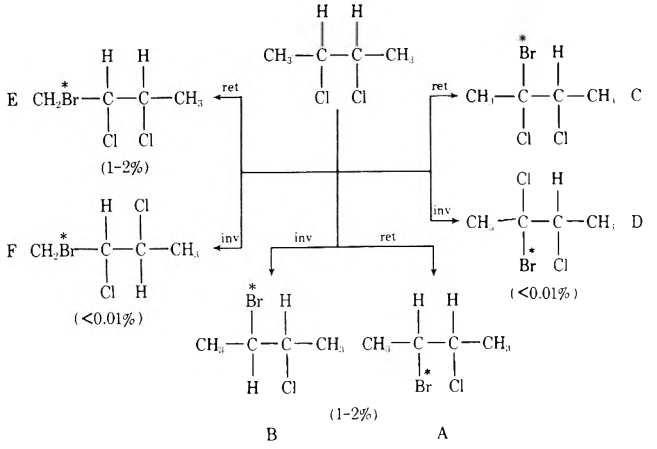

(numbers in parentheses are the radiochemical yields in per cent of total ^{80}Br formed in reaction mixture): (1) the *erythro*-2-bromo-3-chlorobutane as a result of ^{80}Br-for-Cl substitution under retention of configuration (A); (2) the *threo*-2-bromo-3-chlorobutane as a result of ^{80}Br-for-Cl substitution under inversion of configuration; (3) the two diastereomers resulting from ^{80}Br-for-H substitution (with (C) or without (D) retention of configuration); (4) the products formed as a result of ^{80}Br-for-H substitution in one of the methyl group (E and F) (the product was the diastereomers of 1-bromo-2,3-dichlorobutane). (Corresponding products are formed following ^{80}Br substitution in the *d,l* form of 2,3-dichlorobutane.)

Previous ^{80}Br substitution experiments[23] with substrate molecules such as CH_3Cl or CH_2Cl_2 have already indicated that the probability of ^{80}Br-for-H substitution in molecules where the ^{80}Br is given a choice to substitute either a H or Cl (attached to the same carbon atom) is very small compared with ^{80}Br-for-Cl substitution.

A similar trend was observed in the present study where the radiochemical yields of the 2-bromo-2,3-dichlorobutane were found to be too small (<0.01%) to allow a reasonable quantitative determination of the two diastereomers.

As expected ^{80}Br-for-H substitution at the methyl group leading to the 1-bromo-2,3-dichlorobutanes proceeds with a relatively good radiochemical yield (about 1-2%) and leads almost exclusively to the product which has retained its original configuration.

Thus in the following only the relative yields of the products resulting from halogen for halogen substitution will be reported and discussed.

In the first series of experiments the effect of Ar moderator on the stereochemical course of the ^{80}Br-for-Cl substitution in *meso*- and *d,l*-dichlorobutane was studied in the gas phase. The reaction was carried out in a 500-ml Pyrex vessel containing 12 Torr of the substrate, 15 Torr of $CF_3{}^{80m}Br$, which served as the source of ^{80}Br, and 20 Torr of O_2 as scavenger. Various amounts of argon were added to this mixture; the reaction time was 100 min. The results are shown in Figure 1, where the ratio of retention to inversion, *i.e.*, the ratio of ^{80}Br found in the 2-bromo-3-chlorobutane molecule formed under retention and inversion of configuration, respectively, is plotted as a function of the mole per cent argon present and the total pressure of the system. The results clearly suggest that when *meso*-2,3-dichlorobutane is the substrate argon additives have only a small effect on the stereochemical course of the substitution, *i.e.*, on the relative yields of ^{80}Br labeled *erythro*- and *threo*-2-bromo-3-chlorobutane, whereas when the *d,l* form is the substrate under the same experimental conditions a drastic reduction of this ratio from 2.5 to 0.4 representing the ratio of relative yields of ^{80}Br labeled *threo*- to *erythro*-2-bromo-3-chlorobutane can be observed.

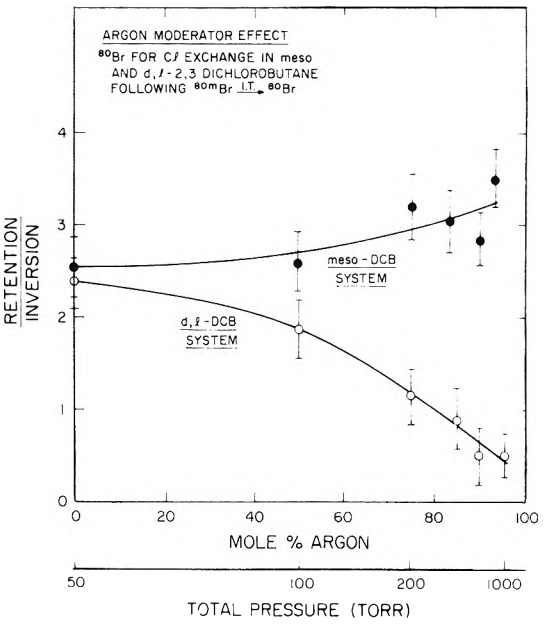

Figure 1. Ratio of ^{80}Br for Cl substitution product formed *via* retention to that formed *via* inversion of configuration plotted as a function of argon concentration and total pressure of the reaction mixture following ^{80m}Br(IT)^{80}Br in *meso*- and *d,l*-2,3-dichlorobutane system (The reaction products are *erythro*- and *threo*-2-bromo-3-chlorobutane, respectively.): substrate pressure: 12 Torr; $CF_3{}^{80m}Br$, 15 Torr; O_2, 20 Torr; reaction volume 500 ml, exposure time 100 min, room temperature.

Since in this series of experiments the moderator concentration was increased by adding additional argon to the reaction mixture which was consistently made up of about 12 Torr of substrate, 20 Torr of CF_3Br, and 20 Torr of O_2 the total pressure of the system increased simultaneously from about 50 to 1000 Torr. Thus the observed effect could be due to either one of the two parameters: increased total pressure or increased argon concentration or both.

The effect of total pressure within the above range on the stereochemistry of the halogen exchange was tested in a second series of experiments, where the composition of the reaction mixture which included over 94 mol % moderator was kept constant, while the total pressure was changed. The fact that within the pressure range under investigation no change in the retention to inversion ratio was observed (Figure 2) clearly indicates that under these experimental conditions the system is insensitive to an about tenfold change in total pressure.[26] The variations in the retention to inversion ratio found in the ^{80}Br-*d,l*-2,3-dichlorobutane system (Figure 1) must therefore be associated with the presence of increasing amounts of argon.

Similarly, moderator experiments have also been carried out for I-for-Cl substitution at constant pressure (15 Torr) in *d,l*-2,3-dichlorobutane using the ^{125}Xe(EC)^{125}I process. The halogen-for-halogen substitution products were now the diastereomers of 2-chloro-3-iodobutane. Inactive xenon was also used as moderator. The trend dis-

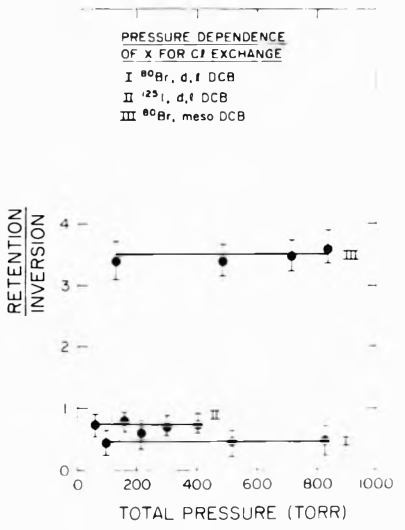

Figure 2. Ratio of halogen for Cl substitution product formed *via* retention to that formed *via* inversion of configuration plotted as function of total pressure. (I) ^{80m}Br(IT)^{80}Br in *d,l*-2,3-dichlorobutane; retention, *threo*-2-bromo-3-chlorobutane; inversion, *erythro*-2-bromo-3-chlorobutane; composition of reaction mixture DCB 1.4%, CF_3 ^{80m}Br 1.8%, O_2 2.5%, and Ar 94.3; reaction volume 500 ml, exposure time 100 min, room temperature. (II) ^{125}Xe(EC) ^{125}I in *d,l*-2,3-dichlorobutane; retention, *threo*-2,iodo-3-chlorobutane; inversion, *erythro*-2-iodo-3-chlorobutane; composition of reaction mixture DCB 4%, Xe 96%; reaction volume 500 ml, exposure time 70 min, room temperature. (III) ^{80m}Br(IT)^{80}Br in *meso*-2,3-dichlorobutane; retention, *erythro*-2-bromo-3-chlorobutane; inversion, *threo*-2-bromo-3-chlorobutane; composition of reaction mixture and experimental conditions same as in I.

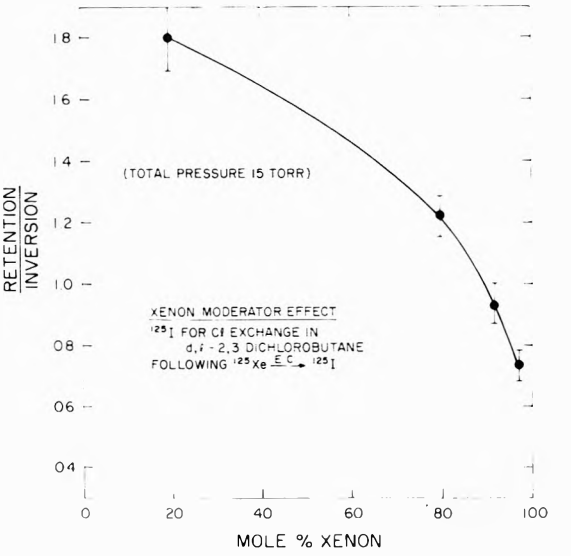

Figure 3. Ratio of ^{125}I for Cl substitution products formed *via* retention to that formed *via* inversion of configuration plotted as function of mole per cent xenon present, following ^{125}Xe(EC)^{125}I in *d,l*-2,3-dichlorobutane: retention, *threo*-2-iodo-3-chlorobutane; inversion, *erythro*-2-iodo-3-chlorobutane; total pressure of reaction mixture 15 Torr; reaction volume 500 ml, exposure time 70 min room temperature.

played by the results shown in Figure 3 (for experimental conditions see legend of figure) is very similar to that observed in the corresponding substitution reactions with ^{80}Br as the reactant, although the absolute radiochemical yields are somewhat lower (0.2% *vs.* 1-2% in the case of Br substitution). It seems that the retention to inversion ratio again approaches a limiting value of about 0.5, which (within the experimental error) is identical with the corresponding value (0.4) found for ^{80}Br substitution.

The results may then be summarized as follows. (1) The ratio retention/inversion is not pressure dependent in the range from 50 to 1000 Torr. (2) The ratio retention/inversion is affected by the addition of moderator only to a small extent if *meso*-DCB is the substrate and approaches a limiting value of approximately 3.2. (3) The ratio retention/inversion decreases drastically with increasing moderator concentration if *d,l*-DCB is the substrate, approaching a value of about 0.4–0.5. This effect seems to be independent of the type of halogen: (^{80m}Br(IT)^{80}Br or ^{125}Xe(EC)^{125}I) and the nature of the rare gas (Ar or Xe) used as moderator.

These findings clearly indicate that the stereochemical course of the nuclear decay-induced halogen-for-halogen substitution leads to results considerably different from those observed with the same substrates when the substituting halogen species are neutral, hot ^{38}Cl or ^{39}Cl produced *via* the ^{37}Cl(n,γ)^{38}Cl or ^{40}Ar(γ,p)^{39}Cl nuclear processes[27,28] where ^{38}Cl (or ^{39}Cl) for Cl substitution in the gas phase results predominantly (>90%) in the formation of products obtained under retention of configuration. Furthermore, the stereochemical course in hot homolytic substitution is not influenced by the addition of moderators.[28a,b]

As mentioned in the Introduction, the basic difference between the halogen species produced *via* (n,γ) or other nuclear reactions and *via* a nuclear decay is that in the former case the initially charged halogen ion undergoes a sufficiently large number of collisions with the surrounding matter to lose its charge long before it reacts chemically, which will be true also in the presence of excess rare gases.[16] On the other hand, the halogen, generated in the nuclear decay, is also formed as a highly charged species,[15] however, it usually acquires much less kinetic energy (as a consequence of the nuclear decay process) and is more likely to reach thermal energies before it becomes completely neutralized,[9] this even more so if the surrounding matter, such as argon or xenon, has an ionization potential which lies between the first and second ionization potential of the bromine (or iodine).

Thus, it can be safely assumed that in the present study, especially in the presence of argon or xenon moderator, the reacting species is a singly charged Br^+ or I^+. The possible contribution of radical species leading to halogen-for-halogen substitution in the diastereomeric 2,3-dichlorobutane was examined by adding 1,3-butadiene as scavenger, which was found to be very efficient to suppress radical reactions in the Rowland and Wai study.[28] The results, as summarized in Table I, do not show any significant effect of the added 1,3-butadiene on the product ratio and therefore do not support the presence of radical recombination mechanisms contributing to the overall substitution under these experimental conditions.

Thus in analogy with previous studies[7,23,25] on the electrophilic reactions of decay produced Br^+, one can postulate a mechanism in which $^{80}Br^+$ ions attack the substrate yielding excited halocarbocation (1), that can either decompose (2), or become stabilized (3) followed by elimination of a proton or halide ion, most likely by transfer to another substrate molecule, yielding the final reaction product.

If one adopts this reaction sequence the observed results can then be explained by the following mechanism. In both systems the halogen species makes its attack prefer-

$$^{80}Br^{+} + CH_3{-}CHCl{-}CHCl{-}CH_3 \longrightarrow [CH_3{-}CHCl{-}CHCl{-}CH_3 \cdots {}^{80}Br]^{+}_{exc} \quad (1)$$

$$[CH_3{-}CHCl{-}CHCl{-}CH_3 \cdots {}^{80}Br]^{+}_{exc} \xrightarrow{\text{decomposition}} \text{fragments} \quad (2)$$

$$[CH_3{-}CHCl{-}CHCl{-}CH_3] \quad (3)$$

(^{80}Br bound to the CHCl carbon)

entially (>70%) from the front side resulting in a three-centered bond structure[17,29,30]

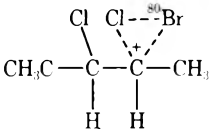

thus yielding a substitution product which retains the original configuration.

To account for the considerable amount of "inversion" which occurred in the case of the *d,l* form upon addition of moderator, one would have to postulate that the resulting complex survives immediate decomposition, *i.e.*, its energy contents is not exceedingly high, however, the complex has sufficient energy for racemization to occur during the lifetime of the complex leading to the observed ratio of erythro to threo product which at high Ar concentrations is close to the thermodynamic equilibrium concentration of the two diastereomers. On the other hand, only a slight increase in the stereospecificity of the substitution reaction occurs when *meso*-2,3-dichlorobutane is the substrate. The initial attack by the electrophile predominantly leads to the erythro form (retention), but the threo product is also formed (possibly by back-side attack). Excitation racemization, if it occurs, will not lead to drastic changes since the two diastereomers are present in yields close to their thermodynamic equilibrium. The thermodynamically less stable threo form will be predominantly affected by excitation racemization giving rise to the erythro form. Indeed, the ratio erythro to threo is seen to slightly increase with increasing moderator concentration.

In order to further test this excitation racemization mechanism one would have to add very efficient energy sinks, which would quickly remove any excess energy from the complex, or strong (gaseous) Brønsted bases to initiate a quick Cl^+ transfer, *i.e.*, to reduce the possibility for racemization either by deactivation of the complex or by shortening the lifetime of the complex.

A preliminary experiment in this direction was done by adding small amounts of methanol (vapor), which is known to be a good energy sink and a relatively strong Brønsted base, to the system. The results, listed in Table I, show a drastic increase in retention of the original configuration if *d,l*-2,3-dichlorobutane is the substrate and Br^+ the electrophile, whereas only a slight change in the stereospecificity is observed when *meso*-2,3-dichlorobutane is the substrate.

The fact that only the *d,l* system is affected by the addition of methanol is in the agreement with the assumptions made above and the findings demonstrated in Figures 1, 3, and 4. Obviously, the postulated "excitation racemization" occurs to a significant extent only in the thermodynamically less stable *d,l* system. In the meso form racemization plays a minor role since a front-side attack of the halogen ion leads preferentially to the thermodynamically stable erythro form whereas in the *d,l* system mostly the thermodynamically less stable erythro diastereomer is initially formed. In this latter case racemization is either kinetically or thermodynamically controlled, depending on the environment.[31] The assumption of two competing processes occurring after the formation of the halocarbocation in the *d,l* system, namely, racemization and Cl^+ transfer (see eq 4) would then explain the trends observed in Figures 1, 3, and 4. As the Ar concentration increases, racemization also increases due to the lacking possibility for Cl^+ transfer to substrate molecules. In the presence of methanol the stereospecificity increases, since Cl^+ transfer to this molecule is more effective than to substrate molecules.

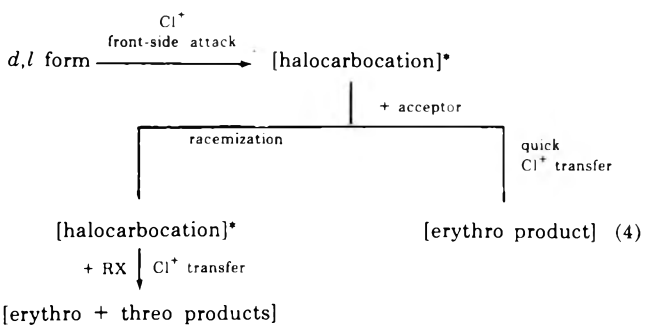

(4)

Additional studies using different Brønsted bases and other good energy sinks which would change the rate of energy and Cl^+ or proton transfer and thus affect the lifetime of the postulated complex are presently carried out to test the proposed mechanism.

TABLE I: ^{80}Br Found in Each of the Two Diastereomers of 2-Bromo-3-chlorobutane (BCB)[a] Following ^{80m}Br(IT)^{80}Br in *meso*- or *d,l*-2,3-Dichlorobutanes (DCB) Under Various Experimental Conditions

Substrate (12 Torr)	Additives, Torr[b]				% ^{80}Br in BCB[c]	
	O_2	Ar	$CH_2{=}CH{-}CH{=}CH_2$	CH_3OH	Erythro	Threo
meso-DCB	20	760			78.2	21.8
	20	760	20		75.4	24.6
	20	760		10	80.2	19.8
d,l-DCB	20	760			70.0	30.0
	20	760	20		62.1	37.9
	20	760		10	8.5	91.5

[a] In % of ^{80}Br incorporated into BCB erythro + threo = 100%. [b] Each sample contains 20 Torr of $CF_3{}^{80m}Br$. Experiments were carried out in a 500-ml Pyrex vessel; reaction time was 100 min at room temperature. [c] Quoted values are the average of four to five experiments.

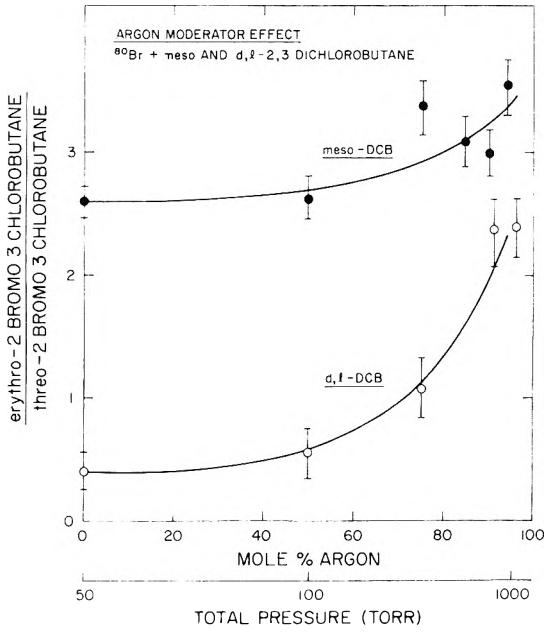

Figure 4. Ratio of ^{80}Br labeled *erythro*- to threo-2-bromo-3-chlorobutane *vs.* mole per cent argon present in reaction mixture following ^{80m}Br(IT)^{80}Br in *meso*- and *d,l*-2,3-dichlorobutane. Experimental condition same as described in Figure 1.

Acknowledgment. The authors are indebted to Mr. M. Schüller, Mr. Jeff Wu, and Dr. L. Bartal for valuable experimental assistance.

Referenes and Notes

(1) Work supported by the U. S. Atomic Energy Commission.
(2) J. B. Nicholas and E. P. Rack, *J. Chem. Phys.*, **48**, 4085 (1968).
(3) J. B. Nicholas, J. A. Merrigan, and F. P. Rack, *J. Chem. Phys.*, **46**, 1996 (1967).
(4) E. Tachikawa, *Bull. Cnem. Soc. Jap.*, **43**, 63 (1970).
(5) E. Tachikawa and T. Kahara, *Bull. Chem. Soc. Jap.*, **43**, 1293 (1970).
(6) E. Tachikawa, *Bull. Chem. Soc. Jap.*, **42**, 1504 (1969).
(7) F. Cacace and G. Stöcklin, *J. Amer. Chem. Soc.*, **94**, 2518 (1972).
(8) M. Yagi, K. Kondo, and T. Kobayashi, *Radiochem. Radioanal. Lett.*, **9**, 123 (1973).
(9) M. D. Loberg and M. T. Welch, *J. Amer. Chem. Soc.*, **95**, 1075 (1973).
(10) J. Okamoto and E. Tachikawa, *Bull. Chem. Soc. Jap.*, **42**, 1504 (1969).
(11) R. R. Pettijohn and E. P. Rack, *J. Phys. Chem.*, **76**, 3342 (1972).
(12) D. W. Oates, R. L. Ayres, R. W. Helton, K. S. Schwartz, and E. P. Rack, *Radiochem. Radioanal. Lett.*, **4**, 123 (1970).
(13) F. Schroth and J. P. Adloff, *J. Chim. Phys.*, **61**, 1373 (1964).
(14) M. J. Welch, *J. Amer. Chem. Soc.*, **95**, 1075 (1973).
(15) For review, *cf.* S. Wexler, *Actions Chim. Biol. Radiat.*, **8**, 107 (1965).
(16) For a review of hot atom reactions, *cf.* (a) A. P. Wolf, *Advan. Phys. Org. Chem.*, **2**, 202 (1964); (b) R. Wolfgang, *Progr. React. Kinet.*, **3**, 124 (1965); (c) G. Stocklin in "Chemie heisser Atome," Verlag Chemie, Weinheim, Germany, 1969.
(17) F. Cacace and M. Speranza, *J. Amer. Chem. Soc.*, **94**, 4447 (1972).
(18) M. C. Lucas and C. W. Gould, Jr., *J. Amer. Chem. Soc.*, **63**, 2541 (1941).
(19) G. A. Olah and J. M. Bollinger, *J. Amer. Chem. Soc.*, **90**, 947 (1968).
(20) M. Delephine and L. Volle, *Bull. Soc. Chim. Fr.*, **23**, 673 (1920).
(21) S. Winstein and E. Grunwald, *J. Amer. Chem. Soc.*, **70**, 836 (1948).
(22) L. Vasaros, H. J. Machulla, and W. Tornau, *J. Chromatogr.*, **62**, 458 (1971).
(23) S. H. Daniel and H. J. Ache, *Radiochim. Acta*, **19**, 132 (1973).
(24) G. Stocklin and W. Tornau, *Radiochim. Acta*, **6**, 86 (1966); **9**, 95, (1968).
(25) E. J. Knust, Report Juel-940-NC (1973).
(26) The reason for this behavior may be seen in the fact that at these high moderator concentrations the reaction products are formed at their equilibrium concentrations. Otherwise, one might expect to see a change in the product ratio due to a shift in the relative probabilities for racemization and X^+ transfer as a function of pressure (*vide infra*).
(27) F. S. Rowland, C. M. Wai, C. T. Tiny, and G. Miller, "Chemical Effects of Nuclear Transformations," Vol. 1, International Atomic Energy Agency, Vienna, 1965, p 333.
(28) (a) C. M. Wai and F. S. Rowland, *J. Phys. Chem.*, **74**, 434 (1970); (b) *ibid.*, **71**, 2752 (1967); (c) H. J. Machulla, Report Jul-873-NC (1972).
(29) G. A. Olah, G. Klopman, and R. H. Schlosberg, *J. Amer. Chem. Soc.*, **91**, 3261 (1969).
(30) G. A. Olah and J. A. Olah, *J. Amer. Chem. Soc.*, **93**, 1251 (1971).
(31) This model is very similar to that postulated for the isomerization of substituted aromatic compounds following the electrophilic attack of $^{80}Br^+$. (H. J. Knust, A. Halpern, and G. Stocklin, *J. Amer. Chem. Soc.*, in press.)

Pulse Radiolysis of Cyclopentane in Aqueous Solutions

Joseph Rabani,*[1a] Miriam Pick,[1b] and Miomir Simic

Hahn-Meitner-Institut fur Kernforschung Berlin GmbH, Bereich Strahlenchemie, 1 Berlin 39, West Germany

(Received October 9, 1973)

Publication costs assisted by Hahn Meitner Institute

The spectra and decay kinetics of C_5H_9 (C_5H_{10} represents cyclopentane) and $C_5H_9O_2$ radicals have been studied. These radicals were generated in aqueous solutions containing cyclopentane and N_2O in the presence and in the absence of O_2. The optical absorption of $C_5H_9O_2$ has a peak at 270 nm, ϵ 1450 ± 150 M^{-1} cm^{-1}. The following reaction rate constants have been measured: $k(C_5H_9O_2 + C_5H_9O_2) = (1.2 \pm 0.15) \times 10^7\ M^{-1}$ sec^{-1}, $k(C_5H_9 + C_5H_9) = (1.0 \pm 0.2) \times 10^9\ M^{-1}$ sec^{-1}, $k(C_5H_9 + O_2) = (4.9 \pm 0.6) \times 10^9\ M^{-1}$ sec^{-1}, and $k(OH + C_5H_{10}) = (4.9 \pm 0.7) \times 10^9\ M^{-1}$ sec^{-1}. Neither C_5H_9 nor $C_5H_9O_2$ transfer electrons to tetranitromethane. $C_5H_9O_2$ does not decompose to produce O_2^-.

Introduction

The existence of O_2^- radicals in living systems[2a] has greatly contributed toward renewed interest in the chemistry and kinetics of various peroxy radicals. Many organic peroxy radicals can also, in principle, participate in cellular metabolism either directly or *via* undesirable side reactions. For most of the organic peroxy radicals direct or indirect decomposition to O_2^- can theoretically take place and in fact in the esr flow experiments[2b] only the latter one could be seen at longer times. On the other hand, considerable evidence is accumulating for the existence of various organic peroxy radicals in aqueous solutions[3-5] at least in the early stages following the reaction of their precursors with oxygen. In view of those uncertainties comprehensive investigation of the reaction of O_2 with various classes of organic radicals in aqueous solutions is desirable. In this work, reactions of cyclopentane radicals with O_2 and the formation of peroxy radicals and their ultimate fate were investigated. Cyclopentane was chosen on the basis of its considerable solubility in water, and the formation of only one type of radical through its reaction with OH.

Experimental Section

Unless otherwise stated, the linear accelerator at the Hahn-Meitner-Institute was used, at 10 MeV and 10-A current. Pulse duration ranged from 5 to 50 nsec. A Tektronix 549 memory scope was used. The light source was 450-W Xe-Hg lamp. Carl Zeiss M4QIII prism monochromator was employed. No scattered light could be observed under our measuring conditions. A flow system composed of Pyrex glass and polyethylene tubing was used to fill and empty the 4-cm long irradiation cell. The cell was emptied and refilled after each pulse. All solutions contained mixtures of N_2O–O_2, except in a few cases where N_2O only was used. The same gas mixtures were used to push the irradiated solutions away from the irradiation cell, to push the solutions to the cell, and to saturate the solutions.

Cyclopentane was added in excess (the maximum gas phase volume above the solutions taken into account) and vigorously stirred with the solutions for at least 30 min. The temperature was 22.5 ± 0.5°. The vapor pressure of cyclopentane at 22.5° is 285 mm.

Materials. Water was first deionized with the aid of an ion exchanger, and then triply distilled. All other materials were of high purity grade and used as received except tetranitromethane, which was washed with water until all yellow materials disappeared. Solutions of tetranitromethane were prepared within 1 hr before use. They were protected from photolysis by means of a glass filter (320-nm cutoff) and a shutter between the lamp and irradiation cell which was opened 1 sec before pulsing.

Results and Discussion

C_5H_9 Radicals. An aqueous solution saturated with cyclopentane, and equilibrated with N_2O, is expected to undergo the following reactions upon pulse irradiation

$$H_2O \longrightarrow e_{aq}^-,\ H,\ OH,\ H_2O_2,\ H_2,\ H_3O^+,\ OH^- \quad (1)$$

$$e_{aq}^- + N_2O \longrightarrow N_2 + OH + OH^- \quad (2)$$

$$OH + C_5H_{10} \longrightarrow C_5H_9 + H_2O \quad (3)$$

The H atoms may either recombine or react with cyclopentane according to

$$H + C_5H_{10} \longrightarrow H_2 + C_5H_9 \quad (4)$$

Since our solutions were buffered, we expect excess of H_3O^+ and OH^- to decay to their equilibrium concentrations. Thus, within less than 0.5 μsec, C_5H_9 is expected to form with a yield $G(C_5H_9) = G(e) + G(OH)$. A fraction of the H atoms probably reacts with the cyclopentane at a slower rate. The spectrum of C_5H_9 radicals is given in Figure 1a. The peak must be at 235 nm or lower in the uv. The extinction coefficient of C_5H_9 at 248 nm, $\epsilon^{248}(C_5H_9)$ 480 M^{-1} cm^{-1}, was calculated by the comparison of the C_5H_9 absorption to the O_2^- absorption observed in a 2 mM formate solution saturated with a N_2O–O_2 gas mixture (ratio 2:1). Dosimetry with a similar solution of 0.1 M formate gave exactly the same $\epsilon^{248}(C_5H_9)$ when the yield in the dosimeter was taken 4% higher (due to scavenging from spurs by 0.1 M formate), and a small correction (~5%) was made for recombination of OH in competition with reaction 4 under the conditions of the measurements. H atoms $(G(H)/[G(OH) + G(e)] = 0.1)$ were assumed not to react quickly with cyclopentane. The C_5H_9 radicals decay away according to

$$2C_5H_9 \longrightarrow C_{10}H_{18} \quad (5)$$

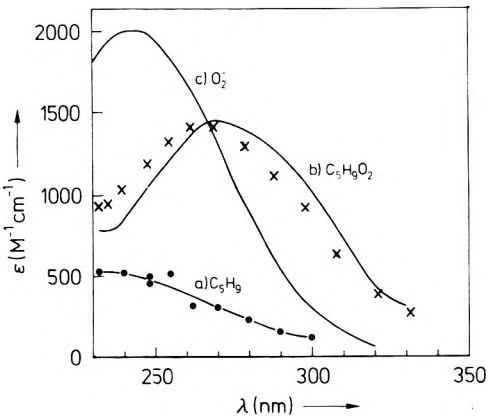

Figure 1. Absorption spectra of C_5H_9, $C_5H_9O_2$, and O_2^- radicals: 2.5 M cyclopentane (saturated solution) at pH 7 (10^{-3} M NaH_2PO_4 + 10^{-3} M Na_2HPO_4). (a) The solution was equilibrated with N_2O; $[C_5H_9] = 1.30 \times 10^{-5}$ M. (b) The solution was equilibrated with N_2O–O_2 gas mixture (4:1 in volume); $[O_2] = 1.7 \times 10^{-4}$ M, $[C_5H_9O_2] = 1.28 \times 10^{-5}$ M. The line represents the extinction coefficient, ϵ, corrected[7] for 14% O_2^- which was present together with $C_5H_9O_2$. The crosses represent the experimental optical densities, when the ϵ scale is multiplied by 5.1×10^{-5}. (c) The absorption spectrum of O_2^- (from ref 7).

and/or

$$\longrightarrow C_5H_{10} + C_5H_8 \qquad (5')$$

A relatively small (about 10%) residual absorption remains. An average value $2k_5 = (2.0 \pm 0.4) \times 10^9$ M^{-1} sec^{-1} was calculated at various initial concentrations of C_5H_9 radicals ranging from 1.6×10^{-6} to 3×10^{-5} M.

When O_2 is also present, it reacts with the C_5H_9 according to

$$C_5H_9 + O_2 \longrightarrow C_5H_9O_2 \qquad (6)$$

As a result, a different absorption spectrum is observed (Figure 1b) with a broad peak at 268 nm. The formation of $C_5H_9O_2$ was followed at 270 nm as a function of O_2 concentration. The results are presented in Table I.

Spectrum and Decay of $C_5H_9O_2$. The absorption spectrum of $C_5H_9O_2$ is presented in Figure 1b. Under our conditions, 14% of the primary radicals (including practically all H atoms, as well as a small fraction of e_{aq}^-) reacted directly with O_2. At pH 7, this resulted in the formation of some O_2^-, according to reactions 7 and 8, and equilibrium 9. The occurrence of these reactions, and the fraction of O_2^- was concluded from the known G values of the primary radicals, and the reaction rate constants of e_{aq}^- with O_2 and with N_2O. It was also confirmed by conductivity and by electron transfer to tetranitromethane measurements, as will be discussed later. Corrections of the spectrum have been carried out for this effect, as well as for about 3% of the C_5H_9 radicals that escape reaction 6, under the conditions of Figure 1b. The extinction coefficient of $C_5H_9O_2$ at 270 nm was measured by the comparison of the absorbance obtained in cyclopentane O_2–N_2O solutions to the absorbance of O_2^- in formate solutions (ϵ^{248} 2000 M^{-1} cm^{-1} used) and to the absorbance of nitroform (ϵ^{350} 14,800 M^{-1} cm^{-1}) in tetranitromethane (TNM) solutions which were irradiated with the same dose using the same gas mixture. We found that in 0.1 M formate, the yield of radicals was 4% higher compared to 2 mM formate. In 1.8×10^{-4} M TNM the yield was 6% higher than in 5×10^{-5} M TNM. An average value $\epsilon^{270}(C_5H_9O_2) = (1450 \pm 150)$ M^{-1} cm^{-1} was obtained

TABLE I: Reactivity of C_5H_9 Radicals toward O_2[a]

$[O_2]$, M	$10^{-9} \times k_6$, M^{-1} sec^{-1}
6.0×10^{-5}	5.5[b]
1.6×10^{-4}	5.7[b]
2.5×10^{-4}	4.5[c]
3.7×10^{-4}	4.0[c]
4.1×10^{-4}	4.5[b]
	Av 4.9 ± 0.6

[a] pH 7.0 (phosphate buffer 10^{-3} M NaH_2PO_4 + 10^{-3} M Na_2HPO_4), 2.5 mM cyclopentane (a saturated solution, vapor pressure 0.375 atm), N_2O present at a partial pressure of (0.625 − 740$[O_2]$) atm. Each value represents an average of 3–4 experiments. A small correction for reaction 5 (5%) was carried out. [b] Initial $[C_5H_9] = 1.2 \times 10^{-5}$ M. [c] Initial $[C_5H_9] = 2.5 \times 10^{-5}$ M.

TABLE II: Measurements of k_{10} at 270 nm[a]

Initial $[O_2^-] \times 10^5$, M	$2k \times 10^{-7}$, M^{-1} sec^{-1}
18.0	2.1
10.0	2.7
3.0	2.5

[a] Each value in the table is an average of three determinations. Solutions contained 1.4×10^{-4} M O_2 and 2.5 mM cyclopentane, and were equilibrated with 0.52 atm of N_2O.

after corrections for variation of yields with the concentrations of solutes, recombination of radicals, and formation of some O_2^- in the cyclopentane solutions. Each of these corrections was always less then 5%.

$$H + O_2 \longrightarrow HO_2 \qquad (7)$$

$$e_{aq}^- + O_2 \longrightarrow O_2^- \qquad (8)$$

$$HO_2 \rightleftharpoons H^+ + O_2^- \qquad pK = 4.8^{6,7} \qquad (9)$$

The decay of the absorbance of $C_5H_9O_2$ was found to be second order. Measurements at 270 nm are presented in Table II. An average rate constant $k_{10} = (1.2 \pm 0.15) \times 10^7$ M^{-1} sec^{-1} was obtained. This value was confirmed by measurements at several other wavelengths and $[O_2]$.

$$2C_5H_9O_2 \longrightarrow (C_5H_9O_2)_2 \qquad (10)$$

Very little, if any, absorbance due to the products of reaction 10 could be observed. A tetroxide, the most likely product of reaction 10, is not expected to have a large absorption in the wavelength region >240 nm. It most likely decomposes in one or more steps to cyclopentanone, cyclopentanol, and O_2.

Transfer to TNM. It has been concluded from the following experiments that neither C_5H_9 nor $C_5H_9O_2$ transfer electrons to tetranitromethane. When solutions containing 6×10^{-5} to 10^{-4} M TNM, cyclopentane (saturated), O_2, and N_2O were pulse irradiated, nitroform (NF^-) was formed with a yield that corresponded to $G(H)$ plus the fraction of e_{aq}^- which was expected to react either with O_2 or with TNM. The rate of NF^- formation in such solutions agreed with $k(O_2^- + TNM) = 2 \times 10^9$ M^{-1} sec^{-1}. This is in agreement with the known[8] value for this rate constant, and supports our suggestion that O_2^- (formed mainly by reaction 7 and equilibrium 9) is responsible for the major part of NF^-. The NF^- yield was always less than 18% of the total yield of radicals. Similar experiments in the absence of O_2 showed that the NF^- formation (~10% of the total yield) could be accounted by the reaction of TNM with H and e_{aq}^- in competition with N_2O.

Conductivity Measurements. Conductivity measure-

ments in solution containing cyclopentane (saturated) and N_2O–O_2 mixtures were carried out at both pH 5.5 ($HClO_4$) and 9.3 (NaOH). The yield of conducting species assumed to be H^+ and O_2^-, measured from the increase in conductivity at pH 5.5 and the decrease in conductivity at pH 9.3 as a result of an electron pulse. At both pH's we found that the yield of conducting species, assumed to be $H^+ + O_2^-$, was about 15% of the total radical yield, and could be accounted for by reactions 7–9, in competition with reaction 2. These experiments are in agreement with the TNM tests, showing (a) a small fraction of the radicals forms conducting species, $H^+ + O_2^-$, as expected, and (b) $C_5H_9O_2$ does not decompose to give O_2^-. The low conductivity at pH 9.3 remained unchanged for at least 0.5 sec decaying to about 50% at 2.5 sec. During that time $C_5H_9O_2$ decayed away. (Initial $[C_5H_9O_2]$ was 1×10^{-6} M.) No indications were found for the formation of hydrotetroxide which at that pH should be in the $ROOOO^-$ form and contribute to the conductivity with $G \cong 3$.

Competition Experiments for the Determination of k_3. We took advantage of the fact that O_2^- reduces TNM while $C_5H_9O_2$ does not to discriminate between the two peroxy radicals. In a TNM solution, equilibrated with N_2O–O_2 gas mixture, and containing both formate and TNM, any OH radicals which react according to (3) will not lead to NF^- formation, while OH radicals that react according to (11) lead to NF^- formation by the reactions

$$OH + HCO_2^- \longrightarrow H_2O + CO_2^- \quad (11)$$

12–14. The effect of [formate] on the yield of NF^- can be

$$CO_2^- + O_2 \longrightarrow CO_2 + O_2^- \quad (12)$$

$$CO_2^- + TNM \longrightarrow CO_2 + NF^- + NO_2 \quad (13)$$

$$O_2^- + TNM \longrightarrow O_2 + NF^- + NO_2 \quad (14)$$

used in order to calculate k_3/k_{11} ratios, according to

$$k_3/k_{11} = ([\text{formate}]/[\text{cyclopentane}])[D^F(NF^-) - D(NF^-)]/[D(NF^-) - D^{CP}(NF^-)] \quad (15)$$

where $D^F(NF^-)$ is the absorbance of NF^- at 350 nm, when all OH radicals react according to (11), $D(NF^-)$ is the absorbance of NF^- at 350 nm under competition conditions, and $D^{CP}(NF^-)$ is the optical density at 350 nm when cyclopentane but no formate is present. The results, given in Table III, give an average $k_3/k_{11} = 1.4 \pm 0.2$. Using $k_{11} = 3.5 \times 10^9$ M^{-1} sec^{-1},[9] we obtain $k_3 = (4.9 \pm 0.7) \times 10^9$ M^{-1} sec^{-1}. (The error limits do not include the error in k_{11}.)

TABLE III: Competition between HCO_2^- and Cyclopentane for OH Radicals[a]

[Formate], mM	$10^2 \times D(NF^-)$	$10^2 \times D^F(NF^-)$	k_3/k_{11}
	5.6	32.7	
0.50	9.2	32.7	1.30
1.30	13.5	32.7	1.26
2.54	17.2	32.7	1.37
5.25	21.5	32.7	1.48
11.2	26.4	32.7	1.36
	3.2	18.5	
2.0	7.7	18.5	1.92
4.0	10.8	18.5	1.60
64	17.7	18.5	1.44

[a] Measured at 350 nm, 1 mM NaH_2PO_4 + 1 mM Na_2HPO_4 buffer; 10^{-4} M TNM; [cyclopentane] = 2.5×10^{-3} M (saturated solution). Each value in the table is an average of two runs.

Conclusions

In the reactions of O_2 and hydrocarbon radicals, such as C_5H_9, hydrocarbon peroxy radicals are formed rather than O_2^-. On the basis of conductivity measurements and the lack of electron transfer processes in TNM solutions, we may exclude spontaneous decay of $C_5H_9O_2$ radicals to O_2^- (at $t < 1$ sec). Formation of a hydrotetroxide $C_5H_9O_4H$ could not be observed either. In that respect its chemistry is comparable to that of non α peroxy radicals, *e.g.*, t-BuOH peroxy radicals which show neither acid–base properties (pH 3–13.6)[10] nor subsequent formation of hydrotetroxides.[11] This sharply contrasts the behavior of α-hydroxy peroxy radicals.[11]

Acknowledgment. We are indebted to Professor A. Henglein for valuable comments and discussions and Dr. J. Lilie for helpful discussions and assistance in conductivity measurements.

One of us (M. S.) acknowledges partial financial support from NIH Grant No. GM-13 557 and AEC Contract No. AT-(40-1)-3408.

References and Notes

(1) (a) Department of Physical Chemistry, The Hebrew University of Jerusalem, Jerusalem 91 000, Israel. (b) In part of the fulfillment of the requirements for M.Sc. degree at the Department of Physical Chemistry, The Hebrew University, Jerusalem 91 000, Israel.
(2) (a) I. Fridovich, *Accounts Chem. Res.*, **5**, 321 (1972); (b) G. Czapski, *Ann. Rev. Phys. Chem.*, **22**, 171 (1971).
(3) M. Simic and E. Hayon, *Biochem. Biophys. Res. Commun.*, **50**, 364 (1973).
(4) T. Eriksen, A. Henglein, and K. Stockhausen, *Trans. Faraday Soc.*, **69**, 337 (1972).
(5) M. T. Downes and H. C. Sutton, *Trans. Faraday Soc.*, **69**, 263 (1973).
(6) J. Rabani and S. O. Nielsen, *J. Phys. Chem.*, **73**, 3736 (1969).
(7) D. Behar, G. Czapski, J. Rabani, L. M. Dorfman, and H. A. Schwarz, *J. Phys. Chem.*, **74**, 3209 (1970).
(8) J. Rabani, W. A. Mulac, and M. S. Matheson, *J. Phys. Chem.*, **69**, 53 (1965).
(9) M. S. Matheson, W. A. Mulac, J. L. Weeks, and J. Rabani, *J. Phys. Chem.*, **70**, 2092 (1966).
(10) M. Simic, P. Neta, and E. Hayon, *J. Phys. Chem.*, **73**, 3794 (1969).
(11) K. Stockhausen, A. Fojtik, and A. Henglein, *Ber. Bunsenges. Phys. Chem.*, **74**, 34 (1970).

Radiolysis of Aqueous Solutions of Cyclopentane and Cyclopentene[1,2]

Turan Soylemez and Robert H. Schuler*

Radiation Research Laboratories, Center for Special Studies and Department of Chemistry, Mellon Institute of Science, Carnegie-Mellon University, Pittsburgh, Pennsylvania 15213 *(Received December 6, 1973)*

Publication costs assisted by the U. S. Atomic Energy Commission and Carnegie-Mellon University

The radiolysis of aqueous solutions of cyclopentane and cyclopentene containing 10^{-2} *M* N_2O or 10^{-3} *M* H^+ has been studied in considerable detail using ^{14}C radio-gas chromatographic methods. In the studies on cyclopentane the initial yields for production of cyclopentene and dicyclopentyl were found to be, respectively, 1.75 and 1.23 for acidic solutions (where e_{aq}^- is converted to H) and 1.95 and 1.36 for those containing N_2O (where e_{aq}^- is converted to OH). The yields for attack on cyclopentane, 6.0 and 6.7, respectively, for the acidic and N_2O containing solutions, agree quite well with the total yields of primary radicals (6.3 and 6.6) so that the material balance is excellent. From the relative yields the disproportionation to combination ratio for reaction between two cyclopentyl radicals in aqueous solution is 1.4 (±0.1). The studies on cyclopentene solutions give a similar ratio for reaction between cyclopentyl and cyclopentyl-2-ol radicals. The product distribution from cyclopentene solutions containing N_2O indicates that 23% of the OH radicals attack cyclopentene by abstraction of an allylic H atom and pulse radiolytic studies give a value for this abstraction ~28%. Auxiliary studies on the rates of the radical reactions and on the esr and optical spectroscopic properties of the intermediate radicals are reported. The optical studies show that cyclopentyl radical absorbs only weakly with the absorption decreasing monotonically with increase in wavelength above 215 nm (ϵ_{215} ~1000 M^{-1} cm^{-1}, ϵ_{300} ~100 M^{-1} cm^{-1}). Cyclopentenyl radical, however, exhibits an intense well-defined absorption band at 242 nm (ϵ_{242} ≥8000 M^{-1} cm^{-1}; width at half maximum = 20 nm). In the radiolysis of saturated aqueous solutions of cyclopentane (2.5×10^{-3} *M*) secondary reactions of H and OH with product cyclopentene become extremely important at doses $>10^{18}$ eV/g (>3% conversion). For the acidic solutions the cyclopentene reaches a plateau of 3×10^{-5} *M*, in accord with expectations from the measured disproportionation-to-combination ratio and the high selectivity (a factor ~60) for addition of H to this product. For the N_2O containing solutions the cyclopentene reaches a higher level (9×10^{-5} *M*) because of the dominant importance of the less selective OH radicals. In general there is very good agreement between the experimental observations on the course of the radiolysis of cyclopentane and predictions based on the yields of radicals produced from the water and the relative rate constants for the different competing reactions which are known either from absolute rate measurements or from the studies on cyclopentene solutions.

Introduction

Except for the recent study of Stevens, Clarke, and Hart[3] on the radiolysis of aqueous solutions of methane there has been no report of a detailed examination of product formation in the radiolysis of aqueous solutions of saturated aliphatic hydrocarbons. Appropriate studies on solutions of this simplest class of organic solutes are, of course, difficult because of their limited solubility although the results of such studies should be of considerable interest to general discussions of the initial and secondary reactions that occur with more complicated substrates. Of particular importance is the fact that direct reaction of hydrated electrons with the aliphatic hydrocarbons does not occur. The lower molecular weight hydrocarbons are sufficiently soluble, and sufficiently sensitive analytical methods are currently available so that significant studies can be carried out. Among liquid saturated hydrocarbons the most suitable choice for such studies would seem to be cyclopentane both because it is the most soluble (2.5×10^{-3} *M*) and because its radical chemistry is expected to be relatively simple since all H atoms are chemically equivalent. We have examined the products formed in the radiolysis of aqueous solutions of cyclopentane by radio-gas chromatographic methods and report the results here. In particular, attention has been focused on the relative importance of the combination and disproportionation reactions of the cyclopentyl radicals produced by the attack of H atoms and OH radicals on the solute. During the initial studies it soon became evident that secondary radical reactions involving product cyclopentene were of considerable importance in determining the overall course of the reaction even at conversions of a few per cent so that an auxiliary study on the radiolysis of aqueous solutions of cyclopentene has also been carried out. It is shown here that information obtained from these latter studies makes it possible to predict the course of the radiolysis of cyclopentane solutions up to doses ~10^{19} eV/g quite accurately. While these studies do not, in retrospect, provide any results that could not have been anticipated reasonably well from appropriate knowledge of the primary yields and the rate constants for the various competing abstraction, combination, and disproportionation reactions, they do serve to point up the various factors which must be considered in obtaining a reasonably complete description for even such a simple system.

Experimental Section

Materials. A 73.8-mg sample of cyclopentane-^{14}C (specific activity 1.9 Ci/mol) was obtained from New England Nuclear Co. This material was purified gas chromatographically and the resultant sample shown to be free of detect-

able traces of radiation-produced product. It was stored on a vacuum line in a vessel sealed with a metallic bellows sealed valve.

Cyclopentene-^{14}C (which was not available commercially) was prepared by dehydrating cyclopentanol-^{14}C (specific activity 1.9 Ci/mol) also obtained from New England Nuclear Co. Dehydration was accomplished by passing the cyclopentanol sample through a 1-m column of activated alumina at 350° together with helium carrier gas at a flow rate of 50 cc/min. These conditions were optimized by studies with inactive cyclopentanol and such that 98% dehydration occurred within the contact period of 2 min. The cyclopentene-^{14}C (20 mg) was then purified chromatographically and stored as above.

Nonradioactive hydrocarbons were Phillips Research Grade. The cyclopentane used in the optical pulse radiolysis studies was chromatographed through silica gel in order to eliminate unsaturated impurities then extracted a number of times with water. The cyclopentene used in the pulse experiments was extracted 5–10 times, first with water and then with strong base, in order to remove impurities which otherwise absorbed strongly at short wavelengths. After extraction, saturated cyclopentene solutions were transparent down to a wavelength of 220 nm. Carboxylic acid derivatives were obtained from Frinton Laboratories. Bromocyclopentane was from K and K Laboratories and cyclopentanol from Matheson Coleman and Bell. Chlorocyclopentane and the reference compounds cyclopentylcyclopentane, 2-cyclopentylcyclopentanol, and 3-cyclopentylcyclopentene were obtained from Chemical Samples Corp. Other chemicals were of the reagent grades usually used in studies such as these.

Sample Preparation and Irradiation. A 0.3-cc sample of triply distilled water (containing 10^{-3} M H_2SO_4 for studies at pH 3) was outgassed on a vacuum line and transferred into a Pyrex irradiation cell 3 cm long and 0.5 cm i.d. The desired amounts of ^{14}C labeled hydrocarbon and N_2O were metered out on the vacuum line, transferred to the irradiation cell, and the cell was sealed. The vapor volume within the cell (0.1–0.2 cc) was noted and the fraction of hydrocarbon in the solution phase calculated from Henry's law as described below. The sample was shaken on a mechanical shaker for at least 1 hr before irradiation. γ-Irradiations were carried out inside ^{60}Co sources at dose rates determined by Fricke dosimetry to be 7.6×10^{16} or 9.7×10^{17} eV g^{-1} min^{-1}. Irradiations were normally from 1 to 10 min and absorbed doses in the range 4×10^{17}–2×10^{19} eV/g.

Radio-Gas Chromatographic Analysis. The radio-gas chromatographic apparatus used was similar to that described by Warman and Rzad.[4] The column effluent, after being examined by a thermal conductivity detector, was oxidized in a CuO furnace at 750°, passed through a dehydrite train to absorb water, and counted in a flow proportional counter having an internal volume of ~50 cc. Helium was used as the eluting gas and methane added to provide a suitable counting mixture. Residence time of the sample within the counter was ~30 sec so that for a specific activity of 2 Ci/mol an activity level equal to the background rate (~200 cpm) corresponded to $\sim 10^{-10}$ mol. Both the integral count and counting rate were monitored. The response of the counting equipment was calibrated during the course of the various experiments using known volumes of toluene-^{14}C of low specific activity. The specific activities of the different samples were intercompared on a liquid scintillation counter.

After irradiation the total sample was introduced into the chromatographic apparatus by breaking the ampoule in the eluting stream as described by Warman and Rzad.[4] This approach (in contrast to using a syringe technique merely to sample the liquid phase) was used because it was desired to obtain total transfer of the sample for a measurement of the hydrocarbon content. The high volatility of the hydrocarbons used makes it difficult to sample the aqueous phase of the irradiated samples accurately.

The radiolysis products were separated from the large volume of water by using Porapak R (Waters Associates Inc.) as the second stage of a two stage column. A preliminary separation of the water, cyclopentane, and cyclopentene from the other products was carried out on the first stage (a 2-m column packed with 25% on 30–60 mesh Chromosorb silicone grease operated at 60°) and these substances were trapped on the Porapak column held at 25°. The Porapak column was replaced by a second silicone grease column and the elution of the remaining products continued by appropriate temperature programming. The cyclopentene and cyclopentane were then eluted from the Porapak column at 150° and separated on a silica gel column at 50°. A typical chromatogram of an irradiated cyclopentene solution is shown in Figure 1 (available on microfilm, see paragraph at end of text regarding supplementary material). In this case the product cyclopentane appears as a very nicely resolved peak in front of the cyclopentene and is readily measurable with high accuracy even at the level of 10^{-6} M. The oxygenated products (cyclopentanone, cyclopentanol, 3(cyclopentyl-2-ol)cyclopentene, and 2-cyclopentylcyclopentanol) exhibit less well-defined peaks and because of tailing their yields are subject to more uncertainty. Cyclopenten-3-ol, which is expected to be produced in the studies of cyclopentene, was missed because it eluted from the first column in 8 min and could not be separated from the water. The cyclopentyl-2-ol dimer (2-cyclopentyl-2-ol-cyclopentanol) eluted at a long time and had a poorly defined peak. In studies of cyclopentane solutions, the product cyclopentene appears on the tail of the cyclopentane so that the background is somewhat higher and measurable levels are in the range upward of 10^{-5} M. In this case the dimers (mostly cyclopentylcyclopentane, 3(cyclopentyl)cyclopentene, and 2-cyclopentylcyclopentanol) were not resolved and the total activity was measured as a unit. The yields, as measured by the activity level, are in terms of molecules of cyclopentene incorporated into the product. The fact that specific activity of the dimers was twice that of the starting material was taken into account in stating these yields.

Examination of Intermediates. The radical intermediates present in the cyclopentane and cyclopentene solutions were examined both by the *in situ* radiolysis-esr technique of Eiben and Fessenden[5] and by the optical pulse radiolysis methods developed by Patterson and Lilie.[6] The latter provides signal averaging capability which is extremely useful for studying the hydrocarbon solutions. Flow systems were used in both cases. For the esr experiments a continuous beam of 2.8-MeV electrons from a Van de Graaff accelerator was used at an absorbed dose rate $\sim 10^{20}$ eV g^{-1} sec^{-1}. The residence time of the sample within the irradiation volume was ~25 msec so that the sample received a dose sufficient to consume ~0.5 mM hydrocarbon. In the pulse radiolysis experiments, exposures (also with 2.8-MeV electrons) were of

~1-μsec duration at currents up to 50 mA for absorbed doses of up to 6×10^{17} eV/g. The samples were changed between pulses. For wavelengths below 260 nm a correction for scattered light of wavelength longer than 290 nm was made from measurements of the intensity of light transmitted by a 2-mm Pyrex 053 filter (290-nm cutoff). The level of scattered light was essentially constant but the total light level decreased continuously with decreasing wavelength so that this correction became important for wavelengths below 250 μm (for transparent samples the scattered light of long wavelength was ~10% of the incident light at 230 nm and ~20% at 220 nm).

Rate Constant Measurements. Second-order rate constants for attack of H atoms on cyclopentane, cyclopentene, and a number of related substances were determined by competitive measurements using the reaction between H atoms and deuterioisopropyl alcohol as the reference reaction (see Neta, Holdren, and Schuler).[7] The rate constant for the latter reaction was taken as 1.05×10^7 M^{-1} sec^{-1} with the latter based on the absolute measurement of 1.0×10^9 M^{-1} sec^{-1} for addition of H atoms to benzoic acid.[8]

Rate constants for OH reactions were determined in competitive pulse radiolysis experiments using the loss of intermediate from the reaction of OH with SCN^- ($k = 1.1 \times 10^{10}$ M^{-1} sec^{-1})[9] or with *p*-nitrobenzoate anion ($k = 2.6 \times 10^9$ M^{-1} sec^{-1})[10] as the indicator.

Absolute second-order rate constants for loss of cyclopentyl and cyclopentenyl radicals were determined by measuring the median lifetimes of the radicals produced at known concentrations in pulse experiments. The total initial radical concentrations were determined by measurement of the absorption of $(SCN)_2^-$ produced by an equivalent dose. The latter was assumed to be produced in N_2O saturated solutions with a yield of 6.0 and to have $\epsilon_{475} = 7600$ M^{-1} cm^{-1}.[11] Doses were intercompared *via* a secondary emission monitor.

Results and Discussion

The solubilities of the hydrocarbons in water are of critical importance in the analysis of the kinetic data obtained in these studies. This situation is true even below the solubility limit because the high vapor pressure of the hydrocarbons results in an appreciable fraction of the hydrocarbon being present in the vapor phase. There is, in fact, relatively little reliable information on the solubilities of liquid hydrocarbons with the most comprehensive summary being the 1966 report by McAuliffe.[12] Other data, where it exists, frequently differ considerably.[13] In the case of cyclohexane, for example, a value a factor of 3 higher than McAuliffe's solubility has been reported.[13a] It was therefore considered desirable to make our own independent determinations. Solutions were saturated with the hydrocarbon in closed vessels, shaken vigorously and, after they had been allowed to stand for 1 day, 0.5-cc portions were withdrawn directly from the aqueous phase into gas-tight syringes through a septum in direct contact with the aqueous phase. The hypodermic needle was not allowed to come into contact with the hydrocarbon phase. These samples were then analyzed by gas chromatographic methods. The sensitivity of the thermal conductivity detector for the individual hydrocarbons was determined by examining known solutions of the hydrocarbons in nonane. The solubilities determined in this work are in quite good agreement with those reported by McAuliffe, as is indicated in Table I. Values for cyclohexane (determined by a related radiochemical method) and cyclohexene were also measured in the present study and these values are reported in Table I along with literature values on the C_5 and C_6 straight chain hydrocarbons which illustrate the trends of solubility with structure. It is seen that the cyclic compounds are a factor of 4–5 more soluble than their straight chain analogs and that the solubility drops off rapidly with increased size. In general the olefins are a factor of 3–4 more soluble than the corresponding alkanes. Of the liquid hydrocarbons cyclopentane and cyclopentene are, from the solubility point of view, obviously the best choices for the present type of study.

TABLE I: Solubilities of Hydrocarbons in Water at 23°

	Solubility, m*M*	
	McAuliffe[a]	Present results
Cyclopentane	2.2	2.5
Cyclohexane	0.65[b]	0.68
Cyclopentene	7.9	8.2
Cyclohexene	2.6	2.6
Pentane	0.53[c]	
Hexane	0.10[c]	
Heptane	0.03	
Octane	0.008	
1-Pentene	2.1	
2-Pentene	2.9	
1-Hexene	0.59	

[a] Reference 12. [b] Values of 0.75 and 1.70 have also been reported (ref 13a and b). [c] Values of 0.54 and 0.21 for pentane and hexane, respectively, have been reported in ref 13c.

In the following it is assumed that below the solubility limit the solutions are ideal and that the hydrocarbon concentration is controlled by Henry's law. Accordingly the fraction of the amount of solute in solution was taken as $(1 + P^0V_g/RTS_{Hyd}V_l)^{-1}$ where P^0 is the vapor pressure of the hydrocarbon, V_l and V_g are the liquid and vapor volumes, S_{Hyd} is the solubility of the hydrocarbon in water, and R and T are the usual gas constant and absolute temperature. For cells having 50% vapor volume these fractions are only 0.13 and 0.28, respectively, for cyclopentane and cyclopentene. It is seen that even where the amount of solute added to the system is below the solubility limit the problem of knowing the exact concentration is, indeed, very severe if there is any vapor volume remaining in the irradiation cell. Detailed kinetic studies on hydrocarbon solutions are made extremely difficult because of uncertainty about the concentration in solution. Because the irradiation periods were short (<10 min) it is assumed in the following kinetic treatments that volatile products did not escape from solution during the period of the irradiation.

Rate Constants for the Reactions of the Primary Radicals. Hydrated electrons should not react with either cyclopentane or cyclopentene so that in the absence of an electron scavenger the hydrated electrons produced from the water presumably will react with H^+ ion to form hydrogen atoms. In the presence of N_2O they will be rapidly converted to OH radicals. If an electron scavenger is not intentionally added to the system it is possible that hydrated electrons might interfere somewhat by reacting with certain radiation produced products such as cyclopentanone.

While the rate constants for reaction of H atoms with both cyclopentane and cyclohexane have previously been measured by an esr method, the values reported (3×10^7 M^{-1} sec^{-1} in both cases) represent the results of single

experiments on saturated solutions and are subject to considerable uncertainty.[14] A pulse radiolytic determination of 4×10^7 M^{-1} sec^{-1} for reaction of H with cyclohexane in aqueous solution has also been reported by Sauer and Mani.[15] Both measurements on cyclohexane are, however, based on a solubility of 1.7 mM and need to be corrected upward to 8 and 10×10^7 M^{-1} sec^{-1} by virtue of the lower solubility indicated in Table I. Because of these solubility problems it was also decided to examine the simple carboxylic acid derivatives where the rate constants should be similar to (but slightly lower than) those for the hydrocarbons[16] and solutions of known concentrations can be prepared more readily. The H_2 and HD yields from solutions containing both isopropyl alcohol-d_7 and the various solutes of interest here are given in Table II (available on microfilm). In these experiments the vapor volume represented only ~20% of the cell volume so that ~37 and ~60% of the cyclopentane and cyclopentene added would be in solution and errors in determining these factors should not affect the results in more than a relatively minor way. The total rate constants for the reaction of H atoms with these solutes relative to the abstraction of H from isopropyl alcohol-d_6 were calculated according to the methods described by Neta, Holdren, and Schuler[7] and are given in the final column. The absolute rate constants obtained on the basis of an assumed value for the reference reaction of 1.05×10^7 M^{-1} sec^{-1} are given in Table III. For the saturated compounds some loss of H atoms by addition to product olefin is evident from the fact that the observed total hydrogen yield is only 2.8–3.2. Since the relative rates are calculated from the observed H_2 and HD yields, such a loss has no effect on the rate constant determinations. For the unsaturated compounds the addition reactions dominate as expected but abstraction also occurs to an important extent, as is manifested by the fact that the H_2 yields are 0.3–0.4 units above the molecular yield (see the entry for acrylic acid). The fraction of H atoms which abstract from the cycloolefins are given in the second column of Table III and the partial rates for the abstraction and addition reactions in the final two columns.

The rate constants given in Table III for cyclopentane and cyclohexane are very reasonable in view of the values of $\sim 5 \times 10^7$ M^{-1} sec^{-1} measured for the carboxylic acids since carboxyl groups are known to decrease H atom abstraction rate constants by a factor of between 1 and 2.[16] The value for cyclohexane agrees well with the previous values obtained in the esr[14] and pulse radiolysis[15] experiments after corrections have been made as indicated above. The esr value for reaction with cyclopentane, which after correction has been made to the solubility of Table I is 20×10^7 M^{-1} sec^{-1}, appears to be unquestionably too high and probably reflects secondary reactions with product cyclopentene at the dose rates employed.

Rate constants for reaction of H atoms with the cycloolefins have not previously been reported but the values are expected to be in the range of $1\text{–}5 \times 10^9$ M^{-1} sec^{-1} typical for addition to unsaturated systems.[17] The values given in Table III appear to be reasonable but may be somewhat high in view of the lower values for addition to the unsaturated acids. The ratio of the rate constant for addition to cyclopentene to that for abstraction from cyclopentane is ~60 and in agreement with the ratio for the corresponding carboxylic acid. This value of the ratio will be used in the following kinetic treatment. The partial rate constant for abstraction from the cycloolefins is considerably higher than that for abstraction from saturated systems and indicates that abstraction occurs predominantly at the allylic positions. For cyclopentene the partial rate per allylic H atom ($\sim 1 \times 10^8$ M^{-1} sec^{-1}) is about a factor of 10 greater than the comparable rate for abstraction from cyclopentane, in agreement with the general conclusions of Witter and Neta[18] from studies on other unsaturated systems. Abstraction from the CH_2 position of cyclopentene should have a partial rate similar to that of cyclopentane and account for less than 1% of the total H atom chemistry.

TABLE III: H Atom Reaction Rates with Aliphatic Hydrocarbons

Hydrocarbon	f^{H}_{abs}[a]	k_{total}[b] $\times 10^{-7}$, M^{-1} cm^{-1}	k_{abs}[b] $\times 10^{-7}$, M^{-1} cm^{-1}	k_{add}[b] $\times 10^{-7}$, M^{-1} cm^{-1}
Cyclopentane		10	10	
Cyclopentanecarboxylic acid		4.8	4.8	
Cyclohexane		7	7	
Cyclohexanecarboxylic acid		5.0	5.0	
Acrylic acid	0.00	210	<5	210
Cyclopentene	0.08	580	50	530
Cyclopentene-1-carboxylic acid	0.06	330	20	310
Cyclohexene	0.09	610	50	560
Cyclohexene-1-carboxylic acid	0.07	310	20	290
Cyclohexene-4-carboxylic acid	0.07	280	20	260

[a] Fraction of H atoms undergoing abstraction reactions calculated on the assumption that the molecular H_2 yield in these solutions is 0.43. [b] Based on a rate constant of 1.05×10^7 M^{-1} sec^{-1} for the abstraction of D from $(CD_3)_2CDOH$.

The rate constants for the reactions of OH with cyclopentane and cyclopentene were determined by measuring the diminution of the absorption of the transient produced by OH attack on p-nitrobenzoic acid (for cyclopentane) or thiocyanate (for cyclopentene) upon saturating a given solution with the hydrocarbon. Values of 3.0 and 7.0×10^9 M^{-1} sec^{-1}, respectively, were obtained. Both values are of the magnitude expected from information on the rates of abstraction from and addition to other saturated and unsaturated systems of similar size.[17] In particular Anbar, Meyerstein, and Neta[19] have reported a value of 4×10^9 M^{-1} sec^{-1} (corrected, see ref 19b) for reaction of OH with cyclopentanecarboxylic acid. It is seen that there is very little selectivity in the reaction of OH radicals. While OH is, of course, expected mainly to add to cyclopentene, H abstraction will also be important. The partial rate constant for abstraction from the allylic positions should be $>1.2 \times 10^9$ M^{-1} sec^{-1} so that 2-cyclopentenyl radical (referred to subsequently as cyclopentenyl) should be an important intermediate. For purposes of making preliminary estimates of the product distribution we will assume that 20% of the OH abstracts H from the 3 position and, as we will see below, a value of this magnitude is borne out by the analysis of the product distribution. Abstraction of H from the 4 position should have a partial rate constant $\sim 0.6 \times 10^9$ M^{-1} sec^{-1} so that the 3-cyclopentenyl radical should account for ~8% of the chemistry.

Radical Intermediates. Esr Studies. If secondary reactions involving product are unimportant, cyclopentyl radical should be the only radical produced from the solute in the case of cyclopentane. This radical is readily identified from its 10 "line" esr pattern where each "line" should have further observable structure resulting from splitting

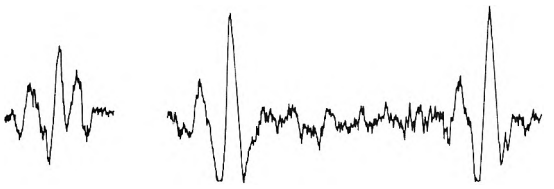

Figure 2. Partial esr spectrum of cyclopentenyl radical produced in the irradiation of N_2O saturated aqueous solution of cyclopentene at pH 13.5. The total spectrum consists of 30 "lines" described by the parameters $a^H(\alpha^*)$ = 14.19 G (two equivalent protons), $a^H(\alpha)$ = 2.81 G (one proton), $a^H(\beta)$ = 22.74 G (four equivalent protons), and g = 2.00265. The second-order patterns of (a) the 16th "line" and (b) the 21st and 22nd "lines" (counting from low to high field) are illustrated. The 2.81-G splitting by the unique proton is illustrated by the separation between "lines" 21 and 22. The hyperfine constants correspond to spin densities of 0.57 at the starred (extreme) and −0.11 at the unstarred (central) position of the allylic system. The observed β-hyperfine constant (22.74 G) is somewhat larger than the value of 20.0 G predicted by multiplying the 35.1-G β hyperfine constant of cyclopentyl radical by the spin density of 0.57 on the adjacent α-carbon atom. If the contributions to the wave function add constructively a spin density of only ~0.02 on the adjacent β-carbon atom is sufficient to explain this difference.

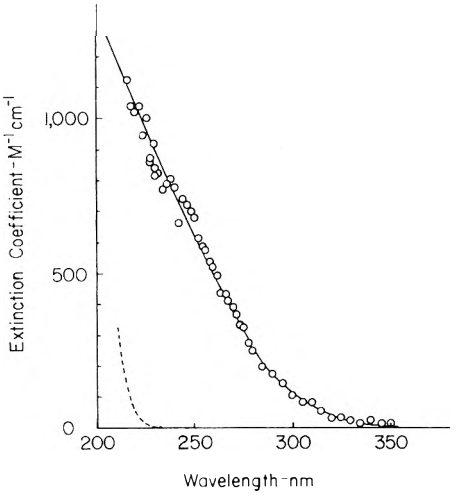

Figure 3. Absorption spectrum of cyclopentyl radical. Measurements were made 3 μsec after a 1 μsec pulse. Each point represents the average of four experiments carried out on N_2O-saturated cyclopentane-saturated aqueous solutions. Doses were ~3 × 10^{17} eV/g (30 μM cyclopentyl radical) and samples were changed between pulses. Appropriate corrections for scattered light have been made and extinction coefficients have been calculated from the dosimetry as described in the text. The absorption spectrum of cyclopentene is given by the dashed curve and that for the cyclopentane lies much further into the uv.[28a]

by the γ protons and by second-order effects.[20] This radical is, in fact, the only one distinguishable during *in situ* esr experiments on neutral solutions (phosphate buffered) saturated both with N_2O (to convert e_{aq}^- to OH) and with cyclopentane. The lines are weak but are readily observable on the high-field side since they are somewhat enhanced by CIDEP effects.[21] The esr parameters in aqueous solution at room temperature are $a^H(\alpha)$ = 20.85 ± 0.10, $a^H(\beta)$ = 35.11 ± 0.03 (four equivalent protons), and $a^H(\gamma)$ = 0.50 ± 0.03 G (four equivalent protons) with g = 2.00256 ± 0.00003 and the observed line width is 0.14 G. The hyperfine constant of the α proton is somewhat lower than the value of 21.48 G reported in liquid cyclopentane at −40°[20] but the β and γ constants are essentially identical with the respective values of 35.16 and 0.53 G previously found. Since α-proton hyperfine constants are expected to decrease with increase in temperature[22,23] the difference between the two studies reflects, to a certain extent, the temperature difference between the measurements. Fischer[24] gives a value of $a^H(\alpha)$ = 21.05 G for cyclopentyl radical in ether solution at room temperature.

Studies similar to the above on a neutral N_2O saturated cyclopentene solution gave only a very weak esr spectrum. The most intense lines were those of the cyclopentenyl radical (see below) indicating that abstraction of the allylic hydrogen atoms by ·OH is a reasonably major process. A large number of weaker lines were also present but the patterns were not sufficiently defined for a detailed assignment. Presumably these lines are attributable to the radical cyclopentyl-2-ol which is expected to be the predominant species present in this case. Cyclopentene was also examined at pH 13.5 where OH is converted to O^- and H atom abstraction by the O^- becomes a very important reaction.[25] The principal radical observed was the cyclopentenyl produced by abstraction of H from the allylic positions of the cyclopentene. This radical has a 30-line esr spectrum (two equivalent α protons at the extremities and one unique α proton at the central position of an allylic system and four equivalent β protons) so that the individual lines are weak as is illustrated in Figure 2. From the observed intensities one can conclude that comparable concentrations of radicals are present at steady state in the respective experiments on solutions of cyclopentane and cyclopentene. The esr parameters of cyclopentenyl in this study are $a^H(\alpha^*)$ = 14.19 (two equivalent protons), $a^H(\alpha)$ = 2.81 and $a^H(\beta)$ = 22.74 G (four equivalent protons), and g = 2.00265. Only a qualitative esr spectrum of cyclopentenyl radical produced in the radiolysis of liquid cyclopentene has previously been reported[26] although unpublished independent measurements by Fessenden and Ogawa in hydrocarbon solutions[27] have given parameters comparable to those observed here. The quantity $2a^H(\alpha^*) - a^H(\alpha)$ = 25.57 G can be compared with the related value of 25.60 G obtained for the assignment of the 14.83 and 13.93 G constants in allyl radical,[20] respectively, to the protons *cis* and *trans* to the unique proton in allyl radical. Krusic and Kochi have previously[28] come to the same assignment from an intercomparison of the hyperfine constants of the *cis*- and *trans*-1-methyl allyl radicals.

Radical Intermediates. Pulse Radiolysis Studies. Pulse radiolysis experiments on cyclopentane solutions at pH 10 (N_2O saturated) gave the absorption spectrum of Figure 3 3 μsec after a 1-μsec pulse. In these experiments the period for OH attack is 0.1 μsec and for H atom attack 3 μsec so that effectively all of the OH and 50% of the H atoms should have been converted to cyclopentyl radicals at the time of observation. From the dosimetry the total initial radical concentration is 30 μM. The correction for loss of radicals by recombination at 3 μsec is estimated from the kinetic results described below to be ~15% so that the yield of radicals present at the time of observation is expected to be 5.4. There will be no important loss of these radicals by reaction with products because the products are formed on a time scale one to two orders of magnitude greater than the initial abstraction reactions. The extinction coefficients given in Figure 3 are based on this yield together with a comparison of the incremental absorbances observed in the cyclopentane solutions with those found at identical doses with SCN^- ($G(SCN)_2^-$ = 6.0; $\epsilon_{490}(SCN)_2^-$ = 7600 M^{-1} cm^{-1}).[28a]

The spectrum of Figure 3 should be attributable to cyc-

lopentyl radical. Sauer and Mani[15] have, however, reported an absorption spectrum for cyclohexyl radical in aqueous solution with a maximum at 240 nm and an extinction coefficient at that wavelength of 1500 M^{-1} cm^{-1}. Since one expects that cyclopentyl and cyclohexyl radicals will have more or less similar absorption spectra the present results appear to be at variance with this previous report. Pulse radiolysis studies on solutions saturated with cyclopentyl bromide or chloride containing *tert*-butyl alcohol to remove OH also gave a component to the absorption assignable to cyclopentyl radical formed by e_{aq}^- attack on the halide which was essentially identical with that indicated in Figure 3. Studies on 10 mM cyclopentanol solutions saturated with N_2O showed some complications at long wavelengths and long times but there was no component at short times which contributed to the absorption in the region of 230–260 nm significantly in excess of that of Figure 3. We conclude that the spectrum of Figure 3 represents cyclopentyl radical and that the absorption increases monotonically with decrease in wavelength. There is no manifestation of any maximum at 240 nm. Cyclopentane itself does not absorb significantly above 200 nm (ϵ_{210} <0.1 M^{-1} cm^{-1}) and cyclopentene absorbs only weakly (ϵ_{210} ~100 M^{-1} cm^{-1}).

The spectrum indicated by the crosses in Figure 4 was observed in the pulse irradiation of N_2O saturated solutions of cyclopentene at pH 10.5. The radicals formed in the addition reactions are expected to exhibit spectra similar to that of Figure 3 so that it would appear that the maximum at ~240 nm can be ascribed largely to cyclopentenyl radicals produced by abstraction of an allylic hydrogen atom. That this is the case is shown by the spectrum at pH 14 (the circles in Figure 4) where a narrow (20 nm at half-maximum) well-defined and moderately intense Gaussian shaped absorption band is observed at 242 nm. The esr studies clearly show that cyclopentenyl is extremely important at this pH and there is little question but that this absorption band can be assigned to cyclopentenyl radical. The growth period of this band is <0.5 μsec for a solution saturated with cyclopentene. Taking the solubility to be <0.008 M the rate constant for O^- attack on the cyclopentene is >2 × 10^8 M^{-1} sec^{-1}. At pH 13 where the ratio of [O^-]:[OH] is ~10:1 the absorption at 242 nm has risen by one-half of the difference between its values at pH 10.5 and 14 so that a rate constant ~7 × 10^8 M^{-1} sec^{-1} is indicated for the reaction of O^-. The contribution of OH at pH 14 is, accordingly, only ~10%. Since the rate constant for addition of O^- to aromatic systems is low[24] we have assumed that addition to cyclopentene and other side reactions of O^- are important and have calculated the extinction coefficients on the basis of a cyclopentenyl yield of 6.0 at pH 14. The values in Figure 4 are, therefore, lower limits with the actual values probably being ~20% larger and somewhat dependent on the relative frequency for abstraction of hydrogen from the 4 position of cyclopentene.

The spectrum observed at pH 10.5 is more complex than that found at higher pH and obviously has a contributing absorption that is somewhat more intense than that of cyclopentyl radical. From the figure a background ~1300 cm^{-1} per OH at the cyclopentenyl maximum is reasonable and if we subtract this background from the observed value of 4100 cm^{-1} per OH and divide by an extinction coefficient of 10,000 M^{-1} cm^{-1} we obtain a value of 28% for the fraction of OH which abstracts an allylic hydrogen atom from cyclopentene. Because of background

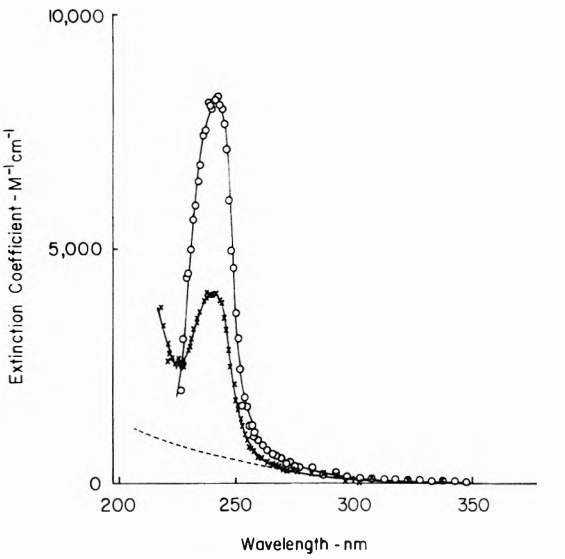

Figure 4. Absorption spectrum of cyclopentenyl radical (O) as observed in the pulse radiolysis of aqueous solutions of cyclopentene at pH 14 (N_2O saturated). Observations are 2 μsec after a 1-μsec pulse which produced an initial concentration ~10^{-5} M. Results represent the average of four experiments. Extinction coefficients are determined on the assumption of a yield of 6.0. Data at pH 10.5 (×), taken under similar conditions, show that cyclopentenyl is produced at the lower pH in reduced yield and that an additional intermediate contributes an underlying absorption in the region immediately above 200 nm. The dashed curve is the spectrum of cyclopentyl radical from Figure 3.

from other radicals and uncertainty in the extinction coefficient this value is regarded as somewhat less reliable than the value of 23% indicated by the chemical measurements described below.

Rate Constants for the Radical–Radical Reactions. Since first-order reactions of the radicals are not expected to compete with the radical–radical reactions even at the lowest dose rates used here, the absolute rates for the second-order processes do not come into the kinetic treatment of product formation in any direct way as long as only one type of radical is present. Where reaction between different types is important, some knowledge of the rate constants for the different combination reactions is useful. Data on the disappearance of cyclopentyl and cyclopentenyl radicals are given in Figures 5 and 6 (available on microfilm). Rate constants for radical disappearance ($2k_{ii}$ where k_{ii} is specified for the reaction $R_i + R_i \rightarrow$ products) were determined from the initial total radical concentration $[R]_0$, as given by the dosimetry, and the observed median lifetime t_m, *i.e.*, the period required for loss of 50% of the radicals ($k_{ii} = (2[R]_0 t_m)^{-1}$). Values of 2.0 and 1.5 × 10^9 M^{-1} sec^{-1} were obtained for, respectively, cyclopentyl and cyclopentenyl. In both cases the decay follows good second-order kinetics out of 90% decay as is illustrated in the figures. In the experiment on cyclopentene at pH 10.5 the decay is more complex and there is a residual absorption which amounts to about 10% of the initial signal. If one corrects for this then the median lifetime of the species absorbing at 242 nm is similar to that at pH 14. It seems likely that this residual may be caused by product cyclopentadiene which has an extinction coefficient ~3000 M^{-1} cm^{-1} at this wavelength. If so the yield of cyclopentadiene is ~0.3 and it is indeed surprising that a larger residual is not observed in the experiment at pH 14 since cyclopentadiene should be even a

TABLE IV: Yields of Products Formed in the γ-Radiolysis of Aqueous Solutions of Cyclopentene Containing 10^{-2} M N_2O[a]

Product	G(product)[b]
Cyclopentanone	~0.55
Cyclopentanol	0.96
3(Cyclopentyl-2-ol)cyclopentene	0.56 × 2 = 1.12[c]
2-Cyclopentylcyclopentanol	0.21 × 2 = 0.42[c]
Cyclopentane	0.31
Total observed	3.36[d]

[a] All of the solutions were saturated with C-14 labeled cyclopentene. [b] Yields are taken from the linear dependences indicated in Figure 4. [c] Given in units of cyclopentene incorporated in the product. The yields of these dimers are one-half the values quoted in the last column. [d] In addition an approximate yield of 1.0 was observed for 2(cyclopentyl-2-ol)cyclopentanol and a yield ~0.7 must be included in the material balance considerations to account for the reformation of cyclopentene. The principal missing product appears to be cyclopenten-3-ol which elutes with the water.

more important product there. The second-order rate constants, as measured in these pulse experiments, show that in spite of its conjugation cyclopentenyl reacts nearly as rapidly as does cyclopentyl so that in the steady-state studies there should be relatively little selectivity between the various possible radical–radical reactions.

Radiolysis of Cyclopentene Solutions. In aqueous solutions of cyclopentene the radiolysis products are, to a large extent, protected from secondary attack by the high reactivity of the cyclopentene so that product formation is expected to be very nearly linearly dependent on dose. As a result, the yields observed at reasonable doses should directly reflect the relative importance of both the different initial reactions and the various competing termination processes. This system will be discussed first since the information obtained is useful in the discussion of the cyclopentane system to follow.

(*a*) *Studies in the Presence of N_2O.* The principal products observed in the radiolysis of cyclopentene solutions were, as has been already indicated in the chromatogram of Figure 1, cyclopentane, cyclopentanone, cyclopentanol, 3(cyclopentyl-2-ol)cyclopentene, and 2-cyclopentylcyclopentanol. For solutions ~8 mM in cyclopentene and 20 mM in N_2O the yields of all products except cyclopentanone increased linearly with dose up to doses of ~6 × 10^{18} eV/g, as is illustrated in Figure 7 (available in microfilm). The yield of cyclopentanone, which is the stable tautomeric form of the cyclopentene-1-ol expected to be produced in the disproportionation of cyclopentyl-2-ol radicals, appears to decrease as the dose increases. Since the cyclopentanone concentration does not rise to the point where the reaction with e_{aq}^- will compete significantly with scavenging by N_2O we must assume that the apparent drop of its yield results from secondary reactions such as electron transfer. The yields indicated by Figure 7 are summarized in Table IV. From the mechanism discussed below one also expects an appreciable yield of both 2(cyclopentyl-2-ol)cyclopentanol and cyclopentene-3-ol and minor yields of cyclopentadiene and the three dimeric products produced from the combination of cyclopentyl and cyclopentenyl radicals. The latter, which from the retention time of cyclopentylcyclopentane should appear just before the 2-cyclopentylcyclopentanol, were produced in such small yields that they were lost in the background. In the chromatographic procedure used, the cyclopentene-3-ol was not observed since it eluted from the silicone grease column along with the water. The dimer 2(cyclopentyl-2-ol)cyclopentanol had such a broad peak that it could not be measured accurately but was produced with a $G \sim 0.5$. A careful examination, which should have detected a yield of even a few tenths, showed no observable cyclopentadiene. While the net yield of this product is certainly low, some should be formed and it seems likely that cyclopentadiene is sufficiently reactive that it is consumed as it is formed by secondary reactions of the radicals.

It is expected that at normal pH values (*i.e.*, <12) the H atoms and OH radicals produced from the water[29] will for the most part add to cyclopentene to give cyclopentyl and cyclopentyl-2-ol radicals although, as indicated above, a significant yield of cyclopentenyl radicals should also be produced by abstraction of hydrogen atoms from the allylic positions. The radicals produced by OH abstraction of hydrogen from the 4 position will give products similar to those of cyclopentenyl and will not be explicitly treated here. As mentioned in the Introduction, reaction of hydrated electrons with hydrocarbons does not occur so that in the presence of N_2O they should be quantitatively converted to OH radicals. If f_{abs}^{H} and f_{abs}^{OH} are the fractions of the reactions of H and OH where abstraction occurs, then the initial chemical reactions can be described by

$$H + c\text{-}C_5H_8 \xrightarrow{1 - f_{abs}^{H}} c\text{-}C_5H_9\cdot \quad (1)$$

$$\xrightarrow{f_{abs}^{H}} c\text{-}C_5H_7\cdot + H_2 \quad (1A)$$

$$OH + c\text{-}C_5H_8 \xrightarrow{1 - f_{abs}^{OH}} c\text{-}C_5H_8OH\cdot \quad (2)$$

$$\xrightarrow{f_{abs}^{HO}} c\text{-}C_5H_7\cdot + H_2O \quad (2A)$$

From the rate studies reported above f_{abs}^{H} can be taken as 0.08 and f_{abs}^{OH} as ~0.2. In the case of neutral N_2O-saturated solutions $G_H = 0.6$ and $G_{OH} = 6.0$[29] so that the yields for cyclopentyl, cyclopentyl-2-ol, and cyclopentenyl radicals produced by reactions 1 and 2 can be estimated to be ~0.56, 4.8, and 1.24, respectively. One of the prime objectives of the analysis of the chemical results is to determine more accurately the yields of the latter two radicals. It can readily be seen that the yield of cyclopentyl radicals must be at least equal to the sum of the yields of cyclopentane and 2-cyclopentylcyclopentanol (*i.e.*, >0.52) and the yield of cyclopentenyl radical must be greater than that of 3(cyclopentyl-2-ol)cyclopentene (>0.56). Given that the ratio between disproportionation and combination of cyclopentenyl and cyclopentyl-2-ol radicals is ~1 the latter yield is more realistically greater than 1.1 so that the above estimates seem very reasonable.

The three radicals produced by these reactions will undergo six sets of combination and disproportionation reactions

$$c\text{-}C_5H_9\cdot + c\text{-}C_5H_9\cdot \rightarrow C_{10}H_{18} \quad (3C)$$

$$\rightarrow c\text{-}C_5H_{10} + c\text{-}C_5H_8 \quad (3D)$$

$$c\text{-}C_5H_8OH\cdot + c\text{-}C_5H_8OH\cdot \rightarrow C_{10}H_{18}(OH)_2 \quad (4C)$$

$$\rightarrow c\text{-}C_5H_9OH + c\text{-}C_5H_7OH(c\text{-}C_5H_8O) \quad (4D)$$

$$c\text{-}C_5H_7\cdot + c\text{-}C_5H_7\cdot \rightarrow C_{10}H_{14} \quad (5C)$$

$$\rightarrow c\text{-}C_5H_8 + c\text{-}C_5H_6 \quad (5D)$$

$$c\text{-}C_5H_9\cdot + c\text{-}C_5H_8OH\cdot \rightarrow C_{10}H_{17}OH \quad (6C)$$

$$\rightarrow c\text{-}C_5H_{10} + c\text{-}C_5H_7OH(c\text{-}C_5H_8O) \quad (6D)$$

$$\rightarrow c\text{-}C_5H_8 + c\text{-}C_5H_9OH \quad (6D')$$

$$c\text{-}C_5H_9OH + c\text{-}C_5H_7\cdot \rightarrow C_{10}H_{15}OH \quad (7C)$$
$$\rightarrow c\text{-}C_5H_8 + c\text{-}C_5H_7OH (c\text{-}C_5H_8O) \quad (7D)$$
$$\rightarrow c\text{-}C_5H_6 + c\text{-}C_5H_9OH \quad (7D')$$
$$c\text{-}C_5H_8\cdot + c\text{-}C_5H_7\cdot \rightarrow C_{10}H_{16} \quad (8C)$$
$$\rightarrow c\text{-}C_5H_8 + c\text{-}C_5H_6 \quad (8D)$$
$$\rightarrow c\text{-}C_5H_6 + c\text{-}C_5H_{10} \quad (8D')$$

with the disproportionation involved in reactions 6–8 proceeding in two possible directions. The mechanism is further complicated by the fact that disproportionation reactions 4D, 6D, and 7D give either cyclopentene-3-ol or cyclopentanone depending on the site from which the H atom is transferred. At the dose rates of these experiments the radical production rates are 1.2×10^{-7} and 1.6×10^{-6} M/sec and from the measured rate constants the mean radical lifetimes are calculated to be 60 and 15 msec. In saturated solutions, addition of the radicals to the cyclopentene will be important if the rate constants for these addition reactions are greater than $\sim 10^2$ M^{-1} sec^{-1}. Rate constants approaching this magnitude seem likely[30] so that addition undoubtedly occurs to at least a small extent and one can expect a loss of radicals by addition reactions at dose rates not too much lower than those employed here. There is, however, no obvious loss of monomeric products nor any apparent dose rate dependence (see Figure 7). In particular the cyclopentyl radicals cannot be adding to cyclopentene significantly since their yield is essentially completely accounted for by the observed cyclopentane and 2-cyclopentylcyclopentanol. Secondary abstraction reactions of the radicals are at least somewhat slower[31] and not expected to be of importance at the solute concentrations of these experiments.

In treating the data it is useful to begin by considering as a first approximation the relative importance of the different reactions as indicated by the above estimates of the individual radical yields. The measured rate constants show that in all cases the radicals disappear at rates approaching the diffusion-controlled limit so that the relative frequency of the competing reactions should be controlled by the encounter rates and not be very far from statistical. For N_2O saturated solutions the reactions of cyclopentenyl radical with itself and with cyclopentyl should be of only minor importance and, because cyclopentyl radicals represent only $\sim$10% of the radicals produced, reaction 3 should account for only $\sim$1% of the total chemistry. The yields for reactions 3–8 should be in the approximate ratios of 1:49:4:14:28:4. It is seen that each of the three sets of reactions involving cyclopentyl-2-ol radicals are important and, in particular, that the reaction between this radical and cyclopentenyl is expected to contribute very significantly. This expectation is borne out by the very high yield observed for the combination product of this reaction.

A more complete description of the scheme represented by reactions 3–8 requires knowledge of the relative rates of disproportionation to combination for each of the reactions and this information must basically be derived from the measured product yields. The disproportionation–combination ratio for reaction between cyclohexyl radicals produced by the photolysis of diphenylmercury in cyclohexane has been determined by Cramer to be 1.1 ± 0.1[32] and a value of this magnitude can be taken as reasonably typical for reactions between radicals resulting from the loss of a secondary hydrogen atom from a saturated system.[33] Analysis of the data is complicated by the fact that reactions 6–8 undergo two different disproportionation reactions. From the relationship given by Holroyd and Klein,[33] which empirically relates the observed relative rates of disproportionation and combination to the entropy difference between the disproportionation products and the dimer of the radical, one can show that the relative importance of reactions 8D and 8D′ is

$$\log k_D/k_{D'} = 0.131\Delta S^\circ \quad (9)$$

where ΔS° is the difference between the standard entropies of the two sets of disproportionation products. The standard entropies of formation of cyclopentane and cyclopentene are, respectively, 70.0 and 69.2 cal deg^{-1} mol^{-1}.[34] The entropy of cyclopentadiene is not available in the API tables but can be estimated as 63.9 cal deg^{-1} mol^{-1} by subtracting the entropy difference[34] of 5.3 cal deg^{-1} mol^{-1} between 2-pentene and *cis*-pentadiene from that of cyclopentene. If Holroyd and Klein's generalization is at all applicable to the present case it can be estimated from the resultant difference of 4.5 cal deg^{-1} mol^{-1} that reaction 8D should be favored over reaction 8D′ by a factor of $\sim$4 and it seems likely that reaction 7D will be similarly favored over 7D′.

The high yield of cyclopentane observed here shows that more than 50% of the cyclopentyl radicals undergo disproportionation processes with the principal contribution being from reaction 6D. The only other sources of cyclopentane are reactions 3D and 8D′ each of which, from the above, should contribute yields of only $\sim$0.015. The yield for reaction 6D can, therefore, be accurately given as 0.28 ($\pm$0.02). Since 2-cyclopentylcyclopentanol is produced only by reaction 6C one obtains a ratio for k_{6D}/k_{6C} of $0.28/0.21 = 1.35$ ($\pm$0.1). This ratio is in reasonable accord with Cramer's value of 1.1 for disproportionation of cyclohexyl radicals. The contribution of reactions 6C and D to the overall chemistry corresponds to a yield of $2(0.31) + 0.42 = 1.04$ or 16% of the total (compared with the 14% *a priori* estimate given above). A cyclopentyl yield of 0.49 is involved in these reactions so that, together with an additional yield $\sim$0.06 from reaction 3, essentially all of the expected cyclopentyl radicals are accounted for. Reaction 8 must occur to some extent but there is obviously very little room for any major contribution.

Both cyclopentyl and cyclopentenyl radicals will disappear mostly by reaction with cyclopentyl-2-ol radicals so that the ratio of 2.6 observed between the products 3(cyclopentyl-2-ol)cyclopentene and 2-cyclopentylcyclopentanol should give an approximate measure of the relative yields of these two radicals. The disproportionation–combination ratio involved in the reactions of cyclopentenyl radicals may be somewhat lower than the value of 1.35 given above[35] so that the observed product ratio should be corrected downward. Taking k_D/k_C as 1, the relative yield for the two radicals is 2.3 from which one can estimate the yield for the cyclopentenyl radicals as 1.4, *i.e.*, 21% of the total radicals. Of this only $\sim$0.05 is ascribed to abstraction of the allylic hydrogens by H and the remainder (1.35) to abstraction by OH. The fractional attack on the allylic hydrogen atoms, f_{abs}^{OH}, is from these chemical results $\sim$0.23. The pulse radiolysis studies discussed above show that the abstraction cannot be more than 50% greater. Taking the total rate for the OH reaction as 7.0×10^9 M^{-1} sec^{-1} the partial rate constant for abstraction from the allylic position is 1.6×10^9 M^{-1} sec^{-1}. Michael and Hart[36] estimate that 30 and 45% of OH abstracts hydrogen from 1,3- and 1,4-cyclohexadiene and that the partial

rate constants are, respectively, 2.9 and 3.4 × 10^9 M^{-1} sec^{-1}.

Cyclopentanol is produced principally by reaction 4D and to a lesser extent by reactions 6D′ and 7D′. A reasonable contribution for the latter two reactions is ~0.10 leaving a yield of 0.86 to be assigned to reaction 4D. If we assume a disproportionation–combination ratio of 1.35 for reaction 4 then the total yield for this reaction is 3.0. Adding to this value yields of 0.49 for reaction 6 and 1.12 for reaction 7, the cyclopentenyl-2-ol radical yield is 4.6. Together with the yield of 1.35 for cyclopentenyl production by H abstraction the total yield for OH attack on the cyclopentene is 5.95 so that the reactions of all of the OH initially produced appear to be accounted for quite well.

As far as the yields indicated in Table IV are concerned an additional yield of ~0.7 should be included for the cyclopentene produced from the disproportionation reactions 3D, 5D, 6D′, and particularly 7D. The remaining yields required for material balance are largely attributed to the oxygenated products 2(cyclopentyl-2-ol)cyclopentanol (measured to be ~2 × 0.5 and, taking k_D/k_C as 1.35, estimated from the above scheme to be 1.3) and cyclopentene-3-ol (estimated by difference as 1.1). It is clear that the latter must be large since reactions 4D, 6D, and 7D should account for 40–50% of the radical combination reactions and the cyclopentanone observed represents less than ½ of the product C_5H_8O. This estimate of the cyclopentene-3-ol indicates that transfer of H from the CH_2 position of the radical occurs twice as often as transfer from the CH(OH) position, *i.e.*, there is little selectivity in this transfer. The unmeasured products from reactions 3, 5, and 8 should not contribute more than 0.2 units so that a total radical yield of ~6.7 is accounted for by the above. There is no evidence in the above yields of any significant addition of organic radicals to the cyclopentene.

(*b*) *Studies at pH 3.* At pH 3 the yields of H atoms and OH radicals are, respectively, ~3.5 and 2.8[29] so that, from the above measurements of f_{abs}^{H} and f_{abs}^{OH}, the initial yields of the organic radicals should be 3.2 for cyclopentyl, 2.15 for cyclopentyl-2-ol, and 0.95 for cyclopentenyl. All reactions except 5 are important and the product distribution becomes qualitatively different and much more complex than that for the N_2O solutions. At this pH cyclopentane is expected to be a major product and since it is measurable with reasonable accuracy attention was focused on its production. The buildup of cyclopentane was found to be linear to a dose of 10^{19} eV/g with the yield being 0.93. Assuming again that reactions 3–8 occur statistically, their relative frequency should be 26:12:2:35:10:15. The cyclopentane yield can be estimated as the sum of contributions from reaction 3D [(1/2)(1.35/2.35)(0.26)(6.3) = 0.47], from reaction 6D (0.80(1.35/2.35)(0.35)(6.3) = 0.51) and from reaction 8D′ (0.20(0.10)1.0/2.0(6.3) = 0.06) for a total of 1.04. The agreement with the observed yield seems reasonably satisfactory. The principal sources of cyclopentane are reactions 3 and 6 which should represent ~60% of the total chemistry or a yield ~3.8. Again it is clear from the high yield of cyclopentane that disproportionation must be an extremely important fate of the cyclopentyl radicals, *i.e.*, that the observed cyclopentane can be accounted for only if $k_D/k_C > 1$.

Radiolysis of Cyclopentane Solutions. In its early stages, the radiolysis of cyclopentane solutions should be very simple in that only cyclopentyl radicals will be produced by the abstraction reactions

$$H + c\text{-}C_5H_{10} \longrightarrow c\text{-}C_5H_9\cdot + H_2 \quad (10)$$

and

$$OH + c\text{-}C_5H_{10} \longrightarrow c\text{-}C_5H_9\cdot + H_2O \quad (11)$$

Initially the only important radical–radical reactions will be 3C and 3D so that cyclopentene and cyclopentyl–cyclopentane should be the only observed products. Their initial yields should be, respectively, $[(G_H + G_{OH})/2][k_D/k_C/(1 + k_D/k_C)]$ and $[(G_H + G_{OH})/2][1/1 + k_D/k_C)]$. Taking k_D/k_C as 1.35 from the above, it is estimated from the primary radical yields that the initial cyclopentene and dimer yields should be 1.80 and 1.35 for solutions at pH 3 and 1.90 and 1.40 for N_2O containing solutions. Both cases have been studied for solutions saturated with cyclopentane. It is found that within experimental error the total dimers build up linearly with dose (to a dose of 10^{19} eV/g) with the yield for the acidic solutions (1.23) being slightly lower than that (1.35) for the N_2O solutions. Subtraction of these values from one-half the expected total radical yields suggests that the disproportionation products have yields of 1.9 and 2.0, respectively, and that k_D/k_C for reaction between cyclopentyl radicals is ~1.5.

The above argument involves an estimate of the importance of disproportionation from the observed absolute yield of dimer and it is obviously much better to compare directly the disproportionation and combination products. It is, however, seen in Figure 8 that the rate of cyclopentene production decreases so rapidly with dose that it is difficult to determine accurately the initial yields of this product. Measurements in the region ~5 × 10^{17} eV/g give yields ~1.8 and 1.2 for the N_2O containing and pH 3 solutions but these values are already somewhat lower than the true initial yields. The cyclopentene content of the samples levels off for doses >5 × 10^{19} eV/g and it is obvious from this fact that the high reactivity of the cyclopentene toward the radicals produced from the water results in a situation where the rate of cyclopentene consumption by reactions 1 and 2 balances its rate of formation.

While reactions 1–8 must, in principle, be considered in addition to reactions 10 and 11 such a general treatment is difficult and it is convenient to proceed to the intermediate stage where one is principally interested in the removal of cyclopentene *via* reactions 1 and 2. Since H atoms are considerably more selective in their reactions with cyclopentene (k_1/k_9 ~ 60) than are OH radicals (k_2/k_{10} ~ 2) reaction 1 comes into play first and is of considerable importance even when cyclopentene is present at the ~1% level, *i.e.*, ~3 × 10^{-5} M. The considerably greater dose dependence for cyclopentene production at pH 3 than for the N_2O containing solutions is readily understood in terms of the relatively greater contribution from H atom reactions in the first instance. We will now attempt to describe the course of the cyclopentene radiolysis in terms of the parameters derived from the kinetic measurements and from the observations on the cyclopentene system.

One can first consider the region below 10^{18} eV/g where the concentration of product cyclopentene is less than 3 × 10^{-5} M and interference by reaction 2 is only of minor importance, *i.e.*, >90% of the OH reactions are with cyclopentane. At these doses the consumption of cyclopentane is <4% so that loss of starting material is not a serious complication. Since cyclopentyl radicals are for the most part re-formed in reaction 1, as a reasonable approximation we can take their yield to be constant and equal to

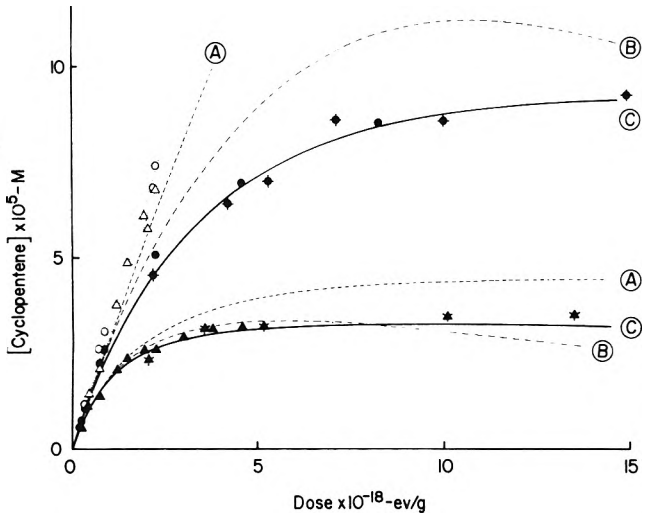

Figure 8. Production of cyclopentene in the radiolysis of cyclopentane solutions (▲,✱) at pH 3 and (●,◆) containing 0.02 M N_2O. Flagged points are at a dose rate of 9.8×10^{17} eV g^{-1} min^{-1}; others at a dose rate of 7.6×10^{16}. Curves A are calculated by integration of eq 12 which takes into account removal of cyclopentene only by the reaction of H atoms ($k_1/k_{10} = 60$). Curves B are calculated by integration of eq 13 and include both a decreased rate of production of cyclopentyl radical as the irradiation progresses and removal of cyclopentene by H and OH ($k_2/k_{11} = 2.3$). The solid curves C represent a similar calculation without the correction for the decreased rate of cyclopentyl production and with k_2/k_{11} taken as 5. The open points (○,△) represent correction of the data at the particular doses by factors relating the solid curves to the initial slope in the latter calculation. The linear dependences (dotted lines) represent initial yields of 1.75 and 1.95.

$G(H) + G(OH)$. The rate for production of cyclopentene then becomes

$$\frac{d(c\text{-}C_5H_8)}{dD} = \frac{10}{N}\left\{[G(H) + G(OH)]\frac{1}{2}\frac{k_D/k_C}{1 + k_D/k_C} - G(H)\frac{k_1[c\text{-}C_5H_8]}{k_1[c\text{-}C_5H_8] + k_9[c\text{-}C_5H_{10}]}\right\} \quad (12)$$

Integration of eq 12 with $k_D/k_C = 1.35$ and $k_1/k_9 = 60$ gives the dashed curves A of Figure 8 for the solutions at pH 3 ($G(H) = 3.5$; $G(OH) = 2.8$) and those containing N_2O ($G(H) = 0.6$; $G(OH) = 6.0$). With $k_D/k_C = 1.35$ one calculates that only 29% of the cyclopentyl radicals are converted to cyclopentene in reaction 3. Since H atoms represent 56% of the initial radicals at pH 3 the rate of cyclopentene production by cyclopentyl disproportionation is balanced by its consumption in reaction 1 when cyclopentene reaches a concentration of 3-4 $\times 10^{-5}$ M (where ~50% of the H atoms react with the cyclopentene). At such a concentration only ~3% of the OH radicals will react with the cyclopentene and contribute a yield of only ~0.1 to its consumption. At doses $<10^{18}$ eV/g we can use calculations based on eq 12 to correct the observations for the loss of cyclopentene *via* reaction 1 to get a better estimate of the initial production rate. Correction of the data by factors obtained from a trial integration of eq 12 shows a linear dependence with a slope corresponding to an initial yield of 1.7. The corrections are, however, appreciable (~60% at 10^{18} eV/g) and a substantial error is possible. For N_2O containing solutions the H atoms are only 9% of the total so that this simplified model predicts that cyclopentene should continue to be produced even when all of the H atoms react with the cyclopentene. Below 10^{18} eV/g the correction factors are small (<15%) and reasonable well known for the N_2O containing solutions. The data appropriately corrected gives an initial slope corresponding to a yield of 1.9. These values indicate a disproportionation to combination ratio of ~1.4.

Considerations on the N_2O containing solutions at higher doses are somewhat more problematical since the reaction of OH with the cyclopentene both reduces the yield of cyclopentyl radicals and also changes the nature of the terminating radical-radical reactions. The H atoms will mainly add to cyclopentene and continue to give cyclopentyl radicals but OH abstraction from the dimer product becomes important and results in a decrease in the cyclopentyl yield. A reasonable (but still approximate) description of the rate for cyclopentene production is

$$\frac{d(c\text{-}C_5H_8)}{dD} = \frac{10}{N}\left\{\left[G(H) + G(OH) \times \frac{[c\text{-}C_5H_{10}]/[c\text{-}C_5H_{10}]_0}{1 + (k_2[c\text{-}C_5H_8]/k_{11}[c\text{-}C_5H_{10}]_0)}\right]\frac{1}{2}\frac{k_D/k_C}{1 + k_D/k_C} - G(H)\frac{k_1[c\text{-}C_5H_8]/k_{10}[c\text{-}C_5H_{10}]_0}{1 + (k_1[c\text{-}C_5H_8]/k_{10}[c\text{-}C_5H_{10}]_0)} - G(OH)\frac{k_2[c\text{-}C_5H_8]/k_{11}[c\text{-}C_5H_{10}]_0}{1 + (k_2[c\text{-}C_5H_8]/k_{11}[c\text{-}C_5H_{10}]_0)}\right\} \quad (13)$$

The initial cyclopentane concentration, $[c\text{-}C_5H_{10}]_0$, is taken as representative of the total saturated hydrocarbon since cyclopentene represents less than 4% of the total. The factor multiplying $G(OH)$ in the first term of eq 13 has been introduced to take into account the decreased importance of OH abstraction from cyclopentane as the irradiation progresses. The last two terms represent the loss of cyclopentene by secondary reactions of H and OH. Integration of eq 13 with k_D/k_C taken as 1.4, k_1/k_{10} as 60 and k_2/k_{11} as 2.3 gives the curves labeled B in Figure 8 ($[c\text{-}C_5H_{10}]$ was evaluated as $[c\text{-}C_5H_{10}] - [c\text{-}C_5H_8] - (G(H) + G(OH))/(1 + k_D/k_C)$). The correction for a decrease in the production of cyclopentyl radicals results in the negative slope at high doses. Since such is not, in fact, observed this correction appears to be somewhat overestimated. The solid curves in the figure are results of integrations of an expression similar to eq 13 but with k_2/k_{11} taken as 5 and without the term correcting for a decreased cyclopentyl production. It is seen that these calculations empirically fit the data extremely well and are used below to extrapolate the data to the initial slope.

For the acidic solutions the terms added to eq 12 serve to correct for the perturbing influence of the OH reactions with a very high degree of accuracy since the concentration of cyclopentene is maintained below 4×10^{-5} M where reaction 2 represents little of the OH chemistry (<3%). Trial integrations of eq 13 shows that the concentration level reached by the cyclopentene is insensitive to the choice of k_2/k_{10} but extremely sensitive to the choice of both k_D/k_C and k_1/k_9, *i.e.*, an increased rate of production by the disproportionation reactions will be compensated for if the relative rate of reaction 1 is, in fact, higher. Given that k_1/k_9 is close to 60 then k_D/k_C must, in fact, be close to the value of 1.4 used in calculating the curves of Figure 1 (and vice versa). Equation 13 also describes the cyclopentene production from N_2O containing solutions up to doses $\sim 3 \times 10^{18}$ eV/g but breaks down somewhat at higher doses since the additional complications resulting from the introduction of other secondary processes become important. In particular in the region of 5×10^{18} eV/g cyclopentene is produced with a net yield

somewhat lower than can readily be accounted for if k_2/k_{11} is as low as 2.3. The *a priori* calculations also predict that in the N_2O containing solutions the cyclopentene should reach a level $\sim 1.1 \times 10^{-4}$ M (at a dose $\sim 10^{19}$ eV/g) whereas the actual plateau is ~25% lower. The differences are, however, small and correspond to a cyclopentene yield which is low by about 0.1 in the region of 10^{19} eV/g where ~25% of the cyclopentene has been consumed. It is seen in Figure 8 that the agreement is excellent if k_2/k_{11} can be taken as large as 5 but it is difficult to see how k_2 can be much greater or k_{11} much smaller than the absolute values given above. It seems likely, therefore, that some minor secondary processes are removing 5–10% more cyclopentene than accounted for by the above mechanism.

Trial integrations of eq 13 can be used to obtain the factors by which the observed cyclopentene yields should be multiplied to correct them to the initial values. Data up to 3×10^{18} eV/g, so corrected, are illustrated in Figure 8 and give initial yields of 1.75 and 1.95 for the acidic and N_2O containing solutions, respectively. The ratios of these yields to those of the dimer (1.23 and 1.36) give values for k_D/k_C of 1.42 and 1.43. (Correcting the N_2O results according to curve B gives an initial yield of 1.85 and k_D/k_C of 1.36.) The disproportionation to combination ratio for the reaction between two cyclopentyl radicals, as determined from these studies on cyclopentane solutions, is, therefore, 1.4 and is regarded as having a very high level of reliability (better than 10%) since it in effect depends only on the measurement of the relative activities in the cyclopentyl–cyclopentane and cyclopentene fractions as extrapolated to zero dose and is not subject to the absolute calibrations implicit in the interpretation of other studies. The total radical yields should be twice the sum of the initial yields of cyclopentene and dimer and are respectively 6.0 and 6.6 for the acidic and N_2O saturated solutions (compared with the expected yields of 6.3 and 6.6) so that the material balance is, in fact, seen to be excellent.

Acknowledgments. The authors wish to thank Professor R. W. Fessenden for his assistance with the esr experiments and Dr. L. K. Patterson and Mr. C. G. Hobaugh for their assistance in the pulse radiolysis studies.

Supplementary Material Available. Table II, Figures 1, 5, 6, and 7, and also a more complete discussion of the esr spectra observed during this study will appear following these pages in the microfilm edition of this volume of the journal. Photocopies of the supplementary material from this paper only or microfiche (105 × 148 mm, 24× reduction, negatives) containing all of the supplementary material for the papers in this issue may be obtained from the Journals Department, American Chemical Society, 1155 16th St., N.W., Washington, D. C. 20036. Remit check or money order for $3.00 for photocopy of $2.00 for microfiche, referring to code number JPC-74-1052.

References and Notes

(1) Supported in part by the U. S. Atomic Energy Commission.
(2) From the dissertation of T. Soylemez submitted to Carnegie-Mellon University in partial fulfillment of the requirements for the degree of Doctor of Philosophy, Oct 1972.
(3) G. C. Stevens, R. M. Clarke, and E. J. Hart, *J. Phys. Chem.*, **76**, 3863 (1972).
(4) J. M. Warman and S. J. Rzad, *J. Chem. Phys.*, **52**, 485 (1970).
(5) K. Eiben and R. W. Fessenden, *J. Phys. Chem.*, **75**, 1186 (1971).
(6) L. K. Patterson and J. Lilie, *Int. J. Radiat. Phys. Chem.*, in press.
(7) P. Neta, G. R. Holdren, and R. H. Schuler, *J. Phys. Chem.*, **75**, 449 (1971).
(8) P. Neta and L. M. Dorfman, *J. Phys. Chem.*, **73**, 413 (1969).
(9) G. E. Adams, J. W. Boag, and B. D. Michael, *Trans. Faraday Soc.*, **61**, 1417 (1965).
(10) P. Neta and L. M. Dorfman, *Advan. Chem. Ser.*, **No. 81**, 222 (1968).
(11) J. H. Baxendale, P. L. T. Bevan, and D. A. Stott, *Trans. Faraday Soc.*, **64**, 2389 (1968).
(12) C. McAuliffe, *J. Phys. Chem.*, **70**, 1267 (1966).
(13) Sources of other data include (a) "Solubilities of Inorganic and Organic Compounds," A. Stephen and T. Stephen, Ed., Vol. 1, Part 1, Pergamon Press, New York, N. Y., 1963, p 726; (b) R. Durand, *C. R. Acad. Sci.*, **226**, 409 (1948); (c) H. D. Nelson and C. L. Deligny, *Recl. Trav. Chim. Pays-Bas*, **87**, 528 (1968).
(14) P. Neta, R. W. Fessenden, and R. H. Schuler, *J. Phys. Chem.*, **75**, 1654 (1971).
(15) M. C. Sauer and I. Mani, *J. Phys. Chem.*, **72**, 3856 (1968).
(16) P. Neta, *Chem. Rev.*, **72**, 533 (1972).
(17) M. Anbar and P. Neta, *Int. J. Appl. Radiat. Isotopes*, **18**, 493 (1967).
(18) R. A. Witter and P. Neta, *J. Org. Chem.*, **38**, 484 (1973).
(19) (a) M. Anbar, D. Meyerstein, and P. Neta, *J. Chem. Soc. B*, 742 (1966); (b) L. M. Dorfman and G. E. Adams, *Nat. Stand. Ref. Data Ser., Nat. Bur. Stand.*, **No. 46** (1973).
(20) R. W. Fessenden and R. H. Schuler, *J. Phys. Chem.*, **39**, 2147 (1963).
(21) R. W. Fessenden, *J. Chem. Phys.*, **58**, 2489 (1973).
(22) R. W. Fessenden and S. Ogawa, *J. Amer. Chem. Soc.*, **86**, 3591 (1964).
(23) I. A. Zlochower, W. R. Miller, Jr., and G. K. Frankel, *J. Chem. Phys.*, **42**, 3339 (1965).
(24) H. Fischer, *J. Phys. Chem.*, **73**, 3834 (1969).
(25) P. Neta, M. Z. Hoffman, and M. Simic, *J. Phys. Chem.*, **76**, 847 (1972).
(26) R. H. Schuler and R. W. Fessenden, "Radiation Research," G. Silini, Ed., North Holland Publishing Co., Amsterdam, 1967, p 99.
(27) R. W. Fessenden and S. Ogawa, unpublished results.
(28) P. J. Krusic and J. K. Kochi, *J. Amer. Chem. Soc.*, **90**, 7157 (1968).
(28) (a) Note Added in Proof. More recent measurements (R. H. Schuler and L. K. Patterson, to be submitted for publication) indicates that the extinction coefficients of cyclopentyl radical are 30% lower than reported in Figure 3.
(29) From the empirical expression given by T. I. Balkas, J. H. Fendler, and R. H. Schuler (*J. Phys. Chem.*, **74**, 4497 (1970)) the yield for scavenging of e_{aq}^- by 10^{-3} M H^+ is 2.9 and by 2×10^{-2} M N_2O is 3.2. Together with the H and OH yields produced directly from the water (0.6 and 2.8, respectively; M. Anbar in "Fundamental Processes in Radiation Chemistry," P. Ausloos, Ed., Interscience, New York, N. Y., 1968, p 651) the H and OH yields should be 3.5 and 2.8 at pH 3 and 0.6 and 6.0 for solutions 0.02 M in N_2O.
(30) A rate constant of 10^3 M^{-1} sec^{-1} has, for example, been reported for the addition of CH_3 to ethylene (K. M. Bansal and S. J. Rzad, *J. Phys. Chem.*, **76**, 2381 (1972).
(31) A rate constant of 20 M^{-1} sec^{-1} has been reported for the abstraction of H from 2,2,4-trimethylpentane by CH_3 (R. H. Schuler and R. R. Kuntz, *J. Phys. Chem.*, **67**, 1004 (1963).
(32) W. A. Cramer, *J. Phys. Chem.*, **71**, 1171 (1967). Values of 1.0–1.5 have been suggested by a number of other investigators but Cramer's determination seems to be the most free of possible complications.
(33) R. A. Holroyd and G. W. Klein, *J. Phys. Chem.*, **67**, 2273 (1963). A relationship between product entropies and disproportionation–combination ratios was first pointed out by J. N. Bradley, *J. Chem. Phys.*, **35**, 748 (1961).
(34) "Selected Values of Properties of Hydrocarbons and Related Compounds," American Petroleum Institute Project 44, Texas A & M University, College Station, Tex.
(35) M. H. Studier and E. J. Hart, *J. Amer. Chem. Soc.*, **91**, 4068 (1969).
(36) B. D. Michael and E. J. Hart, *J. Phys. Chem.*, **74**, 2878 (1970).

Radiation Chemical Studies on Systems Related to Ascorbic Acid. The Radiolysis of Aqueous Solutions of α-Bromotetronic Acid[1]

Mary A. Schuler, Kishan Bhatia, and Robert H. Schuler*

Radiation Research Laboratories, Center for Special Studies and Department of Chemistry, Mellon Institute of Science, Carnegie-Mellon University, Pittsburgh, Pennsylvania 15213 *(Received October 29, 1973)*

Publication costs assisted by the U. S. Atomic Energy Commission and Carnegie-Mellon University

The radiolysis of aqueous solutions of α-bromotetronic acid has been examined in order to provide background information on the radiation chemical reactions of ascorbic acid. It has been shown that in the presence of an H atom donor its reaction with hydrated electrons results very nearly in the quantitative reduction to bromide ion and tetronic acid. Optical pulse radiolysis studies indicate, however, that the radical produced as a result of the attack by hydrated electrons do not abstract hydrogen rapidly. These optical studies suggest that the radical anions expected to result from bromide elimination protonate very rapidly. Conductometric pulse radiolysis experiments confirm that the radicals present at microsecond times are neutral and show that ionic products are produced only at very much longer times following the disproportionation of these radicals. These studies make it evident that radical oxyanions having the structure $-C(O^-)=\dot{C}-$ can protonate very rapidly at the radical site. Oxidation of α-bromotetronic acid by OH produces bromide ion in 28% yield, presumably as a results of addition at the bromine position followed by loss of HBr. The majority of the OH radicals, however, appear to react either by addition to the 3 position or *via* electron transfer and do not yield bromide. Esr and optical pulse radiolysis studies show that the organic radical produced by oxidative debromination is a tricarbonyl radical anion identical with that present in the radiolysis of α-hydroxytetronic acid and very similar to the intermediate present in the oxidation of ascorbic acid. Both optical and conductometric pulse radiolysis studies confirm a yield ~30% for the dehydrobromination process and also show that the loss of HBr occurs rapidly (<1 μsec) and that the resultant radicals, which are relatively unreactive when present by themselves, disproportionate rapidly with other radicals produced in this system ($k \sim 10^9\ M^{-1}\ \text{sec}^{-1}$). The present study shows that with α-bromotetronic acid addition of OH to the double bond is at least as important as electron transfer and indicates that addition is involved to an important extent in the oxidation of α-hydroxytetronic and ascorbic acids by OH radicals.

Introduction

Esr studies of the radicals produced by OH attack on α-bromotetronic acid

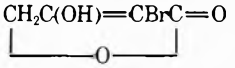

(referred to subsequently as bromotetronic acid or BrTr) have shown that radical I is the principal radical present

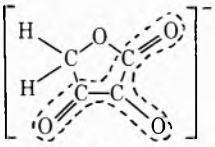

I

at millisecond times.[2] This radical is identical with that produced by oxidation of α-hydroxytetronic acid

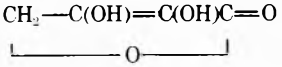

(hydroxytetronic acid or HOTr) with OH radicals and is directly related to the intermediate involved in the oxidation of ascorbic acid in various chemical and biochemical processes.[2] Presumably this radical is produced by attack of OH at the 2 position of bromotetronic acid (which exists as the anion at pH 7) followed by loss of HBr.

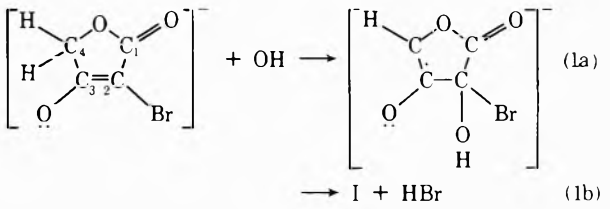

(1a)

(1b)

In these previous studies the esr spectrum of radical I observed during *in situ* radiolysis was only about one tenth as intense as that observed for hydroxytetronic acid under identical irradiation conditions.[2] This observation implies either that this radical is produced very inefficiently (as would be expected if electron transfer to OH is the main source of radical I in the hydroxytetronic acid system) or that it is rapidly removed by reaction with other radicals produced in the radiolysis. The studies of the radiation chemistry of aqueous solution of bromotetronic acid by product analysis and by pulse radiolysis methods which are reported here were carried out in order to investigate the cause of the low intensity of the spectrum of radical I in the esr experiments and to provide background information related to the radiation chemical reactions of ascorbic acid.

Experimental Section

Materials. The initial experiments were carried out on a sample of bromotetronic acid obtained from the Alfred

Bader Chemical Co. This material was chocolate brown in color and contained a significant amount of bromide impurity. The sample was decolorized and the bromide removed by charcoal treatment in ethyl acetate solution followed by recrystallization from ethyl acetate. The resultant sample, used in the initial experiments, showed no detectable bromide (<0.1%) but contained about 1% tetronic acid impurity which made it unsuitable for the liquid chromatographic studies. Subsequently a sample of bromotetronic acid was synthesized according to the method of Kumler.[3] The recrystallized product (white needles) melted with decomposition at 179.0–179.5° (lit. mp 183°) and was shown by liquid chromatographic analysis to contain 0.08% tetronic acid. Titration with NaOH gave nominal equivalent weight of 181.0 (equiv wt BrTr = 179.0) which corresponds to a bromotetronic acid content of 98.9%. A sample of tetronic acid for calibration of the liquid chromatographic system and other ancillary studies was prepared from the bromotetronic acid by reduction with sodium amalgam.[3,4] Liquid chromatographic analysis showed that this material initially obtained contained 7 mol % bromotetronic acid. The tetronic acid was extracted from aqueous solution at pH 2.7 with ethyl acetate and recrystallized from ether. The resultant sample, which melted at 135.5–136.0° (lit. mp 141°), contained 0.3% bromotetronic acid and had a titer corresponding to nominal equivalent weight of 100.8 (equiv wt HTr = 100.0). The latter corresponds to a purity level of 99.2 wt % though the melting point indicates that impurities are present to the extent of several mole per cent. Hydroxytetronic acid was kindly furnished by Y. Kirino who synthesized it by the method of Micheel and Jung.[5] Ascorbic acid was obtained from Calbiochem. Water was distilled in an all glass apparatus and for the more critical experiments was quadruply distilled including stages of basic permanganate and acid dichromate. The electron lifetime in the latter was 30–60 μsec. In most cases samples were buffered to pH 7 with 10^{-3} *M* phosphate (2×10^{-3} *M* KH_2PO_4 neutralized with KOH). Studies in basic solution were at pH 10.7–11.3 (0.5–2 m*M* KOH). Solutions of both the bromotetronic and tetronic acids were very stable, *i.e.*, little change in 10^{-4} *M* solutions was observed over periods of weeks. Hydroxytetronic and ascorbic acids in solution, however, disappeared very rapidly, particularly at low concentrations where the amount of dissolved oxygen was sufficient to react with the starting material. Solutions of the latter purged of oxygen were more stable but it was, in general, difficult to work at concentrations less than 10^{-4} *M*.

Steady-State Irradiations. Where it was desired to examine the reaction of e_{aq}^-, the samples containing 0.01–0.5 *M* *tert*-butyl alcohol were purged of oxygen by bubbling with high purity nitrogen. The reactions of OH were studied with samples saturated with N_2O which both replaced the oxygen and served to convert e_{aq}^- to OH. Product analyses were carried out on samples irradiated with ^{60}Co γ-rays at dose rates of 5.5×10^{16} or 8.2×10^{17} eV g^{-1} min^{-1}. Dosimetry was carried out with the Fricke (ferrous sulfate) system. Where tetronic acid was measured, doses ranged upward from 5.5×10^{15} eV/g (87 rads). The bromide measurements were made in the range $4\text{–}160 \times 10^{17}$ eV/g (6000–250,000 rads).

Bromide Analysis. An Orion 94-35A (bromide) ion selective electrode was used for the bromide measurements in much the same way as previously described in the work with bromouracil.[6] Bromotetronic acid does not hydrolyze measurably so that there was no problem from background production of Br^-. It was, however, necessary to make a small correction for Br^- in the starting material.

Liquid Chromatographic Analysis. The liquid chromatographic apparatus used was that described by Bhatia[7] as modified to operate up to 6000 psi.[8] The columns used to separate the tetronic acids (2.1 mm i.d. × 1 m) were packed with Reeve Angel Pellionex AS or Dupont No. 820505 strong anion exchange material. Water buffered with 0.01 *M* $Na_2B_4O_7$ (pH 9) was used as the eluent. Columns were operated isothermally at 40° and a flow rate of 0.6 ml/min with samples being injected through a loop of 0.189 ml volume. The column effluent was monitored spectrophotometrically at 254 nm (Laboratory Data Control Model 1285 uv monitor). Certain of the chromatographic peaks were collected and their absorption spectra examined with a Cary 14 spectrophotometer.

Pulse Radiolysis Experiments. Optical pulse radiolysis experiments were carried out with the computerized system described by Patterson and Lilie.[9] The signal averaging capabilities of this system were used to particular advantage in the studies within the absorption band of bromotetronic acid where the level of light transmitted by the sample was very low. Van de Graaff electrons (2.8 MeV, ~10 mA, 0.5–2 μsec) were used. Radical concentrations and extinction coefficients were determined by reference to thiocyanate dosimetry with $\epsilon_{490}[(SCN)_2^-]$ taken as 7600 M^{-1} cm^{-1}.[10] Doses were in the range 10^{16}–10^{17} eV/g (200–2000 rads) so that initial radical concentrations were from 1 to 10 μ*M*. A flow system was employed with the sample being replenished between pulses. Because of the large volume of solutions required and the limited supply of the materials being examined most studies were carried out at concentrations ~10^{-4} *M* or lower. In particular studies in the region where the starting materials absorb strongly were carried out at concentrations of ~2×10^{-5} *M* where upward of 15% of the incident light was transmitted by the 2-cm cell. In these cases doses were limited to 2×10^{16} eV/g so that the solute was depleted by <10%.

Conductivity experiments using the 10-MHz bridge described by Lilie and Fessenden[11] were carried out to examine for the production of ionic products. Equivalent conductances were determined by reference to a yield of 3.14 for the production of HCl (Λ = 425 mhos cm^2 $equiv^{-1}$) from saturated CH_3Cl solutes.[12]

Results and Discussion

Rate Constants for Reaction of e_{aq}^- and OH. The rate constants for reaction of e_{aq}^- with bromotetronic, tetronic, and ascorbic acids were measured in phosphate buffered (10^{-3} *M*) solutions by following the absorption of e_{aq}^- at 600 nm in pulse radiolysis experiments. The results, which refer to reaction of e_{aq}^- with the respective monoanions.[13] are summarized in Table I. Schöneshöfer[14] has previously reported a value of 4×10^8 M^{-1} sec^{-1} for the reaction of e_{aq}^- with ascorbate anion.

Experiments on a 32 μ*M* solution of bromotetronic acid at pH 10.7 showed that its loss by reaction with e_{aq}^- could also be followed at 270 nm where the product of the reaction appears to have very little absorption (see below). Measurements at this wavelength gave a reaction period ($t_{1/2}$) of 7.0 μsec which was essentially identical with that of 6.9 μsec for loss of e_{aq}^- (measured at 600 nm). The rate constant of 2.5×10^9 M^{-1} sec^{-1} (after correction for e_{aq}^-

TABLE I: Rate Constants for Reaction of e_{aq}^- and OH[a]

	$k(e_{aq}^-)$, M^{-1} sec^{-1}[a]	k(OH), M^{-1} sec^{-1}
α-Bromotetronic acid	4.4×10^{9}[b]	7.7×10^{9}[c]
Tetronic acid	$\sim 10^{8}$	9.2×10^{9}[d]
α-Hydroxytetronic acid	*e*	4.7×10^{9}
Ascorbic acid	3.0×10^{8}[f]	(7×10^{9})[f]

[a] Measurements were made at pH 7 in 10^{-3} *M* phosphate buffer. At this pH all of the solutes are present in their anionic form (see footnote 13). *tert*-Butyl alcohol (0.1 *M*) was used to remove the OH radicals and the dose per pulse adjusted to produce an initial e_{aq}^- concentration of 10^{-6} where the decay period in the absence of added solute was >30 μsec. The solute concentration was adjusted to give a pseudo-first-order period of 2–5 μsec and the second-order rate constant calculated from the corrected decay period and known solute concentration. At the ionic strength of these solutions (~0.03) the rates for reaction of e_{aq}^- are expected to be ~20% greater than in infinitely dilute solutions. [b] A 32 μ*M* solution at pH 10.5 showed a reaction period of 7.0 μsec from the loss of bromotetronic acid at 270 nm and 6.9 μsec from the loss of e_{aq}^- at 600 nm giving a rate constant of 2.5×10^{9} M^{-1} sec^{-1}. [c] Determined from the loss of BrTr at 258 and also from the production of radical I at 360. [d] Determined from the loss of HTr at 248. [e] Not measured. Assumed to be similar to that of ascorbic acid. [f] Schöneshöfer (ref 14) reports a value of 4×10^{8} M^{-1} sec^{-1} for e_{aq}^- + ascorbate anion and 7×10^{9} M^{-1} sec^{-1} for OH + ascorbate anion.

decay) is, however, somewhat lower than that from the determination at pH 7.

The rate constants for reaction of OH with BrTr and HOTr were measured by following the production of the intermediate radicals at 360 nm. In the case of BrTr the reaction was also followed at 258 nm where a net decrease in absorption occurs (see below). For a 21 μ*M* solution identical periods of 4.3 μsec were determined at the two wavelengths giving a rate constant of 7.7×10^{9} M^{-1} sec^{-1}. The results of the OH rate measurements are summarized in Table I.

Hydrogen atom rates were not measured in the present work but the rate constant for reaction with ascorbic acid has previously been shown to be relatively low (1.1×10^{8} M^{-1} sec^{-1}).[15] While reaction with bromotetronic acid is undoubtedly somewhat faster (perhaps 5×10^{8} M^{-1} sec^{-1}) H atoms should not contribute to any appreciable extent in the steady-state studies and not at all at the short times of most of the pulse experiments.

Reaction of e_{aq}^- with α-Bromotetronic Acid. Hydrated electrons are known to react with many organic halides to produce halide ions in what is believed to be a very rapid dissociative electron capture process. Thus in the case of bromotetronic acid one expects the reaction of e_{aq}^- to result in formation of the tetronic acid radical (radical II), *e.g.*

$$e_{aq}^- + \text{BrTr} \xrightarrow{k_2} \text{II} + Br^- \qquad (2)$$

In the somewhat similar cases of *p*-bromophenol and 5-bromouracil it has recently been shown that bromide elimination is quantitative and that the reaction of the resultant radical with alcohols follows simple scavenging kinetics.[16,17] The rate constants for abstraction of hydrogen from alcohols are quite high, presumably because the reacting entity is a σ radical. On the surface the present case appears to be similar but since reaction of e_{aq}^- is with a highly oxygenated anion one might expect complications. The pulse radiolysis studies described below show

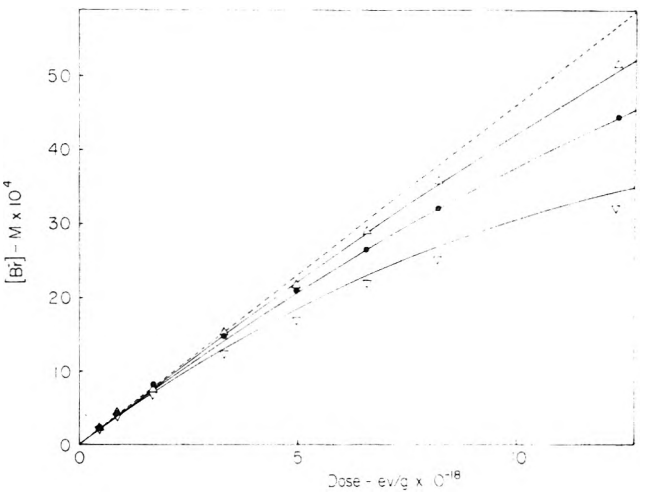

Figure 1. Br^- production resulting from the reaction of e_{aq}^- with bromotetronic acid at pH 7. Solutions were (▽) 0.59, (●) 1.2, and (△) 2.3 m*M* in BrTr and contained m*M* phosphate buffer, and 0.5 *M* *tert*-butyl alcohol to remove OH. The dashed line corresponds to a yield of 2.78 which is the expected initial yield for the 2.3 m*M* solution. The solid curves take into account the effect of product buildup by numerical integration of eq 6 as discussed in the text.

that, in fact, the overall reaction is more complex than simply formation of radical II followed by rapid abstraction from a hydrogen source to produce tetronic acid (HTr), *i.e.*

$$\text{II} + \text{RH} \longrightarrow \text{HTr} + \text{R}\cdot \qquad (3)$$

However, before discussing these pulse radiolysis studies we will present the results of the steady-state experiments.

a. Bromide Production. The production of bromide ion with dose is illustrated in Figure 1 for 0.59, 1.2, and 2.3 m*M* bromotetronic acid solutions containing 0.5 *M* *tert*-butyl alcohol to remove OH. In these experiments it is estimated that the reactions of OH should contribute a Br^- yield of <0.05. The radiation chemical yields measured at a dose ~5×10^{18} eV/g are in the range 2.0 to 2.6 Br^- per 100 eV but it is seen in the figure that at the lowest concentration the yield falls off appreciably with dose. Although there is little curvature at the higher concentrations it is obvious that products of the radiolysis are interfering with the bromide production so that the initial yields should be at least somewhat greater. The liquid chromatographic experiments described below show that in the presence of *tert*-butyl alcohol the principal organic product is tetronic acid. Since, as indicated in Table I, tetronic acid reacts only relatively slowly with e_{aq}^-

$$e_{aq}^- + \text{HTr} \xrightarrow{k_4} \text{products} \qquad (4)$$

i.e. $k_4/k_2 \sim 0.03$, the effect of this product is not expected to be significant at low conversions. The principal additional product which is expected to compete for e_{aq}^- is, of course, the peroxide formed as a molecular product. Although the yield of this product is low (0.7)[18] reaction with e_{aq}^-

$$e_{aq}^- + H_2O_2 \xrightarrow{k_5} OH + OH^- \qquad (5)$$

is important because $k_5/k_2 = 2.8$ ($k_5 = 1.23 \times 10^{10}\ M^{-1}$ sec^{-1}).[19] Taking into account the effects of buildup of tetronic acid and peroxide the differential equation describing the production of bromide becomes

$$\frac{d(Br^-)}{dD} = f_e \frac{G_e D}{10}\left[1\Big/\left(1 + \frac{k_4[HTr]}{k_2[BrTr]} + \frac{k_5[H_2O_2]}{k_2[BrTr]}\right)\right] \quad (6)$$

where G_e is the initial yield for reaction of electrons with the bromotetronic acid at the concentration of the particular experiment and f_e is the fraction of these reactions which gives bromide. If we approximate [BrTr] by $[BrTr]_0 - [Br^-]$, [HTr] by $[Br^-]$ and assume that the peroxide builds up linearly with a G of 0.7 then with f_e taken as 1 and the yields for electron scavenging by the bromotetronic acid as the values (2.67, 2.72, and 2.78) obtained for the particular concentrations from the empirical expression of Balkas, Fendler, and Schuler[12] integration of eq 6 gives the solid curves of Figure 1. Since all of the quantities in eq 6 except f_e are known, these curves constitute an *a priori* prediction of the bromide production on the assumption that f_e is unity. The agreement between the results and the calculated curves is, however, slightly illusory in that upon saturation of these solutions with N_2O a Br^- yield ~0.30 over and above that expected from the failure of the N_2O and alcohol to scavenge e_{aq}^- and OH remains. It seems likely that H atoms, which will not be scavenged by the alcohol at the concentration used, are the source of this additional yield.

One can approximate the initial yields by correcting the observed Br^- concentrations for the fall off resulting from reactions 4 and 5. Since eq 6 describes the course of the radiolysis reasonably well, appropriate correction factors for a particular dose and concentration can be determined by intercomparing the results of trial integrations of this equation with the corresponding initial slope ($f_e G_e D/10$). Data corrected in this manner show good linearity with the slopes corresponding to initial yields of 2.52, 2.72, and 2.83 for the 0.59, 1.2, and 2.3 mM solutions. If we correct for the background Br^- yield of 0.30 indicated above we obtain net yields of 2.22, 2.42, and 2.53 to be ascribed to the reaction of e_{aq}^-. The latter values are 90–95% of the value of 2.70 expected[12] for millimolar bromotetronic acid solutions. It is clear that at these concentrations reaction 2 produces bromide ion very nearly quantitatively.

b. Chromatographic Studies of the Products. Liquid chromatographic examination of irradiated bromotetronic acid solutions containing *tert*-butyl alcohol as an OH scavenger shows that tetronic acid is an extremely important product as has, of course, already been anticipated in writing eq 2 and 3. Illustrative chromatograms are presented in Figure 2. In the initial experiments it was shown that the peak which appears at 11 min had an absorption spectrum similar but not identical with that of either bromo- or hydroxytetronic acid. From the fact that the maximum (248 nm) was shifted to lower wavelengths it was speculated that this product was tetronic acid and subsequent comparison with an authentic sample provided a confirmation.

Appropriate spectroscopic data on the compounds of interest are given in Table II (available on microfilm, see paragraph at end of text regarding supplementary material). The extinction coefficients at 254 nm are sufficiently high (~15,000 M^{-1} cm^{-1}) that products are readily measurable at the 10^{-7} M level (as is illustrated in Figure 2a) and one experiment on 10^{-5} M bromotetronic showed that the tetronic acid impurity present at a concentration of

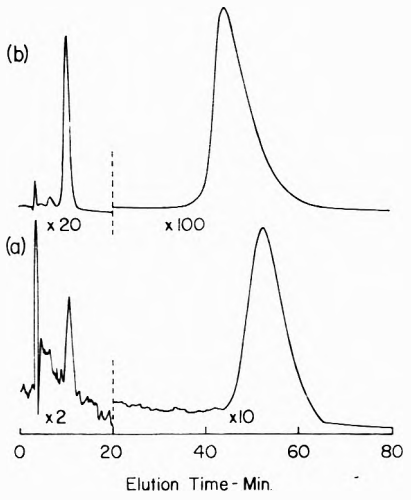

Figure 2. Liquid chromatograms of (a) a 10^{-5} M BrTr solution irradiated to a dose of 5.5×10^{15} eV/g and (b) a 10^{-4} M BrTr solution irradiated to a dose of 5.5×10^{16} eV/g. Solutions were buffered to pH 7, contained 0.02 M *tert*-butyl alcohol to remove OH, and were purged with N_2. The two major peaks correspond to product tetronic acid (recorded at attenuations of 2 and 20) and unreacted bromotetronic acid (recorded at attenuations of 10 and 100). The high sensitivity of the liquid chromatographic approach is illustrated in a where the tetronic acid produced is only 10^{-7} M.

10^{-k8} M was detectable with a signal-to-noise ratio ~2/1. These results substantiate the previous assertions[16] about the high sensitivity potentially available in appropriate liquid chromatographic experiments. The chromatograms of Figure 2 represent experiments carried out on (a) a 10^{-5} M solution irradiated to a dose of 5.5×10^{15} eV/g (87 rads) and (b) on a 10^{-4} M solution irradiated 10 times more.

The production of tetronic acid was determined by comparing its peak height with that of a reference sample and typical results are given in Figure 3. At the doses used here only a small fraction of the BrTr has reacted so that the effects of product buildup can be taken into account reasonably well by methods similar to those described above and the initial slopes determined accurately. At 10^{-3} M BrTr the yield for production of tetronic acid was found to be 2.85 in good agreement with the initial yield of bromide (2.72) although the tetronic acid measurements were made at very much lower doses (~10^{17} eV/g). A yield of 0.25 was observed from N_2O saturated solutions 2.4×10^{-4} M in BrTr both with and without *tert*-butyl alcohol. Since only 0.8% of the e_{aq}^- will escape being scavenged by the N_2O, this yield is attributed mostly to the reduction of radicals resulting from H atom addition. The net yield produced in reactions 2 and 3 is, therefore, 2.63 which is 97% of the yield expected for reaction of e_{aq}^- with the bromotetronic acid at millimolar concentrations.[12] It is clear that provided reaction with secondary products does not interfere (as is commented on below) attack on bromotetronic acid by e_{aq}^- in the presence of an appropriately high concentration of H atom donor results very nearly in its quantitative reduction to tetronic acid.

Data for 10^{-5}, 2.5×10^{-5}, and 10^{-4} M solutions containing 0.02 M *tert*-butyl alcohol are given in Figure 3. The initial yields are, respectively, 1.59, 2.22, and 2.36. Various experiments at 10^{-5} M with different samples of water gave yields which were only 40–60% of the expected 2.6 and showed that, in fact, the yields were dependent on

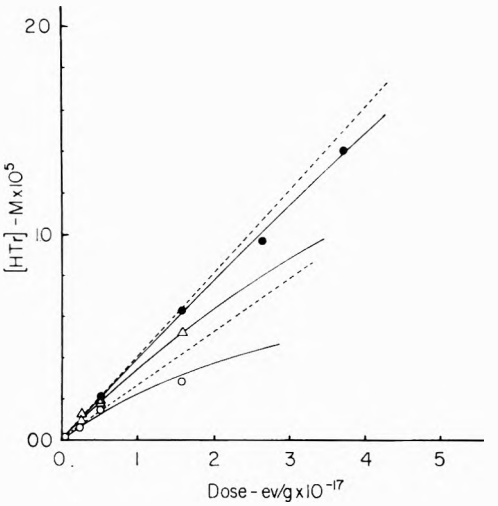

Figure 3. Production of tetronic acid from N_2 purged solutions (○) 1.0×10^{-5} *M*, (△) 2.5×10^{-5} *M*, and (●) 1.0×10^{-4} *M* in bromotetronic acid and 0.02 *M* in *tert*-butyl alcohol (pH 7). The solid curves represent the results of numerical integrations for $d[HTr]/dt$ taken equal to $d[Br^-]/dt$ of eq 6 with $f_e = 0.60$, 0.85, and 0.90. The latter correspond to yields of 1.59, 2.22, and 2.36. The initial slopes at the highest and lowest concentrations are given by the dashed lines in the figure in order to indicate the magnitude of the effect of product buildup. Note the point just above the origin (representing the measurement of Figure 2a) where the yield (1.3) is in very reasonable agreement with the measurements at tenfold higher doses.

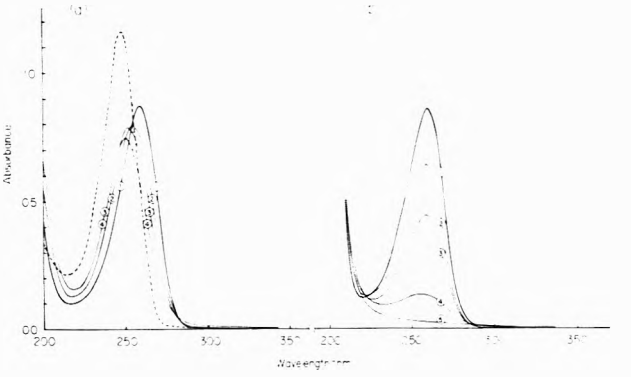

Figure 4. Spectra of irradiated 5×10^{-5} *M* solutions of bromotetronic acid. (a) Solutions purged with N_2 and containing 0.02 *M* *tert*-butyl alcohol at doses of (1) 0, (2) 5.5, (3) 11, and (4) 22×10^{17} eV/g. The dashed curve is the spectrum of tetronic acid normalized to the same concentration. The extinction coefficients are equal to 255 nm (the vertical dashed line) so that an isosbestic point should exist at this wavelength if there is quantitative conversion of BrTr to HTr. Comparison of curves 1 and 3 shows that there is a 6% loss in the absorbance at 255 nm which corresponds to a yield of 0.15 for the net loss of BrTr + HTr at a dose of 11×10^{17} eV/g. (b) Solutions saturated with N_2O at doses of (1) 0, (2) 2.8, (3) 5.5, (4) 12, and (5) 22×10^{17} eV/g. At the lowest dose the loss of absorption corresponds to $G(-BrTr)$ of only 3.0 which by comparison with Figure 12 implies that a product is present which absorbs in the region of 260 nm.

the concentration of *tert*-butyl alcohol used (decreasing with increase in *tert*-butyl alcohol from 0.1 to 0.5 *M*). It is apparent that at this low a concentration of BrTr impurities introduced with the alcohol (very probably ketones) interfere with reaction 2. At 10^{-5} *M* BrTr the period for reaction 2 is 20 μsec which is the magnitude of the electron lifetime observed in pulse experiments. Apparently reactive impurities such as H_2O_2, residual O_2, or other impurities are present at the few micromolar level. In the buffered solutions reaction of e_{aq}^- with $H_2PO_4^-$ will even be important (for 10^{-5} *M* BrTr 10^{-3} *M* $H_2PO_4^-$ is expected to scavenge ~20% of e_{aq}^-). One set of experiments at 10^{-5} *M* BrTr using samples outgassed by the pumping procedure described by Johnson and Allen[20] showed even lower yields. The fact that the yield appears to be low by ~40% at 10^{-5} *M* indicates that the yields will be low by ~20 and 6% at 2.5×10^{-5} and 10^{-4} *M*, respectively. The estimate of 6% at 10^{-4} *M* cannot be far in error and gives a corrected value of 2.51 or ~5% less than expected. Effects of impurities at 10^{-3} *M* should be less than 1%. While sufficient analytical sensitivity is available to carry out experiments readily at solute concentrations even as low as 10^{-6} *M*, spurious reactions, particularly those of e_{aq}^-, mask any fundamental significance of the results obtained. The present studies emphasize the great difficulties involved in attempts to examine quantitatively the reactions of e_{aq}^- with solutes at concentrations below 10^{-4} *M*.

Experiments on N_2O saturated solutions in the absence of alcohol showed, as expected, that OH radicals are not a source of tetronic acid. One can, therefore, examine for the production of this product in the absence of any intentionally added H atom source. Irradiation of a 10^{-4} *M* BrTr solution gave a yield of 1.7. This yield is surprisingly high and gives a hint that protonation of the radical anion (either before or after Br^- elimination) may be important.

c. Spectroscopic Studies of the Reactions. The change in the absorption spectrum of a 50 μ*M* solution of BrTr containing 1 m*M* isopropyl alcohol irradiated to doses of 5.5, 11, and 22×10^{17} eV/g is illustrated in Figure 4a. Superimposed on this figure is the spectrum of tetronic acid at the same concentration. The importance of the conversion of BrTr to HTr is qualitatively evident but at the highest dose complications are obvious from the relatively high absorption in the regions of 200–210 and 270–300 nm. The extinction coefficients of these two compounds are equal at 255 nm so that if conversion were quantitative one should observe an isosbestic point at this wavelength. It is seen, however, that at the higher doses there is a significant decrease in absorption at 255 nm which shows that products other than tetronic acid are formed. At 1.1×10^{18} eV/g the loss of absorbance at 255 nm (curve 3 in Figure 4a) corresponds to a net yield of ~6% of the total reaction expected. The rate of loss increases with dose so that it seems likely that secondary reactions are at least partially responsible. One can also see from Figure 4a that the BrTr concentration can be followed spectrophotometrically at 270 nm with little interference from the absorption of HTr although complications from other products are apparent at the higher doses.

d. Pulse Radiolysis Studies of the Intermediates. Pulse radiolysis studies were undertaken on the assumption that reactions 2 and 3 were mainly responsible for the production of tetronic acid. Extensive investigations, however, failed to confirm such a simple explanation. The pertinent details are briefly summarized in Figures 5a and 6. In the particular set of experiments reported in these figures 0.01 *M* *tert*-butyl alcohol was added to a 3×10^{-5} *M* BrTr solution to remove the OH radicals but approximately 5% of the OH still reacts with the BrTr. In the region of 270 nm the transmission increases with a period of 4.4 μsec which, as mentioned above, corresponds to the decay of e_{aq}^- and the magnitude of the change shows that the bromotetronic acid is essentially quantitatively consumed. However, as is seen in Figure 5a, the increase in transmission below

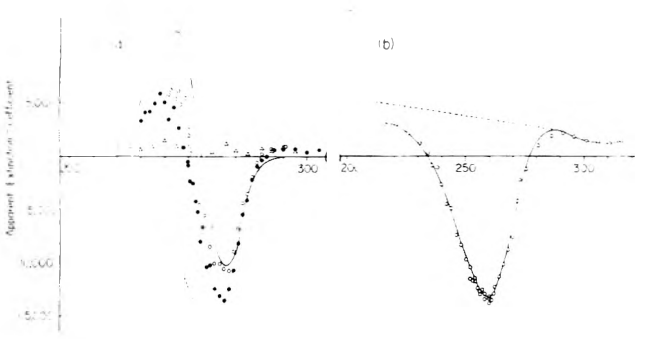

Figure 5. a The differential spectrum resulting from the reaction of e_{aq}^- with BrTr as observed at 150 μsec in the pulse radiolysis of a 30 μM solution at pH 7 (10^{-3} M phosphate; N_2 purged). The dose in these experiments was $\sim 2 \times 10^{16}$ eV/g per pulse and produced 10^{-6} M e_{aq}^-. Solid circles are for a solution containing 0.01 M *tert*-butyl alcohol to remove the OH radicals ($\sim$5% of the OH still reacts with the BrTr and contributes about -1000 units in the region of 260 nm) H atoms are not effectively scavenged by this concentration of *tert*-butyl alcohol and may contribute several thousand units to the decrease provided the rate constant for their reaction is $>10^9$ M^{-1} sec^{-1}. Open circles are for a solution to which 0.1 M methyl alcohol was also added where H atom and OH radicals will be completely scavenged. Triangles are for a solution 0.4 M in methyl alcohol saturated with N_2O. The ordinate scale is based on a yield of 2.6 for reaction of e_{aq}^- with the BrTr. The dashed curve represents the negative of the absorption spectrum of BrTr and the solid curve the difference between the spectrum of HTr and of BrTr. (b) The differential spectrum resulting from the reaction of OH with BrTr as observed at 10 μsec (24 μM BrTr, pH 10.5 N_2O saturated, dose $\sim$1 eV/g per pulse). In this case the ordinate scale is based on a yield of 6.0 for reaction of OH with the BrTr. The product has a significant absorption in the regions of 230 and 280 nm and is assumed to increase monatonically toward lower wavelength in the intermediate region (dashed curve). The solid curve represents the superposition of the BrTr spectrum on this background.

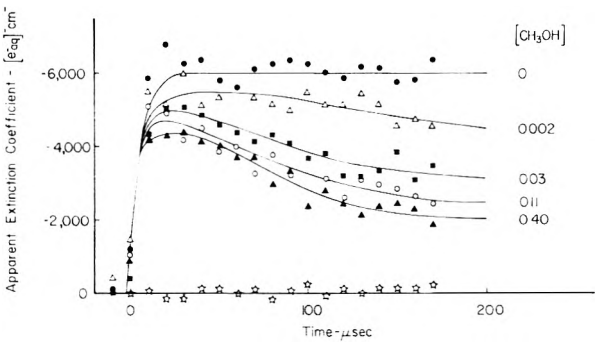

Figure 6. Effect of adding methyl alcohol to solutions containing 30 μM BrTr and 0.01 M *tert*-butyl alcohol as observed at 255 nm (pH 7; N_2 purged). The extinction coefficients of bromotetronic and tetronic acids are equal at this wavelength so that if reactions 2 and 3 are quantitative one expects to see a recovery to the base line with the period being that of reaction 3. The fact that the recovery period does not decrease as expected upon increase in the methyl alcohol at the molar concentrations given in the figure indicates that the relatively small effects observed cannot be attributed to simple radical scavenging by the methyl alcohol. In these experiments the dose was limited to produce an initial radical concentration of only 10^{-6} M. Because of the low wavelength and high absorption of the sample the transmitted light level was low ($\sim$1% of that available at 400 μM) and the incremental signal of the same magnitude as the noise level in the photomultiplier output. It was possible, however, to employ signal averaging methods to give very reasonable data. The data of this figure represent averaging over 25 experiments where each point represents the experimentally measured difference between the light level following a pulse and that in a blank experiment. The points along the abscissa (☆) are for a dummy experiment and illustrate the uncertainty involved in such a subtraction.

260 nm is considerably less than expected from the loss of BrTr so that the species produced by e_{aq}^- attack on the BrTr must absorb intensely in this region. After completion of the scavenging of e_{aq}^- at about 30 μsec the absorbance was constant out to more than 200 μsec. Below 250 nm there is a net absorption by the product. The difference between the differential spectrum and that of bromotetronic acid is very similar to that of tetronic acid but only about 75% as intense. The spectrum observed does not change appreciably upon addition of more *tert*-butyl alcohol (up to 0.1 M), methyl alcohol (up to 0.4 M), or isopropyl alcohol (up to 0.01 M). Since it is not likely that the rate constant for H atom abstraction from *tert*-butyl alcohol by radical II is greater than 10^7 M^{-1} sec^{-1} reaction 3 should not be complete in the experiments at 10^{-2} M at the times of observation, *i.e.*, $\sim$330 μsec. As is seen in Figure 6 addition of methyl alcohol does cause a small increase in absorption on the 100-μsec time scale but the period involved does not continue to decrease as more alcohol is added as is required if scavenging of an intermediate is involved. The results with *tert*-butyl and isopropyl alcohols were similar. In none of these experiments did the net absorption in the region of 245 nm exceed the level indicated for the methanol containing solutions in Figure 5a so that the degree of conversion is not dependent on the alcohol concentration. One concludes that the absorbing species is not product tetronic acid but rather an intermediate that reacts with methanol with a rate constant $<10^5$ M^{-1} sec^{-1}. Radical II is structurally similar to uracilyl and expected to abstract hydrogen from the alcohols quite rapidly.[17] We note at this point that radical II is an anion and suggest rather than the species being observed is its protonated form, radical III, *i.e.*

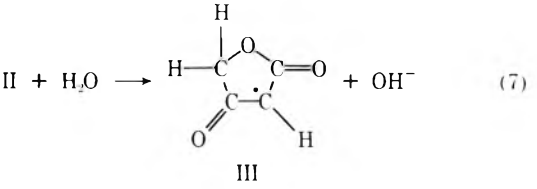

III

Because of the short time scale, at a pH of 7 or greater protonation must involve reaction of radical II directly with water. Radical III is a π radical and should abstract hydrogen relatively slowly.

e. Conductometric Studies. Pulse conductivity studies provide a ready test of the above suggestion since radical III is neutral and reaction 7 replenishes the OH^- consumed by the hydrogen ions initially produced. Conductometric pulse radiolysis studies on a 1.5×10^{-4} M solution containing 0.02 M *tert*-butyl alcohol at pH 10.5 showed traces such as are illustrated in Figure 7a and 7b. The change of conductance expected from reaction 2 is $\Lambda(Br^-) - \Lambda(OH^-) + \Lambda(II) - \Lambda(BrTr^-) \sim -115$ mhos cm^2 equiv^{-1} whereas the net effect of reactions 2 and 7 is $\Lambda(Br^-) - \Lambda(BrTr^-) \sim 0$. Since the equivalent conductance of Br^- is very likely greater than that of bromotetronic acid anion, the latter quantity should, in fact, be somewhat positive. Initially one sees a slight increase in conductance which based on a $G(e_{aq}^-) = 2.6$ corresponds to a change in equivalent conductance of +28 mhos cm^2 equiv^{-1} and it is obvious that protonation occurred.

Over the longer term we see a decrease in conductance which clearly follows second-order kinetics (the initial period is inversely proportional to dose) and is presumably mainly the result of disproportionation of radical III. In

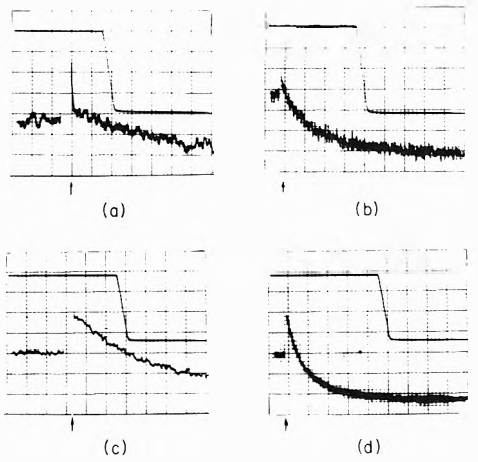

Figure 7. Conductometric pulse radiolysis traces for (a and b) 1.5×10^{-4} *M* BrTr containing 0.02 *M* *tert*-butyl alcohol at pH 10.5 (N_2 purged) and (c and d) 1.2×10^{-4} *M* BrTr saturated with N_2O. Lower traces give the conductivity at (a and c) 20 μsec/division and (b and d) 100 μsec/division. Relative sensitivities are for (a and b) 2 and (c and d) 5. Upper traces give the current integral which corresponds to doses of (a and b) 1.6×10^{16} eV/g per division and (c and d) 3.2×10^{16} eV/g so that the initial total radical concentrations were, respectively, ~7 and 10×10^{-6} *M*. Arrows indicate the termination of the pulse. Note especially the slight initial increase in a and b.

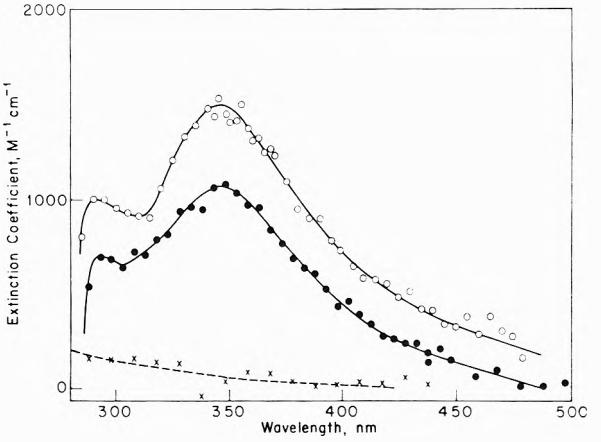

Figure 8. Spectra of radicals III (●) and IV (○). The spectrum of radical III was obtained at 20 μsec from a 10^{-4} *M* BrTr solution containing 0.1 *M* *tert*-butyl alcohol to remove OH radicals (N_2 purged; pH 10.7). Saturation of this solution gives a very low background (×) showing that OH radicals do not contribute. Similar spectra were observed at pH 7 for solutions containing 0.01 and 0.1 *M* isopropyl alcohol. The spectrum of radical IV was obtained at 10 μsec from a 10^{-3} *M* BrTr solution containing 0.1 M KBr (N_2O saturated; pH 10.9). In this experiment the period for oxidation of BrTr by Br_2^- is 1.4 μsec so that oxidation is within 1% of being complete at the time of the measurement. Doses were 5–10 × 10^{16} eV/g per pulse. The points for radical IV represent the data from individual experiments and those for radical III the average over four experiments.

Figure 7b the median lifetime is 120 μsec so that the rate constant is $\sim 1.2 \times 10^9$ M^{-1} sec^{-1}, *i.e.*, the disproportionation is essentially diffusion controlled. Upon disproportionation this radical will either be reduced to tetronic acid or be oxidized to hydroxytetronic acid, both of which are ionized so that the conductance should ultimately change by approximately $\Lambda(Br^-) - \Lambda(OH^-)$, *i.e.*, −115 mhos cm^2 $equiv^{-1}$. The observed change is −122 mhos cm^2 $equiv^{-1}$. If combination reactions involving radical III were important one would expect very little change in conductance so that it is very evident that disproportionation dominates. The radical lifetime in the steady-state experiments is considerably longer (~10^{-2} sec) than in these pulse studies so in that case abstraction reactions may take place in competition with disproportionation. The high yield of tetronic acid in the presence of alcohols suggests abstraction rate constants ~10^4 M^{-1} sec^{-1}.

f. The Absorption Spectrum of Radical III. At this point it seems reasonably clear that the species manifest in the region of 250 nm at microsecond times is radical III. This radical also absorbs in the region above 300 nm as indicated by the solid points in Figure 8. A moderately intense band is observed in the region of 350 nm (ϵ_{350} 1060 M^{-1} cm^{-1}) with a very long tail out to ~500 nm. Saturation of the solutions with N_2O gave a negligible background (crosses) showing that the absorbing species is not produced by unscavenged OH. A similar absorption in the region of 350 nm and at longer wavelengths has been observed for the radical substituted with Br at the 2 position (open circles in Figure 8) and will be discussed below. The fact that these radicals absorb at relatively long wavelengths is readily understandable since in these radicals the unpaired electron is in a π orbital having contributions from both of the carbonyl groups. In radical II the electron (in a σ orbital) is localized on C_2 so that significant absorption is not expected in this region. For example, uracilyl radical, which presumably has an electronic configuration similar to II, does not appear to absorb significantly above 300 nm.[21] The 2-hydroxy analog of radical III (discussed below) has a considerably more intense band at 360 nm but no significant absorption above 400 nm.

g. Summary. The above can be summarized by indicating that in the presence of an appropriate H atom donor e_{aq}^- reacts with bromotetronic acid at low dose rates to produce bromide ion and tetronic acid nearly quantitatively, *i.e.*, with an efficiency >90%. Pulse studies indicate that an intermediate is produced which has an absorption spectrum very similar to but somewhat less intense than that of tetronic acid. From detailed examination of the results of pulse radiolysis studies it is suggested that this intermediate is a neutral entity produced by protonating the anion radical which results from halide elimination following electron capture. Pulse conductivity studies confirm this suggestion and shown that at high concentrations the radicals disappear largely by disproportionation. It is pointed out that in this system the initial radical is an oxyanion which has the unpaired electron coupled to the oxygen through an ethylenic linkage. In this configuration protonation at the radical site becomes readily possible so that the radical chemistry can be qualitatively different from that of other radicals which on the surface seem to be similar. While detailed studies of tetronic acid production can be carried out at very low solute concentrations (*i.e.*, 10^{-5} *M* and below) interference by competing electron scavengers becomes evident and vitiates attempts to use this system to directly measure the yield of e_{aq}^- which reacts with scavengers at low concentrations. Such attempts are further complicated by the fact that secondary conversion of the intermediate radical to tetronic acid is relatively slow.

Reaction of OH with α-Bromotetronic Acid. The studies with OH are, of course, more directly relevant to studies on ascorbic acid since, as mentioned in the Introduction, oxidative debromination is known from esr studies[2] to produce a radical very similar to that present during the

oxidation of ascorbic acid. One hopes from measurements on bromide production to get some insight into the relative frequency for reaction of OH by addition at the C_2 position (reaction 1) and by competing addition at the C_3 position and/or electron transfer. The latter two reactions will have the same net effect, *i.e.*

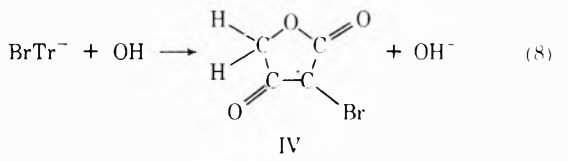

$$BrTr^- + OH \longrightarrow \text{IV} + OH^- \qquad (8)$$

It is of particular importance to know whether or not addition of OH contributes significantly in these systems or whether an electron transfer mechanism dominates.

a. Bromide Production. In this case the bromide production does not appear to be affected to any considerable extent by product buildup since one observes essentially linear yield–dose curves with no pronounced dependence of the yield on concentration even at doses $\sim 10^{19}$ eV/g. The yields measured at a dose of 6×10^{18} eV/g are 1.58, 1.68, and 1.91 for 0.59, 1.2, and 2.30 mM solutions. These yields include small contributions from e_{aq}^- which escape being scavenged by the N_2O (0.05, 0.10, and 0.19, respectively). The OH radical reacts relatively slowly with both Br^- and H_2O_2 ($k(OH + Br^-) = 1 \times 10^9\ M^{-1}\ sec^{-1}$; $k(OH + H_2O_2) = 2 \times 10^7\ M^{-1}\ sec^{-1}$)[19,22] so that neither of these products is expected to interfere significantly. Trial integrations of the appropriate differential equation describing the effect of product buildup shows that there would have been observable curvature to the yield–dose plots if $G(\text{product})k(OH + \text{product})$ were greater than ~20% of $G(OH)k(OH + BrTr)$. Using this ratio as an upper limit the calculations place corresponding limits of 0.13, 0.08, and 0.04 on the differences between true initial yields and the values measured at 6×10^{18} eV/g. Making both of the above corrections the net initial yields ascribable to OH reactions are in the ranges 1.53–1.66, 1.58–1.66, and 1.72–1.76 for the 0.6, 1.2, and 2.3 mM solutions, respectively. From these measurements the yield of bromide ion in millimolar solutions of BrTr can be taken as 1.7 ± 0.1 or 28% of the total OH yield of 6.0 appropriate to N_2O saturated solutions. Bromide elimination in reaction 1 is very rapid (<1 μsec) so that this yield presumably represents an upper limit for the attack of OH at the bromide position.

b. Spectroscopic and Chromatographic Studies. The change in the absorption spectrum of a N_2O saturated 5×10^{-5} M solution of BrTr with dose is illustrated in Figure 4b. The decrease of absorption at 258 nm is approximately linear with dose and gives a lower limit to the yield for consumption of BrTr of 3.0. No contribution from any intensely absorbing product is directly apparent although the fact that the loss in absorption is less than indicated in Figure 9 implies some such contribution. One expects at least a small yield of hydroxytetronic acid which has a strong absorption in this region (see Table II) as a result of disproportionation of radical I. Liquid chromatographic examination of a 1.8×10^{-4} M solution irradiated to a dose of 1.8×10^{18} eV/g showed that hydroxytetronic acid was produced with a yield ~0.9 but the amount detected decreased rapidly as the result of post-irradiation oxidation[23] so that a quantitative study was not feasible (hydroxytetronic acid eluted in front of tetronic acid; the identity of this peak was confirmed by showing its absorption spectrum to be identical with that of an authentic sample). It was possible to follow the consumption of bromotetronic acid in chromatographic experiments and the results are given in Figure 9. The initial yield ($G(-BrTr)$) is 4.1 which is less than the yield of OH (6.0) but considerably greater than that of bromide (1.7). It is clear the OH is consumed in reactions that do not readily yield bromide.

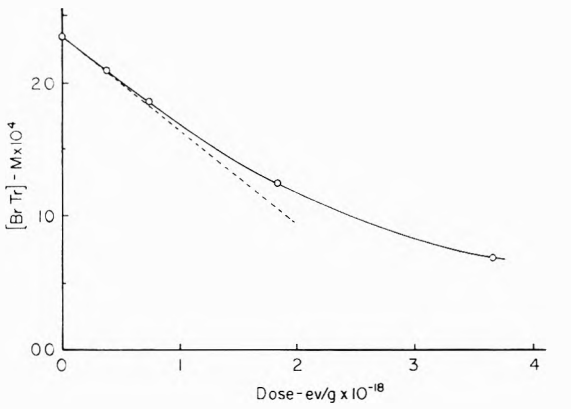

Figure 9. The consumption of bromotetronic acid at pH 7 as measured in liquid chromatographic experiments. The dashed line corresponds to an initial yield of −4.1.

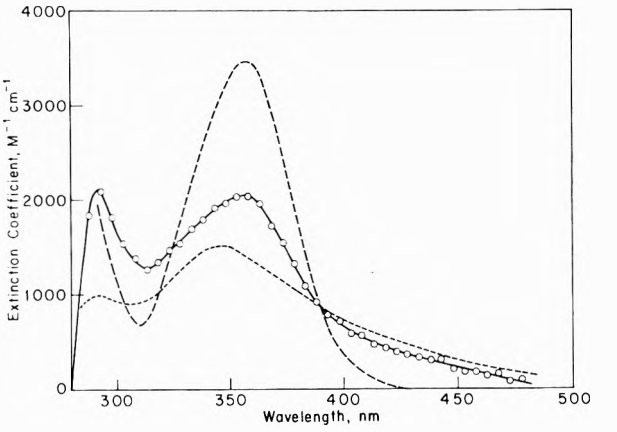

Figure 10. Spectrum observed at 10 μsec for a N_2O saturated 10^{-3} M solution of BrTr at Ph 10.9. The spectra of radical I (– –) and radical IV (- - - -) are superimposed. Doses were ~5 × 10^{16} eV/g per pulse and the points represent the average over four experiments.

c. Pulse Radiolysis Studies. While the *in situ* esr experiments[2] have demonstrated that radical I is an important intermediate they have provided little direct information on the quantitative aspects and one is still not sure at this point that the bromide produced results entirely from reaction 1. It is desirable, therefore, to have auxiliary evidence from pulse radiolysis studies. The experimental points in Figure 10 give the absorption spectrum observed ~5 μsec after pulse irradiation of a nitrous oxide saturated 1 mM solution of bromotetronic acid at pH 10.8 (OH reaction period is ~0.1 μsec). A moderately intense absorption band similar to that reported for the intermediate produced from ascorbic acid[14,24] occurs in the region of 350 nm indicating that radical I is very likely present at μsec times. Similar, but slightly less intense, spectra were observed at concentrations of 10^{-5} and 10^{-4} M.

An authentic spectrum of radical I was obtained by oxidizing 1.5×10^{-4} M hydroxytetronic acid with Br_2^- (produced by reaction of OH with 10^{-2} M Br^-) and is com-

pared in Figure 11 with the spectrum obtained in similar experiments on ascorbic acid. The period for reaction of Br_2^- with the hydroxytetronic acid was 9 μsec (determined by following the loss of Br_2^- at 415 nm where radical I has negligible absorption; $k = 5.0 \times 10^8\ M^{-1}\ sec^{-1}$) so that the reaction was essentially complete 65 μsec after the pulse where the spectrum of Figure 11 was obtained. The extinction coefficients were calculated on the assumption that OH is quantitatively converted to radical I, as seems likely since both electron transfer and addition of Br to either end of the double bond should ultimately lead to this radical. In this case there is essentially no decay of radical I so that the observations can be carried out at relatively long times. As is shown in the figure a spectrum of identical shape was also observed in the reaction of OH with 10^{-4} *M* hydroxytetronic acid but these more direct studies were somewhat susceptible to interference by oxidation products and secondary reactions and the intensities were 15% lower than when the radical was prepared *via* the Br_2^- path. The comparison of the spectrum of radical I with that of the intermediate in the ascorbic acid case shows them to be very similar with the former having a somewhat more Gaussian shape and a lower absorption in the 300–320-nm region. This similarity is, of course, expected since the esr studies show their electronic structures to be very similar (the *g* factors and ^{13}C hyperfine constants[2] are essentially identical and indicate that the unpaired electron is in a highly delocalized orbital with important contributions from spin density on the carbonyl oxygen atoms).

The absorption spectrum of radical I, which has a maximum at 358 nm (ϵ_{358} 3450 $M^{-1}\ cm^{-1}$), is superimposed in Figure 10 on the spectrum observed for OH attack on bromotetronic acid. In the latter case the maximum (356 nm) has been shifted slightly toward lower wavelength but there clearly is a broad underlying absorption which can cause such a shift. One suspects that radical IV is mainly responsible for this underlying absorption, particularly after the assignment of an absorption at 350 nm to radical III. Radical IV was prepared by oxidizing bromotetronic acid with Br_2^-, *i.e.*

$$Br_2^- + BrTr^- \longrightarrow IV + 2Br^- \qquad (9)$$

The rate constant for reaction 9 was determined to be $4.9 \times 10^8\ M^{-1}\ sec^{-1}$ by measuring the disappearance of both Br_2^- and BrTr. The absorption spectrum given by the open circles in Figure 8 appears to be attributable entirely to radical IV.[25] This spectrum, which has a maximum at 346 nm (ϵ_{346} 1500 $cm^{-1}\ M^{-1}$), is very similar to that for radical III, and is superimposed as the dotted curve in Figure 10. Radical IV appears to account for the long wavelength tail observed in the case of OH attack on bromotetronic acid.

All three curves cross at 390 nm indicating that OH is converted almost completely either to radical I or IV. The relatively high absorption in the region of 300–320 nm shows that a small amount of some additional species which absorbs strongly in this region must also be produced. At 350 nm radical IV has an extinction coefficient of 1380 $M^{-1}\ cm^{-1}$. Using successive approximations, with the assumption that the observed extinction coefficient (2050 $M^{-1}\ cm^{-1}$) is the sum of contributions from radicals I and IV, the contribution from I rapidly converges to 990 $M^{-1}\ cm^{-1}$ or 32% of that of the extinction coefficient for the radical produced from hydroxytetronic acid. (The conductometric pulse radiolysis studies described below also indicate that ~30% of the OH attacks bromotetronic acid at the bromide position.) These spectroscopic data show that the yields of Br^- and radical I are identical and therefore indicate that no bromide is produced except for that resulting from reaction 1. One must conclude that the C–Br bond in radical IV remains intact even following disproportionation of the radicals.

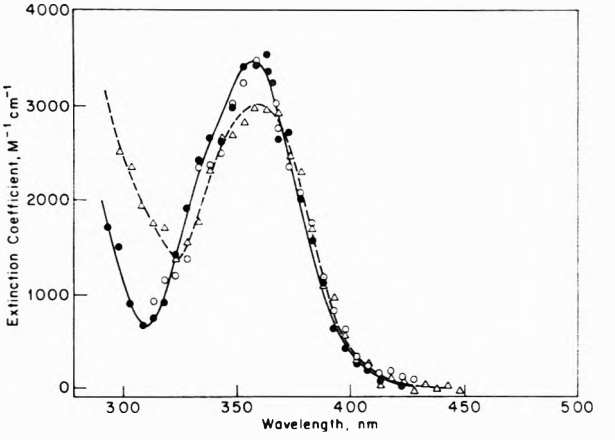

Figure 11. Spectra observed for radical I produced by oxidizing 10^{-4} *M* hydroxytetronic acid with Br_2^- (●) and with OH (○). A comparative spectrum of the radical produced by oxidizing ascorbic acid with Br_2^- (△) is also given. Doses were ~2 × 10^{16} eV/g per pulse and the points represent the average over four experiments.

Pulse radiolysis studies on a N_2O saturated 2×10^{-5} *M* solution of BrTr gave the differential spectrum of Figure 5b at 50 μsec. There is a strong increase in transmission at 258 nm which corresponds to about 80% of the extinction coefficient of BrTr. One sees, however, that a product results in an increased absorption in the vicinity of 230 and 290 nm. If we assume that the background absorption increases monotonically, as is indicated by the dashed line in the figure, then superposition of the negative of the absorption spectrum of BrTr gives excellent agreement with the observations. Because of the correction for the background absorption and also because of the relatively large contribution from scattered light (the transmission of the sample was only 15% at 250 nm and as a result the scattered light correction was ~30%) there is an uncertainty of 10–20% in the magnitude of the loss in absorbance attributable to consumption of BrTr. Both corrections are, however, reasonable so that the loss of BrTr resulting from OH attack appears to be very nearly quantitative at ~100 μsec.

The above results suggest that over the long term bromotetronic acid is in part re-formed as the result of the reduction of radical IV in disproportionation processes. Experiments on a 5×10^{-5} *M* solution irradiated with a dose sufficient to produce 2×10^{-5} *M* of OH radicals showed, in fact, a partial recovery (~15% at 200 μsec) of the absorption of BrTr as the radicals disproportionated. Because of clipping of the initial cusp and additional decay at long times the total recovery is estimated to be somewhat larger (~25 ± 5%) and in reasonable agreement with the amount by which the destruction of BrTr is low in the ^{60}Co experiments (32%).

d. Conductometric Studies. Conductivity studies provide more definitive information on the branching of the OH attack *via* reactions 1 and 8. Typical traces are illustrated in Figure 7c and 7d. For a 10^{-4} *M* bromotetronic acid solution at pH 10.8 (N_2O saturated) one observes an

increase in the conductivity of 60 mhos cm^2 $equiv^{-1}$ immediately after the pulse (based on an OH yield of 6.0). This increase was quite consistent from run to run and is believed to be accurate to ~5%. For reaction 1 one expects an increment in conductance of $\Lambda(Br^-) - \Lambda(OH^-) \simeq -115$ mhos cm^2 $equiv^{-1}$ (assuming that the conductances of radical I and BrTr anion are similar). For reaction 8 the change should be $\Lambda(OH^-) - \Lambda(BrTr^-) \simeq 142$ mhos cm^2 $equiv^{-1}$. The fact that the initial change is appreciably positive indicates qualitatively that reaction 8 is more important than reaction 2. Solution of the expression which equates the observed initial increment to the sum of the contributions from reactions 1 and 8 gives 0.32 as the fractional importance of reaction 1, in very good agreement with the expectations from the bromide and optical measurements. If we assume that reactions 1 and 8 contribute the only conducting species then this measurement is, in fact, the one most free of possible interpretive complications.

As the radicals recombine the conductivity decreases by 126 units and approaches a level of −66 mhos cm^2 $equiv^{-1}$ (see Figure 7d). This decrease clearly follows second-order kinetics (the median lifetime is inversely proportional to dose; $k \sim 1.5 \times 10^9$ M^{-1} sec^{-1}) and very obviously represents the changes resulting from disproportionation reactions. (Radical combination would not be expected to result in significant changes in conductivity and is apparently completely unimportant here.) The magnitude of the decrease indicates that approximately one OH^- is consumed for each radical undergoing disproportionation. Disproportionation will effectively involve the oxidation and reduction of radicals I and IV. Reduction of radical IV will result in the re-formation of bromotetronic acid and account for the recovery of the absorption noted above and also the fact that the yield for consumption of BrTr is only ~70% of the OH yield. Reaction of radical IV with radical I apparently results primarily in its oxidation since reduction would produce a 50% recovery of BrTr and little change in conductivity (disproportionation in this latter direction essentially involves electron transfer to re-form BrTr at the expense of I). We will assume, therefore, that in 20% of the instances radical IV is reduced by disproportionationating with itself, that in 30% of the instances radical I is reduced by disproportionating with IV and that in 50% of the instances radical IV is oxidized. Reduction of I and IV will result in increases in conductivity of 192 and 50 mhos cm^2 $equiv^{-1}$ as a result of the production of OH^- and $BrTr^-$, respectively. Oxidation of IV must, therefore, account for the very large decrease in conductance and it is implied that each radical oxidized must effectively consume at least two OH^-. The most obvious suggestion is that radical IV hydroxylates at the C_2 position but such a reaction would be expected to result in the elimination of bromide along with the formation of 2,3,4-trioxotetrahydrofuran (TTHF), *i.e.*

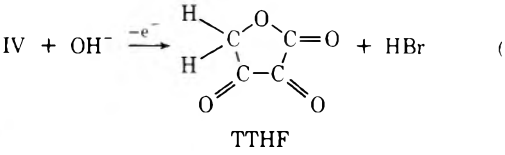

TTHF

In the steady-state experiments no significant bromide is produced over and above that formed in reaction 1. We tentatively suggest, therefore, that hydroxylation occurs at the C_4 position, *i.e.*

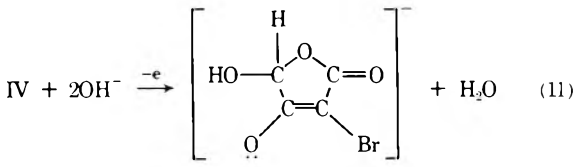

Reaction 11 involves a change in equivalent conductance of ~ −334 mhos cm^2 $equiv^{-1}$. (The change for reaction 10 is −307 mhos cm^2 $equiv^{-1}$.) According to the above, the partial contributions to the observed conductance change will be ~0.30 × 192 = +58 units from the reduction of radical I, ~0.20 × 50 = +10 units from the reduction of radical IV, and ~0.50 × −334 = −167 units from the oxidation of IV. The net conductance change in the disproportionation processes should therefore be ~ −99 mhos cm^2 $equiv^{-1}$ (reaction 10 gives only −84 units). The fact that the observed decrease (−126 mhos cm^2 $equiv^{-1}$) is still higher certainly indicates that the total explanation is very likely more complex and may very well involve ring opening of the oxidized species.

e. Kinetics of the Radical Decay. At this point it is clear that the low intensity of the spectrum of radical I in the esr experiments must be attributed to its removal by reaction with other radicals. This conclusion is confirmed by studies of the decay of the absorption at 360 nm. Radical I at a concentration of 10^{-5} M (prepared by irradiation in a N_2O saturated hydroxytetronic acid solution) does not decay observably over a 400-μsec period so that the second-order rate constant for reaction with like radicals (reaction 12) must be $<10^7$ M^{-1} sec^{-1}. The rate con-

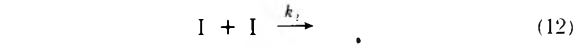

stant for this reaction is, in fact, undoubtedly very similar to the value of 10^5 M^{-1} sec^{-1} found for the radicals from ascorbic acid[24] since the spectral intensities in the two esr experiments are similar. In the experiments on bromotetronic acid, however, the absorption at 360 nm (where I represents 50% of the absorption) decays observably on the 100-μsec time scale with the initial decay rate being proportional to the dose as expected from second-order kinetics. Data are illustrated in Figure 12. At an initial total radical concentration of 9×10^{-6} M the median radical lifetime was 105 μsec so that a second-order rate constant of the magnitude of 10^9 M^{-1} sec^{-1} is indicated. This means, of course, that radical I must be disappearing almost entirely by reaction with radical IV.

Assuming that radicals I and IV are initially present in a ratio *ca.* 30:70 the important radical-radical reactions are

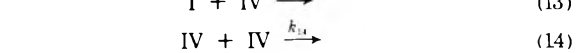

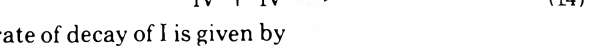

The rate of decay of I is given by

$$d[I]/dt = -k_{13}[I][IV] \quad (15)$$

where IV can be approximated by

$$[IV] = [IV]_0 - ([I_0] - [I]) - \int_0^t 2k_{14}[IV]^2 \, dt \quad (16)$$

i.e., the concentration of IV is equal to the initial concentration less the amounts consumed by disproportionation with I and with itself. Substitution of eq 16 into 15 gives an equation with three basic parameters (k_{13}, k_{14}/k_{13}, and $[IV]_0/[I]_0$) which can be readily integrated by numerical methods. Choosing $[IV]_0/[I]_0 = 2.34$ from the chemical

experiments, the qualitative shape of the decay can be fitted only with k_{14}/k_{13} approximately equal to the expected statistical ratio of 0.5. (If $k_{14} \gg k_{13}$ then radical IV will decay rapidly leaving a residual concentration of I behind and if $k_{14} \ll k_{13}$ then radical I will decay toward zero since an excess of radical IV will always be present.) The concentration of radical I at long times is controlled critically by the ratio k_{14}/k_{13} and best fit with the data at long times requires a value of ~0.32, *i.e.*, I disproportionates with IV somewhat more rapidly that IV does with itself. Incorporation of this value into the integrations then allows an absolute value of $1.6 \times 10^9\ M^{-1}\ \text{sec}^{-1}$ to be determined for k_{13} from the actual decay at short times.

Two points should be made here. First since the two components decay with very nearly statistically equal rates, one does not expect the absorption spectrum to change as the decay progresses. There was, in fact, no significant change in the form of the spectrum with time. Second, that in this case the rate constant for the cross reaction between radicals I and IV is rapid even though radical I is relatively unreactive when present by itself. While reaction 12 involves combination between two charged radicals, single charges do not usually inhibit the rate to any large extent so that the low rate constant for this reaction must be attributed to the high delocalization of electrons[2] in radical I which apparently makes it relatively difficult to be oxidized by disproportionating with itself.

f. Steady-State Concentrations in the Esr Experiment. If reactions 13 and 14 are the only important reactions, solution of the steady-state case gives

$$[\mathrm{I}]_{ss} = \sqrt{\frac{P_\mathrm{I}}{k_{13}}}\sqrt{\frac{2k_{14}}{k_{13}}\frac{P_\mathrm{I}}{P_\mathrm{IV} - P_\mathrm{I}}} \qquad (17)$$

where $[\mathrm{I}]_{ss}$ is the steady-state concentration of radical I and P_I and P_IV are the rates for production of I and IV. With P_IV somewhat greater than P_I this relation can be approximated by

$$[\mathrm{I}]_{ss} \simeq \sqrt{\frac{P_\mathrm{I} + P_\mathrm{IV}}{k_{13}}}\frac{P_\mathrm{I}}{P_\mathrm{IV}}\sqrt{\frac{2k_{14}}{k_{13}}} \qquad (18)$$

For the present case the product of the last two factors is ~0.35, *i.e.*, in the steady-state esr experiments one expects the normalized intensity of radical IV to be 35% of that of radicals known to be produced in high yield and to disappear in diffusion-controlled processes. Comparison of the esr signals from a 0.9 m*M* solution of BrTr and with those from sodium acetate at a dose rate sufficiently low that depletion did not occur shows the relative intensities to be 0.31 (see Fessenden[26] for the validity of such comparisons). The intensities observed in the esr experiments thus appear to be adequately explained by the high rate for the second-order intercombination reaction manifested in the pulse radiolysis experiments.

g. Summary. In summarizing the results of the OH experiments the main points appear to be that ~30% of the OH radicals react at the bromine position leading to radical I as the result of rapid dehydrohalogenation and that reaction of the remaining OH at the C_3 position leads to only a partial yield for destruction of the bromotetronic acid as a consequence of reduction of the resultant radical to the starting material in the disproportionation processes. Oxidation of this radical must also occur but does not appear to yield bromide readily. The low intensity of radical I in the esr experiments on bromotetronic acid (as compared with the intensities observed in similar experiments on hydroxytetronic acid) is adequately explained in terms of the rapid removal of radical I by reaction with radical IV. The fact that in the present case OH appears to add to the C_2 position argues that OH does not oxidize hydroxytetronic and ascorbic acids solely by an electron transfer mechanism.

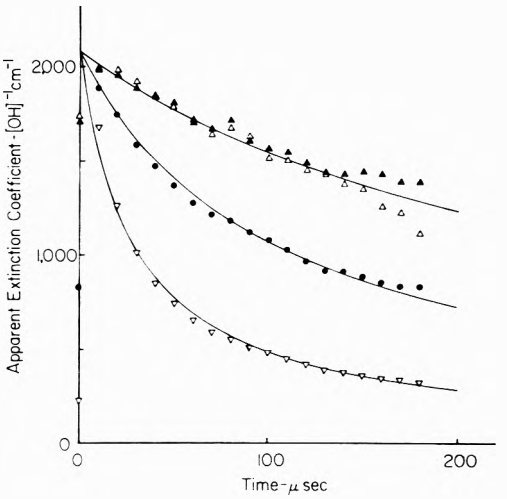

Figure 12. The decay of absorption at 360 nm for a N_2O saturated 10^{-3} *M* BrTr solution at pH 10.9 as measured in pulse radiolysis experiments. Doses were (▽) 29.0, (○) 8.2, (▲) 3.1, and (△) 3.0×10^{16} eV/g per pulse (data are normalized for dose and represent signal averaging over ten experiments). The curves are calculated by numerically integrating eq 15 with $k_{13} = 1.55 \times 10^9\ M^{-1}\ \text{sec}^{-1}$, $k_{14}/k_{13} = 0.32$, and $[\mathrm{IV}]_0/[\mathrm{I}]_0 = 2.34$ with the initial total radical concentration taken from the dose measurements as 29.0, 8.2, and 3.1 μ*M*.

Supplementary Material Available. Table II will appear following these pages in the microfilm edition of this volume of the journal. Photocopies of the supplementary material from this paper only or microfiche (105 × 148 mm, 24× reduction, negatives) containing all of the supplementary material for the papers in this issue may be obtained from the Journals Department, American Chemical Society, 1155 16th St., N.W., Washington, D. C. 20036. Remit check or money order for $3.00 for photocopy or $2.00 for microfiche, referring to code number JPC-74-1063.

References and Notes

(1) Supported in part by the U. S. Atomic Energy Commission.
(2) G. P. Laroff, R. W. Fessenden, and R. H. Schuler, *J. Amer. Chem. Soc.*, **94**, 9062 (1972).
(3) W. K. Kumler, *J. Amer. Chem. Soc.*, **60**, 859 (1938).
(4) L. Wolff and C. Schwabe, *Ann.*, **292**, 231 (1896).
(5) T. Micheel and F. Jung, *Chem. Ber.*, **66**, 1291 (1933).
(6) K. M. Bansal, L. K. Patterson, and R. H. Schuler, *J. Phys. Chem.*, **76**, 2386 (1972).
(7) K. Bhatia, *Anal. Chem.*, **45**, 1356 (1973).
(8) K. Bhatia, *Radiat. Res.*, in press.
(9) L. K. Patterson and J. Lilie, *Int. J. Radiat. Phys. Chem.*, in press.
(10) J. H. Baxendale, P. L. T. Bevan, and D. A. Stott, *Trans. Faraday Soc.*, **64**, 2389 (1968).
(11) J. Lilie and R. W. Fessenden, *J. Phys. Chem.*, **77**, 674 (1973).
(12) T. I. Balkas, J. H. Fendler, and R. H. Schuler, *J. Phys. Chem.*, **74**, 4497 (1970).
(13) Above pH 7 the anionic forms predominate (see ref 3). The p*K* of bromotetronic acid is 2.2 and that of tetronic acid is 3.8. The first p*K* of hydroxytetronic acid is 4.4 and that of ascorbic acid 4.1. In each of the latter cases the equilibrium is attributed to ionization of the OH group at the 3 position with ionization of the OH at the 2 position occurring in the region of pH 12.
(14) M. Schoneshofer, *Z. Naturforsch. B*, **27**, 649 (1972).
(15) P. Neta and R. H. Schuler, *Radiat. Res.*, **47**, 612 (1971).
(16) K. Bhatia and R. H. Schuler, *J. Phys. Chem.*, **77**, 1356 (1973).
(17) K. Bhatia and R. H. Schuler, *J. Phys. Chem.*, **77**, 1888 (1973).

(18) A. O. Allen and R. A. Holroyd, *J. Amer. Chem. Soc.*, **77**, 5852 (1955); A. O. Allen and H. A. Schwarz, *Proc. U. N. Int. Conf. Peaceful Uses At. Energy, 2nd*, **29**, 30 (1958).
(19) M. Anbar and P. Neta, *Int. J. Appl. Radiat. Isotopes*, **18**, 493 (1967).
(20) E. R. Johnson and A. O. Allen, *J. Amer. Chem. Soc.*, **74**, 4147 (1952).
(21) L. K. Patterson and K. M. Bansal, *J. Phys. Chem.*, **76**, 2392 (1972).
(22) L. M. Dorfman and G. E. Adams, *Nat. Stand. Ref. Data Ser., Nat. Bur. Stand.*, **No. 46** (1973).
(23) K. Bhatia, to be submitted for publication.
(24) B. H. J. Bielski and A. O. Allen, *J. Amer. Chem. Soc.*, **92**, 3792 (1970); B. H. J. Bielski, D. A. Comstock, and R. A. Bowen, *ibid.*, **93**, 5624 (1971).
(25) *In situ* esr experiments on a 10^{-4} *M* BrTr solution showed that the addition of 10^{-1} *M* KBr reduced the intensity of the triplet of radical I by 65%. Although the remaining signal could result from secondary reactions at the relatively high dose rates used, the fact that the signal was not eliminated completely indicates that complications may be present.
(26) R. W. Fessenden, Proceedings of the Conference on "Fast Processes in Radiation Chemistry and Biology," Sussex, England, Sept 10–14, 1973.

An Electron Spin Resonance Study of the Radiolysis of Aqueous Solutions of Cyanate Ion[1]

D. Behar and Richard W. Fessenden*

Radiation Research Laboratories, Center for Special Studies and Department of Chemistry, Mellon Institute of Science, Carnegie-Mellon University, Pittsburgh, Pennsylvania 15213 *(Received November 26, 1973)*

Publication costs assisted by the Carnegie-Mellon University and the U. S. Atomic Energy Commission

The *in situ* radiolysis–esr method has been used to investigate the radicals produced in aqueous solutions of cyanate ion (NCO^-) by high-energy electron irradiation. Over the pH range 3.6–12.4, N_2O-saturated solutions give rise to a proton-containing radical with the esr parameters a^N = 13.73, a^H = 10.87 G, and g = 2.00425. From the dependence of the intensity of this spectrum upon flow rate and the concentration of NCO^- it is concluded that the radical is a primary product and most probably has the structure $H\dot{N}CO_2^-$. Over the pH range 6.5–10.5 another radical which contains two nitrogen atoms and has the parameters a^N = 9.82, $a^{N'}$ = 5.90, a^H = 7.84, and g = 2.00404 is observed. This radical can best be assigned as $^-O_2CNH\dot{N}CO_2^-$ formed by a secondary reaction of OH with the dimer of the primary radical. Above about pH 12 yet another radical is found which also seems to be a secondary product. On the basis of earlier studies this radical can be assigned the structure $^-O_2C\dot{N}O_2^-$. No radicals resulting from the reaction of e_{aq}^- with cyanate were found. Radicals which may have the structure $RO_2C\dot{N}^-$ were produced by allowing methyl and ethyl carbamate to react with HOCl and allowing the resultant *N*-chloro compounds to react with e_{aq}^- in basic solution. The spectra for the two esters were similar in their gross features with $a^N \sim 11$ G and $g \sim 2.0048$.

Introduction

The present work continues our investigations of irradiated aqueous solutions of halides[2] and pseudo-halides.[3,4] In a previous paper[4] we identified the carbon-centered radical $H_2\dot{N}CO$ as the product of the reaction of OH with CN^- and a nitrogen-centered radical $HC(OH){=}\dot{N}$ as the product of OH and HCN. The ionized form of this latter radical ($HC(O^-){=}\dot{N}$) was also detected at lower pH. The radical $HC(O^-){=}\dot{N}$ has also been claimed by Ginns and Symons to be produced by irradiating frozen aqueous solutions of alkali metal cyanides[5] and cyanates.[6] However, the hydrogen hyperfine constant of 73 G found by them[5,6] for $HC(O^-)\dot{N}\cdot$ does not agree with the value of 54.5 G found by us[4] so that different radicals seem to be involved. It was hoped that a study of the reaction of e_{aq}^- with NCO^- could help resolve this disagreement. In addition, an identification of the OH reaction product with cyanate would be of value because of its close relationship with thiocyanate. The latter ion is very important in radiation chemistry and is used both as a standard for OH rate constant measurements in competitive situations and for dosimetry in pulse experiments. Although an intermediate radical $NCSOH^-$ has been identified in this latter system by optical methods[3] uncertainties as to the exact structure of the radical still remain. Ideally, esr experiments should be carried out on thiocyanate itself but the presence of sulfur in the adduct radical seems to cause line broadening and no signals were detected in a previous study.[7] Although in that study we also reported no esr signals from solutions of cyanate as well, the use of higher modulation amplitudes and microwave powers as suggested by the work on CN^- [4] did, in fact, allow observation of esr spectra as reported here. New experiments on SCN^- did not lead to observation of any esr lines.

To our knowledge no work has been done on the radiation chemistry of cyanate solutions. Irradiated single crystals of KOCN were studied by Owens, *et al.*,[8] who identified CN radicals. These findings have been criticized by Ginns and Symons[6] who argue that the magnetic parameters of Owens, *et al.*,[8] do not agree with the good characterization of CN by Easley and Weltner.[9] In their own

work on irradiated frozen aqueous solutions of KOCN and NaOCN, Ginns and Symons[6] were able to show the presence of several intermediate species and identified N, $HOCN^-$, and N_2CO^- as the most important ones. No evidence for the formation of an OH adduct to NCO^- ion was found in that work.

Experimental Section

Fisher certified potassium cyanate was used without further purification. Methyl and ethyl carbamates from Baker were used to prepare the *N*-chlorocarbamate derivatives by mixing equimolar concentrations of methyl or ethyl carbamate with Baker analyzed sodium hypochlorite at pH 7, as described by Metcalf.[10] The reaction mixture was diluted to the required concentration and then brought to the required pH without separating the *N*-chlorocarbamates from the reaction mixture. All solutions were prepared with doubly distilled water and deoxygenated by bubbling with either N_2 or N_2O. N_2O was used to convert the hydrated electrons initially produced into hydroxyl radicals. The *in situ* irradiation with a 2.8-MeV electron beam was carried out directly in the esr cavity as previously described.[11,12]

Results and Discussion

Radiolysis of Cyanate Solutions. The esr spectrum obtained on irradiating 10^{-2} *M* KOCN solution saturated with N_2O at neutral pH was composed of two sets of lines of different intensities. The lines are assigned to two different radicals as shown in Figure 1. Both radicals result from a reaction of OH with cyanate since they disappeared when *tert*-butyl alcohol was added to the solution. Spectrum 1, composed of a 19.87-G doublet of 13.73-G triplets with g = 2.00425, seems to result from addition of OH to the carbon nitrogen triple bond.

$$OH + {}^-O{-}C{\equiv}N \longrightarrow {}^-O{-}\overset{OH}{\overset{|}{C}}{=}\dot{N} \qquad (1)$$

The 13.73-G triplet is reasonable for a radical with the unpaired electron on nitrogen but a splitting of 19.87 G for the proton in an OH group seems very unreasonable.[13] We assume, therefore, that a lactim–lactam rearrangement takes place to form the carbamate radical according to reaction 2. The rearrangement in reaction 2 can be very fast as it involves only a proton dissociation and reattachment and equilibrium 2 probably lies to the right since no signals for the lactim form were observed.

$$\underset{\text{lactim}}{{}^-O{-}\overset{OH}{\overset{|}{C}}{=}\dot{N}} \rightleftharpoons \underset{\text{lactam}}{{}^-O{-}\overset{O}{\overset{\|}{C}}{-}\dot{N}H} \qquad (2)$$

An alternative to reaction 1 is addition of OH to the nitrogen to give ^-O-$\dot{C}$=NOH or O=$\dot{C}$-NHOH and these could rearrange to ^-O-CH=NO·, HOCH=NO·, or O=CH-NHO·. In addition to being less likely chemically, these other radicals do not easily explain the magnetic parameters. The first pair of radicals are of the formyl type and should have a low g factor while the second pair are iminoxy radicals and should have larger nitrogen splittings. The fifth radical is of the nitroxide type and should have a g factor ~2.0060 and no proton splitting as large as 19 G. The species $^-O_2C\dot{N}H$ seems, therefore, to be the most likely radical to account for the observed spectrum.

An addition reaction similar to 1 and followed in the same way by a rearrangement like reaction 2 has been

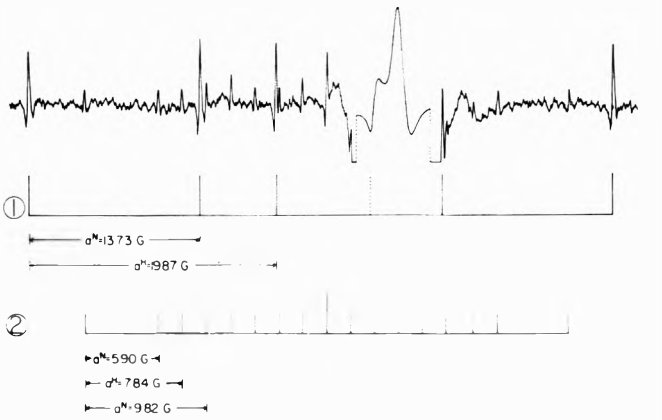

Figure 1. A second-derivative esr spectrum obtained during radiolysis of an N_2O-saturated solution of 10^{-2} *M* KNCO at pH 8.0. The central portion was recorded at reduced gain and contains the signal from the silica cell. Magnetic field increases to the right. The spectra indicated as 1 and 2 are assigned to $H\dot{N}CO_2^-$ and $^-O_2C\dot{N}HNCO_2^-$, respectively.

previously demonstrated with cyanide.[4] In that case the mechanism was established by showing that the same radical, $CONH_2$, was produced either by addition of OH to CN^- or by H abstraction from $HCONH_2$. The same approach of comparing the radicals from cyanate and carbamic acid could not be attempted here because of the instability of carbamic acid. Nevertheless a comparison with the radicals produced from carbamate esters could be carried out as discussed in a later section. Although nitrogen-centered radicals were produced in this way these radicals were not directly comparable to $H\dot{N}CO_2^-$ and so were of limited help in the identification.

The esr spectrum given in Figure 1 is pH dependent. Below pH 3.6 both spectra 1 and 2 disappear. Because the acid HOCN formed at low pH (K_a = 1.2 × 10^{-4}) decomposes in water to ammonia and carbon dioxide[14] it is possible that the disappearance of the lines below pH 3.6 results from the decomposition of the cyanic acid even before irradiation. In our measurements the pH was decreased to pH 3.2 where no spectrum was observed and then increased back to pH 8. After these changes the spectrum was observed again. This experiment proves that the disappearance of the spectrum did not result from decomposition of the starting material. The most probable explanation involves the acid–base equilibrium of the radical

$$H\dot{N}CO_2^- + H^+ \rightleftharpoons H\dot{N}CO_2H \qquad (3)$$

As a result of the proton exchange *via* this equilibrium, line broadening could occur reducing the signal intensity to below the detection limit. In addition the neutral form of the radical would probably react faster than the ionized form, resulting in a lower steady-state concentration of the acid form.

Above pH 10 the intensity of spectrum 1 decreased with increasing pH and completely disappeared above pH 12.5. Meanwhile a new triplet with a^H = 14.39 G and g = 2.00503 started to grow in above pH 11.8. A possible explanation for this new spectrum is the dissociation of $H\dot{N}CO_2^-$ to form $^-\dot{N}CO_2^-$ but the lack of any line broadening associated with the equilibrium would be surprising. In addition, the intensity of this spectrum decreased with flow rate indicating a secondary product. Subsequently, these magnetic parameters were found to match exactly those of a radical assigned the structure $^-O_2C\dot{N}O_2^-$ by

Zeldes and Livingston.[15] In their case the radical was produced by photolysis of a solution containing formate and nitrite. Although the value of a^N is much lower than is usual for nitro anion radicals this fact can presumably be explained by conjugation with the carboxyl group. It should be noted that analogous radicals derived from other hydrogen donors were obtained in a number of cases[15] so the mechanism seems quite straightforward. The great stability of the radical $^-O_2CNO_2^-$ (Zeldes and Livingston could detect the ^{13}C splittings)[15] suggests that in our radiolysis experiments only a small fraction of the total yield of radicals need end up in this form to produce the observed signal. We cannot suggest any simple mechanism to explain the secondary formation of $^-O_2CNO_2^-$ in our system. However, disproportionation of $H\dot{N}CO_2^-$ (in addition to the coupling reaction) could produce $^-O_2CNHOH$ (and $^-O_2CNH_2$) which might be further oxidized to ^-O_2CNO. This nitroso compound could then directly attach OH to form $^-O_2CNO_2^-$.

Spectrum 2 in Figure 1 has 18 lines of the same intensity with two overlapping in the center to form one doubly intense line. Three of the lines are masked under the signal from the silica. This spectrum can be described by three coupling constants $a^N = 9.82$, $a^N = 5.90$, and $a^H = 7.84$ G with $g = 2.00404$. It was found to disappear below pH 6.5 and to decrease in intensity above pH 10.5. In order to produce a radical with two nitrogens there must be some secondary reaction. One of the possibilities is on OH attack on a dimer molecule formed by reaction of $H\dot{N}CO_2^-$.

$$2H\dot{N}CO_2^- \longrightarrow {}^-O_2CNH{-}NHCO_2^- \quad (4)$$

$$^-O_2CNH{-}NHCO_2^- + OH \longrightarrow {}^-O_2CNH{-}\dot{N}CO_2^- \quad (5)$$

This radical can be regarded as hydrazyl with substitution of CO_2^- for two of the hydrogens. Although other possible reaction schemes exist Neta[16] has recently shown that reaction of e_{aq}^- with $^-O_2CN{=}NCO_2^-$ produced by hydrolysis of the diethyl ester leads to the same esr lines as in our spectrum 2. In this case the reaction is clearly electron attachment followed by protonation to give the radical proposed in reaction 5 ($^-O_2CNH\dot{N}CO_2^-$). In the cyanate system the observed decrease in intensity of spectrum 2 with increased NCO^- concentration ($[NCO^-] > 10$ mM) is in accord with reactions 4 and 5. The combination of a double negative charge with the inherent stability of the hydrazyl type of radical indicates that the intensity of spectrum 2 need not represent a very high radical production rate. The identification of $^-O_2CNH\dot{N}CO_2^-$ as responsible for spectrum 2 implies the formation of $^-O_2CNHNHCO_2^-$ and supports rather strongly the identification of $H\dot{N}CO_2^-$ as the primary radical.

The reaction of OH with cyanate (reactions 1 and 2) is similar to that observed with CN^- and HCN in that attack is at the carbon.[4] If a similar reaction occurred with thiocyanate then the radical $H\dot{N}C(=S)O^-$ would be produced. It is difficult to understand how this radical could undergo reaction with further SCN^- to give the accepted[3] pseudo-halogen species $(SCN)_2^-$. On this basis we must conclude that the reaction of thiocyanate is not like that observed with cyanate and that OH attack is on the sulfur to give $NCSOH^-$. The OH group in this radical could readily be replaced by another SCN^- or by halogen ions.

A search has been carried out for radicals resulting from reaction of e_{aq}^- with NCO^-. We were particularly interested in this reaction (which might form $HC(O^-){=}\dot{N}$) because of the disagreement (mentioned above) between Ginns and Symons[5,6] and ourselves[4] concerning the esr parameters of that radical. (The difference in the proton hyperfine constants is far above the experimental errors of both laboratories.) Unfortunately, we could not observe any esr spectrum from a reaction of electrons with cyanate although a rate constant of 1.3×10^6 at pH 11 has been reported.[17] Our observations were made only near neutral pH where the above-mentioned radical was observed from a reaction of OH with HCN.[4] As another alternative we tried to obtain the same radical from an addition reaction of H atoms to the cyanate triple bond. A solution of 10^{-2} M KNCO and 10^{-1} M NaH_2PO_4 at pH 6.5 was irradiated. Under these conditions the electrons would react mainly with the phosphate to produce hydrogen atoms. Again, we failed to observe any spectrum.

Radiolysis of Carbamate Solutions. Radiolysis of solutions of methyl or ethyl carbamate was tried as a possible route to radicals related to $H\dot{N}CO_2^-$ since carbamic acid itself is not stable in aqueous solution. With 10^{-2} M solutions saturated with N_2O only weak spectra with magnetic parameters typical of carbon-centered radicals (see Table I) were obtained. There was no evidence for reaction of the OH radicals with the amino hydrogens.

$$OH + NH_2CO_2CH_3 \longrightarrow \dot{N}H_2CO_2CH_3 + H_2O \quad (6)$$

The hyperfine splittings and the g factors obtained here leave no doubt about the identification of these radicals. The hyperfine structure of the NH_2 group could not be completely resolved, probably because the nitrogen and the hydrogen splittings are of the same magnitude and some overlapping takes place.

In order to obtain the nitrogen-centered radicals we attempted to produce the N-chloro-substituted methyl and ethyl carbamates by allowing the esters to react with hypochlorite as described in the Experimental Section. These reaction mixtures were diluted to a concentration of 5×10^{-3} M (assuming complete reaction of the carbamate) and allowed to react with e_{aq}^- according to reaction 7 in N_2 saturated solution. At neutral pH only very

$$ClNHCO_2CH_3 + e_{aq}^- \longrightarrow H\dot{N}CO_2CH_3 \quad (7)$$

weak unidentified lines (in addition to weak lines of carbon-centered radicals) were observed. On increasing the pH to ~11 new spectra were obtained. The spectra are characterized by an 11-G triplet and a g value in the region of 2.0048. The spectrum obtained with methyl carbamate is shown in Figure 2. The spectrum of the radical derived from the ethyl ester was very similar but in this case the fine structure of each line was composed of four lines with an intensity distribution close to 1:2:2:1. Such a pattern can be explained if it is assumed that the five hydrogens in the C_2H_5 group have, by chance, comparable hyperfine constants and only four out of the six lines with the intensity distribution of 1:5:10:10:5:1 were observed. In each case no large proton splitting as in the case of $H\dot{N}CO_2^-$ was found. The absence of such a splitting forced us to assume that the radical produced in reaction 7 is dissociated at this pH.

$$H\dot{N}CO_2CH_3 \rightleftharpoons [\dot{N}CO_2CH_3]^{\pm} + H^+ \quad (8)$$

The lack of a spectrum in neutral and acid solutions can have several causes. If the radical is not charged (equilibrium 8 to the left), its second-order recombination rate constant will be greater than that of the charged radical and as a consequence its steady-state concentration will

TABLE I: Magnetic Parameters Obtained in the Electron Irradiation of Cyanate and Carbamate Derivatives in Aqueous Solutions[a]

Source	pH	Suggested radical	a^N, G	a^H, G	g
KCNO	8	$HNCO_2^-$	13.73	19.87	2.00425
KCNO	8	$^-O_2CNH-NCO_2^-$	9.82, 5.90	7.84	2.00404
KCNO	11.8–14	$^-O_2CNO_2^{-b}$	14.39		2.00503
$ClNHCO_2CH_3$	10.5	$^-NCO_2CH_3$	11.13	$a(CH_3)$ = 0.51	2.00483
$ClNHCO_2C_2H_5$	11.5	$^-NCO_2C_2H_5$	11.17	$a(C_2H_5)$ = 0.28[c]	2.00479
NH_2CO_2Et	7	$NH_2CO_2\dot{C}HCH_3$	(0.25)[d]	17.55 (α) 24.03 (β)	2.00280
NH_2CO_2Me	7	$NH_2CO_2\dot{C}H_2$	(0.29)[d]	19.72	2.00285

[a] Hyperfine constants accurate to ±0.03 G. The g factors were measured relative to the peak from the silica cell and are accurate to ±0.00005. Second-order corrections have been made. [b] This radical was identified by comparison of the parameters with those reported by Zeldes and Livingston.[15] Their values are a^N = 14.38 G and g = 2.00505. [c] A four-line pattern of approximate relative intensities 1:2:2:1 was observed, see text. [d] Approximate size of splitting, exact pattern, and number of lines not clear.

be lower. In addition, exchange of the proton might cause line broadening which will also reduce the intensity.

Because the chlorinated compounds were not isolated from the reaction mixture some doubts might be raised concerning the identity of the parent molecule and the resulting radical as given in reaction 7. The spectrum of the radical given in Figure 2 was not obtained without allowing the carbamate to react with HOCl, and it disappeared when the solution was bubbled with N_2O to scavenge the solvated electron. This technique of directly using the reaction mixture has not been employed in these laboratories for amides but has been successful for producing amino radicals such as $(CH_3)_2\dot{N}$.[18] From the value of a^N observed there is little doubt that a nitrogen-centered radical has been produced and the expected reaction 7 seems by far the most likely source. It is possible, of course, that some secondary reaction such as that encountered with cyanate in basic solution also occurs here. However, the use of e_{aq}^- as the radical source together with the fact that the hypochlorite reaction is generally very clean[10] and OH is scavenged by the alkyl groups on the esters suggests that no complications should arise.

In our previous investigation of the radiolysis of HCN[4] at neutral pH we claimed to produce a radical with the spectral parameters a^H = 27.44, $a^{H'}$ = 19.78 G, and g = 2.00426. No identification of this species which lacks a ^{14}N hyperfine splitting could be suggested. The parameters for this species resemble those of $H\dot{N}CO_2^-$ found in this work except that the value of a^H (= 27.44 G) is exactly twice the nitrogen splitting for $\dot{N}HCO_2^-$. This similarity brought us to repeat the experiment with HCN and to search for lines which were not observed before. Indeed, one missing line was found superimposed on a satellite of the signal from the cell. (In the previous work the line of the cell was very intense because of high modulation amplitudes.[4]) This missing line changes the 27.44-G hydrogen doublet into a 13.70-G nitrogen triplet and demonstrates the formation of $H\dot{N}CO_2^-$ in the HCN system. The mechanism of formation of this radical in the radiolysis of HCN is not clear but a secondary process is likely. Disproportionation of HC(OH)=$\dot{N}$ could lead, in part, to HOCN introducing cyanate into the cyanide system as a competitor for OH.

Discussion of Hyperfine Constants. Although it is sometimes difficult to use the magnitude of nitrogen hyperfine constants to uniquely identify a radical's structure it is clear that all of the radicals in Table I (with the exception of the last two) are to a large degree nitrogen centered. This conclusion follows from the size of a^H which is generally not above 10 G for radicals without a major contribution from a nitrogen-centered form. (The radical $\cdot CONH_2$ with a^N = 21.6 G[4,19] is a notable exception.) The primary radical derived from cyanate is best described by the structure $H\dot{N}CO_2^-$. This radical can be considered either as $\dot{N}H_2$ substituted with a CO_2^- group or as $\dot{C}O_3^-$ with NH replacing one of the oxygens. Because CO_2^- in the radical $\dot{C}H_2CO_2^-$ causes relatively little change in the magnetic parameters when this radical is compared with methyl itself, the former description seems best. The observed splittings are not greatly different than those of $\dot{N}H_2$ (a^N = 10.4 and a^H = 23.8 G)[20] and substitution can be expected to raise the value of a^N.[21] The radical $H\dot{N}CO_2^-$ is also closely related to the amido radicals $RCO\dot{N}R'$ studied by Danen and Gellert[22] and the parameters match those of the latter radicals ($a^N \sim 15$ G, g = 2.0044–2.0053) rather well. The radical designated as $^-O_2CNH\dot{N}CO_2^-$ is related to $H_2N\dot{N}H$ but with two substitutions. The magnetic parameters for hydrazyl adsorbed on a zeolite[23] are a^N = 8.8, $a^{N'}$ = 11.7, $a^H(NH)$ = 18.8, and $a^H(NH_2)$ = 2.3 G with the two NH_2 protons equivalent only at high temperature. Two other reports of dialkyl hydrazyls have appeared[24,25] with similar values for the nitrogen and NH proton hyperfine constants. The nitrogen hyperfine constants of $^-O_2CNH\dot{N}CO_2^-$ are similar to these various values but are somewhat smaller apparently as a result of delocalization onto the CO_2^- groups. The value of a^H (7.84 G) is considerably larger than the average value of 2.3 G for N_2H_3 but because this value is an average, a larger splitting for one of the NH_2 protons is possible. The radicals assigned as $^-\dot{N}CO_2CH_3$ and $^-\dot{N}CO_2C_2H_5$ are more of a problem as they appear to be dissociated in that no NH splitting is observed. Two structures are possible, namely, the amido form $ROC(=O)-\dot{N}^-$ with the orbital bearing the unpaired electron most likely conjugated with the carbonyl and the imino form $ROC(O^-)=\dot{N}$ with the singly occupied orbit-

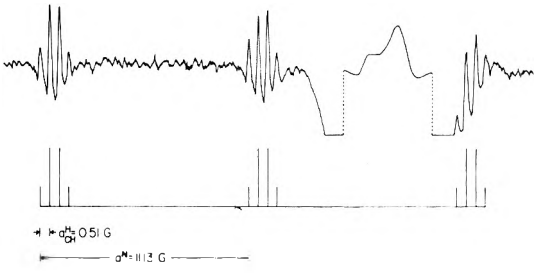

Figure 2. The esr spectrum obtained during the radiolysis of an N_2-saturated solution of methyl *N*-chlorocarbamate prepared as described in the text. The pH was 10.5.

al in the plane of the molecule. The g factor is the best indicator of which structure is present. The two values found are near 2.0048 (see Table I) and match those of $HN\dot{C}O_2^-$ (2.00425) and the other amido radicals (2.0044–2.0053)[22] much more closely than the value of 2.00325 for $HC(O^-)=\dot{N}$.[4] The amido form seems more likely, therefore. The identification, as given, implies that the pK of the NH proton in the ester form is several units lower than in $HN\dot{C}O_2^-$.

Conclusion

Study of the radicals present under conditions of OH attack on cyanate has allowed identification of the initial product as the adduct $HN\dot{C}O_2^-$. A secondary radical $^-O_2CNHN\dot{C}O_2^-$ is ascribed to H abstraction from the dimer of the primary radical. The primary reaction is similar to that observed with CN^- and HCN in that reaction at the carbon occurs. It seems unlikely that reaction of OH with thiocyanate follows a similar path as conversion of the intermediate $NCSOH^-$ to $(SCN)_2^-$ would then be difficult. No radicals resulting from e_{aq}^- reaction with cyanate were found.

References and Notes

(1) Supported in part by the U. S. Atomic Energy Commission.
(2) D. Behar, *J. Phys. Chem.*, **76**, 2517 (1972).
(3) D. Behar, P. L. T. Bevan, and G. Scholes, *J. Phys. Chem.*, **76**, 1537 (1972).
(4) D. Behar and R. W. Fessenden, *J. Phys. Chem.*, **76**, 3945 (1972).
(5) I. S. Ginns and M. C. R. Symons, *J. Chem. Soc., Dalton Trans.*, 185 (1972).
(6) I. S. Ginns and M. C. R. Symons, *J. Chem. Soc., Dalton Trans.*, 3 (1973).
(7) D. Behar and R. W. Fessenden, *J. Phys. Chem.*, **76**, 1706 (1972).
(8) F. Owens, R. A. Breslow, and O. R. Gillian, *J. Chem. Phys.*, **54**, 833 (1971).
(9) W. C. Easley and W. Weltner, *J. Chem. Phys.*, **52**, 197 (1970).
(10) W. S. Metcalf, *J. Chem. Soc.*, 148 (1942).
(11) K. Eiben and R. W. Fessenden, *J. Phys. Chem.*, **75**, 1186 (1971).
(12) D. Behar and R. W. Fessenden, *J. Phys. Chem.*, **76**, 1710 (1972).
(13) The OH proton splitting assigned to $HC(OH)=\dot{N}$ is 0.89 G.[4]
(14) N. V. Sidgwick, "The Chemical Elements and Their Compounds," Vol. I, Oxford, 1950, p 673.
(15) H. Zeldes and R. Livingston, *J. Amer. Chem. Soc.*, **90**, 4540 (1968).
(16) P. Neta, private communication.
(17) M. Anbar and E. J. Hart, as reported by M. Anbar and P. Neta, *Int. J. Appl. Radiat. Isotopes*, **18**, 493 (1967).
(18) R. W. Fessenden and P. Neta, *J. Phys. Chem.*, **76**, 2857 (1972).
(19) R. Livingston and H. Zeldes, *J. Chem. Phys.*, **47**, 4173 (1967).
(20) E. L. Cochran, F. J. Adrian, and V. A. Bowers, *J. Chem. Phys.*, **51**, 2759 (1969).
(21) For instance, the value of a^N for $(CH_3)_2\dot{N}$ in aqueous solution is 15.65 G.[18] (In nonpolar solvents the value is slightly higher, W. C. Danen and T. T. Kensler, *J. Amer. Chem. Soc.*, **92**, 5235 (1970)).
(22) W. C. Danen and R. W. Gellert, *J. Amer. Chem. Soc.*, **94**, 6853 (1972).
(23) R. Fantechi and G. A. Helcke, *J. Chem. Soc., Faraday Trans. 2*, **68**, 942 (1972).
(24) D. E. Wood, C. A. Wood, and W. A. Lathan, *J. Amer. Chem. Soc.*, **94**, 9278 (1972).
(25) V. Malatesta and K. V. Ingold, *J. Amer. Chem. Soc.*, **95**, 6110 (1973).

New Asymmetric Dielectric Relaxations in Two Liquid Triacetates

Eiji Ikada* and Teizo Watanabe

Faculty of Engineering, Kobe University, Nada, Kobe, 657, Japan *(Received August 7, 1973)*

The dielectric properties of liquid glyceryltriacetate and 1,2,6-hexanetriacetate were studied. The dielectric constants and losses were measured over the frequency range from 23 Hz to 3 MHz and at temperatures from −60 to 60°. The measured values of the static dielectric constants of the two triacetates were between 6 and 10 at the experimental temperatures and are much smaller than those of the corresponding hydroxyl-substituted compounds. The two triacetates showed asymmetric dielectric relaxations at low temperatures. The loci of the Cole–Cole plots did not fit those of the Davidson–Cole-type relaxations, but could be expressed by the Havriliak–Negami equation $\epsilon^* - \epsilon_\infty = (\epsilon_0 - \epsilon_\infty)/[1 + (j\omega\tau_0)^{1-\alpha}]^\beta$. It was found that the values of the distribution parameters $(1 - \alpha)$ and β for glyceryltriacetate, 1,2,6-hexanetriacetate, and poly(vinyl acetate) were approximately equal. It was concluded that the asymmetric dielectric relaxations were apt to appear in chain molecules containing multiple polar groups. The relaxation mechanism of these triacetates was discussed in contrast with those of the polyhydroxyl compounds, which showed the Davidson–Cole-type relaxations.

Introduction

It is well known that liquid or supercooled polyhydroxyl compounds such as diols and triols exhibit Davidson–Cole-type asymmetric dielectric relaxations[1-3] which can be expressed by the equation[1]

$$\epsilon^* - \epsilon_\infty = \frac{\epsilon_0 - \epsilon_\infty}{(1 + j\omega\tau_0)^\beta} \qquad (1)$$

where ϵ^* is the complex dielectric constant, ϵ_0 and ϵ_∞ are the limiting low- and high-frequency dielectric constant, respectively, j is the imaginary unit, ω is the angular frequency, τ_0 is the mean relaxation time, and β is the distribution parameter of the relaxation times.

On the other hand, the Cole–Cole plots of the principal relaxations of polar polymers in the glass–rubber transition region (so-called "α relaxation") generally show another asymmetric curve[4,5] which is in most cases flatter than those for the polyhydroxyl compounds.

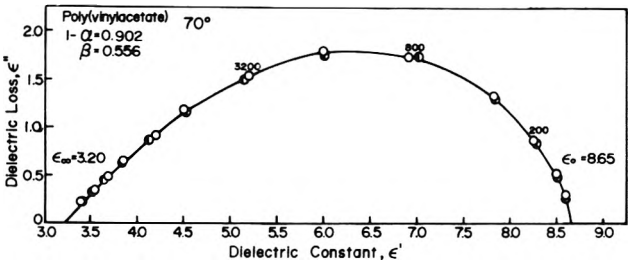

Figure 1. Cole–Cole plot for PVAc. ϵ' and ϵ'' of this plot were measured by Ishida, *et al.* (Y. Ishida, M. Matsuo, and K. Yamafuji, *Kolloid-Z. Z. Polym.*, **180**, 108 (1961).): O, experimental points; ◐, calculated points obtained by using the Havriliak–Negami equation. $(1 - \alpha)$ and β were determined by the method described in Appendix. Numbers beside data points denote frequency in Hz.

Havriliak and Negami[4] suggested a new empirical equation to fit asymmetric α relaxations showing this wider distribution of relaxation times

$$\epsilon^* - \epsilon_\infty = \frac{\epsilon_0 - \epsilon_\infty}{[1 + (j\omega\tau_0)^{1-\alpha}]^\beta} \qquad (2)$$

where each parameter has the same physical meaning as described above, and $(1 - \alpha)$ is another distribution parameter of the relaxation times. Apparently this equation is comprised of both the Cole–Cole[6] and the Davidson–Cole equations. Therefore, for $(1 - \alpha) = 1$, the Havriliak–Negami equation corresponds to the Davidson–Cole equation, and the Davidson–Cole-type relaxation may be considered as a limiting case of the Havriliak–Negami-type relaxation.

As most Davidson–Cole-type relaxations have been generally observed for polyhydroxyl compounds, it was at first concluded that such relaxations were characteristic for polyhydroxyl compounds which formed molecular clusters *via* intermolecular hydrogen bonds. The same type of relaxation was, however, also observed in non-hydrogen-bonded liquids such as isoalkyl halides[7,8] and alkanethiols,[9] therefore, this conclusion was partly denied.

On the other hand, α relaxations of poly(vinyl acetate) (PVAc) have been studied by many workers[10,11] and it has been reported that the Cole–Cole loci of PVAc closely resembled those of the Davidson–Cole-type asymmetric relaxation seen in Figure 1. The apparent similarity in the shape of Cole–Cole curves for the polyhydroxyl compounds and for PVAc is very interesting to us.

The purpose of this work is to study the relationship between the two asymmetric relaxations, *i.e.*, the Davidson–Cole and the Havriliak–Negami-type relaxations. The two triacetates were selected as low-molecular weight model compounds of PVAc, and the dielectric properties of these two triacetates were compared with those of the polyhydroxyl compounds which showed Davidson–Cole-type relaxation.

Experimental Section

Materials. 1,2,6-Hexanetriol (1 mol) was acetylated with 1.5 mol of acetic anhydride and 4.5 mol of pyridine at 100° for 3 hr. The product was distilled twice under reduced pressure to remove pyridine and acetic anhydride. Residual unreacted hydroxyl groups were checked by infrared absorption of the OH stretching vibration and it was found that the quantity of the residual hydroxyl groups was negligibly small. Commercial glyceryltriacetate of the specified grade was used without purification. Density and refractive index were determined by the Lypkin-type pycnometer and by the Pulfrich refractometer, respectively. The physical constants of the two triacetates are collected in Table I.

TABLE I: Physical Constants of the Two Triacetates

Temp, °C	Densities, g/ml	Refractive indices, nD
	Glyceryltriacetate	
10.0	1.1698	
20.0	1.1597	1.4313
30.0	1.1489	1.4272
	1,2,6-Hexanetriacetate	
10.0	1.1045	
20.0	1.0958	1.4389
30.0	1.0861	1.4352

Dielectric Measurement. Dielectric constants and losses were measured by a ratio arm transformer bridge (Ando Electric Co., type TR-1BK) over the frequency range from 23 Hz to 3 MHz. The dielectric cell was a concentric platinum glass cell having a geometrical capacity of 13.0 pF. Temperature measurement of the cell was determined using a Au–Co *vs.* Cu thermocouple and a standard thermometer. The glass cell was immersed in a well-stirred alcohol bath at the lower temperatures and in a water bath at the higher temperatures.

Results and Discussion

Static Dielectric Constant. Temperature dependences as expressed by plots of the static dielectric constants against the reciprocal of absolute temperature are well represented by straight lines as shown in Figure 2. The values of the static dielectric constants of both triacetates vary between 6 and 10 in the experimental temperature range. These values are much smaller than those of glycerol[1] and 1,2,6-hexanetriol,[3] which are equal to *ca.* 60, because the substitution of the hydroxyl groups in the triols by the acetoxyl group leads to the absence of formation of molecular clusters by intermolecular hydrogen bonding OH···O.

The dipole moments of glyceryltriacetate and 1,2,6-hexanetriacetate were calculated from the static dielectric constants by means of the Onsager equation[12]

$$\epsilon_0 = \epsilon_\infty + \frac{\epsilon_0}{2\epsilon_0 + \epsilon_\infty}\left(\frac{\epsilon_\infty + 2}{3}\right)^2 \frac{4\pi N_0 \mu_0^2}{3kT} \qquad (3)$$

where ϵ_0 and ϵ_∞ are the limiting low- and high-frequency dielectric constants, respectively, N_0 is the number of molecules per cubic centimeter, μ_0 is the dipole moment *in vacuo*, and kT is the thermal energy. The calculated values of the dipole moment vary from 2.44 to 2.57 D as the temperature increases from −60 to −7.4° for 1,2,6-hexanetriacetate and from 2.33 to 2.49 D as the temperature increases from −58.1 to 40° for glyceryltriacetate.

Dielectric Relaxation. Both 1,2,6-hexanetriacetate and glyceryltriacetate showed dielectric dispersion and absorption over the experimental frequency and temperature ranges. The plots of frequency dependence of dielectric loss for the two triacetates are broad and asymmetric as often seen in the curves for the diol and the triol, but the shapes of the curves do not change markedly at different measuring temperatures. The Cole–Cole plots of 1,2,6-hexanetriacetate and glyceryltriacetate are shown in Figures 3 and 4, respectively. Apparently, these arcs closely resemble those expressed by the Davidson–Cole equation, but do not coincide with the arc calculated according to this equation, as is shown in Figure 5. Davidson and Cole

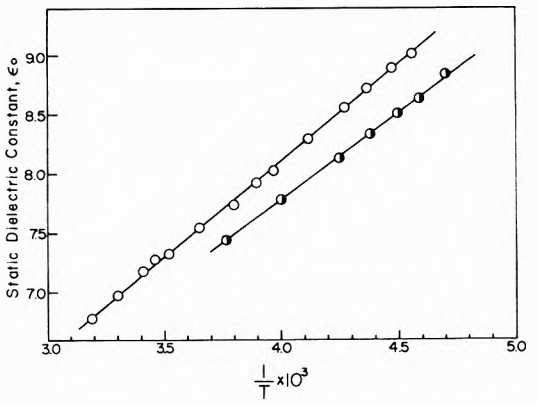

Figure 2. Temperature dependence of the static dielectric constants: O, glyceryltriacetate; ◑, 1,2,6-hexanetriacetate.

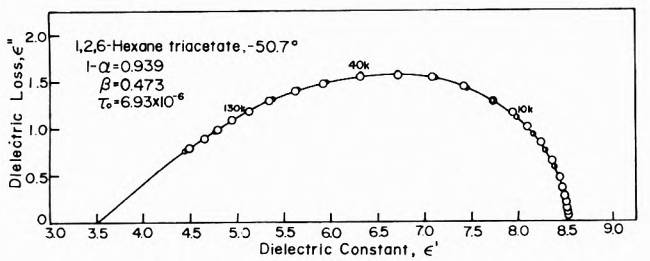

Figure 3. Typical Cole–Cole plot for 1,2,6-hexanetriacetate: O, experimental points; ◑, calculated points.

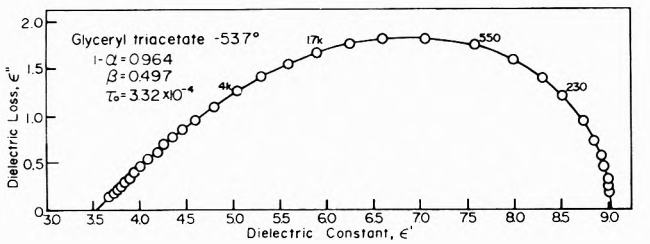

Figure 4. Typical Cole–Cole plot for glyceryltriacetate. In this figure agreement between the calculated points and the experimental points is so good as to render them indistinguishable. The calculated points were therefore omitted from this figure.

reported that the plot of log tan$[\beta^{-1} \tan^{-1}\{\epsilon''/(\epsilon' - \epsilon_\infty)\}]$ against log frequency gives a straight line having a slope of ½ if the observed arc fits the Davidson–Cole-type relaxation.[1] This method was applied for the observed arcs of these triacetates and various values for ϵ_∞ and β were tried. No plot, however, gave a straight line. Typical plots are shown in Figure 6. It can be concluded from this result that the asymmetric dielectric relaxations of the triacetates cannot be represented by the Davidson–Cole equation although the shapes of the Cole–Cole arcs closely resemble those of the Davidson–Cole-type relaxation. The new empirical equation suggested by Havriliak and Negami to describe the asymmetric dielectric relaxation was examined to ascertain its applicability for these experimental loci. Ikada and Watanabe reported that the asymmetric α relaxations of the various kinds of acrylonitrile–butadiene copolymers could be well represented by the Havriliak–Negami equation.[5]

The real and imaginary parts of eq 2 are given by

$$\epsilon' - \epsilon_\infty = (\epsilon_0 - \epsilon_\infty) r^{-\beta/2} \cos \beta\theta \qquad (4a)$$

$$\epsilon'' = (\epsilon_0 - \epsilon_\infty) r^{-\beta/2} \sin \beta\theta \qquad (4b)$$

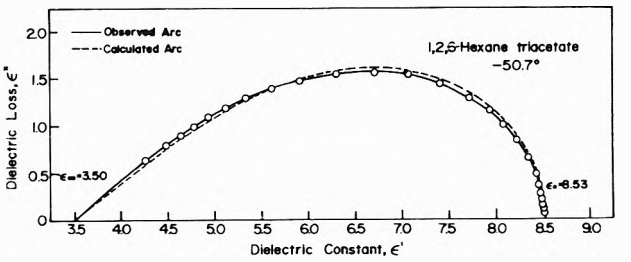

Figure 5. Comparison of the calculated locus of the Davidson–Cole-type relaxation with the experimental locus: O, experimental points at each experimental frequency. Dotted line shows the calculated locus of the Davidson–Cole-type relaxation. The distribution parameter β of the calculated locus is 0.422.

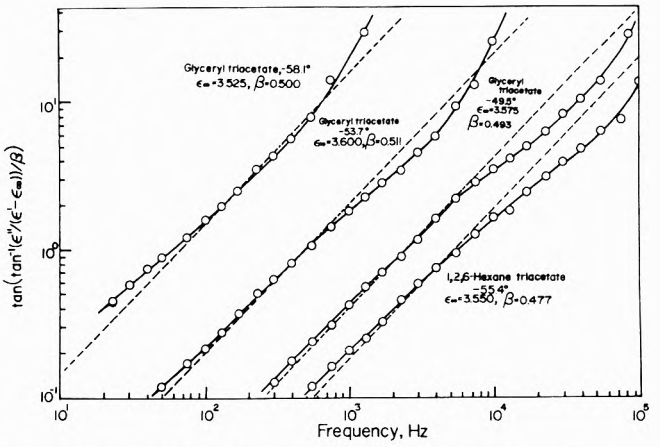

Figure 6. Log tan $[\beta^{-1} \tan^{-1} \epsilon''/(\epsilon' - \epsilon_\infty)]$ *vs.* log frequency.

with

$$r = [1 + (\omega\tau_0)^{1-\alpha} \sin \alpha(\pi/2)]^2 + [(\omega\tau_0)^{1-\alpha} \cos \alpha(\pi/2)]^2 \qquad (4c)$$

and

$$\theta = \tan^{-1}\left[\frac{1 + (\omega\tau_0)^{1-\alpha} \cos \alpha(\pi/2)}{(\omega\tau_0)^{1-\alpha} \sin \alpha(\pi/2)}\right] \qquad (4d)$$

Determination of the five numerical constants $(1 - \alpha)$, ϵ_0, ϵ_∞, β, and τ_0 was carried out by the same method described in Appendix. The calculated ϵ' and ϵ'' at each measuring frequency f were obtained by introducing the five numerical constants and ω $(= 2\pi f)$ into eq 4a–d. The experimental values of ϵ_0, ϵ_∞, $(1 - \alpha)$, β are collected in Table II. Comparison of the calculated values for 1,2,6-hexanetriacetate at −50.7° with the experimental points is shown in Figure 3. The experimental points for glyceryltriacetate at −53.7° agreed almost completely with the calculated values. Other experimental arcs for both triacetates at different temperatures also agreed well with calculated arcs. The Havriliak–Negami equation is therefore considered to be a good representation of the dielectric relaxation of these two triacetates. Although most of the dielectric relaxations of the polar low molecules have been treated by the Debye,[13] the Cole–Cole,[6] and the Davidson–Cole equations, some exceptional relaxations could not be expressed by the above three equations. Recently, the dielectric relaxations of α,ω-dibromoalkanes such as 1,4-dibromobutane, 1,6-dibromohexane, 1,8-dibromooctane, and 1,10-dibromodecane were studied by Garg and coworkers.[14] The shapes of their experimental Cole–Cole arcs also resemble those of the Davidson–Cole-type relaxation, but the observed arcs deviate from the arcs calcu-

TABLE II: Relaxation Parameters of Two Triacetates and PVAc

Temp, °C	ϵ_0	ϵ_∞	$1 - \alpha$	β	τ_0
		Glyceryltriacetate			
−58.1	9.20	3.49	0.915	0.523	2.65×10^{-3}
−53.7	9.03	3.53	0.964	0.497	3.32×10^{-4}
−49.5	8.89	3.55	0.967	0.494	6.50×10^{-5}
−43.5	8.73	3.53	0.954	0.483	8.38×10^{-6}
−39.1	8.56	3.65	0.982	0.484	1.33×10^{-6}
		1,2,6-Hexanetriacetate			
−60.5	8.88	3.55	0.945	0.525	5.69×10^{-4}
−55.4	8.73	3.53	0.888	0.533	2.59×10^{-5}
−50.7	8.53	3.50	0.939	0.473	6.93×10^{-6}
−44.9	8.33	3.50	0.934	0.489	1.52×10^{-6}
−37.7	8.13	3.53	0.936	0.487	3.12×10^{-7}
		Poly(vinyl acetate)[a]			
70.0	8.65	3.20	0.902	0.556	2.24×10^{-4}

[a] Calculated by using the experimental data of Ishida, *et al.*

lated for the Davidson–Cole-type relaxation. A similar result is seen in the measured Cole–Cole arcs of *n*-octyl iodide.[15]

Chain molecules which contain more than two polar groups are likely to show asymmetric dielectric relaxations such as the Davidson–Cole or the Havriliak–Negami-type relaxation. This deduction holds not only for the dielectric relaxations of polyhydroxyl compounds such as diols and triols, but also for those of the triacetates, polar polymers, and α,ω-dibromoalkanes. All of these compounds contain multiple polar groups in a molecule. On the other hand, polar molecules which contain one polar group do not generally show asymmetric relaxation, but show Debye or Cole–Cole-type relaxation, with the exception of some alkane halides. Hence it is considered that the interrelation of the motion of each polar group may be associated with the asymmetric dielectric relaxations.

It is reported that glycerol[1] and 1,2,6-hexanetriol[3] show Davidson–Cole-type relaxations. It is apparent that the significant difference between the triol and the triacetate can be ascribed to whether the hydrogen bond exists in the liquid structure or not. The polyhydroxyl molecules, where breaking and re-forming of the hydrogen bond must occur on relaxation, exhibit Davidson–Cole-type relaxation. Triacetates which do not contain the hydrogen bond show Havriliak–Negami-type relaxation which has the two kinds of distribution of relaxation times. This behavior coincides with the fact that the hydrogen-bonding normal alcohols show the single Debye-type behavior,[16] and the non-hydrogen-bonding mono-substituted alkanes such as *n*-alkyl bromides show a distribution of the relaxation times as seen in the Cole–Cole-type relaxation.[17]

At the same time, it was found that two kinds of the distribution parameters $(1 - \alpha)$ and β seemed to be associated with the acetate molecules. The three acetate molecules PVAc, glyceryltriacetate, and 1,2,6-hexanetriacetate show nearly the same values for $(1 - \alpha)$ and β which are *ca.* 0.9 and 0.5, respectively, as is shown in Table II. Therefore, these values of the two distribution parameters are characteristic of the acetoxyl-substituted chain molecules. It is interesting that long-chain PVAc and short-chain triacetates exhibit the same distribution of relaxation times. Judging from this fact, it may be concluded that the relaxation mechanism is independent of the chain length of the relaxing molecules and that the short-range motional unit takes part in the so-called segmental relaxation in the long-chain molecule.

The distribution parameter β in the Davidson–Cole equation of α,ω-dibromoalkanes reported by Garg, *et al.*, has nearly the same value for various chain lengths. Accordingly, it is supposed that the distribution of relaxation times of these dibromoalkanes is independent of the orientations between the two terminal dipole moments.

The distribution function of the Davidson–Cole-type relaxation indicates that this relaxation consists of cooperative mechanisms. According to Glarum, for example, one of these cooperative mechanisms is dipolar reorientation as a whole and the other is the diffusion of defects such as holes.[18] On the other hand, Litovitz and McDuffie regard the two mechanisms as dipolar reorientation and the breaking and re-forming of hydrogen-bonded clusters.[19]

Hoffman and Pfeiffer proposed a multiple potential barrier model for the dielectric relaxation for a single rotator in a crystalline field and they explained that this jump theory might also be applied in the case of polar long-chain compounds with a number of accessible orientation sites.[20] From their theoretical calculation asymmetric loss curves were obtained for the two-sites model. Recently Jernigan studied theoretically the internal relaxation modes of α,ω-dibromo-*n*-alkanes and also obtained slightly asymmetric Cole–Cole arcs from the dipolar correlation function.[21]

It is similarly supposed from the above discussions of the mechanism of the Davidson–Cole-type relaxation that the cooperative mechanisms may coexist in the relaxation process of chain molecules containing multiple polar groups. When a reference polar group rotates or oscillates perpendicularly to the chain axis, this motion induces the successive rotation or oscillation of neighboring polar groups such as a side chain or a chain-end group consecutively, like the propagation of a wave. The amplitude of the induced oscillation may be smaller than that of the original oscillation of the reference group because the successive motion is attenuated in the viscous medium (propagation along the skeletal chain). Then the induced motion shows shorter relaxation times than those of the reference relaxing group. Hence the asymmetric distribution of the relaxation times appears. Another explanation follows: Polar molecules in a viscous medium generally show dielectric relaxation due to molecular reorientation as a whole in the liquid state. In addition to this relaxation, the polar subgroups of the molecules, such as the side chain and the chain-end group, may show local mode relaxations whose relaxation times are shorter than those of the molecular reorientation. This superposition of the multiple relaxation modes may yield the cooperative phenomenon of the molecular relaxation process. Also several possible motions are considered for the molecular relaxation mechanism of these two triacetates, such as molecular rotation as a whole, internal rotation of the side group perpendicularly to the skeletal chain, and the local motion in the acetoxyl group.

The relaxation times of the triacetates plotted against the reciprocal of the absolute temperature are shown in Figure 7. As can be seen in this figure, the relaxation times of glyceryltriacetate are longer than those of 1,2,6-hexanetriacetate in the experimental temperature ranges. This result is interesting since the molecular diameter of 1,2,6-hexanetriacetate is greater than that of glyceryltriacetate. On the other hand, the relaxation times of glycerol[1] are shorter than those of 1,2,6-hexanetriol[3] as expected

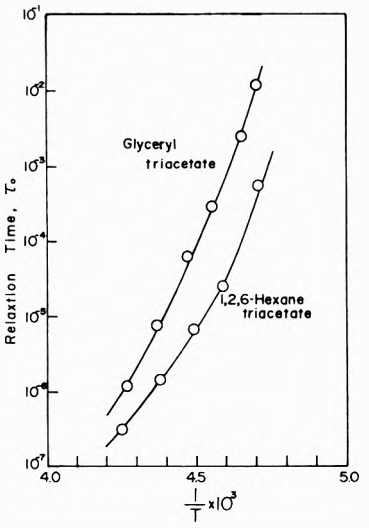

Figure 7. Temperature dependence of relaxation times of the two triacetates.

from their molecular dimensions. It is known that the relaxation times of polar molecules in the liquid state are generally proportional to the molecular diameter. As is seen in Figure 7, the Arrhenius plots of the relaxation times of the triacetates do not show a straight line. This tendency is often seen in the Arrhenius plots of hydrogen bonding liquids and in the α relaxations of polymers, and is known as "WLF-type behavior."

Appendix

The Method of Determination of ϵ_0, ϵ_∞, τ_0, $(1 - \alpha)$, *and* β.[4] The limiting low-frequency dielectric constant ϵ_0 and the limiting high-frequency dielectric constant ϵ_∞ are obtained by extrapolating the experimental locus to the low- and high-frequency intercepts on the real axis, respectively.

Dividing eq 4b by 4a, the following relationship is obtained

$$\tan \phi = \frac{\epsilon''}{\epsilon' - \epsilon_\infty} = \tan \beta\theta \qquad (5)$$

Using eq 4d, we can deduce the following relationship

$$\lim_{\omega\tau_0 \to \infty} \tan \theta = \lim_{\omega\tau_0 \to \infty} \tan (\phi/\beta) = \tan (\phi_L/\beta) = \cot \alpha(\pi/2) \qquad (6)$$

Hence

$$\phi_L = (1 - \alpha)\beta(\pi/2) \qquad (7)$$

where ϕ_L is the high-frequency limiting angle made by the experimental locus with the real axis.

The relaxation time τ_0 is obtained by determining the crossing point of the bisector of the asymptotic angle ϕ_L with the locus. This crossing point corresponds to the relaxation frequency ($\frac{1}{2}\pi\tau_0$). The distribution parameter $(1 - \alpha)$ is obtained from the following relationship

$$\frac{1}{\phi_L} \log \frac{|\epsilon^*_{(\omega\tau_0=1)} - \epsilon_\infty|}{\epsilon_0 - \epsilon_\infty} = -\frac{1}{\pi(1 - \alpha)} \log [2 \sin \alpha(\pi/2)] \qquad (8)$$

where $|\epsilon^*_{(\omega\tau_0=1)} - \epsilon_\infty|$ is the distance between ϵ_∞ and $\epsilon^*_{(\omega\tau_0=1)}$.

References and Notes

(1) D. W. Davidson and R. H. Cole, *J. Chem. Phys.*, **19**, 1484 (1951).
(2) E. Ikada, *J. Phys. Chem.*, **75**, 1240 (1971).
(3) G. E. McDuffie, Jr., and T. A. Litovitz, *J. Chem. Phys.*, **37**, 1699 (1962).
(4) S. Havriliak and S. Negami, *J. Polym. Sci., Part C*, **14**, 99 (1966).
(5) E. Ikada and T. Watanabe, *J. Polym. Sci., Polym. Chem. Ed.*, **10**, 3457 (1972).
(6) K. S. Cole and R. H. Cole, *J. Chem. Phys.*, **9**, 341 (1941).
(7) D. J. Denny, *J. Chem. Phys.*, **27**, 259 (1957).
(8) J. G. Berberian and R. H. Cole, *J. Amer. Chem. Soc.*, **90**, 3100 (1968).
(9) Krishnaji, V. K. Agarwal, and P. Kumar, *J. Chem. Phys.*, **56**, 5034 (1972).
(10) D. J. Mead and R. M. Fuoss, *J. Amer. Chem. Soc.*, **63**, 2832 (1941).
(11) K. Yamafuji, H. Ichikawa, F. Irie, and Y. Ishida, *Kolloid-Z. Z. Polym.*, **181**, 160 (1962).
(12) L. Onsager, *J. Amer. Chem. Soc.*, **58**, 1486 (1936).
(13) See, *e.g.*, C. P. Smyth, "Dielectric Behavior and Structure," McGraw-Hill, New York, N. Y., 1955, Chapter V.
(14) S. K. Garg, W. S. Lovell, C. J. Clemett, and C. P. Smyth, *J. Phys. Chem.*, **77**, 232 (1973).
(15) F. I. Mopsik and R. H. Cole, *J. Chem. Phys.*, **44**, 1015 (1966).
(16) F. X. Hassion and R. H. Cole, *J. Chem. Phys.*, **23**, 1756 (1955).
(17) E. J. Hennely, W. H. Heston, Jr., and C. P. Smyth, *J. Amer. Chem. Soc.*, **70**, 4102 (1948).
(18) S. H. Glarum, *J. Chem. Phys.*, **33**, 639 (1960).
(19) T. A. Litovitz and G. E. McDuffie, Jr., *J. Chem. Phys.*, **39**, 729 (1963).
(20) J. D. Hoffman and H. G. Pfeiffer, *J. Chem. Phys.*, **22**, 132 (1954).
(21) R. J. Jernigan, "Dielectric Properties of Polymers," F. E. Karasz, Ed., Plenum Press, New York, N. Y., 1972, p 99.

Contribution to the Statistical Theory of Polyfunctional Polymerization

P. Luby

Institute of Chemistry, Slovak Academy of Sciences, 809 33 Bratislava, Czechoslovakia *(Received October 31, 1972; Revised Manuscript Received December 17, 1973)*

Molecular size distribution in multichain polymers formed by polyfunctional homopolymerization of a single kind of repeat unit is calculated theoretically. An expression was derived for the weight fraction distribution of isomers of certain composition of units defined by a vector **u**. Molecular size distribution equations were derived explicitly as functions of link distribution. A formula was deduced for the link distribution, more generally than it was done for a linear substitution effect.

1. Introduction

In the last decade the classical statistical theory[1] of the molecular size distribution in polyfunctional polycondensation of a single kind of repeating unit of functionality f has been considerably developed. A variety of theoretical studies[2-7] applying various conceptions contributed to the state of this knowledge.

E.g., Whittle[2] shows an interesting method of specification of a polymerization process making use of the theory of stochastic processes. Besides the cyclization effect his conception allows for the neighboring-group effect which means that the reactivity of any functional group depends on how many other groups of the same unit have already reacted. This effect was involved in stochastic graph theory of Matula, *et al.*,[3] also, who called it the "reorganization heat order." It was also treated by Gordon's statistical mechanical approach and he called it the "first shell substitution effect."

Although there is no attempt at a detailed analysis of the above theories, special attention is devoted to that of Gordon, *et al.*, which appeared to be the most successful.

The latter approach which was verified by experimental evidence[5] allows for the effects of substitution and of intramolecular bonds. The theory of cascade processes based on the so-called probability generating functions (pgf) is a powerful tool to solving this problem. Various statistical moments, gel point, and sol fraction may be calculated in this way, without the need of pertinent summations.

However, a distribution equation expressing directly the fractions of individual $x$mer species is missing, except for the random ideal case and a small linear substitution effect.[4] Instead complicated expansions[6] of the pgf and extractions of certain coefficients of the power functions are necessary. An expression evaluating these quantities directly is needed. For this purpose link distribution functions (ldf, see section 2) were applied in the present paper without the pgf.

As is obvious the use of ldf enables a clear separation of the combinatorial problem from thermodynamical and kinetical considerations.[4] This fact is used in this work also and the distribution equations (17, 18, 21) thus derived are applicable both to the thermodynamically and kinetically controlled reaction of homopolymerization of a single kind of repeating unit of functionality f. The conversion degree α given by the fraction of reacted groups in the system is taken as an independent variable throughout this paper.

Restriction is, however, made to the case, when the influence of any reacted group is limited to the reactivities of groups of the same unit. This effect will be understood when using the term substitution effect (se) hereafter. The problem of higher shell se (these are by far less efficient) as well as intramolecular condensation in the sol phase is beyond the scope of this paper. Calculations related to molecular distribution are not possible without approximations[3] in these cases.

2. Link Distribution Function

All units of the reaction mixture may be divided into $f + 1$ types U_i, where $i = 0, 1 \ldots f$ denotes the number of functional groups of a monomer unit of f that have reacted. The number fractions p_i of these types of units form the link distribution and are equal to the probability that a randomly chosen unit is an U_i. The ldf in the thermodynamically controlled reversible reaction is briefly mentioned in this section. The formula (5) is derived for the ldf in a kinetically controlled (irreversible) reaction with somewhat higher generality than it was done for a linear se (eq 8).

When the reaction is reversible, relation 1 follows directly from the theory of Gordon, *et al.*[4]

$$p_i = P_i \sum_0^f P_i \tag{1}$$

where

$$P_i = {}^fC_i(1-\gamma)^{f-i}\gamma^i \exp\left[-\left(\sum_{m=0}^{i-1}\psi_m/RT\right)\right] \tag{2}$$

${}^fC_i$ denotes a combinatorial number with the parameters f, i. γ is a conversion parameter given as an implicit function of α

$$\alpha = \sum_0^f iP_i / \sum_0^f P_i \tag{3}$$

ψ_m is an additional term to the standard free energy of forming a bond between two units which is responsible for the se of m already reacted groups of the unit under consideration. The se is fully determined by $f - 1$ of these parameters while $\psi_0 = \psi_{-1} = \psi_f = 0$.

The problem of an irreversible (kinetically controlled) reaction was described by the same authors[4] for the so-called linear se. Their treatment may easily be generalized to the case of an ordinary se when modifying the kinetic rate equations in the following way.

$$-\mathrm{d}p_i/\mathrm{d}t = k[(f - i)p_i \exp(\psi_i/RT) - (f - i + 1)p_{i-1} \times \exp(\psi_{i-1}/RT)]\sum_{0}^{f-1}(f - i)p_i \exp(\psi_i/RT) \quad (4)$$

where formally $p_{-1} = 0$. When dividing (4) by the expression $-\mathrm{d}p_0/\mathrm{d}t$ one obtains f linear differential equations which may be integrated subsequently in order $i = 1, 2$ etc. up to $i = f$. General solution of these equations is as follows

$$p_i = \left(\prod_{q=0}^{i-1}\rho_q\right)\sum_{j=0}^{i} p_0^{\rho_j}/\left[\prod_{\substack{m=0\\ m\neq j}}^{i}\right](\rho_m - \rho_j) \quad (5)$$

where any ρ_i is defined as

$$\rho_i = (f - i)\{\exp[-(\psi_i/RT)]\}/f \quad (6)$$

(analogously ρ_j, ρ_q, and ρ_m).

Equation 5 transforms to eq 8 describing a linear se when substituting

$$\psi_i = iRT \ln N^2 \quad (7)$$

in (6) and therefore in (5) (*cf.* ref 4, eq 83)

$$p_i = N^{i(i-1)}\frac{f!}{(f-i)!}\sum_{j=0}^{i}\frac{p_0^{N^2j(f-j)/f}}{\prod_{\substack{m=0\\ m\neq j}}^{i}[(f-m)N^{2m} - (f-j)N^{2j}]} \quad (8)$$

N is a constant determining the character of a linear se f equations of the type (5) together with the trivial relation (9) form a complete system with $f + 1$ variables.

$$\sum_{0}^{f} ip_i = \alpha f \quad (9)$$

3. Derivation of the Weight Fraction Distribution Equation

The first step in deducing the distribution equation from the known ldf is to find the weight fraction $w_x(\mathbf{u})$ of those $x$mers which have the same composition $\mathbf{u}$. A vectorial notation (Clarendon type) is used to designate this composition

$$\mathbf{u} \equiv (u_1, u_2 \ldots u_f)$$

This means that an $x$mer of the type X_u consists of u_1, u_2 $\ldots$ u_f units of the types U_1, U_2 $\ldots$ U_f, respectively, where $u_1 + u_2 + \ldots u_f = x > 1$. The idea of classification of isomers according to their $\mathbf{u}$ vector is not new. It was used by many other authors who solved problems more or less similar to that of ours (*e.g.*, ref 2 and 8).

The value of $w_x(\mathbf{u})$ is equal to the probability of finding a randomly chosen unit to be a part of X_u. If we specify that the randomly chosen unit must be U_i then the corresponding probability $w_{xi}(\mathbf{u})$ will be

$$w_{xi}(\mathbf{u}) = p_i\left[\frac{p_i}{\alpha f}\right]^{u_1}\left[\frac{2p_2}{\alpha f}\right]^{u_2}\cdots\left[\frac{ip_i}{\alpha f}\right]^{u_i-1}\cdots\left[\frac{fp_f}{\alpha f}\right]^{u_f} n_{xi}(\mathbf{u}) \quad (10)$$

Substituting

$$b_i = ip_i/\alpha f \quad (11)$$

we obtain after rearrangement

$$w_{xi}(\mathbf{u}) = \alpha f i^{-1}\mathbf{b}^{\mathbf{u}} n_{xi}(\mathbf{u}) \quad (12)$$

where the expression $\mathbf{b}^{\mathbf{u}}$ denotes

$$\mathbf{b}^{\mathbf{u}} = b_1^{u_1} b_2^{u_2} \ldots b_f^{u_f} \quad (13)$$

Here, any b_i denotes the probability that an arbitrary reacted group is attached to some U_i. This value is given by the quotient of reacted groups of all U_i's (ip_i) and all reacted groups in the system (Σip_i), viz. eq 9, $n_{xi}(\mathbf{u})$ is the number of all possible configurations, in which the remaining part of a given X_u may occur with respect to the U_i under consideration (see Appendix).

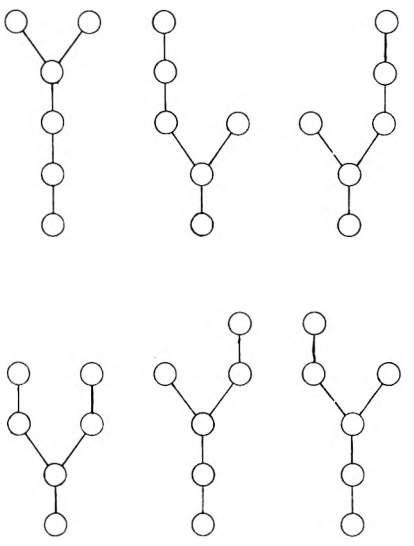

Figure 1. The six distinct ordered trees of composition $u_1 = 3$, $u_2 = 2$, $u_3 = 1$, rooted on a terminal vertex. Their number is given $n_{6,1}(3,2,1) = 4!/2!2!$. Two distinct isomorphic classes are arranged in the upper and the bottom row separately.

In the terminology used in graph theory, any U_i may be called a vertex with i edges. $n_{xi}(\mathbf{u})$ would be the number of distinct ordered trees rooted on a vertex with i edges and consisting of u_1, u_2, $\ldots$, u_f vertices which have one, two, etc., up to f edges, respectively.

It should be emphasized that distinct isomorphic classes of molecular trees may refer to certain $\mathbf{u}$ (Figure 1). The number $n_{xi}(\mathbf{u})$ should therefore be taken as a cumulative one.

Gordons theorem 1 (*cf.* ref 7) proved to be a useful tool for enumeration of this quantity which in our case takes the form

$$n_{xi}(\mathbf{u}) = \frac{iu_i}{u_1} n_{xi}(\mathbf{u}) \quad (14)$$

The problem is thus reduced to enumeration of the cumulative number of distinct ordered trees rooted on a terminal vertex (U_1). The latter obeys an equation (see Appendix)

$$n_{xi}(\mathbf{u}) = (x - 2)!/(u_1 - 1)!u_2!u_3! \ldots u_f! \quad (15)$$

Since the randomly chosen unit may be of any type, the probability $w_x(\mathbf{u})$ is given by the summation

$$w_x(\mathbf{u}) = \sum_{i=1}^{f} w_{xi}(\mathbf{u}) \quad (16)$$

By subsequent substitution from (15) into (14), then in (12) and then in (10) and applying the trivial relation (19) we obtain after rearrangement

$$w_x(\mathbf{u}) = \frac{\alpha f}{x - 1}\left[\begin{matrix} x \\ \mathbf{u} \end{matrix}\right]\mathbf{b}^{\mathbf{u}} \quad (17)$$

where the expression in brackets denotes a combinatorial number $x!/u_1! \ldots u_f!$. Equation 17 represents an important relation denoting weight fraction of a special group of isomers defined by the vector $\mathbf{u}$.

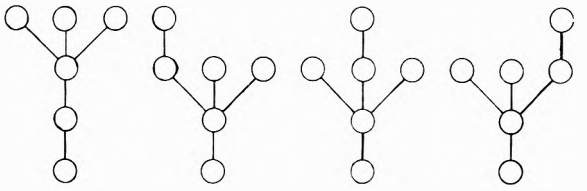

Figure 2. The four distinct ordered trees of composition $u_1 = 4$, $u_2 = 1$, $u_4 = 1$ rooted on a terminal vertex. Their number fulfills the expression $n_{6,1}(4,1,0,1) = 4!/3!$.

To obtain an explicit relation for the weight fraction of any $x$mer as a function of link distribution p_i which is more useful practically, one requires $f - 2$-fold summation of $w_x(\mathbf{u})$; *viz.*, the degrees of freedom of variables $\mathbf{u}$ is diminished by the trivial relations 19 and 20

$$w_x = \sum_{u_f=0}^{m_f} \sum_{u_{f-1}=0}^{m_{f-1}} \cdots \cdots \sum_{u_3=0}^{m_3} w_x(\mathbf{u}) \tag{18}$$

$$x = \sum_{1}^{f} u_i \tag{19}$$

$$2(x-1) = \sum_{1}^{f} i u_i \tag{20}$$

where $x \geq 2$, while $w_1 = p_0$ automatically.

For example, the size distribution of a trifunctional system (which appears to be the most spread case) obeys the equation

$$w_x = \frac{x!3\alpha}{x-1} \sum_{u_3=1}^{m_3} \frac{b_1^{u_1} b_2^{u_2} b_3^{u_3}}{u_1!\, u_2!\, u_3!} \tag{21}$$

where $u_1 = u_3 + 2$, $u_2 = x - 2u_3 + 2$, and $m_3 \leq 0.5x - 1$, and where the b's are found from eq 11.

The upper limits of the summations 18 and 21 may be determined by the assumption that a given $x$mer must contain the highest possible number of units U_1. *E.g.*, m_f may be found from the condition (22) that the molecule contains only units U_1 and U_f

$$m_f = x - u_1 \tag{22}$$

u_1 may be found by a simple stoichiometric consideration.

$$u_1 = f m_f - 2(m_f - 1) \tag{23}$$

Substituting (23) into (22) one obtains

$$m_f \leq (x-2)/(f-1) \tag{24}$$

The inequality sign should be used, because m_f must always be an integer. Similarly m_{f-1} may be found, provided that the molecule contains units U_1, U_f, and U_{f-1} only. It holds in general

$$m_i \leq \left[x - 2 - \sum_{k=i+1}^{f} u_k(k-1) \right] / (i-1) \tag{25}$$

where $2 < i \leq f - 1$.

Appendix

Every $x$mer molecule defined by a vector $\mathbf{u}$ may be represented by a molecular tree having x vertices and $x - 1$ edges (links). These $x - 1$ edges are constructed pair wise from $2x - 2$ reacted functional groups; we can call them shortly "groups" because the unreacted ones are immaterial from the point of ennumeration of $n_{x1}(\mathbf{u})$. This problem requires a combinatorial approach and it is convenient to consider $2(x - 1)$ groups rather than $x - 1$ edges. These $2x - 2$ groups may be classified as those which participate in a link formation with a terminal vertices, U_1 (type A), and those which participate with $U_{i>1}$ (type B). Each x vertices of a given tree (except that of dimer) must have at least one group of type B. Therefore only $x - 2$ groups come into combinatorial consideration whether being a B or A. Provided that the tree is constructed in a special way so that no equivalent vertices (those having the same number of groups) occur beside terminal ones, the number of distinct ordered trees rooted on U_1 should refer to the variation number (*cf.* Figure 2)

$$n_{x1}(u_1, 1, 1, \ldots 1) = (x-2)!/(u_1 - 1)! \tag{26}$$

Nevertheless, a given tree may contain some sets of equivalent vertices and $n_{x1}(\mathbf{u})$ given by eq 26 would include identical configurations. By dividing the right side of (26) by the product of permutation numbers $u_i!$ referring to the series of equivalent vertices, we obtain a more general expression (*cf.* Figure 1)

$$n_{x1}(\mathbf{u}) = (x-2)!/(u_1 - 1)!\, u_2!\, u_3! \ldots u_f! \tag{27}$$

In the case of U_1 vertices the factorial number is diminished by one, because the referential U_1 is taken as the root that does not contribute to the number of identical configurations given by (26).

References and Notes

(1) P. J. Flory, "Principles of Polymer Chemistry," Cornell University Press, Ithaca, N. Y., 1953.
(2) P. Whittle, *Proc. Cambridge Phil. Soc.*, **61**, 475 (1965); *Proc. Roy. Soc., Ser. A* **285**, 501 (1965).
(3) D. W. Matula, L. C. D. Groenweghe, and J. R. Van Wazer, *J. Chem. Phys.*, **41**, 3105 (1964).
(4) M. Gordon and G. R. Scantlebury, *Trans. Faraday Soc.*, **60**, 604 (1964).
(5) M. Gordon and G. R. Scantlebury, *J. Chem. Soc.*, 395 (1967); M. Gordon and K. Kajiwara, *Plaste Kaut.*, **19**, 245 (1972).
(6) I. J. Good, *Proc. Roy. Soc.*, **272**, 54 (1963).
(7) M. Gordon, T. G. Parker, and W. B. Temple, *J. Comb. Theory*, **11**, 142 (1971).
(8) I. J. Good, *Proc. Cambridge Phil. Soc.*, **51**, 240 (1955); W. H. Stockmayer, *J. Chem. Phys.*, **12**, 125 (1944).

Electric and Nonelectric Interactions of a Nonionic–Cationic Micelle

Hiroshi Maeda,* Masa-aki Tsunoda, and Shoichi Ikeda

Department of Chemistry, Faculty of Science, Nagoya University, Nagoya, Japan *(Received August 10, 1973)*

The standard free-energy change accompanying the micelle formation of a nonionic–cationic surfactant is related to the critical micelle concentration after a treatment developed by Aranow, Emerson, and Holtzer. It is shown that electric and nonelectric contributions are experimentally separable. Respective contributions consist of various interactions which can not be separately treated in the case of ionic micelles, such as the effect of charge on nonelectric interaction or the variation of electric free energy due to the addition of a nonionic monomer. An experimental method of the approximate evaluation of these interactions is suggested and applied to the experimental data on aqueous solutions of dimethyldodecylamine oxide. The results can be reasonably interpreted in terms of the effect of charge on the solvent structure around hydrocarbon chains.

Introduction

Stability of micelles can be measured in terms of the standard free-energy change for the reaction of the addition of one more surfactant monomer to the most probable micelle and hence it can be related to the critical micelle concentration (cmc).[1] For ionic micelles electric and nonelectric interactions contribute to the stability. When effects of environmental factors on the stability are considered, such as ionic strength, pH, and temperature, it is desirable to separate each contribution. For ionic surfactants of strong electrolyte, however, the separation is generally difficult to carry out experimentally, because both hydrocarbon part and charge of a monomer can not be added independently to the most probable micelle.

Emerson and Holtzer[2] calculated the electric part of the standard free-energy change and estimated the hydrocarbon part as a difference of the former from the total which was obtained from the values of cmc. In their calculation shape and volume of the most probable micelle were assumed to remain constant even though aggregation number of the micelle and ionic strength might change. The assumption has been criticized on theoretical grounds.[3] Aside from this assumption, results of the calculation were affected by a slight change in the value assigned to the distance of closest approach of counterions.

In the case of nonionic–ionic surfactants, two ways of addition of a monomer to the most probable micelle are possible except for two extreme cases (full charge and no charge): the addition of either a nonionic species or an ionic one. Hence we may expect that in the case of nonionic–ionic surfactants separate evaluation of electric and nonelectric parts can be achieved experimentally.

In the first part of the present paper we show how the standard free-energy change for respective additions of a monomer can be related to the cmc after a reasoning developed previously.[1,2] General expressions are obtained including those for both nonionic and ionic micelles as limiting cases. Moreover, we can understand more clearly the nature of the interactions involved in the parameters describing the stability by means of the obtained general expressions. Titration property of micelles is also discussed, which is one of the most characteristic properties of nonionic–cationic surfactants. In the second part application of the treatment presented in the first part to the experimental data is given, which were obtained on aqueous solutions of dimethyldodecylamine oxide in the presence of sodium chloride. Potentiometric titrations were carried out on the system and the data are analyzed in combination with those of the cmc.

Theoretical

Consider a solution containing four components: water, simple salt, surfactant molecule (nonicnic species), and neutralizing agent (acid). For the sake of brevity, we consider the case of a nonionic–cationic surfactant. Conversion to the case of a nonionic–anionic one can be achieved formally.

At a concentration higher than cmc various micelles are present in solution, each characterized by the aggregation number m' (the total number of surfactant monomers involved in a micelle, either ionic or nonionic) and the number of charges n'. Chemical potential of a micelle ion, $\mu_{m',n'}$, specified by a set of values (m',n') can be written according to a standard treatment of polyelectrolytes.[4]

$$\mu_{m',n'} = \mu^0_{m',n'} + RT \ln C_{m',n'} \tag{1}$$

$$\mu^0_{m',n'} = \mu^0_{m',0} + n'(RT \ln K_m + \mu^0_H) + PT\left[n' \ln (n'/m') + (m' - n') \ln \frac{m' - n'}{m'}\right] + G^{el}(m', n') + G^{ex}(m', n') \tag{2}$$

For both monomers, denoted by D and DH for nonionic and ionic species, respectively

$$\mu_D = \mu^0_D + RT \ln C_1(1 - \alpha_1) \tag{3}$$

and

$$\mu_{DH} = \mu^0_{DH} + RT \ln C_1\alpha_1 \tag{4}$$

Here the superscript zero represents that the signed quantity refers to the standard state. The standard state for each micellar species as well as for each kind of the monomers is defined as a state of unit concentration (M) in an aqueous *salt solution* with respect to each species under consideration, in which the interaction between the species is absent as in the state of infinite dilution.[5] We assume that the ionic strength is high enough that interactions between micelles can be ignored. Accordingly, activity coefficients for micelles and monomers are assumed to arise solely from their interactions with small ions. These activity coefficients are considered to be constant irrespective of pH and the total surfactant concentration

and involved in the chemical potentials of respective standard states. Concentration of a micelle species consisting of m' monomers and n' charges is expressed by $C_{m',n'}$. Concentration of salt and of the total monomer are denoted by C_s and C_1, respectively. The latter is considered to coincide with cmc when the total surfactant concentration is slightly higher than cmc. Degrees of ionization of monomers and micelles are denoted by α_1 and α_m, respectively, and the latter is defined as n'/m'. G^{el} represents the work necessary to charge a micelle from no charge to a final value against the electric repulsion alone. Electric and nonelectric free-energy changes accompanying the introduction of a proton from its standard state to a fully discharged micelle in a given salt solution are given by $RT \ln K_m$, where K_m denotes the intrinsic proton dissociation constant of the micelle. The latter is assumed to be independent of the aggregation number. G^{ex} represents any other nonelectric contributions when more than two charges are present on a micelle. It should be noted that since the electric free energy G^{el} is defined as above, any contributions accompanying ionization other than G^{el} and taken into account by the term K_m is to be involved in the term G^{ex}.

Equilibria for Proton Dissociation. Consider a series of multiple equilibria for proton exchange among those micellar species which have the same aggregation number m'. The distribution curve of charges n' will be characterized with a single maximum located at n. *Hence*

$$C_{m',n(m')} = C_{m',n(m')+1} = C_{m',n(m')-1} \quad (5)$$

Since the values of m' usually encountered are of order of several tens or a hundred, the fluctuation of n' from the most probable value $n(m')$ will be small. We can thus safely ignore the amount of those species present in a solution which have values of n' far from the most probable value n. Differentiation of eq 1 with respect to n' at constant m', pH, and C_s gives

$$\mu_H = (\partial \mu^0_{m',n'}/\partial n')_{m'} \qquad \text{for } n' = n(m') \quad (6)$$

Introduction of eq 2 into eq 6 yields a well-known expression for potentiometric titration of multicharged species.

$$pK \equiv pH + \log(\alpha_m/1 - \alpha_m) = pK_m - (0.434/RT)[\partial(G^{el} + G^{ex})/\partial n]_{m'} \quad (7)$$

Equation 7 shows how the degree of ionization of a micelle is determined by pH. Similarly the degree of ionization of monomer α_1 is related to pH in terms of the dissociation constant for monomer K_1.

$$pH + \log(\alpha_1/1 - \alpha_1) = pK_1 \quad (8)$$

The Most Probable Aggregation Number.[6] A distribution curve with respect to the aggregation number m' can be drawn if the concentration of micelles that have a specified value of m' is plotted against m'. The distribution curve is also expected to have a single maximum located at m. Then

$$C_{m,n(m)} = C_{m+1,n(m+1)} = C_{m-1,n(m-1)} \quad (9)$$

The most probable aggregation number m is determined by the differentiation of eq 1 with respect to m' where n' is replaced by $n(m')$.

$$(\partial \mu_{m',n(m')}/\partial m') = (\partial \mu^0_{m',n(m')}/\partial m') \qquad \text{for } m' = m \quad (10)$$

Behavior of $n(m')$ should be briefly examined here. Generally we can assume that degree of ionization is independent of m' or it decreases as m' increases, *i.e.*, $\partial(n/m')/\partial m' \leq 0$. Since $n(m')$ never decreases as m' increases, the variation of n with m' should obey the following inequalities except for the case that $n = m'$.

$$0 \leq \partial n(m')/\partial m' \leq n/m' < 1$$

Thus we can reasonably obtain the approximate relation

$$n(m'+1) = n(m') = n(m'-1) \quad (11)$$

Combining eq 5, 9, and 11 we find that nine species (the most probable micelle and its nearest neighbors) have the same concentration, which may be written as follows.

$$C_{m,n(m)} = C_{m,n(m)\pm 1} = C_{m\pm 1,n(m)} = C_{m+1,n(m)\pm 1} = C_{m-1,n(m)\pm 1} \quad (12)$$

Addition of Monomers to the Most Probable Micelle. To relate the stability of the micelles to the cmc, consider the following two reactions which demonstrate respective addition of nonionic and ionic monomer to the most probable micelle.

$$D + \text{micelle}[m, n(m)] = \text{micelle}[m+1, n(m)] \quad (13)$$

and

$$DH + \text{micelle}[m, n(m)] = \text{micelle}[m+1, n(m)+1] \quad (14)$$

We can set those concentrations of two micellar species appearing on both sides of each equation be equal owing to eq 12. In terms of eq 1-4 conditions for chemical equilibria for the two reactions can be written as follows

$$RT \ln (\text{cmc}) = \Delta G_{HC} + (\partial G^{el}/\partial m)_n + RT \ln \frac{1-\alpha_m}{1-\alpha_1} \quad (15)$$

for the addition of a nonionic monomer and

$$RT \ln (\text{cmc}) = \Delta G_{HC} + RT \ln (K_m/K_1) + (\partial G^{el}/\partial m)_n + [\partial(G^{el} + G^{ex})/\partial n]_m + RT \ln (\alpha_m/\alpha_1) \quad (16)$$

for the addition of an ionic monomer. In the above ΔG_{HC} is defined as $\partial \mu^0_{m,0}/\partial m - \mu^0_D + (\partial G^{ex}/\partial m)_n$ and represents the most important part of nonelectric contribution to the standard free-energy change associated with the addition of a nonionic monomer to the micelle. The term $(\partial G^{el}/\partial m)_n$ represents a change in electric free energy of the micelle due to a change of its dimensions caused by the addition of a nonionic monomer at a constant number of charges. The last terms of both equations represent respective changes in mixing free energy of charged and uncharged species both in a micelle and in solution, caused by the addition of either species. When intrinsic tendency for protonation of the ionizable group differs in the two states (monomer or micelle), the term $RT \ln (K_m/K_1)$ will appear, which will be discussed later. If the degree of ionization of the most probable micelle is assumed very close to the average degree of ionization of micelles in solution, then α_m as well as α_1 can be experimentally obtained.

Equations 15 and 16 are general expressions relating cmc to the stability of micelles. For nonionic micelles eq 15 reduces to

$$RT \ln (\text{cmc})_0 = \Delta G_{HC}(0) = [\partial \mu^0_{m,0}/\partial m]_{n=m(0)} - \mu^0_D \quad (17)$$

Here $(\text{cmc})_0$, $m(0)$, and $\Delta G_{HC}(0)$ denote that they are evaluated at zero ionization. For ionic micelles formed by strong electrolytes eq 16 becomes

$$RT \ln (\text{cmc}) = \Delta G'_{HC} + (\partial G^{el}/\partial m)_n + (\partial G^{el}/\partial n)_m = \Delta G'_{HC} + (\partial G^{el}/\partial m)_{m=n} \quad (18)$$

(As to the notations appearing in eq 18 see Discussion section.) In this case only the sum of electric and nonelectric

contributions are experimentally determinable. For general nonionic–ionic micelles, however, both terms, $[\partial(G^{el} + G^{ex})/\partial n]_m$ and $\Delta G_{HC} + (\partial G^{el}/\partial m)_n$, can be experimentally determined, which demonstrates electric and nonelectric contributions are separable. When correlation between electric and nonelectric interactions is insignificant, as has been postulated previously,[2] then respective main contributions, $(\partial G^{el}/\partial n)_m$ and ΔG_{HC}, can be experimentally evaluated.

Effect of Charge on Solvent Structure. Further separation of electric and nonelectric contributions may be possible if we examine the dependence of the term $\Delta G_{HC} + (\partial G^{el}/\partial m)_n$ on ionization and ionic strength.

In general, the term $(\partial G^{el}/\partial m)_n$ is negative and increases in magnitude as ionization increases. However, at low ionization the magnitude will be negligibly small, for the effect is significant only when charge density on a micelle is considerably high. The term becomes less negative when ionic strength is raised at a constant ionization.

We assume that difference of solvent structure around charged and discharged micelles is the largest contribution to the term G^{ex}, since the experimental data are well interpreted if the contribution is assumed to be of primary importance in the formation of nonionic micelles.[7] When a polar head is ionized, the structure of water around hydrocarbon chains near the charge will be considerably altered in a direction that the contact between water and hydrocarbons chains is less favored. At low ionization the amount of solvent structure altered by the introduction of charges will be nearly proportional to the number of charges introduced. The effect is thus additive but it is already taken into account through the term $RT \ln K_m$ in eq 2. Accordingly G^{ex} is expected to be approximately zero at low ionization. As ionization proceeds, the structure of water around hydrocarbons becomes destroyed to a different degree from what is expected when the effect is additive, since two or more charges can destroy the same region of solvent structure. In other words, the amount of solvent structure altered by the introduction of a charge is less than that accounted in the term $RT \ln K_m$. This leads to a negative G^{ex}. When ionization becomes so large that structure of water around micelle surface is completely destroyed, then G^{ex} will be the most negative and remain constant upon further ionization. Since major contribution to G^{ex} is assumed to come from charges, the term $(\partial G^{ex}/\partial m)_n$ will be approximately zero for the entire region of ionization, irrespective of ionic strength.

On the other hand, the aggregation number may also change with charge density. When electric interaction alone is considered, the aggregation number is expected to decrease as the charge increases. However, when ionization exceeds an extent that G^{ex} becomes appreciably negative, then we suppose that the aggregation number *increases* so as to reduce the contact area between hydrocarbons and structureless water. Equilibrium aggregation number will then be determined by a balance between electric repulsion and extent of the contact. When micelle surface is completely covered with polar heads, the aggregation number becomes maximum.[8] It should be noted that the described variation of G^{ex} with ionization will not be affected if the aggregation number changes. For, G^{ex} is related to the amount of solvent structure around micelle surface and is, therefore, independent of whether a change in the amount is caused by the perturbation due to charges or by the reduction of the contact area resulting from micelle growth.

The term $\partial\mu^0_{m,0}/\partial m - \mu^0_D$, which is equivalent to ΔG_{HC} in the present context, depends on degree of ionization only through the variation in aggregation number. If aggregation number goes through the minimum as predicted above, the term $\Delta G_{HC} - \Delta G_{HC}(0)$ becomes positive at low ionization, reaches the maximum, and then decreases as ionization proceeds further. The variation of the term, $\Delta G_{HC} - \Delta G_{HC}(0) + (\partial G^{el}/\partial m)_n$, with ionization is expected to resemble in shape what is just described about the term $\Delta G_{HC} - \Delta G_{HC}(0)$.

However, an essentially identical shape will result for the dependence of the term, $\Delta G_{HC} - \Delta G_{HC}(0) + (\partial G^{el}/\partial m)_n$, even if we suppose the opposite situation to be the case that solvent contribution is insignificant. Under this simple situation the term G^{ex} will be negligible at any degree of ionization and aggregation number continuously decreases as ionization proceeds. Accordingly the term $\Delta G_{HC} - \Delta G_{HC}(0)$ will continue to increase in positive direction but the total, $\Delta G_{HC} - \Delta G_{HC}(0) + (\partial G^{el}/\partial m)_n$, will resemble in shape as is described above.

At high ionic strength the term $(\partial G^{el}/\partial m)_n$ will disappear. If we extrapolate to infinite ionic strength the values of $RT \ln [(\mathrm{cmc})(1 - \alpha_1)/(\mathrm{cmc})_0(1 - \alpha_m)]$ obtained at various ionic strengths, we can evaluate the term $\Delta G_{HC} - \Delta G_{HC}(0)$ under the limiting condition. The limiting values will differ from those expected at respective ionic strengths where experimental data are obtained. The difference may arise from both changes in perturbation of solvent structure due to small ions in ionic atmosphere and in aggregation number caused by a change in ionic strength. The dual dependence on ionic strength can not be treated quantitatively at present. However, we assume the difference to be negligible. The approximation may be partly justified if we notice that the quantities under discussion have magnitude of second order as compared with main contributions, $(\partial G^{el}/\partial n)_m$ and ΔG_{HC}. Further, the dual dependence is in the opposite direction and is expected to cancel out each other to some extent. By means of this approximation we can separately evaluate each term.

$$\Delta G_{HC} - \Delta G_{HC}(0) = RT\left[\frac{(\mathrm{cmc})(1 - \alpha_i)}{(\mathrm{cmc})_0(1 - \alpha_m)}\right]_{C_s \to \infty} \quad (19)$$

Note that the term $(\partial G^{ex}/\partial n)_m$ can not be separated from $(\partial G^{el}/\partial n)_m$ in the titration data. Hence, separation of electric and nonelectric contributions is still insufficient in this respect. Nevertheless, the procedure to extrapolate to infinite ionic strength is useful because variation of the limiting values with ionization will provide a measure of the extent of solvent contribution mentioned; whether the limiting values continue to increase or they become negative after passing through the maximum.

Comparison with Experiment

Potentiometric titrations of aqueous solutions of dimethyldodecylamine oxide (DDAO) were carried out at 25° with hydrochloric acid at various sodium chloride concentrations. Titrations at high ionic strengths (0.10–1.0 *M*) were reported by Tokiwa and Ohki.[9] Titrations of the solutions below cmc enabled us to determine α_1 and pK_1. The degree of ionization of solution as a whole, denoted by α, was determined experimentally with the aid of titrations of the solvent, *i.e.*, salt solutions containing no surfactants. Details of the procedure and underlying assumptions have been given.[9] The degree of ionization of micelles α_m, equivalently, the titration curve for the micelle,

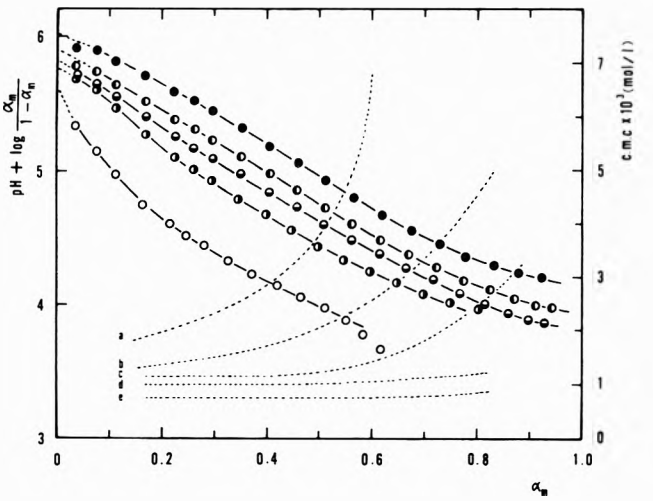

Figure 1. Titration curves of the micelle of DDAO. Data of the cmc are also indicated by dotted lines: salt concentrations (M) 0(○,a), 0.01(◑,b), 0.05(◒,c), 0.1(◐,d), and 0.2(●,e).

TABLE I: Intrinsic Dissociation Constants for Micelle (K_m) and Monomer (K_1) of DDAO

C_s, M	0	0.01	0.05	0.1	0.2
pK_m	5.63	5.76	5.82	5.89	6.01
pK_1	4.78	4.85	4.88	4.88	4.95
$RT \ln (K_1/K_m)$[a]	1.16	1.24	1.28	1.37	1.44

[a] Expressed in kcal/mole.

was evaluated in terms of the following relation

$$\alpha C = \alpha_m(C - C_1) + \alpha_1 C_1 \qquad (20)$$

Here C denotes the total surfactant concentration. Titration curves for the micelle were independent of C and are shown in Figure 1 for different ionic strengths. Extrapolation of pK to zero ionization is made in such a way that pK_m may depend on ionic strength, since the standard states are defined in a salt solution. The values of pK_m are given in Table I together with those of pK_1. Data of the cmc are obtained from the measurement of surface tension of the solutions[10] and are also shown in Figure 1. In Table II are cited the data necessary to discuss the stability of micelles in terms of eq 7 and 15. Values of $RT \ln [(\text{cmc})(1 - \alpha_1)/(\text{cmc})_0(1 - \alpha_m)]$ are plotted in Figure 2 against α_m. At low ionization the value is slightly positive and increases as α_m increases. When ionization proceeds further, a downward trend appears and the value becomes more negative as α_m increases further. The general feature of the curves drawn in Figure 2 is quite consistent with that described in the preceding section. We tried to extrapolate the data to infinite ionic strength as suggested. Extrapolations could be carried out only when the data obtained at 0.2 M NaCl were not taken into consideration.[11] The limiting values thus obtained are shown in Figure 2 by a dashed line. Variation of the limiting values with α_m reveals that solvent contribution is significant since they do not increase monotonously. The behavior implies that the aggregation number decreases or remains almost constant at low ionization (below about 0.3) and then increases as ionization proceeds. Herrmann found that the aggregation number of fully protonated micelle of DDAO was larger than that of fully discharged species.[12] Moreover he found that the fully protonated micelle is rod like in shape,[13] which confirmed that the aggregation number was larger than the maximum value expected for spherical

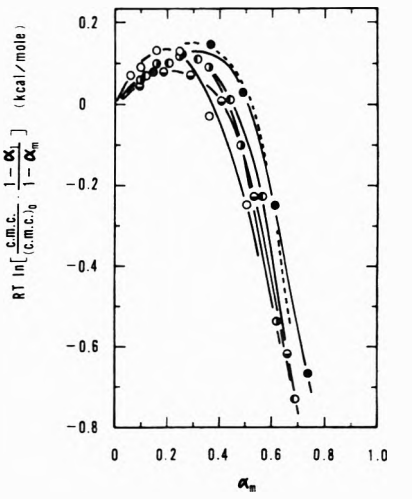

Figure 2. An example of the analysis of experimental data on aqueous solutions of DDAO: salt concentrations (M) 0(○), 0.01(◑), 0.05(◒), 0.1(◐), and 0.2(●). Limiting values of ordinate at infinite ionic strength are shown by a dashed line.

shape.[14] These findings are quite consistent with that predicted by the present analysis about the thermodynamic data. On the other hand there are no experimental data indicating the predicted decrease or invariance in aggregation number at low ionization.

It is to be stated here that although the extrapolation was made in a highly approximate manner, the general trend of the limiting values just described is by no means altered. For example, if the limiting values were assumed to increase continuously with α_m, in a consistent manner with the data corresponding to α_m below about 0.3 in Figure 2, then resulting absolute values of $(\partial G^{el}/\partial m)_n$ would be so large that the term $[\partial(G^{el} + G^{ex})/\partial n]_m + (\partial G^{el}/\partial m)_n$ decreased as α_m increased.

Values of the term $(\partial G^{el}/\partial m)_n$ can be evaluated by means of the limiting values and are given in Table II. They should be taken as representing the minimum values. We can see that the fraction of the term $(\partial G^{el}/\partial m)_n$ to the term $[\partial(G^{el} + G^{ex})/\partial n]_m$ is about 10% or more. Accordingly, neglection of the term $(\partial G^{el}/\partial m)_n$ seems to be not necessarily a good approximation. However, quantitative discussions are impossible about the magnitude of the term $(\partial G^{el}/\partial m)_n$ or of the limiting value shown in Figure 2, if the highly approximate nature of the employed extrapolation is taken into consideration. Therefore, in so far as the micelles of DDAO are concerned, the assumption of Emerson and Holtzer is not necessarily permissible that a charged monomer can be added to a micelle without altering micellar volume.

Discussion

The standard free-energy change associated with the addition of a nonionic monomer to a discharged micelle is $\Delta G_{HC}(0)$, as given in eq 17. When a charged monomer is added to a discharged micelle the corresponding free-energy change is $\Delta G_{HC}(0) + RT \ln (K_m/K_1)$. Although the term $RT \ln (K_m/K_1)$ may include electric interaction, it is to be regarded as representing a part of nonelectric standard free-energy change in question according to the definition introduced. Equation 15 shows that the corresponding change is $\Delta G_{HC} + (\partial G^{el}/\partial m)_n$ if a nonionic monomer is added to a charged micelle. On addition of a charged monomer to a charged micelle the corresponding result is what is given in eq 16. Though the free-energy

TABLE II: Free Energy of Micelle Formation of DDAO[a]

	pH 6.5	6.0	5.5	5.0	4.5	4.0
$C_s = 0.10\ M$, $\Delta G_{HC}(0) = -4.09$						
α_m	0.12	0.21	0.32	0.44	0.56	0.74
RT ln (cmc)	−4.09	−4.09	−4.09	−4.09	−4.06	−4.03
RT ln $[(1 - \alpha_m)/(1 - \alpha_1)]$	−0.07	−0.10	−0.11	−0.01	0.26	0.76
$(\partial G^{el}/\partial m)_n$			−0.04	−0.08	−0.13	−0.16
$[\partial(G^{el} + G^{ex})/\partial n]_m$	0.27	0.67	0.99	1.36	1.73	2.07
$C_s = 0.05\ M$, $\Delta G_{HC}(0) = -4.00$						
α_m	0.10	0.19	0.29	0.41	0.53	0.66
RT ln (cmc)	−4.00	−4.00	−4.00	−4.00	−3.94	−3.79
RT ln $[(1 - \alpha_m)/(1 - \alpha_1)]$	−0.05	−0.08	−0.07	−0.01	0.29	0.83
$(\partial G^{el}/\partial m)_n$				−0.10	−0.21	−0.18
$[\partial(G^{el} + G^{ex})/\partial n]_m$	0.34	0.67	0.99	1.35	1.68	2.02
$C_s = 0.01\ M$, $\Delta G_{HC}(0) = -3.94$						
α_m	0.10	0.16	0.25	0.36	0.48	0.62
RT ln (cmc)	−3.93	−3.91	−3.89	−3.80	−3.69	−3.50
RT ln $[(1 - \alpha_m)/(1 - \alpha_1)]$	−0.05	−0.06	−0.05	0.05	0.35	0.98
$(\partial G^{el}/\partial m)_n$				−0.05	−0.16	−0.23
$[\partial(G^{el} + G^{ex})/\partial n]_m$	0.37	0.65	1.02	1.35	1.66	1.99

[a] Expressed in kcal/mole.

change in this case has been simply written as $\Delta G_{HC} + Ne\psi$,[2] each term contains various contributions, ψ being electric potential at micelle surface. For example, ΔG_{HC} in this case may generally differ from that for nonionic species by what are symbolized by the term RT ln (K_m/K_1) and $(\partial G^{ex}/\partial n)_m$. Hence a slightly different notation $\Delta G'_{HC}$ is used for the case in eq 16. The term RT ln (K_m/K_1) should be interpreted as representing an effect of charge on nonelectric interaction, which is clearly present in the case of strong electrolytes although respective dissociation constants, K_m and K_1, have no physical meaning. Similarly the electric part will be $(\partial G^{el}/\partial m)_{m=n}$ which can be divided, at least conceptually, into two terms as illustrated in eq 18. The term $(\partial G^{el}/\partial n)_m$ is exactly identical with $Ne\psi$.

The difference between pK_m and pK_1, experimentally found in the case of DDAO, should be briefly discussed. The difference is considered to provide a quantitative measure for the effect of charge on nonelectric interaction (hydrophobic interaction in the present context). This interpretation is justified if electric interaction between a charged monomer and its ionic atmosphere is approximately identical with that encountered when the monomer is added to a discharged micelle, and if transfer of a monomer from aqueous solution to a micelle is a proper procedure for measuring the hydrophobic interaction. When we compare the values of $\Delta G_{HC}(0)$ from Table II with those of RT ln (K_m/K_1) from Table I, we can conclude that a charged monomer is more stabilized than a nonionic one by about 30% when they are transferred to a discharged micelle, which is equivalent to say that introduction of a charge destabilizes a monomer by a corresponding amount.

A picture introduced in this paper concerning the effect of charge on solvent contribution may differ from "the electrostatic solvent effect" proposed by Poland and Scheraga.[15] They introduced the idea to explain that heat of micelle formation of ionic micelles is generally less positive than that of nonionic ones.[7] They ascribed the negative contribution to a change in the solvent structure around the charged head. According to our picture, however, it is the contact area between hydrocarbon chains and the solvent that is supposed to be largely diminished when a monomer is transferred to a micelle, and hence accessibility of the charged heads to the solvent is considered not so largely altered by the process, contrary to their supposition. Instead, the effect of charge is to reduce the positive solvent contribution to the enthalpy change which plays a central role for the change in the case of nonionic micelle, since more solvent structure is destroyed by the introduction of a charge in the state of monomer than in micelles.

References and Notes

(1) R. H. Aranow, *J. Phys. Chem.*, **67**, 556 (1963).
(2) M. F. Emerson and A. Holtzer, *J. Phys. Chem.*, **69**, 3718 (1965); **71**, 1898 (1967).
(3) P. Mukerjee, *J. Phys. Chem.*, **73**, 2054 (1969).
(4) A. Katchalsky and J. Gillis, *Recl. Trav. Chim. Pays-Bas*, **68**, 879 (1949); F. E. Harris and S. A. Rice, *J. Phys. Chem.*, **58**, 725 (1954); R. A. Marcus, *J. Chem. Phys.*, **23**, 1057 (1955).
(5) The use of the term "reference state" will be more appropriate in place of the term "standard state" here employed. However, we use the latter for the sake of consistency, since the term $-RT$ ln (cmc) or ΔG_{HC} has been conventionally termed as "standard" free-energy change.
(6) If the most probable aggregation number m is defined as such that $m'C_{m',n(m')}$ instead of $C_{m',n(m')}$ is the maximum at $m' = m$, then corresponding aggregation numbers should be multiplied to respective concentrations in eq 9 and a term RT/m' should be added to left-hand side of eq 10. However, the difference will be unimportant for the range of values of m usually encountered.
(7) L. Benjamin, *J. Phys. Chem.*, **68**, 3575 (1964).
(8) I. Reich, *J. Phys. Chem.*, **60**, 257 (1956); D. C. Poland and H. A. Scheraga, *ibid.*, **69**, 2431 (1965).
(9) F. Tokiwa and K. Ohki, *J. Phys. Chem.*, **70**, 3437 (1966).
(10) M. Tsunoda, H. Maeda, and S. Ikeda, manuscript in preparation.
(11) When C_s is smaller than about 0.1 *M*, values of RT ln $[(\text{cmc})(1 - \alpha_1)/(\text{cmc})_0(1 - \alpha_m)]$ gradually increase as C_s^{-1} decreases, if they are plotted against the latter at constant α_m. Steep increase is observed, however, when C_s is larger than about 0.1 *M* and extrapolation of the curve to infinite ionic strength becomes difficult. The observed trend to tend to infinity as ionic strength approaches infinity is quite inconsistent with the expectation from our theoretical treatment. The cause for this discrepancy will be considered to arise from the limitation of our treatment rather than to arise from experimental error. A possible limitation will be that lamellar micelles are present at high ionic strength which are quite different from the assumed model that they are dispersed in a solution as independent particles.
(12) K. W. Herrmann, *J. Phys. Chem.*, **66**, 295 (1962).
(13) K. W. Herrmann, *J. Phys. Chem.*, **68**, 1540 (1964).
(14) C. Tanford, *J. Phys. Chem.*, **76**, 3020 (1972).
(15) D. C. Poland and H. A. Scheraga, *J. Colloid Interface Sci.*, **21**, 273 (1966).

Phase Diagrams of Reciprocal Molten Salt Systems. Calculations of Liquid–Liquid Miscibility Gaps[1a]

M. L. Saboungi,*[1b] H. Schnyders, M. S. Foster, and M. Blander

Chemical Engineering Division, Argonne National Laboratory, Argonne, Illinois 60439 *(Received January 2, 1974)*

Publication costs assisted by Argonne National Laboratory

Liquid–liquid miscibility gaps of ternary reciprocal molten salt systems may be calculated *a priori* from conformal ionic solution theory utilizing data for the four subsidiary binary systems and the four pure constituents. Using a modification of the second-order theory, we calculated miscibility gaps for hypothetical systems containing two cations, A^+ and B^+, and two anions, C^- and D^-; the results show that the sizes of miscibility isotherms depend on the standard free-energy change for the metathetical reaction AC + BD ⇄ AD + BC as well as on the binary interaction parameters whereas the asymmetry in the shape and position of miscibility isotherms depends only on the binary interaction parameters. The calculated sizes and positions of miscibility isotherms in the Na, Tl||Br, NO_3 system are in good agreement with measurements.

Introduction

The conformal ionic solution (CIS) theory[2a] has been shown to lead to predictions of liquidus temperatures *a priori* which are in good agreement with measurements for a variety of reciprocal salt systems.[2b,3,4] This lends confidence in the theory for predictions in systems which exhibit fairly large deviations from ideal solution behavior. A preliminary discussion has been given of miscibility gaps and upper consolute temperatures[2b] as well as some limitations of the theory.[3] However, no detailed examination of the theory has been undertaken for systems in which deviations from ideality are so large that liquid–liquid miscibility gaps occur. A large number of such systems are known[5] and it is important to examine the applicability and limitations of this second-order perturbation theory for such systems. In this paper we present a test of the theory for the system Na, Tl || Br, NO_3. In addition, we discuss the influence of particular parameters and ionic interactions on the shapes and position of miscibility gaps. An empirical generalization of the theory is suggested to eliminate one of its limitations.

CIS Theory for Ternary Reciprocal Systems[2a]

A ternary reciprocal system contains two cations (A^+, B^+) and two anions (C^-, D^-) and is represented by the symbol A, B || C, D. There are four constituents (AC, AD, BC, BD), any three of which may be chosen as independent components.[6] The activity coefficients, γ_i, can be calculated from the CIS theory. For BD, for example, the activity coefficients are given by

$$RT \ln \gamma_{BD} = X_A X_C \Delta G^\circ + X_A X_C(X_C - X_D)\lambda_A + X_C(X_A X_D + X_B X_C)\lambda_B + X_A(X_A X_D + X_B X_C)\lambda_D + X_A X_C(X_A - X_B)\lambda_C + X_A X_C(X_A X_D + X_B X_C - X_B X_D)\Lambda \quad (1)$$

where X_i is the ion fraction of ion i (*e.g.*, $X_A = n_A/(n_A + n_B)$, $X_C = n_C/(n_C + n_D)$ where n's are number of moles of ions indicated), ΔG° is the standard molar Gibbs free-energy change for the reaction

$$AC(l) + BD(l) \rightleftharpoons AD(l) + BC(l) \quad (2)$$

λ_i is an energy parameter in the second-order equation for the excess free energy of binary systems with the common ion i

$$\Delta G_A^E = X_C X_D \lambda_A \quad (3)$$

$$\Delta G_B^E = X_C X_D \lambda_B \quad (4)$$

$$\Delta G_C^E = X_A X_B \lambda_C \quad (5)$$

$$\Delta G_D^E = X_A X_B \lambda_D \quad (6)$$

and Λ is approximated by

$$\Lambda = -(\Delta G^\circ)^2/2ZRT \quad (7)$$

All the parameters may be estimated from available data, ΔG° from data on the pure salts, λ_i from data on the binary systems, and Z is a coordination number and has been taken as 6. Consequently, the theory utilizes data obtained from lower order systems to calculate properties of ternary systems.

Equations similar to eq 1 can be obtained for the activity coefficients of the other constituents AD, BC, and AC by changes in the subscripts in eq 1 and the constituents of equilibrium (2) as follows: for AD, change A → B and B → A; for AC, change A → B, B → A, C → D, and D → C; for BC, change C → D and D → C. The chemical potential of BD is given by

$$\mu_{BD} - \mu_{BD}^\circ = RT \ln a_{BD} = RT \ln X_B X_D \gamma_{BD} = \Delta\mu_{BD} \quad (8)$$

where μ_{BD}^0 in the chemical potential of pure liquid BD and a_{BD} is the activity of BD in solution.

Calculation of Liquid–Liquid Miscibility Gaps

The thermodynamic conditions for defining miscibility gaps for ordinary ternary systems are relatively simple.[7] Because ternary reciprocal systems contain not three but four entities and have four possible constituents, the conditions for defining miscibility gaps must be stated differently although the fundamental equations are the same. If one defines the three components as BC, AD, and BD then the molar Gibbs free energy of mixing, ΔG_m, is given by the expression

$$\Delta G_m = X_C\Delta\mu_{BC} + X_A\Delta\mu_{AD} + (X_D - X_A)\Delta\mu_{BD} \quad (9)$$

where the chemical potentials of any constituent, as for example BD, may be calculated by equations as[6]

$$\Delta\mu_{BD} = (\partial n\Delta G_m/\partial n_B)_{n_A} + (\partial n\Delta G_m/\partial n_D)_{n_C} \quad (10)$$

where n is the total number of moles ($n = n_A + n_B = n_C + n_D$), and the derivative is taken at constant T and P. If at constant T and P one considers the surface for ΔG_m with the magnitude of ΔG_m plotted in the coordinate perpendicular to the composition square, then one may define the conditions for miscibility gaps geometrically in terms of this surface.[7] Any two compositions on this surface which are in equilibrium with each other must be in a single plane which is tangent to the ΔG_m surface at two points k' and k'' which correspond to these two compositions. If the two points are represented by a prime ($'$ for k') and double prime ($''$ for k'') then we can express this condition by the equations

$$(\partial\Delta G_m/\partial X_B)_{X_D}' = (\partial\Delta G_m/\partial X_B)_{X_D}'' \quad (11)$$

$$(\partial\Delta G_m/\partial X_D)_{X_B}' = (\partial\Delta G_m/\partial X_D)_{X_B}'' \quad (12)$$

and

$$\Delta G_m' - \Delta G_m'' = (X_B' - X_B'')(\partial\Delta G_m/\partial X_B)_{X_D}' + (X_D' - X_D'')(\partial\Delta G_m/\partial X_D)_{X_B}' \quad (13)$$

Equations 11 and 12 state that the tangent planes to the points k' and k'' are parallel or coincide and eq 13 constrains them so that they must be the same plane. From eq 10 for BD and similar ones for the other constituents it can be shown that

$$\Delta\mu_{AC} = \Delta G_m - X_B(\partial\Delta G_m/\partial X_B)_{X_D} - X_D(\partial\Delta G_m/\partial X_D)_{X_B} \quad (14)$$

$$\Delta\mu_{AD} = \Delta G_m - X_B(\partial\Delta G_m/\partial X_B)_{X_D} + X_C(\partial\Delta G_m/\partial X_D)_{X_B} \quad (15)$$

$$\Delta\mu_{BC} = \Delta G_m + X_A(\partial\Delta G_m/\partial X_B)_{X_D} - X_D(\partial\Delta G_m/\partial X_D)_{X_B} \quad (16)$$

$$\Delta\mu_{BD} = \Delta G_m + X_A(\partial\Delta G_m/\partial X_B)_{X_D} + X_C(\partial\Delta G_m/\partial X_D)_{X_B} \quad (17)$$

From eq 11–17 one deduces the well-known conditions

$$\Delta\mu_{AC}' = \Delta\mu_{AC}'' \quad (18)$$

$$\Delta\mu_{AD}' = \Delta\mu_{AD}'' \quad (19)$$

$$\Delta\mu_{BC}' = \Delta\mu_{BC}'' \quad (20)$$

$$\Delta\mu_{BD}' = \Delta\mu_{BD}'' \quad (21)$$

which is statement that any constituent of the two solutions in equilibrium with each other has the same chemical potential in both solutions. Only three of these four equations are independent. Consequently, any three of the four eq 18–21 or the three eq 11–13 may be utilized in conjunction with eq 1, 8, or 9 to calculate the pairs of immiscible compositions which are in equilibrium with each other. In our computer calculations we generally utilized three of the eq 18–21 and occasionally checked the self-consistency of the results from eq 11–13.

For any given temperature, the problem of finding conjugate pairs of liquid compositions which are at equilibrium with each other (*i.e.*, tie lines) is reduced to the problem of finding a composition which simultaneously satisfies three of the four eq 18–21. An analytic approach to the problem is precluded because of the logarithmic terms and one must resort to numerical methods.

The calculation utilizes a method for minimizing the sum of the squares of nonlinear functions of several variables developed by Powell.[8,9] (See paragraph at end of text regarding supplementary material.)

Using this computational method, we calculate many pairs of points at fixed temperatures which define the isothermal cut of the dome of immiscibility. As the temperature is increased, the area of these isothermal cuts decreases until it shrinks to a point at the upper consolute temperature, T_c. Above this temperature the salts are completely miscible.

The calculation of upper consolute temperatures from the CIS theory has been discussed.[2b] An approximate expression is

$$T_c = \frac{\Delta G^\circ}{5.5R} + \frac{\lambda_A + \lambda_B + \lambda_C + \lambda_D}{11R} \quad (22)$$

An examination of the theory[3] for a hypothetical case in which $\lambda_A = \lambda_B = \lambda_C = \lambda_D = \lambda$ has shown that an artifact is introduced into the calculations of miscibility gaps from the theory for $Z \leq 5.3$ when $\lambda = 0$. This artifact also occurs for cases in which the binary interaction parameters, λ_i, are negative enough so that the ratio of the term in Λ to the others in eq 1 is greater than the ratio when $Z = 5.3$. This artifact in the calculations occurs because the theory has only been carried out to second order and the dependence of this artifact on values of λ makes the self-consistent treatment of miscibility gaps impossible for some systems without modification of the equations.

The calculations made previously[3] suggest a modification to the term Λ in eq 1 which leads to a self-consistent treatment of miscibility gaps such that the artifact will not appear in the calculations for very negative values of λ. This modification is

$$\Lambda = -\left(\Delta G^\circ + \frac{\Sigma\lambda_i}{2}\right)^2 / 2ZRT \quad (23)$$

If one expands (23), the form of the added terms in (23) appear to be consistent with third- and fourth-order terms in the CIS. The term in $(\Delta G^\circ)(\Sigma\lambda_i)$ is probably related to some of the third-order terms and the term in $(\Sigma\lambda_i)^2$ is probably related to some of the fourth-order terms. The purpose of this paper is to test the eq 1, 7, and 23 and we will show that we obtain a good representation in the Na, Tl || Br, NO_3 system. In addition, we will calculate miscibility gaps in hypothetical systems to gain an understanding of the influence of the different parameters in the theory on the location, shape, and size of the miscibility gaps. These considerations provide some insight into the interpretation of the topological characteristics of miscibility gaps and illustrate features which are observed.

Miscibility Gaps in Hypothetical Systems

In this section, we calculate miscibility gaps from eq 1 and 23 to see what influence the parameters ΔG°, λ_i, and Z have on the shape and size of the miscibility gaps and on the positions of the tie lines which connect individual pairs of points which are in equilibrium. All the calculations in Figure 1 were made for $\Delta G^\circ = 18.0$ kcal mol^{-1}.

The calculations in Figure 1a were for the case in which all λ_i's are zero and $Z = 6$, in Figure 1b when all λ_i's are zero and $Z = 5.5$, in Figure 1c when three λ_i's are zero, $\lambda_A = 1500$ cal mol^{-1}, and $Z = 6$, and in Figure 1d when three λ_i's are zero, $\lambda_A = -1500$ cal mol^{-1}, and $Z = 6$. Figures 1a and 1b are universal curves which are the same for any

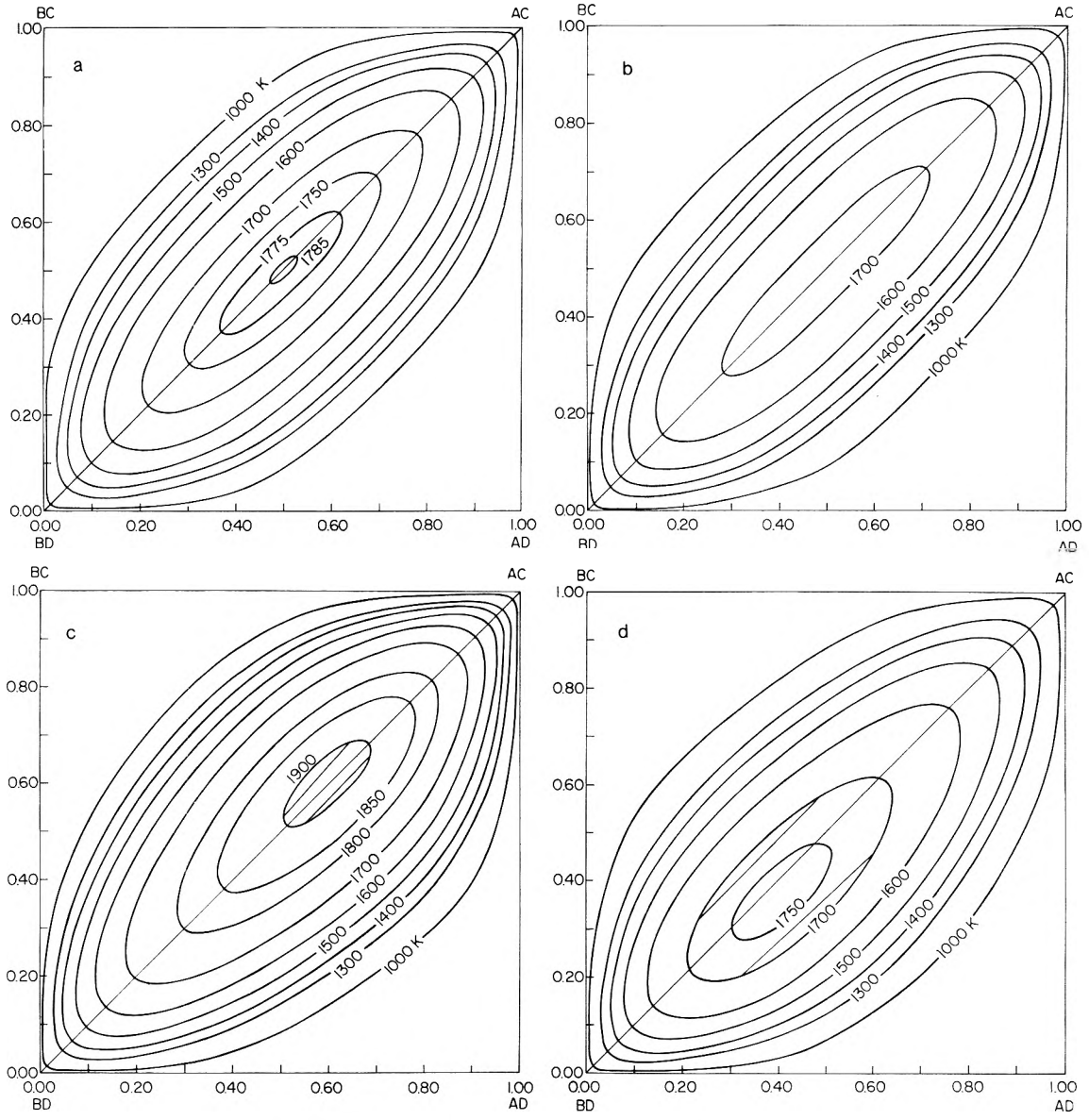

Figure 1. Calculated miscibility gaps for hypothetical systems: (a) ΔG° = 18 kcal mol^{-1}, Z = 6, $\lambda_A = \lambda_B = \lambda_C = \lambda_D$ = 0; (b) ΔG° = 18 kcal mol^{-1}, Z = 5.5, $\lambda_A = \lambda_B = \lambda_C = \lambda_D$ = 0; (c) ΔG° = 18 kcal mol^{-1}, Z = 6, λ_A = 1.5 kcal mol^{-1}, $\lambda_B = \lambda_C = \lambda_D$ = 0; (d) ΔG° = 18 kcal mol^{-1}, Z = 6, λ_A = −1.5 kcal mol^{-1}, $\lambda_B = \lambda_C = \lambda_D$ = 0.

other value of ΔG° for temperatures such that values of $(\Delta G^\circ/RT)$ are the same as for the curves in Figures 1a and 1b.

The miscibility domes in Figures 1a and 1b rise steeply at low reduced temperatures and flatten out at higher temperatures. At low temperatures there is little difference between Figures 1a and 1b. The flattening of the top of the dome occurs at slightly lower temperatures for Z = 5.5 and is more pronounced than for Z = 6 with the isotherms at higher temperatures being narrower and more elongated for Z = 5.5 than for Z = 6. The shapes are somewhat elliptical except at low reduced temperatures where the shapes tend to straighten so as to conform to the two corners of the composition diagram near the stable pair (AC + BD). Because of symmetry, the tie lines for these two cases in which all λ's are zero are all parallel to the stable diagonal connecting the AC and BD corners. In Figure 1c for the case in which Z = 6, λ_A is positive and $\lambda_B = \lambda_C = \lambda_D$ = 0, it can be seen that the isotherms subtend a larger area than in Figure 1a; they are also displaced toward the AC corner and are asymmetric in a way such that the miscibility gap subtends a somewhat larger area in the AC-BC-BD triangle than in the AC-AD-BD triangle. In Figure 1d for the case in which Z = 6, λ_A is negative and $\lambda_B = \lambda_C = \lambda_D$ = 0, the isotherms subtend a smaller area than in Figure 1a; they are also displaced toward the BD corner and are asymmetric such that they subtend a somewhat larger area in the AC-AD-BD triangle than in the AC-BC-BD triangle. Further, the tie lines are no longer parallel to the diagonal AC-BD, but are displaced in a manner as is illustrated in Figures 1c and 1d. These reflect the complex changes in relative solution properties for these idealized systems and indicate that for a proper thermodynamic analysis one needs measurements covering the entire composition square rather than only along the stable diagonal.

These considerations provide us with an insight into the influence of particular ionic interactions on miscibility gaps and are significant for the interpretation of measurements.

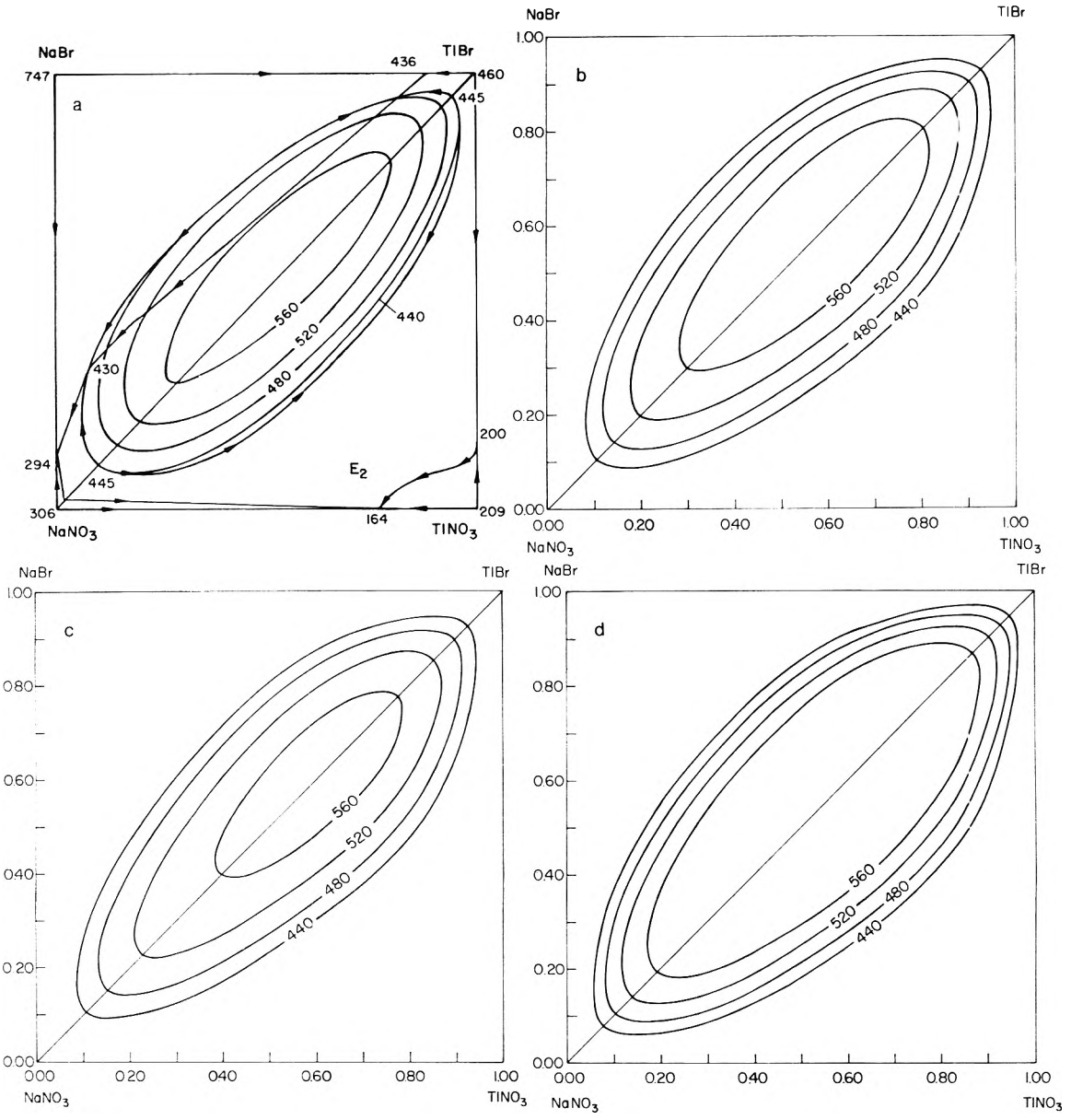

Figure 2. Experimental and calculated miscibility gaps for the reciprocal system (Na, Tl || NO_3, Br): (a) measured (ref 10); (b) calculated miscibility isotherms with $\Delta G^\circ = 8720 - 1.1T(K)$ cal mol^{-1} and $Z = 6$; (c) calculated miscibility isotherms with $\Delta G^\circ = 9240 - 1.1T(K)$ cal mol^{-1} and $Z = 6$; (d) calculated miscibility isotherms for $\Delta G^\circ = 8720 - 1.1T(K)$ cal mol^{-1} and $Z = 5.5$.

TABLE I: Values of the Interaction Parameters Used in the Calculations

Binary	λ_i, cal mol^{-1}
$NaNO_3$–NaBr	360
$TlNO_3$–TlBr	1120
$NaNO_3$–$TlNO_3$	230
NaBr–TlBr	0

Miscibility Gaps in the Na, Tl || Br, NO_3 System

The system Na, Tl || Br, NO_3 has been studied by Sinistri, Franzosini, and Flor[10] who have measured isothermal liquid–liquid miscibility gaps at 440, 480, 520, and 560° given in Figure 2a as well as the intersection of the miscibility dome with liquidus surfaces. This work was chosen as it constitutes the most complete and detailed study of immiscibility in reciprocal systems which is suitable for our calculations. The values of the binary interaction parameters for this system are small or positive. The values of λ_i given in Table I were taken from the calorimetric data of Kleppa and Meschel[11] for the $TlNO_3$–TlBr binary and calculated from the phase diagrams for the NaBr–$NaNO_3$ and $NaNO_3$–$TlNO_3$ systems.[12] There are no measurements for the NaBr–TlBr system and the phase diagram cannot be utilized because of solid solutions. We have assumed that $\lambda_{Br} = 0$. This is not too different from predictions of small values of λ_{Br} one makes from theoretical correlations.[6,13] ΔG° was calculated from available tabulated data[14,15] and is represented by $\Delta G^\circ = 8720 - 1.1T(K)$ cal mol^{-1}. The miscibility isotherms calculated from eq 1 and 23 with $Z = 6$ are given in Figure 2b and are to be compared with the measured isotherms. For comparative purposes, the isotherms for the case in which $\Delta G^\circ = 9240 - 1.1T(K)$ cal mol^{-1} and $Z = 6$ are given in Figure 2c and for the case in which $\Delta G^\circ = 8720 - 1.1T(K)$ cal mol^{-1} and $Z = 5.5$ are given in Figure 2d.

The correspondence between the measured isotherms and the calculations represented in Figure 2b is remarkably good. The shapes and positions of the measured and

TABLE II: Calculated and Measured Compositions Along the Miscibility Gaps at the Stable Diagonal in the Na, Tl||NO_3, Br System

	Mole fraction of TlBr							
T, °C	Measd		Calcd (Figure 2b)		Calcd (Figure 2c)		Calcd (Figure 2d)	
440	0.10	0.95	0.10	0.93	0.08	0.95	0.10	0.92
480	0.13	0.92	0.14	0.90	0.10	0.93	0.15	0.90
520	0.19	0.88	0.20	0.87	0.14	0.90	0.23	0.85
560	0.28	0.80	0.30	0.80	0.19	0.87	0.40	0.78

calculated isotherms are very close. The isotherms are asymmetrically displaced somewhat in the direction of the TlBr corner and subtend a somewhat larger area in the $NaNO_3$-NaBr-TlBr triangle than in the TlBr-$TlNO_3$-$NaNO_3$ triangle. This is consistent with the fact that λ_{TlI} is the largest and predominant interaction parameter influencing the shapes and position of the isotherms. Since λ_{Tl} is positive, this system is analogous to the system illustrated in Figure 1c with λ_{TlI} being analogous to λ_A. Thus we see a confirmation of the predicted displacements of the position of the miscibility gaps which result from the influence of interactions related to the binary interaction parameters.

Discussion

The correspondence of the measured and calculated phase diagrams illustrates the potential of the theory in predicting miscibility gaps. This is further exhibited in Table II where we list measured and calculated compositions along the stable diagonal. The correspondence is remarkably good. The calculations are sensitive to the value of $\Delta G°$. As can be seen in Figures 2b and 2c, a change of 500 cal mol^{-1} makes a significant difference in the size of the miscibility gap when temperatures are not too far from the upper consolute temperature. We see that the size of the gap depends on $\Delta G°$ and on the interaction parameters whereas the asymmetry depends only on the relative values of the interaction parameters. Fairly small uncertainties in $\Delta G°$ may lead to significant uncertainties in the size of the gap. The influence of the size of Z is illustrated in Table II and in Figure 2 with the gap being somewhat smaller for $Z = 5.5$ than for $Z = 6$.

We have utilized eq 23 for Λ. Had we utilized eq 7 with $Z = 6$ the gap would have been wider. We obtain results similar to Figure 2b using eq 7 with a value of $Z = 5$. When λ_i's are positive as in this case, the size of the term Λ in eq 1 relative to the other terms is smaller than when the λ_i's are zero if eq 7 is used for Λ. It is this relative size that leads to the artifact in the equations discussed previously[3] with the artifact appearing when Λ gets relatively large. This artifact is manifested by a double maximum in the calculated miscibility gap. Thus, in this case, the artifact does not appear when eq 7 is used even when $Z = 5$ whereas it appears when $Z < 5.3$ when all the λ_i's are zero. Conversely, when the λ_i's are negative, such artifacts may appear even for values of Z much larger than 5.3.

For example, we have performed calculations for the Li, Cs || F, Cl system in which there are large negative deviations from ideality in the LiF-CsF and LiCl-CsCl binaries. Using eq 7 with $Z = 6$ led to difficulties in calculation and the calculations we obtained were characterized by two (rather than one) maxima in the miscibility dome. With the use of eq 23 these artifacts were suppressed. Our calculations in this system led to a calculated miscibility gap which, within the uncertainties in the parameters, was as long and asymmetric as the measurements of Bukhalova and Sementsova[16] and Sholokhovich, *et al.*,[17] along the stable diagonal (LiF-CsCl) but was much wider than indicated in the measurements along the unstable diagonal (LiCl-CsF). The reasons for this discrepancy remain unclear. The measurements in the Li, Cs || F, Cl system are only of the intersection of the miscibility dome with the liquidus curves. A full test of the theoretical calculations requires much more detailed data on the entire miscibility dome.

Our calculations illustrate that the theory is in accord with the most completely studied system suitable for our calculations. Only one other system, the Rb, Tl || NO_3, Br system appears to have been studied in detail adequate for a similar comparison.[5] Unfortunately, this system is very close in character to the one we studied. Clearly, more data on systems which are decidedly different from the Na, Tl || NO_3, Br system are necessary for a real test of the range of applicability of the theory. It appears that the use of eq 1 and 23 with $Z = 6$ are adequate for the calculation of miscibility gaps and should also be suitable for the calculation of liquidus temperatures. This is the only example of which we are aware for which the entire miscibility gap may be predicted *a priori* from solution theory.

Acknowledgment. One of us (M. L. S.) would like to acknowledge support received from the C.N.R.S. of Lebanon.

Supplementary Material Available. The description of the method of calculation will appear following these pages in the microfilm edition of this volume of the journal. Photocopies of the supplementary material from this paper only or microfiche (105 × 148 mm, 24× reduction, negatives) containing all of the supplementary material for the papers in this issue may be obtained from the Journals Department, American Chemical Society, 1155 16th St., N.W., Washington, D. C. 20036. Remit check or money order for $3.00 for photocopy or $2.00 for microfiche, referring to code number JPC-74-1091.

References and Notes

(1) (a) This work was largely supported by the U. S. Atomic Energy Commission. (b) On a fellowship from the C.N.R.S., Beirut, Lebanon.
(2) (a) M. Blander and S. J. Yosim, *J. Chem. Phys.*, **39**, 2610 (1963); (b) M. Blander and L. E. Topol, *Inorg. Chem.*, **5**, 1641 (1966).
(3) M. L. Saboungi and M. Blander, *High Temp. Sci.*, in press.
(4) M. L. Saboungi, C. Vallet, and Y. Doucet, *J. Phys. Chem.*, **77**, 1699 (1973).
(5) C. Sinistri, P. Franzosini, and M. Rolla, "An Atlas of Miscibility Gaps in Molten Salt Systems," Institute of Physical Chemistry, University of Pavia, Italy, 1968.
(6) M. Blander, "Thermodynamic Properties of Molten Salt Solutions," in "Molten Salt Chemistry," M. Blander, Ed., Interscience, New York, N. Y., 1964.
(7) I. Prigogine and R. Defay, "Chemical Thermodynamics," Translated by D. H. Everett, Wiley, New York, N. Y., 1954.
(8) M. J. D. Powell, *Comp. J.*, **8**, 303 (1965).
(9) Quantum Chemistry Program Exchange, University of Indiana, Bloomington, Ind.
(10) C. Sinistri, P. Franzosini, and G. Flor, *Gazz. Chim. (Rome)*, **97**, 275 (1967).
(11) O. J. Kleppa and S. V. Meschel, *J. Phys. Chem.*, **67**, 688 (1963).

(12) P. Franzosini and C. Sinistri, *Ric. Sci.*, **A3**, 439 (1963).
(13) J. Lumsden, "Thermodynamics of Molten Salt Mixtures," Academic Press, London, 1966.
(14) D. R. Stull and H. Prophet, *Nat. Ref. Data Ser., Nat. Bur. Stand.*, **No. 37** (1971).
(15) F. D. Rossini, *et al.*, *Nat. Bur. Stand. Circ.*, **No. 500** (1952).
(16) G. A. Bukhalova and D. V. Sementsova, *Russ. J. Inorg. Chem.*, **10**, 1027 (1965).
(17) M. L. Sholokhovich, D. S. Lesnykh, G. A. Bukhalova, and A. G. Bergman, *Dokl. Akad. Nauk. SSSR.* **103**, 261 (1955).

Kinetic Studies of Bis(chloromethyl) Ether Hydrolysis by Mass Spectrometry

J. C. Tou,* L. B. Westover,

Analytical Laboratories

and L. F. Sonnabend

Designed Polymers Research, Dow Chemical U. S. A., Midland, Michigan 48640 *(Received October 10, 1973)*

Publication costs assisted by the Dow Chemical Co.

The hydrolysis of bis(chloromethyl) ether (bis-CME) was studied in 2 *N* NaOH, 1 *N* NaOH, water, 1 *N* HCl, and 3 *N* HCl. From the measured values of ΔS_0^* and E^*, it was interpreted that the mechanism of the hydrolysis of bis-CME was Sn1 in character in basic solution and shifted to an Sn2 like mechanism in acidic solution.

Introduction

Chloromethyl methyl ether (CMME) is a commonly used chloromethylating agent in the manufacturing of commercial ionic resins. One of the impurities present in CMME has been found to be bis(chloromethyl) ether (bis-CME). Bis-CME has been shown recently to be a very strong carcinogen in experiments involving skin painting,[1] subcutaneous injection,[1] and inhalation.[2] Since these findings, possible industrial exposure to this simple molecule has been of very much concern. Analytical techniques for analysis of ppb levels of bis-CME in air have then been developed quite recently.[3,4]

Unlike CMME, which has been extensively studied,[5] the hydrolysis of bis-CME in solution has not been investigated to the best of our knowledge. In this report, the rates of bis-CME hydrolysis were determined in 2 *N* NaOH, 1 *N* NaOH, water, 1 *N* HCl, and 3 *N* HCl. The Arrhenius expressions for the hydrolysis rates were also determined. The systematic changes of the determined values of ΔS_0^* and E^* from basic solution to acidic solution are discussed in terms of the changes of the hydrolysis mechanisms.

The least-squares linear fits of the rate and arrhenius plots were achieved with use of an IBM 1130 computer.

Experimental Section

Due to the high toxicity of bis-CME, any exposure to this molecule must be avoided. The rate determinations were, therefore, carried out at very low concentration levels of the order of 1 ppm. Bis-CME dissolves in aqueous solution very slowly. To facilitate a fast dispersion of bis-CME in aqueous solution, a 1% bis-CME–acetone solution was used. Here, acetone acted as a carrier for dispersion. The hydrolysis apparatus is shown in Figure 1. The bis-CME–acetone solution (20 μl) was injected into a sealed 160-cc vessel filled with the appropriate solution in which the hydrolysis rate was to be determined. Assuming no prior hydrolysis took place, the concentration so prepared was *ca.* 1 ppm. The vessel was placed in a thermal bath and completely filled with the appropriate solution so that no air space remained into which bis-CME might volatize thus changing the concentration of the solution. The solution was constantly stirred. The syringe used for injecting the bis-CME–acetone solution served for sealing the opening used for the injection. To avoid any bis-CME escaping into the atmosphere, the syringe was not removed until after the bis-CME in the aqueous solution reached an undetectable level. The concentration of bis-CME in the aqueous solution was monitored using a CEC 21-110 double focusing mass spectrometer coupled with a 15-head semi-membrane silicone fiber probe. The development of the fiber probe was published elsewhere by Westover, Tou, and Mark.[6] In order to detect the anticipated weak signals, an amplifier with a gain of about 30 was installed to amplify further the mass spectrometer output.

A few milligrams of benzene in a 500-cc reservoir at 200° was bled into the mass spectrometer through a molecular leak. The purpose for this was twofold. One was for calibration as an internal mass marker for the peaks to be monitored. The second was for checking whether or not there were variations of the instrument sensitivity during each experiment. The resolution of the mass spectrometer was adjusted to *ca.* 2000, which was enough to resolve a doublet peak at *m/e* 79 due to $C_5{}^{13}CH_6^-$ and $C_2H_4OCl^-$. The former ion is the ^{13}C molecular ion of benzene. The latter ion, $C_2H_4OCl^-$, which was monitored, is the most intense ion in the mass spectrum of bis-CME and is generated from the molecular ion, $ClCH_2OCH_2Cl^{\cdot+} \rightarrow ClCH_2O^+{=}CH_2 + \cdot Cl$. The intensity of the $C_2H_4OCl^-$ peak is directly proportional to the concentration of bis-

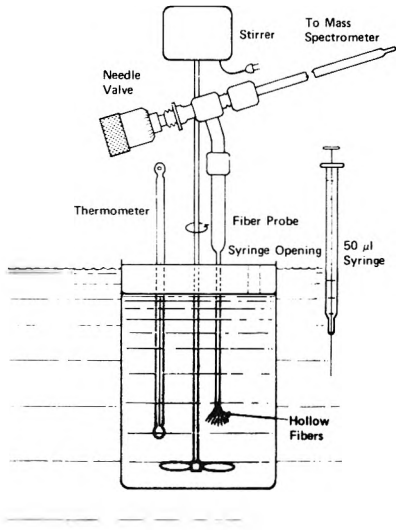

Figure 1. Bis-CME hydrolysis apparatus.

CME in solution. The doublet at m/e 79 was repetitively scanned at a rate of ~1.3 sec per data point and recorded using a light beam oscillograph.

Results and Discussion

The monitored intensity of the $C_2H_4OCl^+$ peak was found to be dependent upon rates of mixing and hydrolysis. In order to determine the rate of mixing, acetone was used and the rate measured by monitoring the molecular ion of acetone. Acetone was found to reach equilibrium in the solution in *ca.* 20 sec. The recorded intensity change of the $C_2H_4OCl^+$ peak can be considered to be solely due to hydrolysis only after bis-CME is uniformly dispersed in the solution. The rate of mixing was found to be dependent on temperature and viscosity of the solutions being studied. These dependences are easily recognizable from the intensity changes of the $C_2H_4OCl^+$ peak. The peak intensities monitored gradually increased to their maxima as mixing occurred and then followed a decay controlled by the bis-CME hydrolysis rate in solution at the experimental temperature. The log of the intensity of the $C_2H_4OCl^+$ peak after reaching its maximum was plotted against time. The rate of hydrolysis can then be derived from the slope of a least-squares fit straight line. Two rate curves are shown in Figures 2 and 3 to serve as representative cases. Because the signals monitored are weak, scattering of the data points is expected. Generally speaking, the lower the temperature and the weaker the signal, the larger the scattering. These are clearly demonstrated in Figures 2 and 3. Even though the data points are scattered, a linear plot was obtained in every case studied which indicates the hydrolysis is a pseudo-first-order reaction.

The rates determined at different temperatures can be expressed in the Arrhenius form

$$k = Ae^{-E^*/RT} = 2.1 \times 10^{10} T e^{\Delta S^*/R} e^{-E^*/RT} \qquad (1)$$

where k is the rate at temperature T, A the Arrhenius frequency factor, R the gas constant, ΔS^* the entropy of activation, and E^* the energy of activation. Hence the plot of log k against $1/T$ will yield a straight line, from which E^* can be derived from the slope and A from the intercept. The Arrhenius plot with least-squares fit is shown in Figure 4 for the hydrolysis of bis-CME in 3 N HCl as a representative case. The values of A, ΔS_0^*, and E^* along

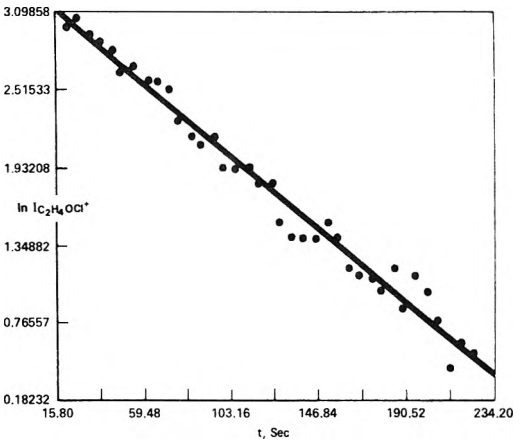

Figure 2. Hydrolysis of bis-CME in 3 N HCl at 294.5°K.

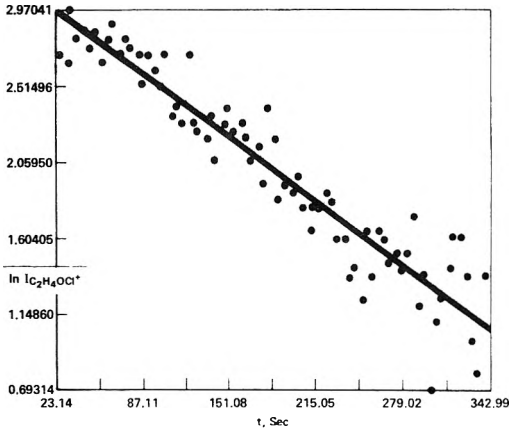

Figure 3. Hydrolysis of bis-CME in 3 N HCl at 288.4°K.

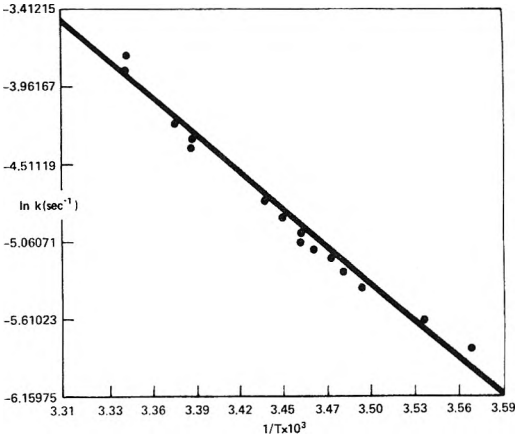

Figure 4. Arrhenius plot of bis-CME hydrolysis in 3 N HCl.

with the standard deviations were calculated and are summarized in Table I.

As shown in Table I, a systematic change in A, ΔS_0^*, and E^* is clearly demonstrated as the hydrolysis media changed from being basic to being acidic. The decrease of the activation energy from acidic solution to basic solution highly suggests that the hydrolysis of bis-CME is a nucleophilic reaction. It has been reported that the solvolysis of CMME, similar to that of *tert*-butyl chloride in many respects, has an unusually low activation energy and entropy of activation. Values of E^* from 8.6 to 13 kcal mol^{-1} and of ΔS_0^* from −43.7 to −15.6 eu have been re-

TABLE I: A, ΔS_0^*, and E^* for the Hydrolysis of bis-CME in NaOH (aqueous), H_2O, and HCl (aqueous)

Solution	A	ΔS_0^*, eu	E^*, kcal/mol	k, sec^{-1} 0°	20°	40°	$\pm \Delta k$, sec^{-1}
2 N NaOH	1.15×10^5	−35.2	8.96 ± 0.3	0.0079	0.024	0.064	0.002
1 N NaOH	1.34×10^8	−21.2	12.9 ± 1.0	0.0064	0.032	0.13	0.003
H_2O	1.08×10^{10}	−12.5	15.8 ± 0.4	0.0025	0.018	0.10	0.006
1 N HCl	1.94×10^{11}	−6.73	17.5 ± 0.05	0.0019	0.018	0.12	0.002
3 N HCl	8.37×10^{11}	−3.82	18.6 ± 0.11	0.0011	0.011	0.088	0.002

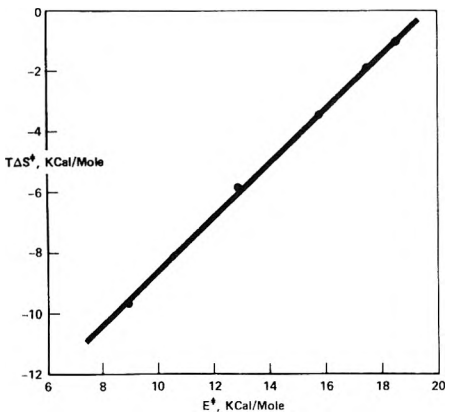

Figure 5. The compensation effect plot of $T\Delta S^*$ against E^* at 0°.

ported in various solvents.[5a,7] In the case of solvolysis of primary alkyl halides, values of E^* are *ca.* 20 to 25 kcal mol^{-1} and of ΔS_0^* *ca.* −4 to −12 eu.[3] The former case is typical of the transition state involving an ion-pair like configuration (S_N1 mechanism), and the latter case involves a covalent bond like configuration (S_N2 mechanism). Comparing our values shown in Table I with those discussed above, the mechanism of the hydrolysis of bis-CME is S_N1 in character in basic solutions and shifts to an S_N2 like mechanism in acidic solutions. In basic solutions, the formation of the ion-pair like transition state would be facilitated by charge delocalization, $[ClCH_2OCH_2^+]Cl^- \rightarrow [ClCH_2\text{-}O^+{=}CH_2]Cl^-$. However, the carbonium ions will be destabilized due to the protonation on the ether oxygen atom in acidic solutions. In this case, the attack of a nucleophile, ^-OH, on the α carbon is anticipated and, therefore, the S_N2 reaction is favored.

In a considerable number of kinetic studies involving a series of solvents, plots of $T\Delta S^*$ against E^* have been found to be straight lines of approximately unit slope.[8] As shown in Figure 5, the linear relationship was indeed found to be true in the present case and exhibited a slope of about 0.92. The positive slope indicates that energies of activation and entropies tend to compensate each other, so that the changes in free energy are small. The irregular variations of the rate constants calculated in different solvents at different temperatures, as shown in Table I, are believed to be real and to be caused by the alleged compensation effect[8] which determines both the slopes (E^*) and the intercepts (ΔS^*) in the Arrhenius rate plots. The directions of the variations in the rate constants determined in different solvents are controlled by the crossings of the rate curves in the Arrhenius plots.

Conclusion

The hydrolysis of bis-CME was found to be a pseudo-first-order reaction in all of the cases investigated. The decrease of the activation energy from acidic solution to basic solution highly suggests that the hydrolysis of bis-CME is a nucleophilic reaction. Comparing the values of ΔS_0^* and E^* measured for bis-CME with those for CMME and primary alkyl halides, it can be rationalized that the mechanism of the hydrolysis of bis-CME is S_N1 in character in basic solutions and shifts to an S_N2 like mechanism in acidic solutions.

Acknowledgment. The authors would like to express their great appreciations to T. Alfrey, G. J. Kallos, and D. R. Carter for their helpful discussions.

References and Notes

(1) B. L. VanBuuren, A. Sivak, B. M. Gold Schmidt, C. Katz, and S. Milchonne, *J. Nat. Cancer Inst.*, **43**, 481 (1969).
(2) S. Laskin, M. Kuschner, R. T. Drew, V. P. Cappielle, and N. Nelson, *Arch. Environ. Health*, **23(8)**, 135 (1971).
(3) L. Collier, *Environ. Sci. Tech.*, **6**, 980 (1972).
(4) L. A. Shadoff, G. J. Kallos, and J. S. Woods, *Anal. Chem.*, **45**, 2341 (1973).
(5) (a) T. C. Jones and E. R. Thornton, *J. Amer. Chem. Soc.*, **89**, 4863 (1967), and the references therein; (b) T. J. Ribar and M. J. Glavas, *Glas. Hem. Drus., Beograd*, **33**, 517 (1968).
(6) L. B. Westover, J. C. Tou, and J. H. Mark, *Anal. Chem.*, **46**, 568 (1974).
(7) P. Salomaa, *Ann. Univ. Turku.*, **A14** (1953).
(8) K. J. Laidler, "Chemical Kinetics," McGraw-Hill, New York, N. Y., 1965, p 251.

Partial Molal Volumes of Ions in Organic Solvents from Ultrasonic Vibration Potentials and Density Measurements. II. Ethanol and Dimethylformamide

F. Kawaizumi and R. Zana*

C.N.R.S., Centre de Recherches sur les Macromolécules, 67083 Strasbourg-Cedex, France *(Received November 16, 1973)*

The partial molal volumes of monovalent ions in ethanol and dimethylformamide (DMF) have been obtained from ultrasonic vibration potential data and density data for solutions of uni-univalent electrolytes. The use of Hepler's equation has permitted us to split ionic partial molal volumes into geometric and electrostrictive contributions. The results obtained in this work together with those previously reported for ions in water and methanol indicate that the parameters which determine ionic partial molal volumes are (1) the size of solvent molecules, (2) the degree of steric hindrance of the poles of the dipole of the solvent molecule, and (3) the properties of the layer of atoms 3–4 Å thick around ions. The geometric contribution depends on 1 and 2 while 2 and 3 appear to determine the contribution of electrostriction.

Introduction

In the first paper[1] in this series, partial molal volumes of monovalent ions in methanol were obtained from the combination of ultrasonic vibration potential (uvp) data and density data for solutions of uni-univalent electrolytes. The purpose of this paper is to report similar data in ethanol and dimethylformamide (DMF).

As will be seen below these data show that the empirical methods of Mukerjee[2] and of Conway, *et al.*,[3] for obtaining ionic partial molal volumes do not hold in DMF. They also provide new informations about the parameters which determine ionic partial molal volumes.

The apparatus and the experimental procedures used in this work have been previously described.[1]

Partial Molal Volumes of 1-1 Electrolytes at Infinite Dilution in Ethanol and DMF

Density data for electrolytes in ethanol and DMF are quite scarce in the literature. For this reason, as a part of this work measurements of density as a function of concentration were performed for solutions of ten 1-1 electrolytes in ethanol and thirteen 1-1 electrolytes in DMF. The apparent molal volume φ_2 of the salts have been calculated using eq 3 in ref 1. The partial molal volumes $\bar{V}_2^0$ of the salts at infinite dilution were obtained by extrapolating to zero concentration the curves $\varphi_2 = f(c^{1/2})$, where c is the concentration, according to Masson's equation.[4]

The results are shown in Figures 1–4. They indicate an overall error of about ±1 cm³/mol on $\bar{V}_2^0$ values. The error on $\bar{V}^0$(CsI) in ethanol may be larger because the limited solubility of CsI prevented the investigation of a sufficiently large range of concentration (the extrapolation was performed by assuming for the line $\varphi_2 = f(c^{1/2})$ the same slope as for RbI). Within the experimental error we found that small additions of water resulted in negligible changes of φ_2 and $\bar{V}_2^0$ (see Figure 3).

The values of $\bar{V}_2^0$ and of the slopes S_V' of the lines $\varphi_2 = f(c^{1/2})$ are listed in Table I where are also given the results of other workers.[5,6] The result of Butler and Lees[5a] for LiCl in ethanol is in good agreement with that found in this work. For DMF differences well above the experimental error appear between the results of Gopal, *et al.*,[6] and those found in this work. It must be pointed out, however, that the results of these authors[6] were obtained at 35°. They are cited in Millero's review[7] as a "private communication" but have not appeared in the Chemical Abstracts up to now. We were thus unable to find the source of these discrepancies. For this reason our results were preferred when calculating ionic partial molal volumes.

The results of Table I indicate that within the experimental error the values of $\bar{V}_2^0$ obey the additivity rule.[7] A number of results listed in Table I were obtained using this rule because the solubility of several electrolytes (mostly chlorides in ethanol) is too low to permit measurements of density with the accuracy required for apparent molal volume determination.

Ultrasonic Vibration Potential of Electrolytes in Ethanol and DMF

The results of the measurements performed in the range 3×10^{-4} to 3×10^{-2} M for most of the electrolytes of Table I are given in Table II. The sign of the uvp Φ was assigned as previously reported.[1,8] Small additions of water (up to 1%) were found to have no effect on the measured uvp.

As for electrolytes in methanol, in all instances but $LiNO_3$, the uvp show a decrease at concentrations above 3×10^{-3} to 10^{-2} M. These decreases are relatively small for bromides and nitrates but become significant for iodides thus showing the same trend as that observed for electrolytes in methanol.[1] Two processes may be responsible of these variations of Φ: (1) ion-pair formation which occurs at lower concentrations in organic solvent than in water, owing to their lower dielectric constant (as pointed out in ref 1 ion pairs may give rise to dipole vibration potentials);[9] (2) formation of complex ions such as triple ions.[10]

The concentration of ion pairs and complex ions increases with the electrolyte concentration c. One may therefore expect an influence of these two processes on the measured uvp at higher c, as is experimentally found. At this point it is worth recalling that in some soap solutions Φ is concentration dependent both in the submicellar and

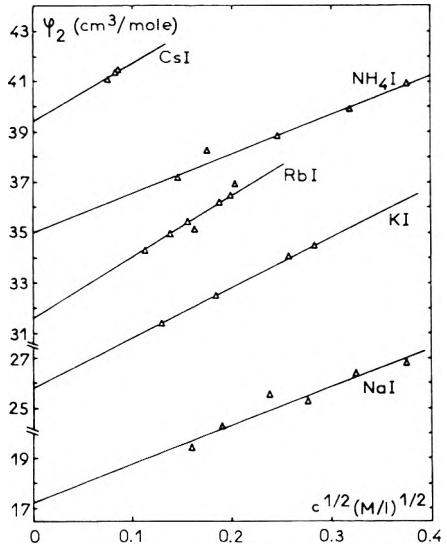

Figure 1. Apparent molal volumes of alkali metal and ammonium iodides *vs.* (molar concentration)$^{1/2}$ in ethanol at 25°.

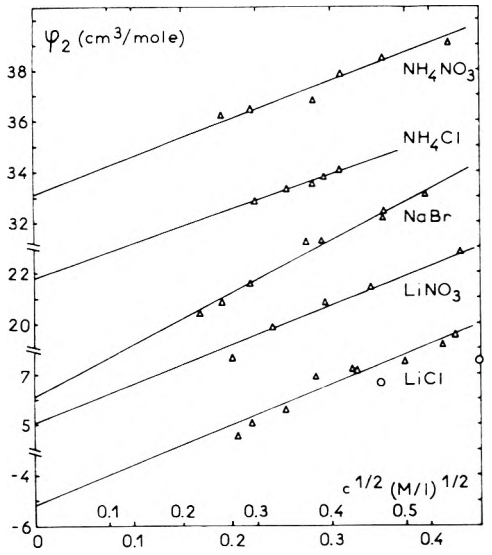

Figure 2. Apparent molal volumes of NH_4NO_3, NH_4Cl, NaBr, $LiNO_3$, and LiCl (our results, Δ, results from ref 5a, O) *vs.* (molar concentration)$^{1/2}$ in ethanol at 25°. The inner concentration scale is for LiCl.

in the micellar ranges of concentration[11] because of submicellar association and micelle formation.

The results of Table II show that in most instances Φ varies only slightly with c in the range 3×10^{-4} to 3×10^{-3} M. For this reason the values of Φ listed in column c in Table II and which were used in calculating ionic partial molal volumes have been taken in this range.

Calculation of Ionic Partial Molal Volumes

The calculation of partial molal volumes of anions ($\bar{V}_-^0$) and cations ($\bar{V}_+^0$) at infinite dilution makes use of eq 1 and 2 in ref 1. It involves the knowledge of the cation and anion transport numbers t_+ and $t_- = 1 - t_+$ and of the amplitude a_{s0} of the velocity of ions in the ultrasonic field.

The transport numbers have been obtained from the limiting equivalent conductivities of ions in ethanol and DMF compiled by Kratochvil and Yeager,[12] and the values of t_+ are listed in Table I. At the onset it must be

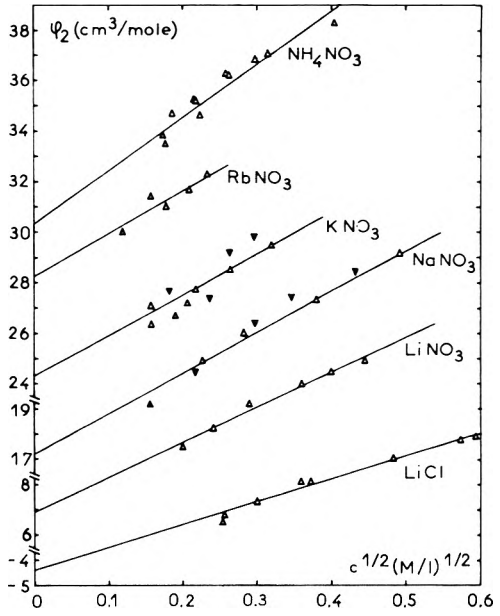

Figure 3. Apparent molal volumes of ammonium, rubidium, potassium, sodium, and lithium nitrates and lithium chloride *vs.* (molar concentration)$^{1/2}$ in DMF (Δ) and in 99% DMF–1% H_2O (▼) at 25°.

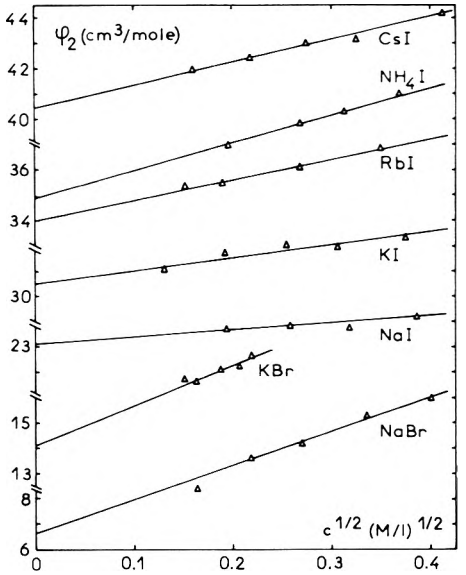

Figure 4. Apparent molal volumes of alkali metal iodides, ammonium iodide, and potassium and sodium bromides *vs.* (molar concentration)$^{1/2}$ in DMF at 25°.

pointed out that transport numbers in DMF are less accurate than in water, methanol, and ethanol. For example, Prue and Sherrington[13] results, which were adopted in this work, yield $t^0(K^+) = 0.359$ in KCl solution while data from other workers[14] give 0.342 for the same quantity. This fact introduces an additional error of up to 2 cm^3/mol in the calculation of ionic partial molal volumes in DMF.

For ions in ethanol, a_{EtOH} was determined using the same graphical procedure as for methanol.[1] Its average value was found to be 11.1 cm/sec. Table III gives in column a the ionic partial molal volumes in ethanol calculated using $a_{EtOH} = 11.1$ cm/sec and the $\bar{V}_2^0$ and Φ data of Tables I and II. For each ion the value in column a is an average over the results for all of the electrolytes of Table

TABLE I: Partial Molal Volumes of Electrolytes and Cation Transport Numbers at Infinite Dilution in Ethanol and DMF at 25°

	Ethanol				DMF			
	$\bar{V}_2^0$, cm³/mol				$\bar{V}_2^0$, cm³/mol			
	This work	Other works	S_v', cm³/mol$^{3/2}$	t_+[c]	This work	Other works	S_v', cm³/mol$^{3/2}$	t_+[c]
HCl		3.0[d]		0.733				
LiCl	−5.2	−4.4[e]	12	0.438	−4.4		9	0.312
$LiNO_3$	5.1		15.3	0.390	6.9		14	0.304
NaCl	4.0[a]			0.482	5.9[a]			0.352
NaBr	6.1		20.5	0.480	6.6		13.5	0.358
NaI	17.2		15.5	0.430	23.1	21.3[f]	2.7	0.364
$NaNO_3$	15.3[a]			0.432	17.2	24.5[f]	16	0.343
KCl	12.6[a]			0.518	13.0[a]			0.359
KBr					14.1		15.5	0.365
KI	25.8		20	0.466	30.5	35.8[f]	5	0.371
KNO_3	23.9[a]			0.469	24.3		16	0.350
NH_4Cl	21.8		13.5	0.486	18.9[a]			0.413
NH_4I	35.0		15.7	0.434	34.9	38.4[f]	10	0.425
NH_4NO_3	33.1		15	0.437	30.3	41.7[f]	21	0.403
RbCl	18.4[a]			0.533	17.0[a]			0.370
RbI	31.6		24	0.481	34.0		8	0.383
$RbNO_3$	29.7[a]			0.484	28.3		16.5	0.361
CsCl	26.2[a]			0.547				
CsI	39.4[b]		23	0.495	40.4		9.3	0.397
$CsNO_3$	37.5[a]			0.498	34.8[a]			0.376

[a] Values obtained using the additivity rule. [b] The error on $\bar{V}^0$(CsI) is probably larger than for other salts owing to the low solubility of CsI in ethanol. The values of $\bar{V}^0$(CsCl) and $\bar{V}^0$($CsNO_3$) in ethanol are likely to be affected by the same error. [c] Values calculated using the results compiled in ref 12. [d] Reference 5b. [e] Reference 5a. [f] Reference 6.

TABLE II: Ionic Vibration Potential Φ (in μV) of Uni-univalent Electrolytes at Various Concentrations (in *M*) in Ethanol and DMF at 22°[a]

	Concentration											
	3×10^{-4}		10^{-3}		3×10^{-3}		10^{-2}		3×10^{-2}		Φ[c]	
Electrolyte[b]	EtOH	DMF	EtOH	DMF	EtOH	DMF	EtOH	DMF	EtOH	DMF	EtOH	DMF
HCl (1,0)	−4.5		−4		−4		−3.5				−4[d]	
$LiNO_3$ (0,1)		−22.5		−22		−20		−12.5		−9		−22
NaCl (2,1)	5	14.5	2.5	23	3						3[d]	16[d]
NaBr (1,2)	−23.5	−25	−24.5	−23.5	−24.5	−24	−27	−24.5	−30.5	−26	−24.5	−24
NaI (1,1)	−62	−53.5	−66.5	−53	−70	−58	−73.5	−62	−78.5	−67	−68	−53.5
$NaNO_3$ (4,2)	−12	−8	−13	−9.5	−16	−9	−21	−7.5		−8	−14.5	−9
KCl (2,2)	9.5	14	12.5	24.5	13	30					12.5[d]	16[d]
KBr (0,1)		−14		−13.5		−14		−16		−18		−14
KI (1,2)	−43	−53	−46	−53.5	−47	−58	−51.5	−62	−60	−65	−46.5	−53.5
KNO_3 (2,2)	−5.5	−8	−4	−8.5	−5.5	−7		−5		−6.5	−5[d]	−8[d]
NH_4Cl (1,1)	−8	−1.5	−7	−6.5	−6.5	−9	−7				−7	−3
NH_4I (0,2)		−63		−70.5		−70.5		−72		−74		−68
NH_4NO_3 (3,2)	−22.5	−17	−24	−16.5	−25.5	−18	−28	−19	−30	−20.5	−25	−17
RbCl (2,1)	36	42.5	39	47							39	45
RbI (1,1)	−13.5	−20	−16.5	−21.5	−20.5	−26.5	−24.5	−34			−18.5	−21
$RbNO_3$ (1,1)	17.5	26.5	19.5	26.5		23		18.5		15.5	19.5	26.5
CsCl (2,1)	64		70.5		71						71	
CsI (1,1)	9	−4	8	−4.5	5.5	−9		−13		−17	8[d]	−4.5[d]
$CsNO_3$ (3,1)	51.5	49		50.5		47.5		42			51.5	49.5

[a] Prior to measurements in organic solvents, measurements were carried out on aqueous solutions of CsCl and RbCl in order to obtain the value of the velocity amplitude a_W in water.[1] The average value of a_W was found to be 10.35 cm/sec and the uvp's measured in organic solvents have all been multiplied by $10.35/a_W$ to give the values of Φ listed above. [b] The numbers in parentheses represent the numbers of independent runs performed on each electrolyte; the first number is for to ethanol (EtOH) and the second for DMF. [c] Values of Φ selected for ionic partial molal volume calculations (see text). [d] Salt for which the sign of the uvp has been obtained as explained in ref 1.

I involving this ion. The values of $\bar{V}^0(Na^+)$, $\bar{V}^0(Cl^-)$, $\bar{V}^0(NO_3^-)$ and $\bar{V}^0(I^-)$ yield results in good agreement with those which can be calculated from the $\bar{V}_2^0$ data of Table I. For this reason the ionic partial molal volumes have been recalculated using these four values as references and the $\bar{V}_2^0$ data of Table I, yielding the set of values listed in column b. The values of $\bar{V}^0(Br^-)$ in columns a and b differ by 5.7 cm³/mol while for all of the other ions the differences are below 2 cm³/mol, *i.e.*, within the experimental error which is estimated to be ±2-3 cm³/mol for all ions except Cs^+ for which the error may be somewhat larger.

For ions in DMF, a_{DMF} was taken as 10.5 cm/sec. Indeed the use of eq 5 in ref 1 and the calibration of the apparatus with aqueous solutions of known uvp show that for DMF one should have $10.35 \leq a_{DMF} \leq 10.7$ cm/sec. The results of these calculations are given in Table IV. The values of the partial molal volume of a given ion, cal-

TABLE III: Ionic Partial Molal Volumes in Ethanol at 25° (cm^3/mol)

Ion	This work[a]	This work[b]	Mukerjee's method[c]	Water[d]
H^+		−15.5		−5.7
Li^+		−19.2	−20.2	−6.6
Na^+	−9.8 (1.5)	−9.8	−10.5	−6.9
K^+	−2.5	−0.4	−1.9	3.3
Rb^+	6.8	5.5	3.9	8.4
Cs^+	15.2	13.3	11.7	15.6
NH_4^+	7.0	8.9	6.8	12.2
Cl^-	12.3 (2.6)	12.5	15.0	23.5
Br^-	20.8	15.1	16.6	30.4
I^-	26.7 (3.4)	26.7	27.7	41.9
NO_3^-	23.8 (1.6)	23.8		34.7

[a] The numbers in parentheses represent the root mean square deviations obtained as in ref 1, for a velocity amplitude a_{KOH} = 11.1 cm/sec. [b] Average values calculated using $\bar{V}^0(Cl^-)$ = 12.5 cm^3/mol, $\bar{V}^0(Na^+)$ = 9.8 cm^3/mol, $\bar{V}^0(I^-)$ = 26.7 cm^3/mol, $\bar{V}^0(NO_3^-)$ = 23.8 cm^3/mol, and the $\bar{V}_2^0$ data of Table I. [c] Values calculated using Mukerjee's method[2] and the $\bar{V}_2^0$ data of Table I. [d] Values obtained from the data compiled in ref 7 with $\bar{V}^0(Cl^-)$ = 23.5 cm^3/mol (see ref 3 and 8).

TABLE IV: DMF Ionic Partial Molal Volumes in cm^3/mol and at 25° Calculated from the Data of Tables I and II with a_{DMF} = 10.5 cm/sec

	Chlorides	Bromides	Iodides	Nitrates
A. Results for Cations				
Li^+				−24.1
Na^+	−22.4	−25.4	−26.4	−17.5
K^+	−11.4	−20.4	−14.5	−7.1
Rb^+	−9.2		−13.3	−8.4
Cs^+			2.2	0.9
NH_4^+	−1.0		−4.0	−2.1

Salts of Li^+		Na^+	K^+	Rb^+	Cs^+	NH_4^+
B. Results for Anions						
Cl^-		28.3	24.4	26.2		19.9
Br^-		32.0	34.5			
I^-		49.5	45.0	47.3	38.2	38.9
NO_3^-	31.0	34.7	31.4	36.7	33.9	32.3

culated from the results for several electrolytes containing this ion, show a greater scatter than in the case of methanol[1] and ethanol. For example, the calculated values of $\bar{V}^0(I^-)$ range from 38.2 to 49.5 cm^3/mol with an average values of 43.8 cm^3/mol and a root mean square deviation of 4.5 cm^3/mol. For NO_3^-, however, the values of $\bar{V}^0(NO_3^-)$ calculated for the six nitrates studied in this work are quite consistent, ranging from 31 to 36.7 cm^3/mol with a root mean square deviation of 2 cm^3/mol from the mean of 33.3 cm^3/mol. For this reason this value of $\bar{V}^0(NO_3^-)$ was adopted as reference and used together with the $\bar{V}_2^0$ data of Table I to calculate the set of ionic partial molal volumes given in column b in Table V. For comparison are given in column a the average ionic partial molal volumes calculated from the results of Table IV. The comparison of columns a and b shows that for Li^+, K^+, Cs^+, NH_4^+, and Cl^- the difference between the two sets of data is less than 3 cm^3/mol. For Na^+, Rb^+, and I^- this difference is about 5.5 cm^3/mol. This last value is slightly above the estimated maximum error on ionic partial molal volumes in DMF (±4 cm^3/mol). The case of Br^- is more difficult to understand. Indeed the difference between the results of columns a and b is larger than 10 cm^3/mol. The behavior of Br^- in DMF is similar to that

TABLE V: Ionic Partial Molal Volumes in DMF in cm^3/mol and at 25°

Ion	This work[a]	This work[b]	Mukerjee's method[c]	Water[d]
Li^+	−24.1	−26.4	−19.4	−6.6
Na^+	−22.1 (3.6)	−16.3	−9.1	−6.9
K^+	−11.0 (3.0)	−9.0	−2.0	3.3
Rb^+	−10.3 (2.2)	−5.0	2.0	8.4
Cs^+	1.6	1.5	8.5	15.6
NH_4^+	−2.4 (1.2)	−3.1	3.9	12.2
Cl^-	24.7 (3.1)	22.0	15.0	23.5
Br^-	33.3	22.9	15.9	30.4
I^-	43.8 (4.5)	39.0	32.3	41.9
NO_3^-	33.3 (2.0)	33.3	26.6	34.7
$(C_2H_5)_4N^+$		125.5[e]		143.4
$(C_3H_7)_4N^+$		198[e]		208.7
$(C_4H_9)_4N^+$		266.4[e]		270.1
$(C_5H_{11})_4N^+$		336.7[e]		333.5

[a] Average values calculated from the results of Table III. For Na^+ and K^+ the results obtained with the bromides have not been taken into account (see text). The root mean square deviations are given in parentheses. [b] Calculated from the $\bar{V}_2^0$ data of Table I with $\bar{V}^0(NO_3^-)$ = 33.3 cm^3/mol. [c] Calculated using Mukerjee's method and the data of Table I. [d] Obtained from the data compiled in ref 7 with $V^0(Cl^-)$ = 23.5 cm^3/mol (see ref 3 and 8) [e] Obtained from the $\bar{V}_2^0$ data for tetraalkylammonium halides of Gopal, *et al.*,[6] cited in ref 7 with $\bar{V}^0(I^-)$ = 39 cm^3/mol.

observed in ethanol. The purity of the bromides used in the experiments is not involved as NaBr and KBr were both Merck purissimum compounds (purity >99.9%) and yielded identical values for $\bar{V}_2^0$ and Φ when used without further purification and after an additional recrystallization.

Before discussing ionic partial molal volumes in terms of geometric and electrostrictive contributions it is interesting to compare the "experimental" ionic partial molal volumes obtained in this work with those that can be calculated using the method of Mukerjee[2] and the extrapolation procedure of Conway, *et al.*[3]

Mukerjee's method assumes the ionic partial molal volume $\bar{V}_i^0$ of an ion i to depend only on its ionic radius r_i. The $\bar{V}_i^0$'s are then obtained by setting the value of the partial molal volume of a certain ion such that all other ionic partial molal volumes calculated from this chosen value and $\bar{V}_2^0$ data fall on a single curve when plotted as a function of r_i^3. Mukerjee's method can be used in each instance where a sufficient number of values of $\bar{V}_2^0$ are known. When applied to the data of Table I in conjunction with Pauling's ionic radii, this method yielded the two sets of values listed in column c in Tables III and V. For ethanol the differences between the experimental results (column b) and those of column c are of about 1–2 cm^3/mol, *i.e.*, within experimental accuracy. For DMF, however, the differences are of about 7 cm^3/mol. Thus Mukerjee's method does not apply in DMF in contradistinction to water,[8] methanol,[1] and ethanol. This conclusion is discussed below.

The extrapolation method of Conway, *et al.*,[3] makes use of the partial molal volumes of tetraalkylammonium (TAA) halides. An extrapolation to zero cation molecular weight then yields the partial molal volume of the halide ion. There are no data available for TAA halides in ethanol. In DMF the use of Gopal, *et al.*,[6] results extrapolated to 25° yields $\bar{V}^0(I^-) = -4 \pm 5$ cm^3/mol. This value is more than 40 cm^3/mol below that in column b of Table V and shows that as for methanol[1] the extrapolation method

does not hold for DMF. The same conclusion is likely to be true for ethanol.

Discussion

As for ions in methanol[1] and water[8] the equation proposed by Hepler[15] will be used to split ionic partial molal volumes in DMF and ethanol into a geometric contribution and a contribution of electrostriction. This equation is given by[15]

$$\bar{V}_i^0 = Ar_i^3 - B/r_i \qquad (1)$$

where A and B are two constants. The first term in the right side of eq 1 represents the geometric contribution and the second term the electrostrictive contribution. This equation has been shown to give a good description of ionic partial molal volumes in water[8] and methanol.[1] For these two solvents A and B have been found to depend only on r_i and not on the sign of the ionic charge.[1,8]

Figures 5 and 6 show the plots of $\bar{V}_i^0 r_i$ *vs.* r_i^4 (Pauling's ionic radii) for ions in ethanol and DMF. For each solvent the points relative to alkali metal ions and halide ions define two straight lines (referred to as 1 and 2, respectively) as predicted by eq 1. For DMF the difference between lines 1 and 2 is well above the experimental accuracy and there is a clear dependence of A and B on the sign of the ionic charge. For ethanol, such a clear cut conclusion cannot be reached on the basis of the results of Figure 5. The difference between lines 1 and 2 is larger than that found for methanol (see Figure 6 in ref 1). Moreover the slopes of lines 1 and 2 are different while in methanol these lines run parallel.[1] Nevertheless, Figure 5 shows that line 1′ which corresponds to the results of column c of Table III (Mukerjee's method) is compatible with the experimental points for all of the alkali metal and halide ions (values in column b) if we assume a maximum error of ±4 cm³/mol for $\bar{V}^0(Cs^-)$ (owing to the limited accuracy on the value of $\bar{V}^0(CsI)$) and for $\bar{V}^0(Br^-)$ (whose abnormal behavior has been pointed out above). With the same assumption the correspondence method of Criss and Cobble[16] appears to hold for ions in ethanol and yields $(\bar{V}_i^0)_{EtOH} = 0.72 (\bar{V}_i^0)_{H_2O} - 3$.

The values of A and B for alkali metal and halide ions obtained from the plots of Figures 5 and 6 and the results for TAA ions in DMF calculated from the data of Gopal, *et al.*[6] (see line 3 on Figure 6), are given in Table VI. For comparison we have also given the results for ions in water[8] and methanol.[1] As will be seen now these results will permit us to find which parameters determine ionic partial molal volumes. The discussion which follows is restricted to the values of A and B obtained from line 1′ both for ethanol and methanol (see Figure 6 in ref 1).

Discussion of the Values of A. The results of Table VI show the three following salient features: (1) within experimental accuracy A is independent of the sign of the ionic charge for alkali metal and halide ions in water, methanol, and ethanol but depends on this parameter in DMF; (2) for the three organic solvents the values of A for alkali metal and halide ions are smaller than in water; and (3) TAA ions are characterized by identical values of A in water, methanol, and DMF.

These results can be interpreted in terms of size of solvent molecules and of specific interactions between ions and solvent dipoles.

Indeed, one may expect the contact between alkali metal ions and solvent dipoles to occur at the negative

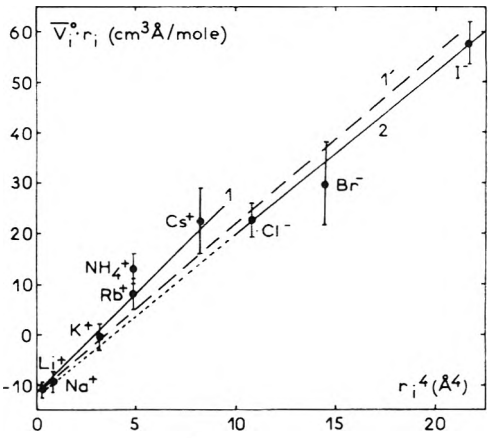

Figure 5. Variation of $\bar{V}_i^0 r_i$ *vs.* r_i^4 for ions in ethanol. Lines 1 and 2 correspond to the results of column b in Table III and line 1′ corresponds to the results of column c obtained by means of Mukerjee's method.

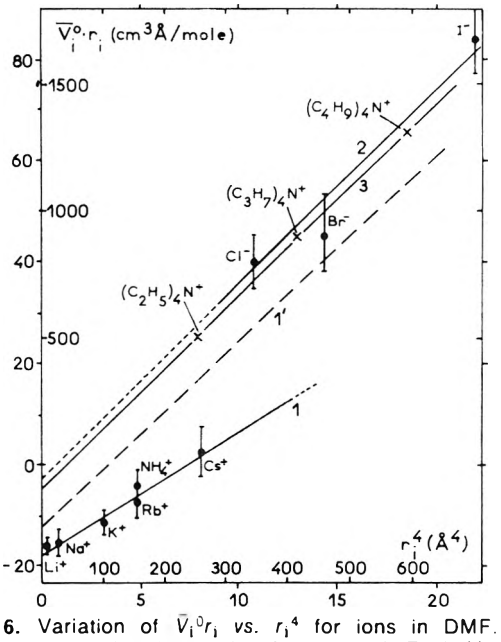

Figure 6. Variation of $\bar{V}_i^0 r_i$ *vs.* r_i^4 for ions in DMF. Lines 1 and 2 correspond to the results of column b in Table V and line 1′ corresponds to the results of column c obtained by means of Mukerjee's method. The inner scales are associated with line 3 which shows the results for TAA ions.

pole of the dipole, *i.e.*, at the oxygen atom of the solvent molecule, for the four solvents of Table VI. On the other hand, for all of these solvent molecules there is only little steric hindrance about the oxygen atoms and those may be considered as equally accessible to cations. It is therefore meaningful to compare the geometric contributions to the partial molal volume of a given cation in these solvents. Table VI shows that for alkali metal cations A increases as the size of the solvent molecule decreases, *i.e.*, as the average volume of the holes in the solvent structure decreases. Thus for a given type of ion–solvent dipole contact the perturbation of the packing of solvent molecules brought about by a given cation decreases as the size of the solvent molecule increases, resulting in smaller values of A.

The same reasoning holds for halide ions in water, methanol, and ethanol where the contact halide ion–solvent dipole occurs at the hydrogen atom of the solvent hydroxyl group. It must be added that the hydrogen atom is

TABLE VI: Values of A (cm³/Å³ mol) and B (cm³ Å/mol) at 25°

	Methanol		Ethanol		DMF		Water[a]	
	A	B	A	B	A	B	A	B
Halide ions	3.5 ± 0.2	17.5 ± 2	3.3 ± 0.2	12 ± 3	3.8 ± 0.4	2 ± 5	4.75 ± 0.2	10 ± 2
Alkali metal ions					2.5 ± 0.3	18 ± 3		
TAA ions	2.4 ± 0.2	90 ± 20			2.4 ± 0.2	100 ± 20	2.4 ± 0.2	15 ± 5

[a] From ref 8.

TABLE VII: Comparison between Experimental and Calculated Values of B for Water, Methanol, Ethanol, and DMF at 25°

Solvent	D[a]	$10^{11}K_T$, cm²/dyn	$10^{11}(\mathrm{d} \ln D/\mathrm{d}P)$, cm²/dyn	B_{calcd}, cm³ Å/mol	B_{expt}, cm³ Å/mol
Water	78.4	4.57[a]	4.71[c]	4.2	10 (alkali metal, halide and TAA ions)
Methanol	32.6	12.55[a]	11.3[c]	24.2	17 (alkali metal and halide ions)
					90 (TAA ions)
Ethanol	24.3	11.4[a]		32.6	12 (alkali metal and halide ions)
DMF	36.7	6.20[b]		11.7	18 (alkali metal ions)
					2 (halide ions)
					100 (TAA ions)

[a] From ref 22. [b] Calculated using eq 3 and 4 and the data in ref 22 and 24. [c] From ref 20 and 21.

as accessible to anions as is the oxygen atom to cations and one should not expect important differences of organization of solvent molecules about anions and cations in these three solvents. Therefore the A values should depend only slightly on the sign of the ion charge. In going to DMF the situation changes drastically. Indeed the nitrogen atom is sterically very hindered and thus not accessible to halide ions. Important differences of organization of DMF molecules about anions and cations must be therefore expected and this may very well explain the difference between the values of A for halide and alkali metal ions (see Table VI and Figure 6). One is also led to predict closer values of A for these two types of ions in formamide where the N atom is much less hindered than in DMF and thus more accessible to anions. Ionic partial molal volume determination in formamide thus appears worthwhile.

In the above the concept of volume fraction statistics[17,18] which has permitted other workers[18] to obtain the value of A for ions in water has not been used. Indeed, as already pointed out[1] this concept supposes (1) a mixture of two types of spherical objects while methanol, ethanol, and DMF molecules are not spherical and (2) that contacts between the two types of objects occur at random. This is clearly not the case, especially with DMF.

Table VI indicates that for TAA ions, A is independent of the nature of the solvent. With the radii of TAA ions given by Robinson and Stokes,[19] A has been found to be very close to the value which can be calculated for a rigid sphere immersed in a continuous solvent, *i.e.*, 2.52 cm³/mol Å³.[2] The simplest explanation for this last result is to be found in the large size of TAA ions. Indeed the smallest TAA ion (tetramethylammonium ion) has approximately the same size as DMF molecules, *i.e.*, the largest solvent of Table VI. It must be pointed out, however, that if the experimental value of A depends on the choice of TAA ion radii, the fact that identical values of A were found for water, methanol, and DMF is not affected by this choice.

Discussion of the Values of B. The expression of B for monovalent ions,[20,21] given by eq 2, provides a theoretical basis for discussing the values of B of Table VI. In eq 2, B is expressed in cm³ Å/mol, D is the dielectric constant and P the pressure in dyn/cm².

$$B = \frac{6.9 \times 10^{12}}{D} \frac{\mathrm{d} \ln D}{\mathrm{d}P} \qquad (2)$$

B has been calculated to be[20,21] 4.2 and 24.2 cm³ Å/mol for water and methanol, respectively, as the value of the derivative d ln D/dP is known for these solvents. For ethanol and DMF this quantity is not known. However with an approximation of about 10% this derivative can be set equal to the isothermal compressibility K_T of the solvent. Indeed the values of d ln D/dP and of K_T given in Table VII check this approximation. K_T is known for ethanol[22] but not for DMF. For this solvent K_T was calculated from the adiabatic compressibility K_S using eq[23] 3 and 4 where

$$K_T = K_S + TV\alpha^2/C_p \qquad (3)$$

$$K_S = 1/dc^2 \qquad (4)$$

T is the temperature, V the molar volume of the solvent, α the isobaric expansibility, C_p the molar heat at constant pressure, d the density, and c the velocity of ultrasound. As all of these quantities are known[22,24] for water, methanol, and ethanol the validity of eq 4 was checked before using it to obtain K_T for DMF. The values of K_T and of B_{calcd} calculated by means of eq 2-4 are given in Table VII together with the experimental results, B_{expt}, from Table VI.

The comparison between the values of B_{expt} and B_{calcd} shows that the solvent continuum model does not permit the explanation of any of the experimental results. It is not possible however to decide whether this failure of the continuum model is due to the model itself or to the form used for the geometric contribution because the value of B obtained from eq 1 depends on this form. Therefore the comparison of B in various solvents using eq 1 may not be correct if the geometric contribution is not proportional to r_i^3 in all solvents as previously pointed out by Millero.[20b] In this respect, the determination of the fraction of void space in a mixture of spheres (ions) and ellipsoids or cylinders (solvent molecules) in the same manner as in Robinson and Stokes[18] work would be very interesting.

In our study of ions in methanol,[1] we were led to interpret the values of B in water and methanol in terms of dielectric properties of the first layer of atoms, 3-4 Å thick, in contact with the ion rather than in terms of dielectric properties of the solvent in the bulk. The results obtained in this work give a strong support to this interpretation as is shown now.

(1) For the four solvents of Tables VI and VII the layer of atoms in contact with alkali metal ions contains essentially oxygen atoms[25] and hydrogen atoms which are either covalently bound (water, methanol, ethanol) or close (DMF) to oxygen atoms. Thus the content of this layer depends much less on the nature of the solvents than would appear from their chemical formulas. This explains that the values of B_{expt} are all between 10 and 18 cm^3 Å/mol while those of B_{calcd} range from 4 to 32 cm^3 Å/mol.

(2) In water, methanol, and ethanol halide ions are in contact with hydroxylic hydrogen atoms,[25] however, the hydroxylic oxygen atoms are in their close neighborhood. Therefore for these three solvents the layer of atoms 3-4 Å thick, *i.e.*, about the diameter of a hydroxylic group or of a methyl group, around halide ions has about the same content as around alkali metal ions. Owing to this behavior, B_{expt} does not depend on the sign of the ionic charge for the three above solvents. In DMF, halide ions have a tendency to surround themselves with nitrogen atoms. However, as pointed out above, these atoms are very sterically hindered compared to the oxygen atom of DMF. Therefore the distance between halide ions and nitrogen atoms remains large and results in a smaller electrostriction than for alkali metal ions. These results are to be compared with those of Laliberté and Conway[26] in their study of the electrostriction of water by $R_xH_{4-x}N^+$ ions with $0 < x < 4$. These authors have shown that when the steric hindrance at the nitrogen atom is increased by increasing x or the length of the alkyl group R, the electrostriction of water decreases rapidly because of the increasing average distance between water dipoles and the ion center of charge. Although a reverse situation occurs for halide ions in DMF where negative ions cannot get close to the positive pole of the solvent dipole the end result remains the same. The distance ion-dipole is too large to give rise to a strong electrostriction. The small value of B_{expt} for halide ions in DMF indicates that these ions are very slightly "solvated." A similar conclusion was reached by other workers[13] on the basis of ionic limiting equivalent conductivities.

(3) The values of B_{expt} found for TAA ions in methanol and DMF can be considered as equal within the experimental error. On the basis of the above model such a result is to be expected as in both solvents methyl groups tend to surround TAA ions. In water however TAA ions are of necessity in contact with OH groups. Therefore eq 4 when applied to the effective content of the layer of atoms in contact with TAA ions will yield much larger values of B for organic solvents than for water. This is because the dielectric constant of a system containing mostly OH groups is larger than that of a system containing essentially CH_3 groups; the reverse is true for the quantity $d \ln D/dP$ (compare D values and K_T values for water and *n*-alkanes[22]). From the above one is also led to predict values of B practically identical for TAA ions in all solvents containing methyl groups. However a different result should be obtained with formamide. This again emphasizes the interest of measurements of ionic partial molal volumes in this solvent.

Conclusions

The results obtained in parts I and II of our work on ionic partial molal volumes in organic solvents indicate that the parameters which determine the values of these quantities are (1) the size of solvent molecules and the degree of steric hindrance of the poles of the solvent dipole; and (2) the properties of the layer of atoms 3-4 Å thick around ions.

Our results also show the specificity of ion-solvent interactions and the necessity to use a molecular model to account for these interactions.

Acknowledgment. The authors are pleased to thank Dr. J. Francois for her assistance in the density measurements.

References and Notes

(1) F. Kawaizumi and R. Zana, *J. Phys. Chem.*, **78**, 627 (1974).
(2) P. Mukerjee, *J. Phys. Chem.*, **65**, 740, 744 (1961).
(3) B. E. Conway, R. E. Verrall, and J. E. Desnoyers, *Trans. Faraday Soc.*, **62**, 2738 (1966); *Z. Phys. Chem.*, **230**, 157 (1965).
(4) D. O. Masson, *Phil. Mag.*, **8**, 218 (1929).
(5) (a) J. V. Butler and A. Lees, *Proc. Roy. Soc., Ser. A*, **131**, 382 (1931); (b) J. Sobkowski and S. Minc, *Rocz. Chem.*, **35**, 1127 (1959).
(6) R. Gopal, *et al.*, cited in ref 7 as private communication.
(7) F. J. Millero, *Chem. Rev.*, **71**, 147 (1971).
(8) R. Zana and E. B. Yeager, *J. Phys. Chem.*, **71**, 521, 4241 (1971).
(9) A. Weinmann, *Proc. Phys. Soc. (London)*, **73**, 345 (1959); **75**, 102 (1960).
(10) J. O. Bockris and A. K. Reddy in "Modern Electrochemistry," Plenum Press, New York, N. Y., 1970, p 450.
(11) R. Zana and E. B. Yeager, *J. Chim. Phys. Physicochim. Biol.*, **65**, 467 (1968); **66**, 252 (1969).
(12) B. Kratochvil and H. L. Yeager, *Fortschr. Chem. Forsch.*, **27**, 1 (1972).
(13) J. Prue and P. Sherrington, *Trans. Faraday Soc.*, **57**, 1795 (1961).
(14) R. Paul, J. Singla, and S. Narula, *J. Phys. Chem.*, **73**, 741 (1969).
(15) L. G. Hepler, *J. Phys. Chem.*, **61**, 1426 (1957).
(16) C. Criss and J. W. Cobble, *J. Amer. Chem. Soc.*, **86**, 5385 (1964).
(17) B. J. Alder, *J. Chem. Phys.*, **23**, 263 (1955).
(18) R. H. Stokes and R. A. Robinson, *Trans. Faraday Soc.*, **53**, 301 (1957).
(19) R. A. Robinson and R. H. Stokes, "Electrolyte Solutions," 2nd ed, Butterworths, London, 1959, p 125.
(20) (a) F. J. Millero, *J. Phys. Chem.*, **75**, 280 (1971); (b) *ibid.*, **72**, 3209 (1968).
(21) J. Padova and I. Abrahamer, *J. Phys. Chem.*, **71**, 2112 (1967).
(22) J. Riddick and W. Bunger, "Techniques of Chemistry: Organic Solvents," Vol. II, 3rd ed, Wiley-Interscience, New York, N. Y., 1970; "Handbook of Chemistry and Physics," 49th ed, The Chemical Rubber Publishing Co., Cleveland, Ohio, 1968.
(23) J. Lamb, "Physical Acoustics," Vol. IIA, W. P. Mason, Ed., Academic Press, New York, N. Y., 1965, p 212.
(24) W. Schaafs, "Molekularakustik," Springer ed, Berlin.
(25) G. W. Stockton and J. S. Martin, *J. Amer. Chem. Soc.*, **94**, 6921 (1972).
(26) L. Laliberté and B. Conway, *J. Phys. Chem.*, **74**, 4116 (1970).

Apparent Molal Volumes of Some Dilute Aqueous Rare Earth Salt Solutions at 25°[1]

F. H. Spedding,* P. F. Cullen, and A. Habenschuss

Institute for Atomic Research and Department of Chemistry, Iowa State University, Ames, Iowa 50010
(Received October 17, 1973)

Publication costs assisted by Ames Laboratory, USAEC

The apparent molal volumes, ϕ_V, of aqueous solutions of La, Nd, Gd, and Lu perchlorate, Pr, Sm, Eu, Gd, Tb, Dy, Ho, Tm, and Lu nitrate, and Eu, Tm, and Lu chloride were determined from 0.0015 to about 0.15 *m* at 25°. The apparent molal volumes were calculated from the specific gravities determined by a magnetically controlled float. The concentration dependences of the apparent molal volumes showed significant deviations from the simple limiting law at the lowest concentrations measured. However, except for the light rare earth nitrates, they could be represented by the extrapolation function of Owen and Brinkley which includes the effect of the $\mathring{a}$ parameter. Including other available ϕ_V data on the rare earth salts, La, Pr, Sm, Eu and Gd nitrate required an additional term in the extrapolation function to compensate for positive deviations, probably caused by complex formation. The deviation of ϕ_V for $Nd(NO_3)_3$ was too large to allow use of the extrapolation function. When the apparent molal volumes at infinite dilution of a rare earth anion series are plotted against rare earth ionic radius, ϕ_V^0 decreases from La to Nd and from Tb to Lu but increases from Nd to Tb with decreasing ionic radius. This variation was found to be independent of the anion. An analysis of the components comprising ϕ_V^0 indicated that the trend was present in the term reflecting rare earth ion–water interactions. This is in agreement with the suggestion that a shift between two inner water coordination spheres of the rare earth ions occurs in the region from Nd to Tb.

Introduction

The rare earths all exist as trivalent ions in solution and behave very similarly except for the regular decrease in ionic size across the series due to the lanthanide contraction. They form an ideal group of ions for the study of thermodynamic properties of aqueous solutions as a function of ionic size. For this reason the Ames Laboratory has a continuing program for the determination of the thermodynamic and transport properties of rare earth solutions from infinite dilution to saturation. These measurements are confined to two-component systems of water and stoichiometric rare earth salts of strong acids. This paper is one in a series presenting these data.

A previous study of the apparent molal volumes, ϕ_V, of some lanthanide chlorides and nitrates[2] has revealed that while all the chlorides studied and also La, Er, and Yb nitrate appeared to conform to the Debye-Hückel theory up to about 0.05 *m* when the effect of the $\mathring{a}$ parameter was included, $Nd(NO_3)_3$ showed a large positive deviation from the theoretical limiting slope. Furthermore, the apparent molal volumes at infinite dilution for a given rare earth anion series did not decrease regularly with decreasing ionic radius as one might expect, but fell into two decreasing series with Sm and Gd being intermediate.

The objective of this research was to investigate the dilute rare earth perchlorate solutions where it can be assumed that no appreciable complexing occurs. It also was desired to determine if any of the other lanthanide nitrate solutions, which are known to form complexes at low concentrations, showed deviations similar to $Nd(NO_3)_3$. Finally, it provided a check on whether or not the trends in the apparent molal volumes at infinite dilution, found previously, persisted for all the chlorides and nitrates, and extended to the perchlorates.

Experimental Procedure

The experimental details have been discussed previously[2] so only a few additional comments are necessary.

1. Preparation of Materials. In addition to the oxide and sulfate methods of analysis described in the earlier paper, an EDTA weight titration was used. A weighed amount of rare earth salt solution was diluted to about 100 ml with a sodium acetate–acetic acid buffer solution (pH 5) and titrated with EDTA using Xylenol Orange as an indicator. The mean deviation for a triplicate analysis was less than 0.05%. A given stock solution was analyzed by two of the three methods. The independent analyses generally agreed to within 0.1%, and the mean value of the independent results was taken to be the concentration of the stock solution.

2. Apparatus. The apparent molal volume of a solution may be calculated from

$$\phi_V = \frac{1000}{c}(1 - S) + \frac{M_2}{\rho_0} \qquad (1)$$

where c is the molar concentration; S is the specific gravity of the solution; M_2 is the molecular weight of the solute; and ρ_0 is the density of the solvent taken as 0.9970751 g/ml, at 25°.

The specific gravities of the solutions were measured by a magnetically controlled float using method 1, described earlier.[2] Of two floats used in the course of the work, only one was found to give equilibrium currents dependent on the atmospheric pressure. A calibration was made for this effect and the equilibrium currents obtained during a specific gravity run were corrected to an average pressure for the run.

The experimental errors were comparable to those found previously. There is a probable error in ϕ_V of ±0.15 ml/mol resulting from an average analysis error of ±0.05%

in the stock solution. The probable error in the specific gravity is less than $\pm 5 \times 10^{-7}$. This contributes significantly to the error in ϕ_V only for solutions below 0.01 m. The probable error in ϕ_V^0 was estimated to be ± 0.2 ml/mol or less.

Results

The specific gravities and apparent molal volumes of the solutions studied are given in Table I.[3] The data for each salt were fitted to a polynomial of the form

$$\phi_V = a_0 + a_1 m^{1/2} + a_2 m + a_3 m^{3/2} \quad (2)$$

by the method of least squares. The points were weighted using the inverse of the square of the probable error in ϕ_V. The coefficients for eq 2 are given in Table II with the standard deviations, rmsd. These coefficients may also be used to calculate the partial molal volume from the equation

$$\bar{V}_2 = a_0 + \frac{3}{2}a_1 m^{1/2} + 2a_2 m + \frac{5}{2}a_3 m^{3/2} \quad (3)$$

Equations 2 and 3 are useful for interpolating over the concentration range studied.

The apparent molal volumes at infinite dilution were evaluated using the extrapolation function of Owen and Brinkley[4] given by the equation

$$\phi_V - 27.44\Omega_V c^{1/2} = \phi_V^0 + \tfrac{1}{2}K_V c + Nc^{3/2} \quad (4)$$

where

$$\Omega_V = \left(\frac{1}{1 + \kappa\mathring{a}} \frac{\partial \ln D}{\partial P} - \frac{\sigma\beta}{3}\right)\left(\frac{\partial \ln D}{\partial P} - \frac{\beta}{3}\right)^{-1} \quad (5)$$

with

$$\sigma = \frac{3}{(\kappa\mathring{a})^3}\left[1 + \kappa\mathring{a} - \frac{1}{1 + \kappa\mathring{a}} - 2 \ln (1 + \kappa\mathring{a})\right] \quad (6)$$

N is a constant and the other symbols have their usual meanings. For a 3:1 electrolyte, $\kappa\mathring{a}$ equals[4] $0.8051\mathring{a}c^{1/2}$ and 27.44 is the theoretical limiting slope. $Nc^{3/2}$ is an additional term added to the extrapolation function for some of the salts to fit the data at higher concentrations. The $\mathring{a}$ parameters were obtained from activity coefficient or conductivity data,[5] or, if not available, estimated from the values for nearby rare earths. The values for β and $\partial \ln D/\partial P$ were taken from Kell,[6] and Owen, *et al.*,[7] respectively. The parameters ϕ_V^0, $\frac{1}{2}K_V$, and N were determined by least squares and are listed in Table III with the $\mathring{a}$ parameters and standard deviations.

Discussion

1. Concentration Behavior. In 1931, Redlich and Rosenfeld[8] derived the following expression for the apparent molal volume from the Debye–Hückel expression for the activity coefficient

$$\phi_V = \phi_V^0 + KW^{3/2}c^{1/2} \quad (7)$$

where W is the valence factor, $\frac{1}{2}\Sigma\nu_i z_i^2$, and K is a function of temperature, solvent properties, and fundamental constants. In a review article, Redlich and Meyer[9] have established $K = 1.868$ at 25° for water. This value combined with the valence factor for 3:1 electrolytes yields the limiting slope of 27.44 used in eq 4. All the salts studied were found to approach this limiting slope as the concentration approached infinite dilution but deviated rapidly at finite concentrations.

Owen and Brinkley[4] derived an extrapolation function

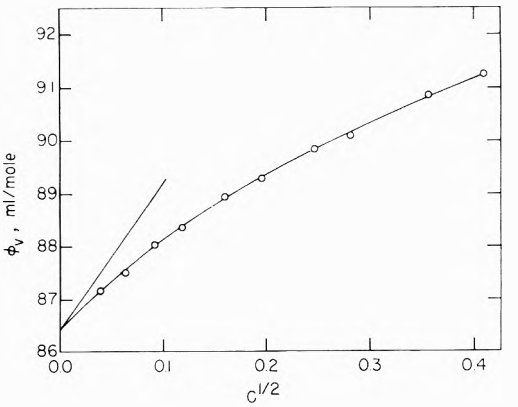

Figure 1. Apparent molal volume of $Lu(ClO_4)_3$ at 25°.

TABLE II: Empirical Coefficients for Calculating ϕ_V and $\bar{V}_2$ from Eq 2 and 3

Salt	a_0	a_1	a_2	a_3	Rmsd
$EuCl_3$	12.08	24.81	−40.83	39.67	0.04
$TmCl_3$	9.03	31.85	−71.69	84.52	0.06
$LuCl_3$	7.88	25.22	−41.56	41.27	0.03
$Pr(NO_3)_3$	45.20	32.44	−26.53	2.66	0.06
$Sm(NO_3)_3$	45.60	32.80	−16.09	−36.65	0.07
$Eu(NO_3)_3$	46.49	33.65	−51.98	44.20	0.04
$Gd(NO_3)_3$	46.73	32.24	−56.24	50.71	0.07
$Tb(NO_3)_3$	46.96	32.07	−68.78	80.51	0.03
$Dy(NO_3)_3$	46.35	34.42	−80.82	93.60	0.04
$Ho(NO_3)_3$	46.05	17.10	5.92	−42.72	0.04
$Tm(NO_3)_3$	43.98	24.92	−37.65	31.42	0.03
$Lu(NO_3)_3$	42.28	26.31	−44.57	43.73	0.07
$La(ClO_4)_3$	93.37	24.31	−50.53	56.14	0.04
$Nd(ClO_4)_3$	88.91	19.32	−26.63	22.38	0.04
$Gd(ClO_4)_3$	91.91	23.13	−48.95	52.49	0.07
$Lu(ClO_4)_3$	86.43	19.64	−30.69	28.19	0.03

for ϕ_V which includes the effect of the ion size, the $\mathring{a}$ parameter. If the variation of the $\mathring{a}$ parameter with pressure is assumed small and neglected, their expression reduces to eq 4 without the $Nc^{3/2}$ term. Though this assumption is open to question, particularly if a change in the effective hydration number of the ions occurs with pressure, this simplification will be made to arrive at eq 4 which may be tested against the data.

The concentration dependence of ϕ_V and the extrapolation of ϕ_V using eq 4, for $Lu(ClO_4)_3$, are shown in Figures 1 and 2, respectively. These curves are generally typical of all of the chlorides and perchlorates studied and the nitrates from Tb to Lu, including those cited in the previous paper.[2] The smooth curve in Figure 1 was obtained from a polynomial similar to eq 2 in $c^{1/2}$ and the straight line is the theoretical limiting slope. The straight line in Figure 2 is given by the two parameter ($N = 0$) Owen–Brinkley equation. The circles represent the experimental points.

Figures 3 and 4 show the analogous graphs for $Eu(NO_3)_3$. The straight line in Figure 4 was obtained, again, from the two-parameter Owen–Brinkley function and clearly does not adequately represent the data. This type of behavior was found for the nitrates from La through Gd. However, all of these salts, except $Nd(NO_3)_3$, could be represented by the three parameter function given by eq 4.

It is known that the nitrates form appreciable amounts of rare earth nitrate complexes at low concentrations. There are several determinations of the stability constants of the rare earth nitrate complexes in the literature.[10-14] Although these measurements are only in qualitative

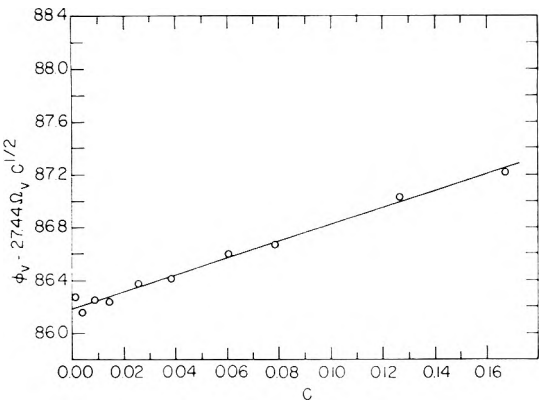

Figure 2. Owen–Brinkley extrapolation of ϕ_V for $Lu(ClO_4)_3$.

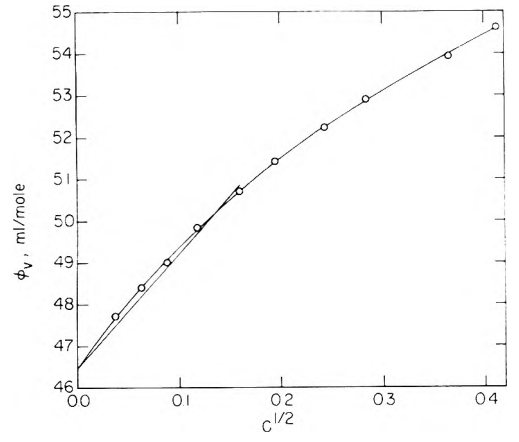

Figure 3. Apparent molal volume of $Eu(NO_3)_3$ at 25°.

agreement, the stability constants of the light rare earth complexes are larger than those of the heavy rare earths, with a maximum somewhere near Sm. In addition, there are indications that some inner-sphere as well as outer-sphere nitrate complexation occurs in dilute solutions.[15-23] The assumption that inner-sphere nitrate complexation occurs in dilute solutions is compatible with the deviations found in the apparent molal volumes.

The formation of a rare earth nitrate complex would effect the apparent molal volume in two ways. First, some 3:1 electrolyte would be replaced by a 2:1 electrolyte (and possibly at higher concentrations than studied here, with some 1:1 or even neutral salt[19]). Since the limiting slope of the apparent molal volume for a 2:1 electrolyte is only 9.7, the presence of this complex would cause the ϕ_V curve to rise less steeply with concentration. Second, the apparent molal volume at infinite dilution for the 2:1 electrolyte would be greater than for the noncomplexed 3:1 electrolyte due to the lesser electrostriction of the water. The ϕ_V curve would rise more rapidly with concentration as the complexes are formed than for an uncomplexed 3:1 electrolyte. While at infinite dilution we assume there are no complexed species, they would form in very dilute solutions and the ϕ_V curves would rise more rapidly than the limiting slope for a 3:1 electrolyte, resulting in positive deviations. Evidently, in very dilute solutions this second effect dominates, as can be seen from Figures 3 and 4, but as the concentration increases the first effect probably plays a significant role.

This analysis is in agreement with the data for the rare earth nitrates from La to Gd, where an additional parameter, Nc^{3} [2], was required to fit the data. The nitrates from Tb to Lu, which complex less than the light rare earth nitrates at comparable concentrations, can be represented by the two-parameter Owen–Brinkley function since the smaller complexing effect can be compensated for, to a certain extent, by the two adjustable parameters, ϕ_V^0 and $\frac{1}{2}K_V$. The failure of the three parameter function to represent $Nd(NO_3)_3$ may be due to the fact that Nd^{3+} is possibly complexing to a greater extent than the other rare earth ions. On the other hand, a shift in another equilibrium (that between two possible inner-sphere water coordination numbers of the uncomplexed rare earth ions beginning around Nd^{3+} in the rare earth series) might also contribute to this failure.

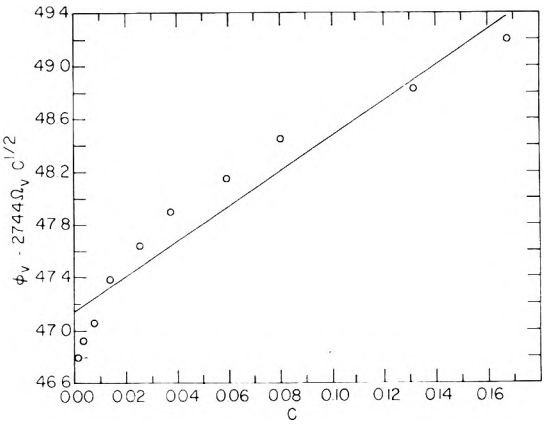

Figure 4. Owen–Brinkley extrapolation of ϕ_V for $Eu(NO_3)_3$.

TABLE III: Parameters for Owen–Brinkley Extrapolation Function

Salt	ϕ_V^0	$\frac{1}{2}K_V$	N	Rmsd	$\mathring{a}$, Å
$EuCl_3$	12.09	7.71		0.06	5.6[a]
$TmCl_3$	9.44	10.47		0.12	5.8[b]
$LuCl_3$	7.95	9.32		0.07	6.0[c]
$Pr(NO_3)_3$	45.46	64.67	−117.67	0.07	4.5[c]
$Sm(NO_3)_3$	45.86	79.06	−169.22	0.08	4.4[d]
$Eu(NO_3)_3$	46.87	35.11	−53.20	0.08	4.4[c]
$Gd(NO_3)_3$	47.00	29.50	−54.35	0.08	4.4[e]
$Tb(NO_3)_3$	47.30	9.17		0.09	4.6[c]
$Dy(NO_3)_3$	46.84	7.61		0.11	4.8[c]
$Ho(NO_3)_3$	45.66	7.04		0.06	5.1[d]
$Tm(NO_3)_3$	44.06	8.22		0.08	5.8[c]
$Lu(NO_3)_3$	42.45	9.95		0.10	6.1[c]
$La(ClO_4)_3$	93.36	7.00		0.05	7.0[e]
$Nd(ClO_4)_3$	88.55	4.37		0.06	6.0[e]
$Gd(ClO_4)_3$	91.77	3.27		0.07	6.4[e]
$Lu(ClO_4)_3$	86.18	6.30		0.04	7.4[c]

[a] F. H. Spedding, P. E. Porter, and J. M. Wright, *J. Amer. Chem. Soc.*, **74**, 2781 (1952). [b] F. H. Spedding and J. L. Dye, *ibid.*, **76**, 879 (1954). [c] Estimated from values of nearby rare earths. [d] D. J. Heiser, Ph.D. Dissertation, Iowa State University, Ames, Iowa, 1958. [e] F. H. Spedding and S. Jaffe, *J. Amer. Chem. Soc.*, **76**, 884 (1954).

It should be noted that the $\mathring{a}$ parameters of the rare earth nitrates, listed in Table III, reflect the trends in the stability constants for the nitrates. The $\mathring{a}$ parameters are lower for the light rare earth nitrates than for the heavy rare earths. Since one would expect a smaller distance of closest approach for a complexed ion than for an uncomplexed ion, the smaller $\mathring{a}$ parameters of the light rare earth nitrates are in agreement with their higher stability constants. This would be true for both inner- and outer-sphere complexes, but should be more marked for inner-sphere complexes. Therefore, the smaller than expected

values for the $\mathring{a}$ parameters of the nitrates, as opposed to the more reasonable $\mathring{a}$'s of the chlorides and perchlorates, support the contention that some inner-sphere complexation occurs in very dilute nitrate solutions, since the $\mathring{a}$'s were obtained from very dilute (below 0.001 M) conductance and activity data.[5]

Since the chlorides complex to a lesser extent than the nitrates,[11,19,23-26] and the perchlorates presumably even less,[27,28] the apparent molal volumes for these salts should also be well represented by the two-parameter Owen-Brinkley function. This was found to be the case.

2. The Partial Molal Volumes at Infinite Dilution. Figure 5 shows the partial molal volumes at infinite dilution (equal to ϕ_V^0) for the rare earth nitrates plotted against the rare earth ionic radii of Templeton and Dauben.[29] This curve is identical, within experimental error, with that for the rare earth chlorides shown in the previous paper,[2] but displaced by the difference between the partial molal volumes of three nitrate ions and three chloride ions. The incomplete rare earth perchlorate series data also show the same trend.

At infinite dilution, the assumption may be made that the electrolyte is completely ionized and no ion-ion interactions are occurring. The partial molal volume at infinite dilution for a rare earth salt may then be given by the expression

$$\bar{V}_2^0(RX_3) = \bar{V}^0(R^{3+}) + 3\bar{V}^0(X^-) \qquad (8)$$

where $\bar{V}^0(R^{3+})$ and $\bar{V}^0(X^-)$ are the ionic partial molal volumes of the rare earth ion and the anion, respectively. For a given rare earth anion series, the contribution to V_2^0 due to the anions is constant. Any trends prevailing across a rare earth anion series must then be independent of the anion. This is in agreement with our results.

Millero has reviewed the methods for determining ionic partial molal volumes.[30] He concluded that the best value for $\bar{V}^0(H^+)$ is -5.4 ml/mol. Based on this value, the ionic partial molal volumes for Cl^- and NO_3^- are 23.2 and 34.4 ml/mol, respectively, at infinite dilution.[30] Using these values, the partial molal volumes at infinite dilution for the rare earth ions were calculated from the chloride and nitrate data and the average values are given in Table IV. The values for Ce^{3+} and Pm^{3+} were estimated from Figure 5 and a similar figure for the chlorides.

The partial molal volume of an ion at infinite dilution may be given by the equation

$$\bar{V}^0(R^{3+}) = V_{int} + \Delta V \qquad (9)$$

V_{int} is the intrinsic volume occupied by 1 mol of ions and may be estimated to be about 1.5–3 ml/mol[29] for the rare earth ions. ΔV reflects the ion–solvent interactions and is the change in volume of an infinite amount of solvent on adding 1 mol of ions. For the rare earth ions, ΔV is the dominant term in $\bar{V}^0(R^{3+})$, and is negative.

For the rare earth ions having a given coordination of solvent molecules about the ions, V_{int} would be expected to decrease smoothly with decreasing ionic radius. Due to the increasing surface charge density of the rare earth ions with decreasing ionic radius, the total hydration (interaction with the first sphere waters and with the water molecules further out) should increase smoothly from La to Lu as is shown by the conductivity[31] and viscosity[32,33] measurements. Since this interaction implies a breakdown of the hydrogen-bonded water structure around the rare earth ion which increases in extent from La to Lu, one would expect a decrease in ΔV across the rare earth series reflecting this increase in total hydration. This is in agreement with the data from La^{3+} to Nd^{3+} and from Tb^{3+} to Lu^{3+}. On the other hand, the increase in $\bar{V}^0(R^{3+})$ from Nd^{3+} to Tb^{3+} has been attributed to a shift in an equilibrium between two inner-sphere water coordination numbers of the cation.[2]

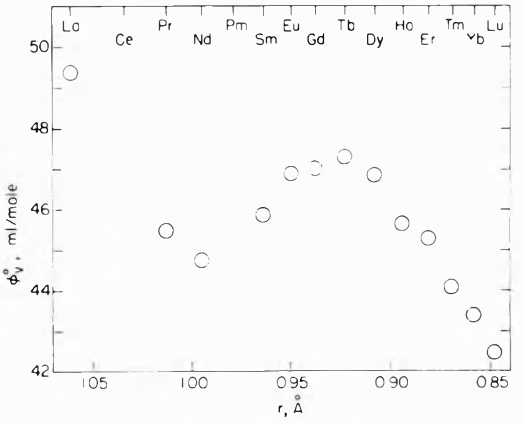

Figure 5. ϕ_V^0 for the rare earth nitrates.

TABLE IV: Partial Molal Volumes at Infinite Dilution of the Trivalent Rare Earth Ions[a]

R^{3+}	$\bar{V}^0(R^{3+})$	R^{3+}	$\bar{V}^0(R^{3+})$
La	−54.5	Tb	−56.1
Ce	(−56.7)	Dy	−56.6
Pr	−58.2	Ho	−57.7
Nd	−58.9	Er	−58.4
Pm	(−58.8)	Tm	−59.6
Sm	−57.9	Yb	−60.1
Eu	−56.9	Lu	−61.2
Gd	−56.4		

[a] Based on $\bar{V}^0(H^+) = -5.4$ ml/mol, $\bar{V}^0(Cl^-) = 23.2$ ml/mol, and $\bar{V}^0(NO_3^-) = 34.4$ ml/mol.

In the previous paper[2] it was suggested that in rare earth solutions there exists an equilibrium between two inner-sphere water coordination numbers for the rare earth cation. For the larger ions from La to Nd, the species with the higher inner coordination number is preferred. For the smaller ions from Tb to Lu, the form with the lower inner coordination number predominates. For the ions from Nd to Tb, the equilibrium is shifting with decreasing ionic radius from the higher to the lower inner-sphere coordination number. It was further suggested that coordination numbers of 9 and 8 would be compatible with the data. Since the effective volume of a water molecule in the first hydration sphere should be smaller than its effective volume outside this sphere, a decrease in the inner-sphere coordination should result in a less negative ΔV and a consequent increase in $\bar{V}^0(R^{3+})$ from Nd^{3+} to Tb^{3+}.

At the present there seems to be some controversy in the literature as to whether a change in the inner-sphere coordination occurs in the rare earth series. Some workers have argued that such a model is not supported by their data.[23,34] We believe there is ample evidence that such an effect does exist. Since the variation of $\bar{V}_2^0$ of the three anion series[35] is the same within experimental error (except for an anion shift), the two-series effect is not a result of cation–anion interaction. Therefore, the effect must be due to a change in the cation–solvent interaction. Further, this same two-series effect is present in most of the thermodynamic and transport properties that have been determined for these solutions. And finally, X-ray

diffraction[36] data on these solutions, to be published shortly, show that there are nine first sphere water molecules for the light rare earth ions and eight first sphere waters for the heavy rare earth ions. We prefer to delay further comment on the controversy until all of the data available to us have been published.

Supplementary Material Available. Table I will appear following these pages in the microfilm edition of this volume of the journal. Photocopies of the supplementary material from this paper only or microfiche (105 × 148 mm, 24× reduction, negatives) containing all of the supplementary material for the papers in this issue may be obtained from the Journals Department, American Chemical Society, 1155 16th St., N.W., Washington, D. C. 20036. Remit check or money order for $3.00 for photocopy or $2.00 for microfiche, referring to code number JPC-74-1106.

References and Notes

(1) This paper is based, in part, on the Ph.D. Dissertation of P. F. Cullen submitted to the Graduate Faculty of Iowa State University, Ames, Iowa, 1969.
(2) F. H. Spedding, M. J. Pikal, and B. O. Ayers, *J. Phys. Chem.*, **70**, 2440 (1966).
(3) See paragraph at end of text regarding supplementary material.
(4) B. B. Owen and S. R. Brinkley, Jr., *Ann. N. Y. Acad. Sci.*, **51**, 753 (1949). See also H. S. Harned and B. B. Owen, "The Physical Chemistry of Electrolytic Solutions," 3rd ed, Reinhold, New York, N. Y., 1958.
(5) See footnotes in Table III.
(6) G. S. Kell, *J. Chem. Eng. Data*, **12**, 66 (1967).
(7) B. B. Owen, R. C. Miller, C. E. Milner, and H. L. Cogan, *J. Phys. Chem.*, **65**, 2065 (1961).
(8) O. Redlich and P. Rosenfeld, *Z. Phys. Chem.*, **A155**, 65 (1931).
(9) O. Redlich and D. M. Meyer, *Chem. Rev.*, **64**, 221 (1964).
(10) B. M. L. Bansal, S. K. Patil, and H. D. Sharma, *J. Inorg. Nucl. Chem.*, **26**, 993 (1963).
(11) D. F. Peppard, G. W. Mason, and J. Hucher, *J. Inorg. Nucl. Chem.*, **24**, 881 (1962).
(12) G. R. Choppin and W. F. Strazik, *Inorg. Chem.*, **4**, 1250 (1965).
(13) N. A. Coward and R. W. Kiser, *J. Phys. Chem.*, **70**, 213 (1966).
(14) A. Anagnostopoulos and P. O. Sakellaridis, *J. Inorg. Nucl. Chem.*, **32**, 1740 (1970).
(15) G. R. Choppin, D. E. Henrie, and K. Buijs, *Inorg. Chem.*, **5**, 1743 (1966).
(16) K. Bukietynska and G. R. Choppin, *J. Chem. Phys.*, **52**, 2875 (1970).
(17) R. Garnsey and D. W. Ebdon, *J. Amer. Chem. Soc.*, **91**, 50 (1969).
(18) H. B. Silber, N. Scheinin, G. Atkinson, and J. J. Grecsek, *J. Chem. Soc., Faraday Trans. 1*, **68**, 1200 (1972).
(19) K. Nakamura and K. Kawamura, *Bull. Chem. Soc. Jap.*, **44**, 330 (1971).
(20) I. Abrahamer and Y. Marcus, *Inorg. Chem.*, **6**, 2103 (1967).
(21) J. Knoeck, *Anal. Chem.*, **41**, 2069 (1969).
(22) D. L. Nelson and D. E. Irish, *J. Chem. Phys.*, **54**, 4479 (1971).
(23) J. Reuben and D. Fiat, *J. Chem. Phys.*, **51**, 4909 (1969).
(24) G. R. Choppin and P. J. Unrein, *J. Inorg. Nucl. Chem.*, **25**, 387 (1963).
(25) T. Goto and M. Smutz, *J. Inorg. Nucl. Chem.*, **27**, 663 (1965).
(26) N. N. Kozachenko and I. M. Batyaev, *Russ. J. Inorg. Chem.*, **16(1)**, 66 (1971).
(27) P. A. Baisden, G. B. Choppin, and W. F. Kinard, *J. Inorg. Nucl. Chem.*, **34**, 2029 (1972).
(28) M. M. Jones, E. A. Jones, D. F. Harmon, and R. T. Semmes, *J. Amer. Chem. Soc.*, **83**, 2038 (1961).
(29) D. H. Templeton and C. H. Dauben, *J. Amer. Chem. Soc.*, **76**, 5237 (1954).
(30) F. J. Millero in "Water and Aqueous Solutions," R. A. Horne, Ed., Wiley-Interscience, New York, N. Y., 1972, Chapter 13.
(31) F. H. Spedding and J. A. Rard, *J. Phys. Chem.*, submitted for publication.
(32) F. H. Spedding and M. J. Pikal, *J. Phys. Chem.*, **70**, 2430 (1966).
(33) F. H. Spedding, D. Witte, L. E. Shiers, and J. A. Rard, *J. Chem. Eng. Data*, submitted for publication.
(34) G. Geier, U. Karlen, and A. v. Zelewsky, *Helv. Chim. Acta*, **52**, 1967 (1969).
(35) Although only four perchlorates were measured in this work, pycnometric densities of all the rare earth perchlorates have been determined in this laboratory. The trend in the $\bar{V}_2$'s at the lowest concentrations, ~0.02 *m*, across the rare earth series are identical, within experimental error, to the $\bar{V}_2^0$ of the chlorides and nitrates.
(36) F. H. Spedding and L. L. Martin, to be submitted for publication.

Thermodynamic Calculations of Equilibrium Constants for Ion-Exchange Reactions between Unequally Charged Cations in Polyelectrolyte Gels[1]

G. E. Boyd,* G. E. Myers,[2a] and S. Lindenbaum[2b]

Oak Ridge National Laboratory, Oak Ridge, Tennessee 37830

(Received December 3, 1973)

Publication costs assisted by Oak Ridge National Laboratory

Experimental measurements of the equivalent water contents and volumes of lightly cross-linked polyelectrolyte gels were employed in thermodynamic calculations of the mass law concentration product quotient, K_m, for the zinc–sodium ion-exchange reaction between cross-linked polystyrenesulfonates and dilute aqueous mixtures of sodium and zinc nitrate. The calculated K_m values were in satisfactory agreement with those measured directly in ionic partition experiments except with the most heavily cross-linked exchangers. The magnitude of K_m was governed mainly by the interactions between zinc and sodium ions in the exchanger. The reversal in the preference of zinc over sodium ion observed with increased crosslinking was explained by the thermodynamic calculations. A general framework is suggested for the prediction of selectivity coefficients for ion-exchange reactions.

Introduction

Ion-exchange reactions between like but unequally charged ions in aqueous solution and synthetic organic ion exchangers have become of increasing interest because of their widespread occurrence and importance. However, as yet very few carefully planned quantitative studies have

been conducted on them to determine their equilibrium constants, and hence the dependence of the ionic selectivity on gel cross linking and ionic composition, and on the external solution composition.

A striking illustration of the neglect of heterovalent ion exchange can be found in what may be the most important of all known reactions, namely, those involved in the water softening cycle (*i.e.*, Ca^{2+} and Mg^{2+} with Na^+ ion). Equilibrium isotherms have been reported[3-5] only for nominal 8% DVB cross-linked polystyrenesulfonate gel in equilibrium with aqueous mixtures of $CaCl_2$-NaCl or $MgCl_2$-NaCl varying between 0.1 and 5 *N* in total concentration, and for a range in divalent ion equivalent fraction (*i.e.*, "loading") in the exchanger between 0.1 and 0.9. Measurements for the magnesium-hydrogen,[6,7] magnesium-potassium,[8] copper-hydrogen,[9] and uranyl-hydrogen[6] ion-exchange reactions with dilute aqueous electrolyte mixtures and various cross linkings have been published, but no attempt has been made to relate the selectivity coefficients for these reactions to either the cross linking, or, for that matter, to the ionic composition of the exchanger. Recently, an extensive series of measurements on the ion exchange reactions of microconcentrations (tracer) of calcium, strontium, cobalt, nickel, zinc, and cadmium ions with hydrogen ion in nominal 1, 2, 4, 8, 12, and 16% divinylbenzene (DVB) cross-linked poly(styrenesulfonic acid) gels has been reported.[10] In subsequent publications[11,12] attempts to predict the observed mass law concentration product ratios were made. Good quantitative agreement with the experimental data was not obtained, although the trend in the ionic selectivity with increased cross linking was reproduced.

This paper will report on the application of an exact thermodynamic treatment to our previously reported selectivity coefficient measurements[13] on the exchange reaction at 25° between zinc and sodium ions in dilute aqueous mixtures and variously cross-linked polystyrenesulfonates. The Gibbs-Donnan model will be assumed to derive an equation which relates the values of the molal concentration product quotient, K_m, for the reaction to the cross linking of the copolymer and to the ionic interactions in the polyelectrolyte gel and in the external aqueous electrolyte mixture. The use of this equation to calculate K_m independently of direct measurements of the equilibrium, to predict the dependence of K_m on cross linking and ionic composition, and to detect the effects of physical or chemical nonuniformity in the gel will be pointed out. Information on the ion-exchange behavior of zinc in aqueous media is of environmental interest, because of the possible appearance of this metal in wastes from the zinc plating industry. The ion-exchange behavior of zinc ion also appears to be germane to its role in metabolic processes.

Experimental Section

Materials and K_m Measurements. The poly(styrenesulfonic acid) cation exchangers nominally cross linked with 2, 4, 8, 12, 16, and 24% divinylbenzene (DVB) used in this research were the same preparations as employed earlier.[13] In addition, a very lightly cross-linked exchanger (*i.e.*, nominal 0.5% DVB), which served as a "reference" preparation, was examined. The capacities and water contents of the cross-linked exchangers are presented in Table I. Equivalent water contents, x_w, of the homoionic sodium and zinc forms in equilibrium with aqueous 0.1 *N* $NaNO_3$ or with 0.1 *N* $Zn(NO_3)_2$ solutions were determined with the "reference compound" technique.[14] It is of

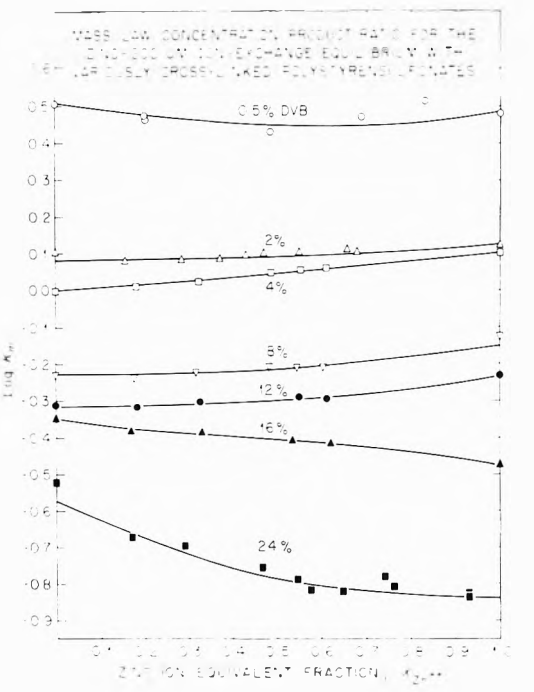

Figure 1. Mass law concentration product ratio for the zinc-sodium ion-exchange equilibrium with variously cross-linked polystyrenesulfonate gels and $NaNO_3 + Zn(NO_3)_2$ at 0.1 *N*.

TABLE I: Capacities and Equivalent Water Contents of Cross-Linked Polystyrenesulfonate Cation Exchangers

Nominal % DVB	Capacity, mequiv/g of dry H form	Water content, g of H_2O/equiv[a]	
		NaR	ZnR_2
0.5	5.00	1928	806
2	5.28	535	427
4	5.15	347	319
8	5.19	176	188
12	5.08	142	160
16	4.75	122	141
24	4.67	88.0	109

[a] In equilibrium with 0.1 *N* $NaNO_3$ or with 0.1 *N* $Zn(NO_3)_2$ solution, respectively.

interest to note that for exchangers containing more than 4% DVB cross linking the zinc form possessed more water than the sodium form.

Values of log K_m derived from previously reported measurements[13] and the x_w values of Table I are plotted in Figure 1 as a function of the Zn^{2+} ion equivalent fraction in the exchanger, x_{ZnR_2}. The water content of a given cross-linked exchanger was assumed to vary linearly with x_{ZnR_2}. Note that the equilibrium constant as measured by K_m *decreases* with increasing cross linking, and becomes less than unity for preparations with a nominal DVB content greater than 4%.

Equivalent Water Content Measurements with the Reference Exchanger. A gravimetric isopiestic vapor pressure comparison procedure[19] was employed to measure x_w values as a function of water activity, a_w, for the homoionic sodium, zinc, and the mixed sodium-zinc salt forms of the nominal 0.5% DVB "reference" exchanger (Table II). Equilibrium was approached from both directions and the measurements were performed in duplicate. Water contents of 4249 and 2187 g/equiv, respectively, for

TABLE II: Equivalent Water Contents (g of H_2O/equiv) of the Sodium and Zinc Salts of Nominal 0.5% DVB Cross-Linked Polystyrenesulfonate as a Function of Water Activity and Zinc Ion Equivalent Fraction

Equivalent fraction	−Log a_w												
x_{ZnR_2}	0.00346	0.00877	0.03395	0.04484	0.07438	0.09307	0.12332	0.14978	0.20901	0.27687	0.36896	0.48149	0.64878
0.000	880	476	183	153	122	107	91.8	83.4	67.7	57.3	49.3	40.0	33.0
0.358	722	426	191	165	133	120	104	95.3	78.6	67.6	58.7	48.9	41.0
0.564	639	399	196	172	140	127	112	103	85.7	74.0	64.4	54.0	45.8
0.772	555	372	201	178	148	136	121	112	94.9	82.6	72.3	60.8	51.5
1.000	481	349	204	183	153	142	127	120	104	91.8	81.4	68.9	58.6

TABLE III: Values of Constants from Least-Squares Fit of Data of Table II to Eq 1

−Log a_w	a	b	c	σ_{fit}
0.00081	2990	−1487	−582	37
0.00125	1997	−1265		21
0.00346	880.5	−470.1	68.7	2.7
0.00877	476.2	−151.6	23.9	0.93
0.03395	183.2	21.4		0.66
0.04484	153.8	30.3		0.48
0.07438	122.2	31.8		0.75
0.09307	107.5	35.1		0.68
0.12332	91.2	37.3		0.91
0.14978	82.7	37.0		0.86
0.20901	66.6	36.4		0.57
0.27687	57.3	24.7	9.8	0.39

$-\log a_w = 0.0$ were determined on the homoionic sodium and zinc forms of the 0.5% DVB cross-linked exchanger with the "reference" compound technique. Isopiestic vapor pressure measurements also were performed with mixtures of sodium poly(styrenesulfonate) (NaPSS) and $Zn(PSS)_2$ polyelectrolyte solutions for zinc ion equivalent fractions of 0.00, 0.225, 0.520, 0.761, and 1.00 and values of $-\log a_w = 0.00081$ and 0.00125, respectively. These data and those of Table II were fitted to polynomials of the form

$$x_w = a + bx_{ZnR_2} + cx_{ZnR_2}^2 \quad (a_w = \text{constant}) \qquad (1)$$

by least-squares methods. Values of the constants in eq 1 for various water activities are given in Table III.

Equivalent Volume Measurements. Equivalent volume, V_e, determinations on the homoionic sodium and zinc forms and on a mixed sodium–zinc form with $x_{ZnR_2} = 0.50$ were performed with the 4% DVB exchanger using pycnometric techniques described elsewhere.[15] A plot of the experimental results (Figure 2) shows that the increase in V_e (ml equiv^{-1}) with x_w expressed in moles of H_2O per equivalent is approximately linear, except at small hydrations. A least-squares fit was made to an empirical equation of the form

$$V_e = V_a + \phi_w^0 x_w^2/(a + x_w) \qquad (2)$$

where V_a is the observed volume per equivalent of anhydrous exchanger, and ϕ_w^0 is the apparent molal volume of pure water (18.069 ml mol^{-1}) at 25°. Numerical values for the constants in eq 2 are presented in Table IV.

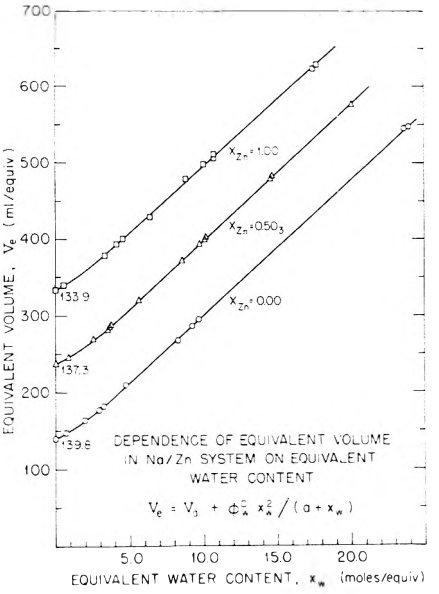

Figure 2. Dependence of the equivalent volume in zinc–sodium ion-exchange gels on the equivalent water content.

Treatment of Experimental Data

Thermodynamic Framework. The possibility of a quantitative description of the dependence of the classical mass law concentration product ratio for exchange reactions by like, singly-charged ions on the ionic composition and cross linking of polyelectrolyte gels and on the external aqueous electrolyte concentration has been demonstrated in previous researches[14-17] in which the Gibbs–Donnan equation[18] was applied. This equation

$$\log K_a = \pi(z_2\bar{v}_1 - z_1\bar{v}_2)_r \qquad (3)$$

relates the thermodynamic equilibrium constant, K_a, to the configurational free-energy change in the molecular network of the ion exchanger. The latter may be expressed as a product of the isotropic strain, π, produced in the exchanger by swelling, and the partial molal volume change, $\Delta\bar{v} = (z_2\bar{v}_1 - z_1\bar{v}_2)$, in the exchanger caused by the exchange of ions 1 and 2 of charges z_1 and z_2, respectively. An equation for the mass law concentration product ratio, K_m, defined by

$$K_m = (m_2^{z_1})_r(m_1^{z_2})_w/(m_1^{z_2})_r(m_2^{z_1})_w \qquad (4)$$

may be derived by substitution of eq 4 into eq 3

$$\log K_m = \pi(z_2\bar{v}_1 - z_1\bar{v}_2)_r + \log(\gamma_1^{z_2}/\gamma_2^{z_1})_r - \log(\gamma_1^{z_2}/\gamma_2^{z_1})_w \qquad (5)$$

where the subscripts r and w, respectively, denote the exchanger and aqueous phases. The special form of eq 5 which applies to the exchange reaction between zinc and sodium ion in the exchanger and in dilute aqueous nitrate mixtures may be written

$$\log K_m = \pi(2\bar{v}_{NaR} - \bar{v}_{ZnR_2}) + \log(\gamma_{NaR}^2/\gamma_{ZnR_2}) - \log(\gamma_{NaX}^4/\gamma_{Zn(NO_3)_2}) \qquad (6)$$

Evaluation of the Configurational Free Energy. The first term on the right-hand side of eq 6 consists of the product of the quantity, π, the strain in a cross-linked ion exchanger when it is in equilibrium with aqueous 0.1 N

TABLE IV: Least-Squares Parameters for the Variation of the Equivalent Volumes (V_r, ml equiv^{-1}) with Equivalent Water Content (x_w mol equiv^{-1}) According to Eq 2

x_{ZnR_2}	V_a(obsd)	a	σ_{fit}	Range of x_w
0.00	139.8	1.263	2.1	0.0–24.0
0.503	137.3	1.264	1.0	0.0–20.1
1.00	133.9	1.164	2.8	0.0–17.8

electrolyte solution, and the partial molal volume change, $(2\bar{v}_{NaR} - \bar{v}_{ZnR_2})$, for the exchange reaction between Na^+ and Zn^{2+} ions at equilibrium. The evaluation of π for a given cross-linked exchanger is based on the formula[19]

$$\pi = (RT/\bar{v}_w) \ln (a_w'/a_w) \quad (7)$$

for constant x_w and x_{ZnR_2}, where $\bar{v}_w$ is the partial molal volume of the water in the exchanger, a_w' is the water activity in the cross-linked exchanger in equilibrium with 0.1 N electrolyte, and a_w is the water activity in the reference exchanger (*i.e.*, nominal 0.5% DVB) when it possesses the same water content per equivalent, x_w, as the cross-linked preparation (Table I). Equation 7 may be simplified to the form[15]

$$\pi(\text{atm}) = 3118(-0.007824\nu m\phi - \log a_w) \quad (8)$$

where ν, m, and ϕ are the number of ions per mole, the molality, and the osmotic coefficient, respectively, for the electrolyte. Values of $-\log a_w$ for constant exchanger composition (*i.e.*, x_{ZnR_2}) and for x_w values taken from Table I were found by graphical interpolation with a large scale plot of the data of Table II.

The evaluation of the partial molal volume change was based on the data in Table IV and the equation[16]

$$(2\bar{v}_{NaR} - \bar{v}_{ZnR_2}) = (2V_{NaR} - V_{ZnR_2}) - \int_0^{x_w} \left(\frac{\partial \bar{v}_w}{\partial x_{ZnR_2}}\right)_{x_w} dx_w \quad (9)$$

for x_{ZnR_2} = constant. The partial molal volume of water in the exchanger, $\bar{v}_w = (\partial V_r/\partial x_w)x_{ZnR_2}$, was found by differentiating eq 2. The coefficient, $(\partial \bar{v}_w/\partial x_{ZnR_2})x_w$, was determined from plots of $\bar{v}_w$ *vs.* x_{ZnR_2}, and the definite integral in eq 9 was evaluated numerically using the values of x_w listed in Table I for each cross-linked ion exchanger. The quantity $\Delta\bar{v} = (2\bar{v}_{NaR} - \bar{v}_{ZnR_2})$ was positive and varied from 13.5 ml mol^{-1} for the 2% DVB exchanger to 13.1 ml mol^{-1} for the most highly cross-linked preparation. This result contrasts with the exchange reactions between the alkali-metal cations[16] where $\Delta\bar{v}$ was always negative. The assumption is sometimes made that $\Delta\bar{v}$ is given to a good approximation by the difference between the partial molal volumes of the ions in aqueous solution at infinite dilution (*i.e.*, $\Delta\bar{v} = 2\bar{v}^0(Na^+) - \bar{v}^0(Zn^{2+})$). The value $\Delta\bar{v}$ thus estimated is 19.2 ml mol^{-1} which is 43% larger than the correct value derived from density measurements with eq 9.

Evaluation of the Activity Coefficient Ratio for Na^+ and Zn^{2+} Ions in the Exchanger. The second term appearing on the right-hand side of eq 5 may be regarded as a measure of the ionic interaction free energy in the exchanger. It was evaluated with eq 10 (see Appendix I for derivation).

$$\log (\gamma_{NaR}^2/\gamma_{ZnR_2}) = \log [(\gamma_{NaR}^*)^2/(\gamma_{ZnR_2}^*)] + \log (x_w/x_w^*) - 111.05 I_R \quad (10a)$$

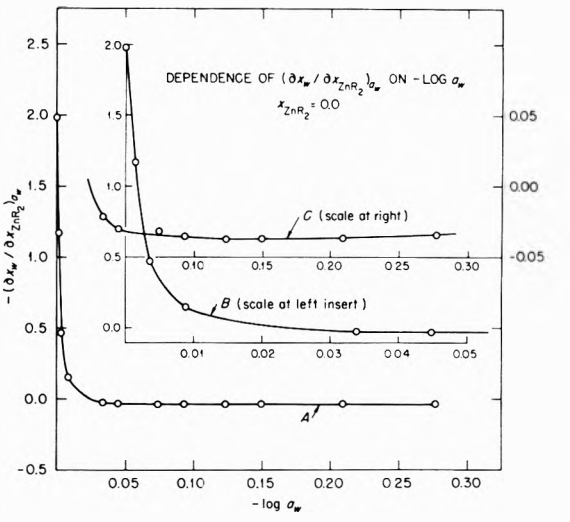

Figure 3. Variation of the differential coefficient, $(\partial x_w/\partial x_{ZnR_2})_{a_w}$, in eq 10b on $-\log a_w$ when $x_{ZnR_2} = 0.0$.

where

$$I_R = \int_{-\log a_w'}^{-\log a_w} (\partial x_w/\partial x_{ZnR_2})_{a_w} d(-\log a_w) \quad (10b)$$

Limiting values for the activity coefficient ratio $(\gamma_{NaR}^2/\gamma_{ZnR_2})$ for $-\log a_w = 0$ cannot be computed because no theory exists for the extrapolation of the measurements at higher concentrations, and because it has not been possible to perform isopiestic measurements on gels sufficiently dilute to satisfy the condition that $\log [(\gamma_{NaR}^*)^2/\gamma_{ZnR_2}^*] = 0$. The integration indicated in eq 10b therefore was performed by substituting the water activity, a_w^*, of the "reference" exchanger (*e.g.*, 0.5% DVB) for which $\pi\Delta\bar{v}$ is negligibly small when it is in equilibrium with 0.1 N zinc-sodium nitrate mixtures. The value of $\log [(\gamma_{NaR}^*)^2/\gamma_{ZnR_2}^*]$ therefore is given as a special case of eq 6

$$\log [(\gamma_{NaR}^*)^2/\gamma_{ZnR_2}^*] = \log K_m^* + \log [\gamma_{NaNO_3}^4/\gamma_{Zn(NO_3)_2}^3] \quad (11)$$

The quantity x_w^* in eq 10a is the equivalent water content of the reference exchanger in equilibrium with 0.1 N electrolyte, and the quantity K_m^* in eq 11 is the mass law concentration product ratio for the zinc–sodium ion-exchange reaction between the reference exchanger and 0.1 N electrolyte. The magnitude of K_m^* must be determined experimentally.

The values of x_w, the equivalent water contents of the cross-linked exchangers, like x_w^* must be determined from experiment. The differential coefficient, $(\partial x_w/\partial x_{ZnR_2})_{a_w}$, which appears in the integral in eq 10b was computed with eq 1. The $-\log a_w$ values which appear in the upper limit of the integral are for the variously cross-linked exchangers. They are the same as those employed in eq 7 and are listed in column 4 of Table V. The integral in eq 10b was evaluated numerically as a function of $-\log a_w$ with a computer. The variation of $(\partial x_w/\partial x_{ZnR_2})_{a_w}$ with $-\log a_w$ for $x_{ZnR_2} = 0.0$ is shown in Figure 3; note that its magnitude changes from a negative to a positive quantity at approximately, $-\log a_w = 0.025$. This behavior has not been observed in previous thermodynamic calculations on the exchange reactions between the alkali-metal cations, or between the halide ions. It is, of course, a reflection of the relatively greater hydration of zinc compared with sodium ion in highly cross-linked polyelectrolyte gels.

TABLE V: Computation of the Equilibrium Mass Law Product Quotient, K_x, for the Zinc–Sodium Ion Exchange Reaction

Nominal % DVB	x_{ZnR_2}	x_w	$-\log a_w$	$\log K_x^*$	$-111.02I_R$	π, atm	$\Delta\bar{v}$, ml	$\pi\Delta\bar{v}/2.3RT$	Log K_x(calcd)	K_x(calcd)	K_x(obsd)	K_x(calcd)/K_x(obsd)
2.0	0.00	535	0.00735	0.1173	0.3057	18	13.5	0.0043	0.4273	2.67	2.35	1.14
	1.00	427	0.00500	0.4150	0.2072	12	13.5	0.0029	0.6251	4.21	3.39	1.24
4.0	0.00	347	0.01378	0.1173	0.3879	39	13.5	0.0093	0.5145	3.26	2.85	1.14
	1.00	319	0.01130	0.4150	0.3001	32	13.5	0.0076	0.7227	5.28	4.16	1.27
8.0	0.00	176	0.03605	0.1173	0.4247	108	13.4	0.0256	0.5676	3.69	3.36	1.10
	1.00	188	0.04195	0.4150	0.2926	128	13.4	0.0303	0.7379	5.46	4.15	1.31
12.0	0.00	142.4	0.05489	0.1173	0.3447	167	13.3	0.0393	0.5103	3.24	3.44	0.94
	1.00	160.4	0.06692	0.4150	0.2049	206	13.3	0.0485	0.6684	4.66	3.66	1.27
16.0	0.00	122.2	0.07349	0.1173	0.2835	225	13.2	0.0526	0.4534	2.84	3.69	0.76
	1.00	141.3	0.09546	0.4150	0.1023	294	13.2	0.0689	0.5862	3.85	2.23	1.73
24.0	0.00	88.0	0.13500	0.1173	0.0428	416	13.1	0.0968	0.2569	1.81	3.41	0.53
	1.00	109.1	0.18585	0.4150	−0.2668	576	13.1	0.1339	0.2821	1.91	1.38	1.38

Discussion

Substitution of eq 10 and 11 into eq 6 gives

$$\log K_m = \pi(2\bar{v}_{NaR} - \bar{v}_{ZnR_2}) + \log (x_w/x_w^*) - 111.05I_R \quad (12)$$

Computations of log K_m for x_{ZnR_2} = 0.0, 0.5, and 1.0 were carried out and the results for x_{ZnR_2} = 0.0 are shown in Figure 4 where the contributions of the separate terms on the right-hand side of eq 12 are indicated. The calculated log K_m values are plotted against the weight normality of the cross-linked exchanger, $\bar{N}_m = 1000/x_w$, as a solid line; the experimentally measured log K_m are shown as points plotted against their respective $\bar{N}_m$ values taken from Table I. A satisfactory concordance between the calculated and observed K_m values appears to hold for four of the six differently cross-linked exchangers. The values for the nominal 16 and 24% DVB preparations, however, differ by more than the error either in the calculation or in the experimental determination of K_m.

Clearly, the most important contribution to the calculated log K_m is the log (x_w/x_w^*) term. This term determines the value of log $(\gamma_{NaR}^2/\gamma_{ZnR_2})$ as may be seen from the following equation for x_{ZnR_2} = 0.0

$$\log (\gamma_{NaR}^2/\gamma_{ZnR_2}) = \log K_m^* + \log \Gamma + \log (x_w/x_w^*) - 111.02I_R \quad (13)$$

where $\Gamma = [\gamma_{NaNO_3}^4/\gamma_{Zn(NO_3)_2}^3] = 1.508$ for trace $Zn(NO_3)_2$ in 0.1 N $NaNO_3$ solution.[13]

The contribution of the copolymer strain free energy, $\pi\Delta\bar{v}$, to log K_m is seen from Figure 4 to be small and positive for all cross linkings. This result arises from the fact that $\Delta\bar{v}$ is small and positive in contrast to the exchange reactions of the alkali-metal cations with Na^+ ion where $\Delta\bar{v}$ is of nearly the same magnitude but is negative.

The contribution of the integral, I_R, in eq 12 to log K_m is positive, but, again in contrast to the exchange reactions of the alkali-metal cations with Na^+ ion, I_R passes through a maximum with increasing cross linking and appears to approach zero for $\bar{N}_m \sim 11.6$, which value corresponds closely to the water content of the sodium form of the 24% DVB preparation (Table I). The unusual dependence of I_R on $\bar{N}_m$ is a consequence of the fact that $(\partial x_w/\partial x_{ZnR_2})_{a_w}$ changes from a negative to a positive value, or, fundamentally, because for $-\log a_w$ values exceeding *ca.* 0.025 the equivalent water content of the zinc poly(styrenesulfonate) exceeds that of the sodium salt.

A more direct relationship with the ion-exchange reaction isotherm is obtained if the mass law product quotient

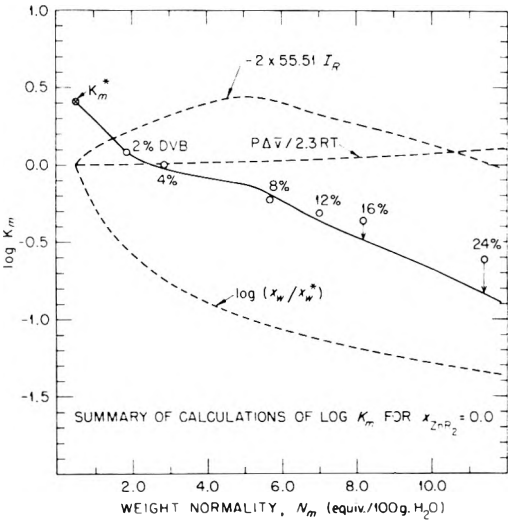

Figure 4. Summary of the thermodynamic calculations of log K_m for the exchange of tracer zinc with the sodium form of variously cross-linked polystyrenesulfonate gels.

is expressed in terms of the equivalent fractions of zinc and sodium ions in the exchanger and in the mixed aqueous electrolyte, respectively. Thus

$$K_x = x_{ZnR_2}x_{Na^+}^2/x_{NaR}^2x_{Zn^{2+}} \quad (14)$$

Substitution of eq 14 in eq 12 gives a form convenient for calculations showing the dependence of the ionic selectivity on the composition of the exchanger

$$\log K_x = 2\pi(\bar{v}_{NaR} - \bar{v}_{ZnR_2}) + \log K_x^* - 111.05I_R \quad (15)$$

where $\bar{v}_{NaR}$ and $\bar{v}_{ZnR_2}$ are now partial equivalent volumes, and K_x^* is the value of K_x measured with the "reference" exchanger. The quantity K_x is related to K_m by $K_x = K_m(\bar{N}_m/N_m)$ where N_m and $\bar{N}_m$ are the weight normalities of the external electrolyte mixture and of the polyelectrolyte gel phase, respectively.

The calculations summarized in Table V were carried out to determine if the observed dependence of K_x on the equivalent fraction of zinc ion in the exchanger, x_{ZnR_2}, could be reproduced using eq 15. Inspection of this table reveals a satisfactory agreement between the calculated and the experimentally measured K_x values for all but the two most heavily cross-linked exchangers. Although the differences between K_x(calcd) and K_x(obsd) vary between 15 and 30% for the nominal 2, 4, 8, and 12% DVB cross-

linked exchangers. The dependence of K_x(obsd) on x_{ZnR_2} is reproduced by the calculation. It seems likely that K(obsd) for the exchange reaction between tracer zinc ion (*i.e.*, $x_{ZnR_2} = 0.0$) and the sodium form of the 24% DVB cross-linked exchanger is in error. The discrepancy between the K_x(calcd) and K(obsd) values in Table V may seem large on first sight. However, it is to be remembered that, because of inherent experimental difficulties, the accuracy of the K(obsd) values is probably no better than ±5%. Additionally, errors from several sources contribute to the term $111.02I_R$ in eq 15. A significant uncertainty exists in the quantity $(\partial x_x/\partial x_{ZnR_2})_{a_w}$ because its value is derived by differentiating the isopiestic data relating x_w to x_{ZnR_2} at constant water activity. Error is present also in the value of $-\log a_w$ which appears as the upper limit in the integral (*cf.* eq 10b). The magnitude of $-\log a_w$ was estimated by graphical interpolation of the data in Table II using the experimentally determined x_w values listed in Table I. Thus, I_R is probably known no better than to ±15%.

The concordance between calculation and experiment found in this research on the zinc–sodium ion-exchange reaction leaves much to be desired; however, it appears to be far better than the agreement reported recently[11] where a significantly different program of calculations for $x_{ZnR_2} = 1.0$ was performed based on eq 3. Thus, for the reaction of *microconcentrations* of Na^+ ion in 0.1 *m* $Zn(ClO_4)$ solution with variously cross-linked zinc poly(styrenesulfonate), K_m(calcd)/K_m(obsd) varied from 1.4 for 2% DVB to 4.3 for 16% DVB exchanger. If the experimental measurements are correct, it seems likely that the failure of this calculation can be traced to the neglect of interionic interaction in the ion exchange gel. The activity coefficient ratio, $(\gamma_{MR}^2/\gamma_{MR_2})$, was estimated with the Gibbs–Duhem equation from osmotic coefficient measurements made with binary NaPSS and with binary $Zn(PSS)_2$ aqueous polyelectrolyte solutions, respectively. It then was assumed that γ_{NaR} and γ_{ZnR_2} for the gel were given by the values for γ_{NaPSS} and $\gamma_{Zn(PSS)_2}$ each at the concentration existing in the gel which effectively was pure ZnR_2. The values of $(\gamma_{MR}^2/\gamma_{MR_2})$ employed in this paper were obtained by applying equations derived from the thermodynamics of ternary aqueous mixtures (see Appendix I) to experimental data on ternary mixtures. This latter method is sound and does not require extrathermodynamic assumptions. However, because of its mathematical form calculations with it require that isopiestic measurements be made with considerable accuracy.

Limitations of the Thermodynamic Calculations. The achievement of a fair agreement between the thermodynamically calculated and the experimentally measured mass law concentration product quotients, K_m and for K_x, for the exchange reaction between trace Zn^{2+} ion and Na^+ ion in 0.1 *N* $NaNO_3$ solutions has been demonstrated in this research with nominal 2, 4, 8, and 12% DVB cross-linked polystyrenesulfonate cation exchangers, but not with the 16 and 24% DVB preparations. Some comment on possible causes for disagreement observed with the most highly cross-linked ion exchangers would seem justified, apart from the observation made earlier that significant errors are present both in the experimentally measured and in the calculated K_m values.

(a) An essential assumption in the thermodynamic calculations is that the properties of the cross-linked exchangers studied are identical with those of the reference exchanger (*i.e.*, nominal 0.5% DVB cross linked) when the equivalent water contents, x_w, of all of the preparations are the same and a correction has been made for differing strain free energies, $\pi\Delta\bar{v}$. This assumption requires that the introduction of divinylbenzene as a cross linker in polystyrenesulfonate gels does not change their thermodynamic properties perceptibly.

(b) All exchangers are presumed to have the same equivalent weight as the reference exchanger, a condition that scarcely holds for the preparations used in this research (*cf.* Table I).

(c) It is implicitly assumed that the cross-linked ion exchangers may be treated as homogeneous polyelectrolyte gels whose average properties (*i.e.*, exchange capacity, equivalent volume, and water constant) are well-defined thermodynamic quantities. Physical and/or chemical heterogeneity are assumed to be absent, a condition that becomes more difficult to realize the greater the cross linking. Thus, it may not be surprising that the properties of the most highly cross-linked exchangers used in this research cannot be computed from those of lightly cross-linked exchangers.

(d) The thermodynamic treatment employed for the evaluation of the activity coefficient ratio, $\log (\gamma_{NaR}^2/\gamma_{ZnR_2})$, assumed a ternary mixture consisting of ZnR_2, NaR, and water. Therefore, values of K_m only for ion-exchange equilibria with dilute aqueous $NaNO_3$–$Zn(NO_3)_2$ mixtures may be derived. With concentrated electrolyte mixtures invasion of the cross-linked polyelectrolyte gels will produce five component mixtures which require a more elaborate thermodynamic treatment.

Appendix I. Derivation of Equation for Activity Coefficient Ratio

The derivation of eq 10 for the mean molal activity coefficient ratio for the ions (Na^+ and Zn^{2+}) in the exchanger is parallel to that already given for exchange reactions between singly charged cations[16] or anions.[15] It rests on the Cauchy cross-differentiation identity whose utility was first pointed out by McKay and Perring.[20]

To begin we write their eq 4 where species 1 = Na^+, species 2 = Zn^{2+}

$$0.018\left(\frac{\partial \ln m\gamma_1}{\partial \ln a_w}\right)_{x_1} = -\frac{k_1}{m} - \frac{k_1}{m}\left(\frac{\partial \ln m}{\partial \ln x_2}\right)_{a_w} \quad \text{(A1a)}$$

$$0.018\left(\frac{\partial \ln m\gamma_2}{\partial \ln a_w}\right)_{x_2} = -\frac{k_2}{m} - \frac{k_2}{m}\left(\frac{\partial \ln m}{\partial \ln x_1}\right)_{a_w} \quad \text{(A1b)}$$

The concentration, m, on a weight of solvent basis is any linear combination of the form

$$m = k_1m_1 + k_2m_2 \quad \text{(A2)}$$

and the fractions x_1 and x_2 are defined by $x_1 \equiv k_1m_1/m$ and $x_2 \equiv k_2m_2/m$.

Multiplying eq A1a by two and subtracting eq A1b gives

$$0.018\left[\frac{\partial \ln (m\gamma_1)^2}{\partial \ln a_w} - \frac{\partial \ln (m\gamma_2)}{\partial \ln a_w}\right]_x = \frac{1}{m}(k_2 - 2k_1) - \frac{2k_1}{m}\left(\frac{\partial \ln m}{\partial \ln x_2}\right)_{a_w} + \frac{k_2}{m}\left(\frac{\partial \ln m}{\partial \ln x_1}\right)_{a_w} \quad \text{(A3)}$$

Assuming $k_1 = 1$ and $k_2 = 2$ gives the concentration as weight normality, $m = m_1 + 2m_2$, and x_2, x_2 as equivalent fractions. Equation A3 becomes

$$0.018\left[\frac{\partial \ln (m\gamma_1)^2}{\partial \ln a_w} - \frac{\partial \ln (m\gamma_2)}{\partial \ln a_w}\right]_{x_2} =$$
$$-\frac{2}{m}\left(\frac{\partial \ln m}{\partial \ln x_2} - \frac{\partial \ln m}{\partial \ln x_1}\right)_{a_w} = -\frac{2}{m}\left(\frac{\partial \ln m}{\partial x_2}\right)_{a_w} =$$
$$2\left[\frac{\partial (1/m)}{\partial x_2}\right]_{a_w} = 2\left(\frac{\partial x_w}{\partial x_2}\right)_{a_w} \quad \text{(A4)}$$

Integrating eq A4 gives

$$\ln\left[\frac{(m\gamma_1)^2}{(m\gamma_2)}\right]_{a_w^*}^{a_w} =$$
$$-2 \times 55.51 \int_{-\log a_w^*}^{-\log a_w} (\partial x_w/\partial x_2)_{a_w} \, d(-\ln a_w) \quad \text{(A5)}$$

Finally, evaluating the left-hand member of eq A5 gives

$$\log\left(\frac{\gamma_1^2}{\gamma_2}\right) = \log\left[\frac{(\gamma_1^*)^2}{\gamma_2^*}\right] + \log\left(\frac{m^*}{m}\right) - 2 \times 55.51 \times$$
$$\int_{-\log a_w^*}^{-\log a_w} \left(\frac{\partial x_w}{\partial x_2}\right)_{a_w} d(-\log a_w) \quad \text{(A6)}$$

Equation A6 is identical with eq 10 of the text.

References and Notes

(1) Research sponsored by the U. S. Atomic Energy Cmmission under contract with the Union Carbide Corp
(2) (a) Research Division, Lockheed Propulsion Co., Redlands, Calif. (b) Department of Pharmacology, University of Kansas, Lawrence, Kan.
(3) W. F. McIlhenny, M.S. Thesis, Texas A & M University, Jan 1958.
(4) W. C. Bauman, J. R. Skidmore, and R. H. Osmun, *Ind. Eng. Chem.*, **40**, 1350 (1948).
(5) W. C. Bauman and J. Eichorn, *J. Amer. Chem. Soc.*, **69**, 2830 (1947).
(6) O. D. Bonner and L. L. Smith, *J. Phys. Chem.*, **61**, 326 (1957).
(7) O. D. Bonner and R. R. Pruett, *J. Phys. Chem.*, **63**, 1420 (1959).
(8) H. P. Gregor, O. R. Abolafia, and M. H. Gotlieb, *J. Amer. Chem. Soc.*, **58**, 984 (1954).
(9) O. D. Bonner and F. L. Livingston, *J. Phys. Chem.*, **60**, 530 (1956).
(10) M. M. Reddy and J. A. Marinsky, *J. Macromcl. Sci.-Phys.*, **B5**, 135 (1971).
(11) M. M. Reddy, S. Amdur, and J. A. Marinsky, *J. Amer. Chem. Soc.*, **94**, 4087 (1972).
(12) J. A. Marinsky, M. M. Reddy, and S. Amdur, *J. Phys. Chem.*, **77**, 2128 (1973).
(13) G. E. Boyd, F. Vaslow, and S. Lindenbaum, *J. Phys. Chem.*, **71**, 2114 (1967).
(14) G. E. Boyd and S. Lindenbaum, *J. Phys. Chem.*, **69**, 2378 (1965).
(15) G. E. Boyd, S. Lindenbaum, and G. E. Myers, *J. Phys. Chem.*, **65**, 577 (1961).
(16) G. E. Myers and G. E. Boyd, *J. Phys. Chem.*, **60**, 521 (1956).
(17) A. Schwarz and G. E. Boyd, *J. Phys. Chem.*, **69**, 4268 (1965).
(18) F. G. Donnan and E. A. Guggenheim, *Z. Phys. Chem.*, **162A**, 346 (1932).
(19) G. E. Boyd and B. A. Soldano, *Z. Elektrochem.*, **57**, 162 (1953).
(20) H. A. C. McKay and J. K. Perring, *Trans. Faraday Soc.*, **49**, 163 (1953).

Adsorption Anomaly in the System Zinc Oxide–Water

Tetsuo Morimoto* and Mahiko Nagao

Department of Chemistry, Faculty of Science, Okayama University, Okayama, Japan

(Received August 8, 1973; Revised Manuscript Received November 5, 1973)

The adsorption anomaly which is associated with the appearance of a jump in the water adsorption isotherm on ZnO has been investigated by measuring water adsorption isotherms, and by electron-microscopic observation, on several samples which differ from each other in origin and pretreatment. The sample ZnO-A, made by burning zinc metal, has the most perfect surface crystallinity and yields the largest jump in the water adsorption isotherm, whereas samples ZnO-B and -C, prepared by the pyrolysis of zinc hydroxide and oxalate, have smaller jumps, corresponding to less surface crystallinity. Heat treatment of the samples decreases surface crystallinity, resulting in a smaller jump in the adsorption isotherms. It is suggested that the peculiar arrangement of surface hydroxyl groups on fully hydroxylated surfaces of ZnO, *i.e.*, a completely hydrogen-bonded structure of surface hydroxyl groups on the well-developed $(10\bar{1}0)$ plane of ZnO, is responsible for these phenomena. Such surfaces may act as uniform surfaces, with a weak adsorbing force for water molecules, giving rise to a mobile adsorption of water molecules followed by two-dimensional condensation.

Introduction

Recent studies on the interaction between ZnO surfaces and water molecules have revealed interesting phenomena which have never been observed on other oxides:[1-5] (1) the surface water content of ZnO, that is the amount of chemisorbed water, decreases remarkably by degassing the ZnO at 200–450°, higher temperatures than in the cases of other oxides;[1] (2) the monolayer capacity of water obtained by applying the BET method to the adsorption isotherm is invariable after degassing ZnO at lower temperatures, but increases markedly after treatments at temperatures over 200°;[1] (3) the heat of immersion of ZnO in water is almost constant for the samples degassed at 100–200°, increases sharply after degassing at temperatures over 200° and attains a maximum value by 400° pretreatment;[2] (4) the adsorption isotherms of water have a vertical discontinuity, which has been named "hump"[1,3] or "jump,"[4,5] near the relative pressure of 0.2–0.3.

It should be noticed that this adsorption anomaly, that is the appearance of a jump in water adsorption isotherms, is observed in the process of physisorption of water on fully hydroxylated surfaces of ZnO. Most metal oxides adsorb water molecules physically as well as chemically, but they do not show such a jump in adsorption isotherms. Fisher and McMillan[6] and Ross, *et al.*,[7-10] described many adsorption systems having such a jump, systems which are composed of adsorbents with uniform surfaces such as graphite and alkali halides and nonpolar adsorbates such as inert gases and hydrocarbons. The present system of ZnO-H_2O, however, is a unique example in that it consists of a polar adsorbent and a polar adsorbate, hence the terminology: "adsorption anomaly."

Ross, *et al.*,[7-10] elucidated the appearance of a jump in terms of two-dimensional condensation on uniform surfaces. Also, for the present system of ZnO-H_2O, from measurements of isosteric heats of adsorption and adsorption entropies, it has been reported that the fully hydroxylated surfaces of ZnO act as homotattic ones for the physisorption of water.[5]

The present study was undertaken to investigate this adsorption anomaly more deeply, by measuring the adsorption isotherms on various ZnO samples which differ in origin and pretreatment, and by observing the surfaces with an electron microscope.

Experimental Section

Materials. Three kinds of ZnO used in this study were the same as those described previously.[4] One of them was the sample prepared by burning zinc metal in air (ZnO-A). The other two (ZnO-B and -C) were obtained by the pyrolysis of $Zn(OH)_2$ and ZnC_2O_4 which were precipitated by mixing zinc nitrate solution with ammonia water and with oxalic acid solution, respectively. These precipitates were washed sufficiently with distilled water and calcined at 500° for 4 hr. For the investigation of the effect of heat treatment on the water adsorption, each sample was calcined again at 700° as well as at 1200° for 2 hr. X-Ray analysis showed all these samples to be well-developed crystals of ZnO.

Surface Area Measurement. The specific surface area of the samples was computed by introducing the nitrogen adsorption data obtained at 77°K into the BET equation, where the assumption was made that the area of a nitrogen molecule is 16.2 $Å^2$.

Water Adsorption Measurement. The adsorption of water on ZnO was measured by using a conventional volumetric adsorption apparatus equipped with an oil manometer to read out more exactly the equilibrium pressure. Prior to the measurement of water adsorption, a sample of about 10 m^2 measured by N_2 adsorption was degassed at 450° for 4 hr *in vacuo* of 10^{-5} Torr to remove naturally adsorbed water and carbon dioxide. After the measurement of the first adsorption isotherm at 18°, the sample was exposed to saturated water vapor for 10 hr, degassed at room temperature for 4 hr in 10^{-5} Torr in order to remove physisorbed water, and then used for the measurement of the second adsorption isotherm at 18°. Adsorption equilibrium was attained within 30 min in the second adsorption, though it took 1 or 2 hr in the first adsorption. In every case, desorption isotherms obtained after determination of the second adsorption isotherm did not show hysteresis, which gives evidence that the samples are nonporous.

Water Content. ZnO stored exposed to the atmosphere maintains physisorbed and chemisorbed water, which can be removed progressively by heating *in vacuo*. The amount of chemisorbed water which is named water content was determined by the successive ignition loss method.[11] In this procedure, a certain amount of CO_2 was found in the gas evolved, but it was separated and eliminated from the value of the water content.[4]

Electron Micrograph. The electron-microscopic observation was carried out by using a scanning electron microscope with high resolution, Model HSM-2A, manufactured by the Hitachi Co.

Results

Adsorption Isotherm of Water. The first and second adsorption isotherms of water on ZnO-A, -B, and -C are given in Figures 1-3, where the adsorbed amount is expressed in milliliters (STP) per unit surface area obtained from nitrogen adsorption. All the isotherms show a jump at a relative pressure of 0.2-0.3 as reported in the previous papers,[1,3-5] though the height of the jump depends on the origin and pretreatment of the samples. Generally, the jump decreases when the samples are treated at higher temperatures. In summary, the jump for the original sample of ZnO-A is the largest and that of 1200° treated ZnO-B is the smallest.

Ratio of H_2O:OH. The quantitative relation between the amounts of physisorbed and chemisorbed water on metal oxides often gives important informations about the adsorption state or adsorption mechanism of water. Contrary to the simplicity of calculating the ratio of H_2O:OH in the cases of TiO_2, α-Fe_2O_3,[12] and Al_2O_3[13] where no jump appears, the calculation on the surface of ZnO is rather complicated.

Table I[14] shows the ratio obtained from the first and second adsorption isotherms, obtained according to the method described in the preceding paper.[4,5] *Vm* is the monolayer capacity computed by applying the BET method to the first adsorption isotherm; this involves both the physisorbed and chemisorbed water. The second adsorption isotherm should reflect only physisorbed water, because the preevacuation of water-saturated surfaces at room temperature has been shown to leave fully hydroxylated surfaces.[1,5] Accordingly, Vp_1, which is obtained by applying the BET method to the initial part of the second adsorption isotherm, gives the amount of physisorption up to the beginning of the jump. Previous considerations have led to the conclusion that the total amount of physisorbed water *Vp* should be taken at the so-called "B" point which appears just after the accomplishment of the jump.[4,5] Vp_2, which is obtained by subtracting Vp_1 from the total physisorption *Vp*, indicates the amount of physisorbed water in the region of the jump.

On the other hand, the amount of chemisorbed water *Vc* is obtained by subtracting Vp_1 from *Vm*. There is another portion of chemisorbed water that is water content, *Vh*, which is retained on the surface before the measurement of the first adsorption isotherm. The total amount of chemisorbed water is therefore given by the sum of *Vc* and *Vh*. Table I gives the same result as described previously in that the ratio of H_2O:OH approximates 1,[4] which leads us to infer that the first physisorbed layer is practically complete when each of the surface hydroxyl groups is covered by a molecule of water. More striking is that this general relation is true for all the samples tested, in contrast to results found for surfaces of TiO_2, α-Fe_2O_3,[12] and Al_2O_3.[13] where the ratio is found to be 0.5.

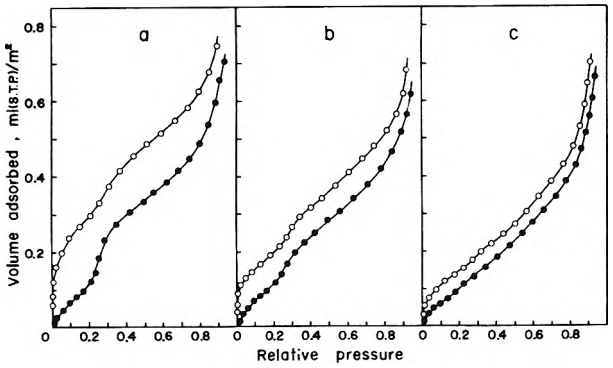

Figure 1. Adsorption isotherm of water on ZnO-A: original (a), 700° treated (b), 1200° treated (c); O, first adsorption; ●, second adsorption.

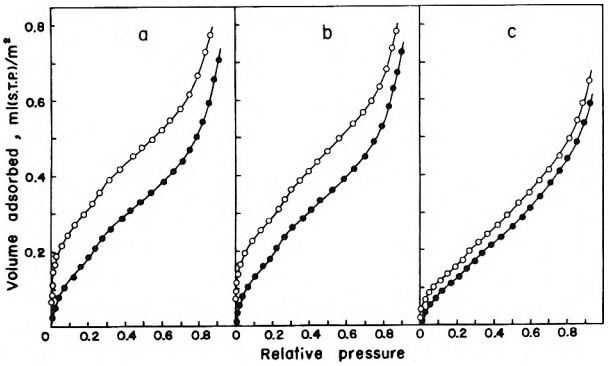

Figure 2. Adsorption isotherm of water on ZnO-B: 500° treated (a), 700° treated (b), 1200° treated (c); O, first adsorption; ●, second adsorption.

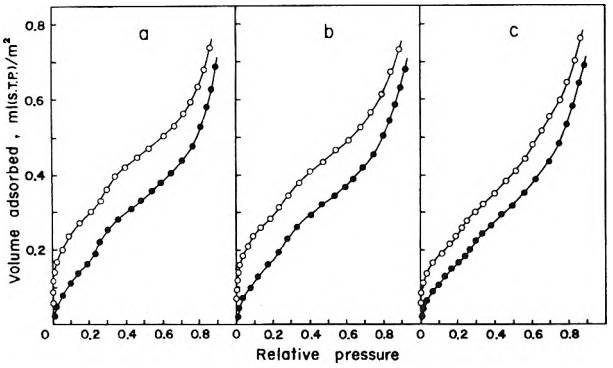

Figure 3. Adsorption isotherm of water on ZnO-C: 500° treated (a), 700° treated (b), 1200° treated (c); O, first adsorption; ●, second adsorption.

Electron-Microscopic Observation. Scanning electron micrographs of the ZnO samples are illustrated in Figure 4. It can be seen from this figure that the crystallinity of the original sample of ZnO-A is the best of all the samples tested. It is well known that the crystal structure of ZnO is of the wurtzite type and that the cleavage is perfect on the (0001), (000$\bar{1}$), and (10$\bar{1}$0) planes.[15-17] The photograph in Figure 4a clearly reveals hexagonal prisms, which testify to the wurtzite structure of ZnO. Furthermore, it was observed under the electron microscope that ZnO formed by burning zinc metal exhibits a number of needles just after preparation, which later change to prisms which are both wider and shorter, though photographs of this latter phenomenon are not included in the present figures. The particles of original ZnO-A are substantially more well defined than those of ZnO-B and -C. It should be further noted that the surface crystallinity decreases remarkably when the samples are treated at higher temperatures, despite the fact that the bulk crystallinity found by X-ray diffraction remains unchanged by the heat treatment.

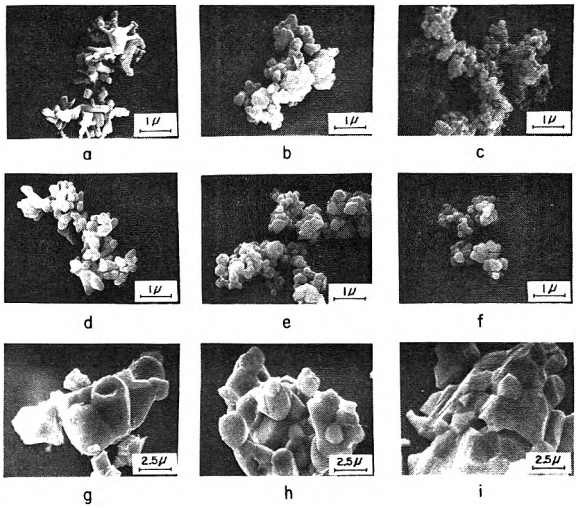

Figure 4. Scanning electron micrographs: ZnO-A, original (a), 700° treated (d), 1200° treated (g); ZnO-B, 500° treated (b), 700° treated (e), 1200° treated (h); ZnO-C, 500° treated (c), 700° treated (f), 1200° treated (i).

Discussion

A number of adsorption systems which give a jump in adsorption isotherms have been reported; in all of these cases adsorbent and/or adsorbate have been nonpolar substances, which result in a fairly weak interaction. The adsorbents dealt with had uniform surfaces, *e.g.*, graphite[9,10,18,19] which has conducting and well-defined surfaces, and alkali halides[6-8] which have homopolar surfaces composed of an equal number of alternately arranged alkali ions and halogen ions.

With such systems as TiO_2-H_2O[20] and ThO_2-H_2O,[21] which are composed of a polar adsorbent and a polar adsorbate, discontinuities in the adsorption isotherms have recently been reported, but they seem to have arisen under nonequilibrium conditions. It should, on the contrary, be emphasized that the present system of ZnO-H_2O gives a reversible and reproducible jump in the adsorption isotherms.

As described above, the height of the jump in the water adsorption isotherm differs depending on the origin and pretreatment temperature of ZnO (Figures 1-3); the jump is greatest on the original sample of ZnO-A. Furthermore, the jump decreases by treating samples at elevated temperatures, corresponding to the decrease in the Vp_2 values in Table I.[14]

The same trend is observable in electron micrographs. In the scanning electron micrographs of ZnO-A (Figure 4a), we can find many sharply delineated hexagonal prisms which have grown along the c axis and, accordingly, have well-developed (10$\bar{1}$0) faces. Furthermore, it is evident that the surface crystallinity decreases by the heat treatment at higher temperatures. This heat treatment will cause the transfer of surface atoms to introduce disorder in the (10$\bar{1}$0) face, that is a decrease in the surface homogeneity. With ZnO-B and -C, the photographs do not permit one to decide which plane prevails more ex-

tensively, but they positively indicate the progression of sintering by heat treatment. From comparison of the results of the water adsorption isotherm and electron micrograph, it is clear that the appearance of a jump is closely related to the development of the (10$\bar{1}$0) face.

In the ZnO crystal of wurtzite structure, the component atoms of both zinc and oxygen are tetrahedrally coordinated. On the (0001) face, which is one of the planes of perfect cleavage, zinc atoms occupy half the trigonal sites formed by the lattice oxygens (Figure 5a,c).[16] For the conservation of electroneutrality on the surface, one oxygen is further bonded to two zincs.[17] Water molecules, when the surfaces are hydrated, will first be chemisorbed in such a way that hydroxyls are bonded to surface zincs and hydrogen atoms to surface oxygens, which brings about a completion of tetrahedral coordination of the surface atoms which is similar to that of the lattice atoms in the bulk.

On the (000$\bar{1}$) face, which is formed at the same time with the (0001) face, each zinc is bonded to an underlying lattice oxygen. Since such a surface structure is reasonably unstable, surface zincs transfer to trigonal sites formed by lattice oxygens.[16] For the requirement of electroneutrality here, one oxygen is bonded to two zincs. The hydration of such a reconstructed surface will produce a hydroxylated surface similar to that on the (0001) face (Figure 5a,d).

Hydroxyl groups thus formed on the (0001) and (000$\bar{1}$) faces are coplanar and separated from each other by a distance equal to the lattice constant. This distance will be too great for hydrogen bonds to occur between neighboring hydroxyl groups.[17]

On the (10$\bar{1}$0) face, which is parallel to the *c* axis and is dominant on the surfaces of ZnO-A, the centers of zinc and oxygen atoms are coplanar and each of them coordinates three counter ions (Figure 5b,e,f). Moreover, it should be noted that an equal number of zincs and oxygens are present on this face and that they are arranged in pairs parallel to the c axis. When hydration occurs on such surfaces, hydroxyl will be bonded to zinc and hydrogen to oxygen, which leads to the completion of tetrahedral coordination of both surface zincs and oxygens. Hydroxyl groups thus formed on (10$\bar{1}$0) face do not produce a coplanar surface, contrary to the cases of the (0001) and (000$\bar{1}$) faces.

On the hydroxylated (10$\bar{1}$0) face, there are prominent rows of hydroxyl groups (Figure 5b), neighboring rows being separated by a short distance, resulting in a narrow channel between rows. Such an arrangement will produce closed hydrogen bondings as follows: each hydrogen bonded to oxygen in the original coplanar Zn–O surface is in a suitable position to enter into hydrogen bonding with oxygen in the hydroxyl which is newly bonded to zinc. At the same time, hydrogen in the newly bonded hydroxyl will be favorably oriented with respect to oxygen in the neighboring hydroxyl on the same row (Figure 5e,f).

The hydration of the (10$\bar{1}$0) face thus leads to a geometry such that all zinc and oxygen atoms on the bare (10$\bar{1}$0) face, together with oxygen atoms newly bonded to zinc atoms, will form complete tetrahedral coordination, and such that all hydrogens in the surface hydroxyl groups will be used to form hydrogen bonds (Figure 5f). The combination of all sites which can possibly form hydrogen bonds on the hydroxylated (10$\bar{1}$0) faces can therefore produce a closed structure, which results in only weak adsorption forces on incoming water molecules. Figure 5b shows the planar view of the hydroxylated (10$\bar{1}$0) faces.

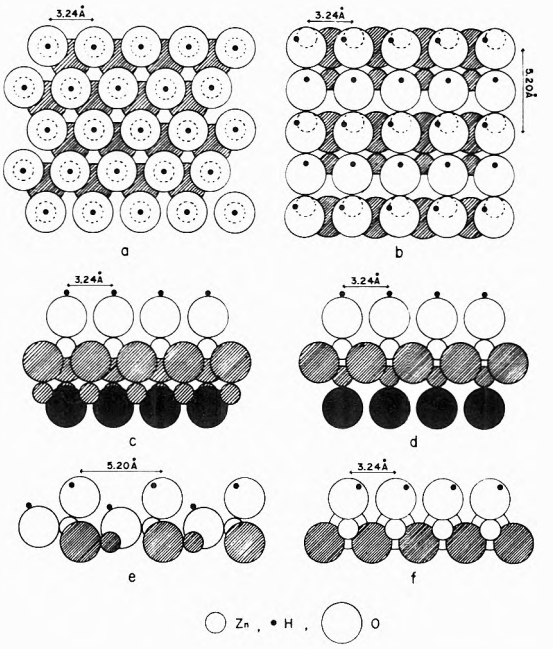

Figure 5. Structural model of hydroxylated ZnO surface: planar view of (0001) face (a) and (10$\bar{1}$0) face (b); side view of (0001) face (c), (000$\bar{1}$) face (d), (10$\bar{1}$0) face perpendicular to *c* axis (e), and (1010) face parallel to *c* axis (f).

Let us consider, next, the water physisorption process on the hydroxylated surfaces of ZnO where the surface crystallinity is excellent, and (0001), (000$\bar{1}$), and (10$\bar{1}$0) faces are well developed. The hydroxylated (0001) or (000$\bar{1}$) faces will be more active for the adsorption of water than the hydroxylated (10$\bar{1}$0) face, because the former has isolated hydroxyl groups which are not hydrogen bonded, contrary to the latter which has no non-hydrogen-bonded hydroxyl groups. Any particles of ZnO should have such surface defects as corners, edges, steps, and others; these sites will act still more actively than those on the (0001) and (000$\bar{1}$) faces.

Physisorption of water will occur initially on the sites having the highest energy, such as the defects stated above, next on isolated hydroxyl groups, and finally on the uniformly hydroxylated (10$\bar{1}$0) faces. Water molecules adsorbed on stronger sites must be immobile, while those on less active sites of completely hydrogen-bonded hydroxyl groups will have a great possibility of moving two dimensionally.[5] A jump in the adsorption isotherm of water may thus appear on surfaces of ZnO having excellent surface crystallinity.

In conclusion, the adsorption anomaly which appears in the physisorption of water on ZnO can be ascribed to the formation of a peculiar structure of surface hydroxyl groups, which results in weaker interaction forces on water molecules coming toward the surface. Heat treatment at higher temperatures may cause enhanced surface heterogeneities of the (10$\bar{1}$0) face as well as a larger decrease in the area of the (10$\bar{1}$0) face compared to the other faces, both of which result in a decrease in the height of the jump and, at the same time, an increase in the initial portion of the water adsorption isotherms (Figures 1–3).

Similarly, a series of surface phenomena occurring in the system ZnO–H_2O, as stated above, can be explained on the basis of characteristic arrangements of atoms on ZnO surfaces. For example, the desorption of surface hydroxyl groups completely hydrogen bonded to each other

on the (10$\bar{1}$0) face will be delayed and take place rather in one rush at relatively higher temperatures.

Supplementary Material Available. Table I will appear following these pages in the microfilm edition of this volume of the journal. Photocopies of the supplementary material from this paper only or microfiche (105 × 148 mm, 24× reduction, negatives) containing all of the supplementary material for the papers in this issue may be obtained from the Journals Department, American Chemical Society, 1155 16th St., N.W., Washington, D. C. 20036. Remit check or money order for $3.00 for photocopy or $2.00 for microfiche, referring to code number JPC-74-1116.

References and Notes

(1) T. Morimoto, M. Nagao, and F. Tokuda, *Bull. Chem. Soc. Jap.*, **41**, 1533 (1968).
(2) T. Morimoto, M. Nagao, and M. Hirata, *Kolloid-Z. Z. Polym.*, **225**, 29 (1968).
(3) M. Nagao and T. Morimoto, *J. Phys. Chem.*, **73**, 3809 (1969).
(4) T. Morimoto and M. Nagao, *Bull. Chem. Soc. Jap.*, **43**, 3746 (1970).
(5) M. Nagao, *J. Phys. Chem.*, **75**, 3822 (1971).
(6) B. B. Fisher and W. G. McMillan, *J. Amer. Chem. Soc.*, **79**, 2969 (1957).
(7) S. Ross and H. Clark, *J. Amer. Chem. Soc.*, **76**, 4291 (1954).
(8) S. Ross, J. P. Olivier, and J. J. Hinchen, *Advan. Chem. Ser.*, **No. 33**, 317 (1961).
(9) J. P. Olivier and S. Ross, *Proc. Roy. Soc., Ser. A*, **265**, 447 (1962).
(10) W. D. Machin and S. Ross, *Proc. Roy. Soc., Ser. A*, **265**, 455 (1962).
(11) T. Morimoto, K. Shiomi, and H. Tanaka, *Bull. Chem. Soc. Jap.*, **37**, 392 (1964).
(12) T. Morimoto, M. Nagao, and F. Tokuda, *J. Phys. Chem.*, **73**, 243 (1969).
(13) T. Morimoto, M. Nagao, and J. Imai, *Bull. Chem. Soc. Jap.*, **44**, 1282 (1971).
(14) See paragraph at end of text regarding supplementary material.
(15) S. Dana and W. E. Ford, "A Textbook of Mineralogy," Wiley, New York, N. Y., 1960, p 480.
(16) A. L. Dent and R. J. Kokes, *J. Phys. Chem.*, **73**, 3781 (1969).
(17) A. Atherton, G. Newbold, and J. A. Hockey, *Discuss. Faraday Soc.*, **52**, 33 (1971).
(18) W. R. Smith and D. G. Ford, *J. Phys. Chem.*, **69**, 3587 (1965).
(19) B. W. Davis and C. Pierce, *J. Phys. Chem.*, **70**, 1051 (1966).
(20) P. T. Dawson, *J. Phys. Chem.*, **71**, 838 (1967).
(21) H. F. Holmes, E. L. Fuller, Jr., and C. H. Secoy, *J. Phys. Chem.*, **72**, 2293 (1968).

Determination of the Equivalence Point of the N + NO Titration Reaction by Electrical Conduction

S. E. Schwartz* and S. M. Butler

Department of Chemistry, State University of New York, Stony Brook, New York 11790 (*Received January 24, 1974*)

Publication costs assisted by the Petroleum Research Fund and the State University of New York

Electrical conduction has been measured in mixtures of atomic nitrogen and oxygen in N_2 formed by allowing NO to react with N in a flowing afterglow. Ionic species may be extracted by electric fields of ~5 V/cm, established between parallel stainless steel electrodes, at pressures of 60 to 1300 Pa. Any remaining conduction, measured subsequent to extraction, vanishes sharply at the equivalence point of the titration reaction $N + NO \rightarrow N_2 + O$ (1) and is thus attributed to ionic species formed by reaction of atomic nitrogen. The rate of ionization exhibits a first-order dependence on [N] for [O]/[N] > 100, and this first-order contribution to the ionization rate exceeds higher order contributions for [O]/[N] > 10. Several mechanisms for chemiionization are considered; such ionization may take place by the reaction $O(^1S) + N(^4S) \rightarrow NO^+ + e^-$. Measurement of saturation current is found to serve as a sensitive indicator of the equivalence point of (1).

Introduction

The rapid reaction

$$N(^4S) + NO \longrightarrow N_2 + O(^3P) \qquad (1)$$

is commonly used in flowing afterglow systems as a titration reaction for atomic nitrogen,[1-11] and as a source of atomic oxygen.[12,13] Typically molecular nitrogen is partially dissociated in an electrical (often microwave) discharge, and NO is added to the flowing N_2–N mixture downstream from the discharge. Successful application of the technique requires precise determination of the NO flow equal to the N atom flow. This "equivalence point" is most frequently determined by monitoring molecular electronic chemiluminescence present under conditions of insufficient or excess NO flow.[1-3] Other means of determining this equivalence point have included esr,[4-6] vacuum uv absorption,[7] and mass-spectrometric measurements of neutral[8] and ionic[9] concentrations. The validity of the equivalence point determined by electronic luminescence has been confirmed by these several techniques, from the total pressure decrease accompanying reaction 1,[10] and from mass-spectrometric product analysis.[11] This work has been recently reviewed.[14a,15]

Because of its sensitivity and convenience, measurement of electronic luminescence remains favored as an equivalence point indicator for reaction 1. The details of the several mechanisms responsible for these luminescence systems are complex, incorporating highly specific populating and depopulating processes. Nevertheless, it is possible to describe the intensities of these emission systems, at constant pressures in the range of 100 to 1000 Pa and at low atom concentrations, as proportional to the concentrations of the reactant species[3,14b,16-23]

$$N(^4S) + N(^4S) \longrightarrow N_2^* \longrightarrow h\nu(\text{yellow}) \qquad I_y \propto [N]^2 \quad (2)$$

$$N(^4S) + O(^3P) \longrightarrow NO^* \longrightarrow h\nu(\text{uv, blue}) \qquad I_{uv} \propto [N][O] \quad (3)$$

$$O(^3P) + NO \longrightarrow NO_2^* \longrightarrow h\nu(\text{green}) \qquad I_g \propto [O][NO] \quad (4)$$

Reactions 3 and 4 are utilized as indicators for the equivalence point of (1), since the intensities I_{uv} and I_g exhibit a first-order dependence on the degree of under- or overtitration, respectively, the concentration of atomic oxygen remaining effectively constant near the equivalence point. The intensity I_y, which decreases quadratically as the equivalence point is approached, is not a sensitive indicator, since the ratio of this intensity to the amount of undertitration becomes vanishingly small near the equivalence point.

We consider here measurement of gas-phase electrical conduction as an additional, independent indicator of the equivalence point of (1). The presence of ionized species is well known in the nitrogen afterglow.[9,14c,24-29] Ionization is substantially increased by partial titration with NO, indicating the occurrence of chemiionization reactions in this system.[29-31] The primary ionic reaction products are reported to be NO^+ and free electrons, and the rate of ionization to be proportional to $[N]^3[O]$. This concentration dependence has been interpreted in terms of a mechanism involving the participation of excited states of N_2 and NO formed by atom recombination,[30] but this mechanism has recently been questioned.[32] If the reported third-order dependence of the ionization rate upon [N] in fact obtains, then ion formation would not serve as a useful equivalence point indicator for (1). We find, however, that the ion formation rate exhibits a first-order dependence on [N] near the equivalence point, and is thus potentially suitable as a titration indicator. We describe an apparatus for measurement of electrical conduction for this purpose and present measurements demonstrating the applicability and sensitivity of this technique.

Experimental Section

The essential features of the discharge flow system are shown in Figure 1. The electrode assembly was fabricated from 10-mm i.d. Pyrex tube using W-Ni feedthroughs. Two identical pairs of electrodes (6 × 27 × 0.25 mm) were fabricated from stainless steel and spot welded to the Ni leads. The electrodes were seated loosely against the walls of the tube; the resulting spacing between the electrodes was about 8 mm. The distance between the electrode pairs E_1 and E_2 was 5 cm. The electrode assembly was surrounded by a grounded chassis box. Polarizing voltages (up to 250 V) were provided by dry cells to exclude extraneous leakage paths between E_1 and E_2 or to ground. For routine measurements 25 V has been found to be satisfactory. Ion currents were measured with a Keithley Model 417 picoammeter, having a sensitivity of 1×10^{-14} A.

Near-uv and visible radiation was monitored by 1P21 photomultiplier tubes with Corning 7-39 and 3-66 filters, respectively. The principal luminescence detected near the equivalence point of (1) was from the $v' = 0$ levels of the β system of NO[3,19-21] in the near-uv, and from the air afterglow in the visible.[3] The limiting aperture to each photomultiplier was 6 mm located 8 cm from the flow tube.

N_2 (Linde High Purity) was further purified by passage over Cu at 900 K, then through a glass-wool packed trap at 77 K, and then through P_2O_5.[19] NO (Matheson) was passed through silica gel at 195 K and P_2O_5 before being condensed at 77 K. The microwave discharge (2450 MHz, 100 W, ¼-wave cavity[33]) and the titration were carried out at pressures of 60 to 1300 Pa. For a typical N_2 flow rate (700 μmol/sec) and pressure (800 Pa) the atom concentration was generally 0.1%, or less depending on the amount of by-pass flow. Occasional experiments were performed with a trace of dry air added before the microwave discharge; the addition of air somewhat enhanced dissociation (up to twofold) but otherwise yielded results essentially similar to those without added air.

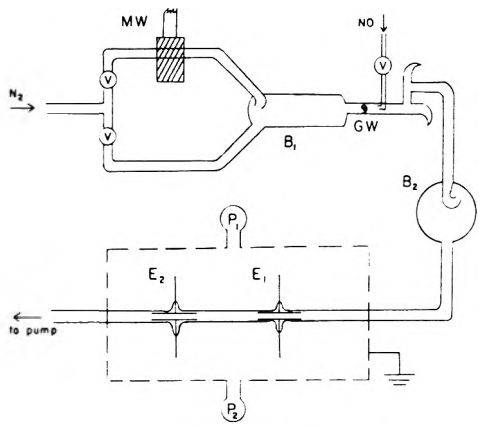

Figure 1. Block diagram of flow system and electrode assembly: MW, microwave cavity; B_1, B_2, ballast volumes (2 dm^3, 1 dm^3, respectively); GW, glass wool plug; P_1, P_2, photomultipliers; E_1, E_2, electrode pairs; V, flow regulating valves.

Gas flows were determined from the pressure drop across a calibrated capillary,[34] or directly from the pressure decrease of a reservoir of known volume.

All experiments were conducted at room temperature, 290–300 K. An air blower was directed on the flow tube just downstream from the microwave discharge to promote cooling of the heated gas. A glass wool plug removed excited species prior to the NO titration inlet.

Results and Interpretation

(*a*) *Mechanism of Saturation.* In agreement with previous investigators[30,31] we find that electrical conduction in this system depends strongly upon the degree of titration. The conduction first increases as NO is added to the nitrogen afterglow and then decreases sharply as the equivalence point is approached. At low applied voltages ($\lesssim 0.5$ V) the current depends linearly upon the applied voltage, but saturation is observed typically at 3–6 V, Figure 2, and the current increases only slightly (or occasionally is found to decrease somewhat) with increasing voltage as high as 250 V. Such saturation might be due either to the formation of a plasma sheath,[35,36] at high ion concentration, or alternately to total extraction of ionic species,[37] at low ion concentration. Hence it is important to determine the process responsible for the saturation observed in the present experiments. Examination of the current at the downstream electrode pair E_2, in the presence of voltage applied at the upstream electrodes E_1, should permit this determination. If extraction occurred at E_1, then the measured current at E_2 would be substantially reduced, unless the ionic concentration was rapidly restored by reactions of neutral species. However, the conduction of a shielded plasma would be minimally affected by prior application of an electric field.

In Figure 3 are shown the results of such an extraction study as a function of NO flow, for fixed N-atom flow, near the equivalence point of reaction 1. (This study was conducted without the ballast B_2.) Upon application of polarization voltage to E_1, i_2, the saturation current at E_2, is substantially reduced. This reduction is a function of the NO flow relative to a fixed N-atom flow, but exceeds two orders of magnitude beyond the equivalence point, establishing that mobility limited extraction[37] takes place

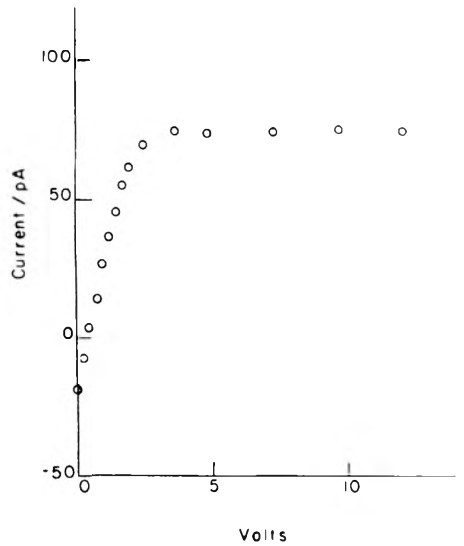

Figure 2. Current–voltage plot in the flowing afterglow near the equivalence point of reaction 1. The current was measured at E_2, E_1 not polarized. Ballast B_2 was omitted; the contact time from the NO inlet to E_2 was *ca.* 10 msec, $[N_2]$ = 800 Pa, F_{N_2} = 800 μmol/sec, atom concentration = 0.1%. The asymmetry is ascribed to stray fields, perhaps due to a voltage exerted by the picoammeter.

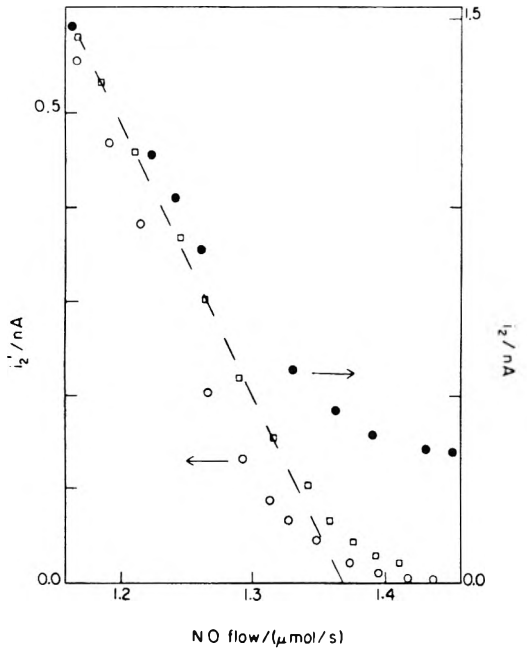

Figure 3. Ion and uv photomultiplier currents *vs.* NO flow: ●, i_2, saturation current at E_2, E_1 not polarized; ○, i_2', saturation current at E_2, E_1 polarized (25 V); □, uv photomultiplier current, arbitrary units; ballast B_2 was omitted, $[N_2]$ = 800 Pa, F_{N_2} = 600 μmol/sec.

when E_1 is polarized, and is responsible for the observed saturation. The magnitude of the observed saturation voltage is consistent with that requisite for NO^+ or another ion of similar mobility to drift the interelectrode distance within the time spent between the electrodes, as determined by the linear flow velocity. Before the equivalence point the apparent extraction of ionic species by E_1 is less efficient. The apparent transmittance of ionic species increases with increasing undertitration, so that well before the equivalence point there is but a slight decrease in i_2 upon application of polarizing voltage to E_1. Such an apparent lack of extraction has been noted previously[26] for active nitrogen. Since it is established that extraction of ionic species at E_1 is highly efficient, the present experiment demonstrates that the current i_2', measured at E_2 with E_1 polarized, is due to ionization resulting from reactions of neutral species present in the flowing gas between E_1 and E_2. It is also established that atomic oxygen in the absence of atomic nitrogen does not produce significant ionization under these conditions. It is further established that the current measured without polarization of E_1 may be due in large part to residual ionic species in the flowing gas.

The decrease in current at E_2 was found to be independent of the direction of the polarizing voltage applied to E_1, ruling out the possibility that the apparent extraction was due to an interaction between the two pairs of electrodes. Occasionally, especially well before the equivalence point, there was a time lag of the order of several seconds before the extraction reached a steady level. In a study of mass-spectrometric sampling of ions in active nitrogen Spokes and Evans[27] noted a similar time lag, which they attributed to surface charging effects. Despite the time lag noted here, the response of the current at E_2 to changes in the NO flow near the equivalence point was always quite rapid (better than 0.1 sec).

(*b*) *Debye Lengths.* The possibility that the decrease in apparent extraction at undertitration is due to plasma shielding at the somewhat higher ion densities here, rather than to the presence of ionic species formed subsequent to extraction, may be further examined by evaluating the Debye length. In order for a plasma to shield itself against an applied electric field it must develop at each electrode a space-charge sheath, the thickness of which must be several Debye lengths.[36b] If the dimensions of the plasma do not greatly exceed the Debye length, then a sheath cannot develop and extraction will occur upon application of an electric field.

Evaluation of the Debye length, $h = (\epsilon_0 kT_e/ne^2)^{1/2}$, requires knowledge of the electron temperature T_e, and the number density of charged species, n. These quantities may be obtained in two ways. First, if it is assumed that saturation is due to formation of a plasma sheath, then the double-probe analysis[35] may be applied. For the data of Figure 2, T_e = 4500 K and $n = 3 \times 10^4$ cm^{-3}, and h = 3 cm (*cf.* the electrode spacing 0.8 cm). Hence the data of Figure 2 are inconsistent with the existence of a plasma, and it is inappropriate to apply plasma theory to interpret Figure 2.

Alternately, assuming extraction, it is possible to identify the measured current with the rate of arrival of ion pairs in the flowing afterglow to the measuring electrodes. Thus $n = i/ef$, where e is the electronic charge and f is the volume flow rate. For the conditions of Figure 2, $n = 1.5 \times 10^5$ cm^{-3}. The electron temperature is estimated as 7000 K from the appropriate Townsend factor[38a] ($E/p \approx$ 1 V m^{-1} Pa^{-1} at saturation); the resulting Debye length, 1.5 cm, is consistent with the assumption of extraction.

For currents of 10^{-13} to 10^{-9} A, the number densities calculated in this way ranged from 10^3 to 10^7 cm^{-3}, and the corresponding Debye lengths from 20 to 0.2 cm. Thus the apparent lack of extraction, measured at undertitration, is due, as assumed above, to chemical reactions of neutral species, and not to plasma shielding.

(*c*) *Effect of Contact Time.* Before proceeding we point out the necessity, in gas-phase titrations, of allowing sufficient contact time between the admixed gases for reaction to proceed to completion prior to measurement of a physical property indicative of the equivalence point. In the experiment shown in Figure 3 insufficient contact time (~10 msec) was provided, resulting in a trailing-off of both the ion current i_2', and the uv photomultiplier cur-

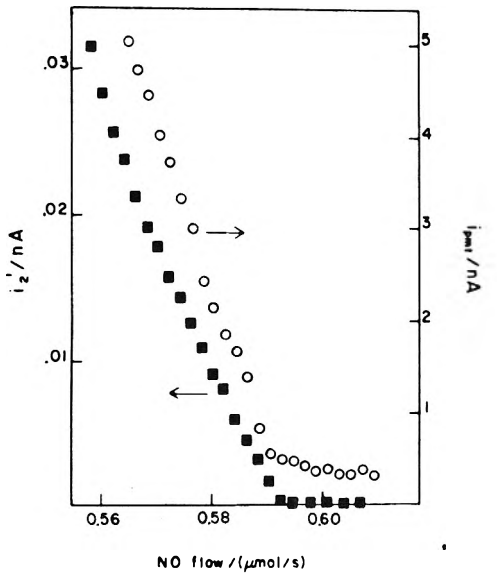

Figure 4. Ion and uv photomultiplier currents near the equivalence point of reaction 1. E_1 was polarized; with ballast B_2 the contact time was 0.5 sec: ■, i_2', ion saturation current; O, uv photomultiplier current; $[N_2]$ = 1000 Pa; F_{N_2} = 800 μmol/sec.

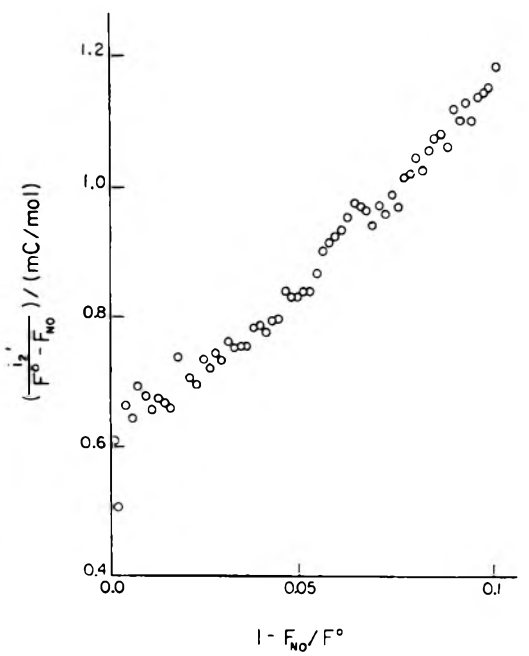

Figure 5. Ion current per N-atom flow *vs.* degree of undertitration. The equivalence point was determined from I_{uv}. $[N_2]$ and F_{N_2} are the same as in Figure 4.

rent, I_{uv} (reaction 3), beyond an apparent equivalence point obtained by linear extrapolation of I_{uv} measured before the equivalence point. With an initial atom concentration of 4×10^{14} cm^{-3}, the half-life of reaction 1 is initially 0.1 msec.[39] However, for equivalent flows of the two reagents the rate of reaction decreases as the reaction proceeds in proportion to the remaining concentration of reagents. Thus, for example, 10 msec is required for 99% completion, even if perfect mixing of the reagents is assumed; the trailing-off in Figure 3 may thus reasonably be attributed to the finite rate of reaction 1. For this reason we have inserted the ballast B_2 (Figure 1) between the NO inlet and the point of monitoring the reaction. This bulb provides an average contact time of 500 msec under typical conditions.

(d) Dependence of Saturation Current on NO Flow. A series of studies was conducted to determine the dependence of the saturation current i_2' (measured with the ballast B_2, and subsequent to extraction at E_1) upon the NO flow rate for fixed N atom flow rates. In these studies the NO flow was established somewhat in excess of the N atom flow and allowed to decrease as the reservoir pressure decreased.[3b] The measured NO flows were fit as a function of time to allow the ion and uv photomultiplier currents to be determined as a function of the NO flow rate, F_{NO} (Figure 4). Both currents exhibit a sharp onset that occurs at the same NO flow within an uncertainty of better than 0.1%. This agreement was observed in all instances except at the lowest pressures (<100 Pa) where the uv emission intensity was so low that the equivalence point could not be determined from the photomultiplier current. The equivalence point so determined was in close agreement as well with that derived from the disappearance, with decreasing NO flow, of the visible luminescence due to reaction 4.

While the saturation current i_2' near the equivalence point was found to rise sharply with decreasing NO flow, indicative of a first-order dependence on the degree of undertitration, these data exhibited substantial upward curvature that indicated the presence of a higher order contribution as well. Since the present study is not directed toward mechanisms of ion formation we defer consideration of the order dependence of this curvature. Nevertheless it is important to establish that the principal contribution to the saturation current at low [N] is first order in the degree of undertitration. Figure 5 is a plot of $\Gamma \equiv i_2'/(F^0 - F_{NO})$, where F^0 is the NO flow equal to N atom flow, as determined from the onset of the uv photomultiplier current, *vs.* the degree of undertitration. The nonzero intercept Γ^0 represents the contribution to the saturation current that is first order in $(F^0 - F_{NO})$. This first-order contribution exceeds the higher order contribution throughout the last 10% of the titration.

In Figure 6 the saturation current and the uv photomultiplier current, principally due to NO β emission,[3,19-21] are compared. Here it is established that near the equivalence point these two quantities increase proportionately over two orders of magnitude; this proportionality is valid within 1% of the equivalence point. There is substantial evidence[2,3,19-21] that the uv intensity increases linearly with $(F^0 - F_{NO})$ near the equivalence point of (1), and thus linearly with [N]. Therefore a linear variation with [N] is ascribed to the saturation current, and in turn to the rate of formation of ionic species.

Saturation Current as an Equivalence Point Indicator

We find that the onset of saturation current provides a sensitive indication of the onset of undertitration when NO is used to titrate atomic nitrogen by reaction 1. Further, this technique permits sensitive real-time control of the NO flow rate when reaction 1 is used to generate atomic oxygen. This sensitivity is due both to the sharp onset of current with insufficient NO flow and to the constant, low value of the background current, *i.e.*, the current measured at overtitration. This background current is due to leakage and with reasonable precaution may be kept as low as 5×10^{-14} A for an applied voltage of 25 V. This magnitude of current corresponds to a saturation current i_2' typical of 0.01% undertitration.

An area of potential concern with the present technique is that substantial atom recombination might be catalyzed by the stainless steel electrodes. Such catalysis is characteristic of metals and metal oxides for both atomic oxygen and nitrogen.[14d,40-42] We have not systematically

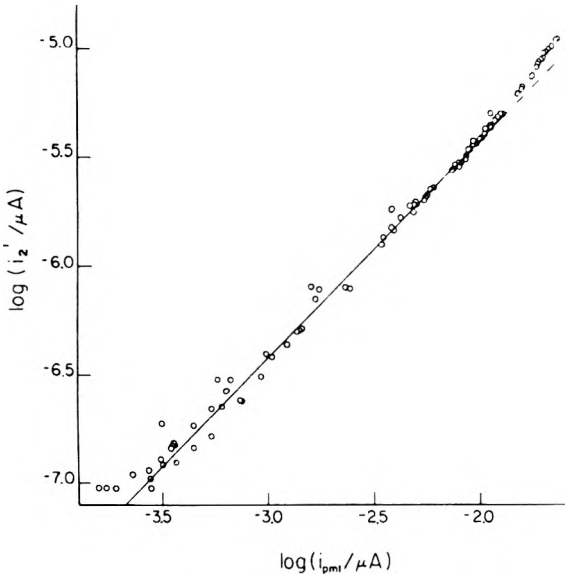

Figure 6. Comparison of ion and uv photomultiplier currents near equivalence point of (1). The solid line (slope = 1) fits data within 1% of equivalence point: $[N_2]$ = 1300 Pa; F_{N_2} = 1200 μmol/sec; F^0 = 0.6 μmol/sec.

explored this possibility here; however no substantial decrease is noted in the concentrations of either atomic species, as estimated from visual observations of luminescence intensities before and after the electrode assembly.

The technique we have described has been found to be applicable throughout the entire range of pressure (60–1300 Pa), N_2 flow rate (5–1400 μmol/sec), and N-atom flow rate (0.13–1.3 μmol/sec) that has been investigated.

Discussion

(*a*) *Origin of Conduction.* It is established by demonstration of extraction of ionic species upon application of an electric field to the flowing N–O afterglow that electrical conduction in this system is substantially due to the motion of these species in the applied field. Further, any conduction subsequent to extraction, such as is measured at E_2 and which forms that basis for the present technique must be attributed to ionization brought about by reactions of neutral species present in the afterglow.

In this respect the present technique is to be distinguished from that noted by Ferguson, *et al.*[9] These investigators pointed out that ionic species present in flowing afterglows, specifically O_2^+ and N_2^+, rapidly undergo charge exchange with NO, as soon as this species becomes present in appreciable concentration, *i.e.*, beyond the equivalence point of reaction 1.

$$O_2^+ + NO \longrightarrow NO^+ + O_2 \quad (5)$$

$$N_2^+ + NO \longrightarrow NO^+ + N_2 \quad (6)$$

Thus the rapid decrease in, for example, O_2^+ current beyond the equivalence point would serve as an equivalence point indicator. Since reactions 5 and 6 require the presence of ionic species and conserve the total ionic concentration, these processes are distinct from those taking place in the present system, in which net ionization results from reactions of neutral species.

(*b*) [*N*] *Dependence of the Ionization Rate.* Because of the simultaneous extinction of ionization and the NO β emission as a function of the flow of the NO titrant, we attribute the ionization in this system to a reaction of ground-state atomic nitrogen, or to a species whose concentration is related to [N(^{4}S)] by a rapid steady state. The apparent first-order dependence of the ionization rate upon [N] may be expressed as

$$R_I = k_I[N] \quad (I)$$

where k_I is a pseudo-first-order rate constant, that may depend on concentrations other than [N]. If the current measured at E_2 is attributed to ions formed within the time, τ, of flow between E_1 and E_2, then k_I may be estimated from Figure 5, as $\Gamma^0/F\tau$, where **F** is the Faraday constant. For the conditions specified $k_I = 3 \times 10^{-6}$ sec^{-1}. The existence of a contribution to the ionization rate that is first order in [N] requires a mechanism distinct from that proposed previously[30] to account for the concentration dependence of ionization in N–O systems

$$R_{II} = k_{II}[N]^3[O] \quad (II)$$

A contribution to the ionization greater than first order in [N], such as (II), is observed here as well, and represents approximately half of the total ionization at 10% undertitration. We conclude that at least two mechanisms for ion formation operate in the N–O system. The contribution first order in [N] has not been reported previously; however, the data of Young and St. John (Figure 1 of ref 30c) appear to indicate a rise in ionization with undertitration that is significantly sharper than indicated by (II) alone.

A quantitative comparison of the ion formation rate measured here with that reported by Young and St. John[30c] may perhaps be useful, since the rate coefficient reported by these authors has been questioned as unreasonably large.[29] For 10% undertitration the data in Figure 5 yield a total ion formation rate of 7×10^7 cm^{-3} sec^{-1}; the contribution that might be ascribed to R_{II} is no more than half this value. This is an order of magnitude less than that computed for this system using the rate coefficient $k_{II} = 7 \times 10^{-46}$ cm^{-9} sec^{-1} (ref 30c). The reason for this discrepancy is not apparent. However Fontijn[29] has noted that impurities substantially enhance the rate of ionization in this system (while preserving the $[N]^3[O]$ dependence) and has suggested that impurities may account for the large ionization rate of ref 30c. Alternately,[29] the ionization rate may be influenced by surface effects; this possibility is considered in the following section.

(*c*) *Surface Effects.* Ion formation in active nitrogen and in N–O mixtures has generally been considered to be a homogeneous process. Rayleigh[24c] established that measured currents in active nitrogen were substantially independent of the material that comprised the measuring electrodes. Gatz, *et al.*,[30b] in measurements of ion currents in N–O mixtures reported similar measurements for electrodes of carbon, aluminum, or gold. Young and St. John,[30c] however, reported that unspecified atom-surface reactions at the electrodes had perturbed the measurements of Gatz, *et al.*,[30a,b] these authors indicated that they were able to overcome these effects by coating their electrodes with a thin layer of metaphosphoric acid.

The effect of electrode composition and surface condition on measurements of gas-phase conduction does not appear to have been investigated at all systematically.[43] Reduction of positive ions to neutral species at the cathode is thought[38b] to take place by an auger process, and except for ions of low potential energy, such as the alkalis, to take place with high efficiency. Nevertheless it might be expected that different materials would exhibit differing behavior with respect to the rate of reduction of positive ions. This in turn might be exhibited in the amount and rate of surface charging, as has been proposed by Spokes and Evans.[27] We have not explored this possibility here. Nonetheless the present demonstration of extraction by polarized electrodes suggests that at least after a transient period the cathode becomes effective in bringing

about reduction at a rate equal to the rate at which ions in the flowing afterglow arrive at the electrode assembly.

In addition to any influence of the electrode composition or surface condition upon measurement of ionic concentrations, a potential role of electrodes in formation of ions should perhaps be considered. Thus, for example, while the reaction

$$N(^4S) + O(^4P) \longrightarrow NO^+ + e^- \qquad \Delta H^\circ = 265 \text{ kJ/mol} \quad (7)$$

may be excluded in the gas phase on energetic grounds, the possibility arises that chemiionization might be feasible at an electrode surface where it would be aided by the work function of the metal. This process would be analogous to, but distinct from, surface ionization, in that chemical energy would be used to supply the difference in energy between the electrode work function and the ionization potential of the gas-phase ion formed.[44] This process would be strongly influenced by electrode temperature and surface condition. While we have not explored this at all systematically, we note that we have used aluminum electrodes in place of E_2 (in a somewhat different configuration than that shown in Figure 1) and have successfully monitored the equivalence point of (1) by conduction measurements with these electrodes as well. No quantitative comparison of different electrode surfaces has yet been undertaken.

(*d*) *Gas-Phase Mechanisms.* We consider here possible mechanisms for formation of ionic species in the gas phase that would support the first-order [N] dependence that is obtained near the equivalence point of reaction 1. As noted above any potential gas-phase mechanism at low temperatures suffers from severe energetic requirements. One energetically feasible reaction of ground-state species is the NO-catalyzed recombination of atomic nitrogen[25,26,45]

$$N(^4S) + N(^4S) + NO \longrightarrow N_2 + NO^+ + e^- \qquad \Delta H^\circ = -50 \text{ kJ/mol} \quad (8)$$

In the presence of excess N (undertitration) NO is present in a low, steady-state concentration that is governed by the reaction

$$N + O + M \longrightarrow NO + M \quad (9)$$

followed by (1). The rate of ion formation according to this mechanism is

$$R_{III} = \frac{k_8 k_9}{k_1}[N]^2[O][M] \quad (III)$$

Because (III) does not support the observed first-order [N] dependence, it appears that (8) is not the source of the ionization near the equivalence point.

Other possible reactions to form NO^+ would require the participation of at least four ground-state species, or of excited atomic[25] or molecular[25,30] species. Such excited species might be present in the flowing gas, having been formed in the discharge, or at large [N] prior to the NO inlet, or alternately, might be continuously generated in the afterglow subsequent to the titration. The former possibility appears unlikely since the rate of ion formation per [N] is not substantially decreased by insertion of the ballasts B_1 and B_2, which have delay times of 1 and 0.5 sec, respectively. Therefore an acceptable mechanism for chemiionization in this system *via* an excited species must include processes for generation of this species as well.

Gatz, Young, and coworkers,[30] and Fontijn and Vree[31] have interpreted the $[N]^3[O]$ dependence of ion formation in terms of electronically excited states of NO and N_2. Such a mechanism gives rise to a high order in [N] unless these species are quenched preferentially by N, and not by O. Since this mechanism does not support a first-order dependence of chemiionization upon [N], it is ruled out as the source of the electrical conduction that forms the basis of the present technique.

The metastable excited nitrogen atom $N(^2P)$ (345 kJ/mol) is known to be present in small concentration in active nitrogen from emission of the forbidden line at 347 nm,[14e,46,47] from atomic absorption,[7,48] and from its contribution to the N^+ current in electron beam ionization studies.[49] This species has been proposed[32] as a possible precursor of chemiionization in the N–O system through the reaction

$$N(^2P) + O(^4P) \longrightarrow NO^+ + e^- \qquad \Delta H^\circ = -80 \text{ kJ/mol} \quad (10a)$$

Meyer, *et al.*,[50] and Golde and Thrush[32] have reported that $N(^2P)$ is produced continuously by

$$N(^4S) + N_2(A^3\Sigma_u^+) \longrightarrow N(^2P) + N_2(X^1\Sigma_g^+) \quad (11a)$$

It is removed principally by the quenching reactions[32]

$$N(^2P) + N(^4S) \longrightarrow \text{products} \quad (12)$$

and

$$N(^2P) + O(^3P) \longrightarrow \text{products} \quad (10)$$

$N_2(A^3\Sigma_u^+)$ is in turn present in a steady state[50,51] governed by

$$N(^4S) + N(^4S) + N_2 \longrightarrow N_2(A^3\Sigma_u^+) + N_2 \quad (13)$$

$$N(^4S) + N_2(A^3\Sigma_u^+) \longrightarrow \text{products} \quad (11)$$

and

$$O(^3P) + N_2(A^3\Sigma_u^+) \longrightarrow \text{products} \quad (14)$$

This mechanism predicts an ionization rate

$$R_{IV} = \frac{k_{10a}k_{11a}k_{13}}{k_{10}k_{14}}\frac{[N]^3[N_2]}{[O]}\left(1 + \frac{k_{12}[N]}{k_{10}[O]}\right)^{-1}\left(1 + \frac{k_{11}[N]}{k_{14}[O]}\right)^{-1} \quad (IV)$$

The estimated values of k_{12} and k_{10} (ref 32) and of k_{11} and k_{14} (ref 50a) allow the last two factors in (IV) to be set equal to unity for $[O] > 10[N]$. A first-order dependence on [N] is not obtained, and this mechanism may be rejected as the source of the ionization near the equivalence point.

Electronically excited $O(^1S)$ (404 kJ/mol) is known to be present in the N–O system from emission of the auroral line at 558 nm.[50,52] This species may give rise to chemiionization *via* the exothermic bimolecular reaction[25]

$$N(^4S) + O(^1S) \longrightarrow NO^+ + e^- \qquad \Delta H^\circ = -139 \text{ kJ/mol} \quad (15)$$

In the absence of N the concentration of $O(^1S)$ may be calculated in terms of the Chapman[53] mechanism

$$3O(^3P) \longrightarrow O_2(X^3\Sigma_g^-) + O(^1S) \quad (16)$$

$$O(^3P) + O(^1S) \longrightarrow \text{products} \quad (17)$$

This mechanism predicts an ionization rate

$$R_V = \frac{k_{15}k_{16}}{k_{17}}[O]^2[N] \quad (V)$$

that exhibits the presently observed first-order dependence on [N]. By equating R_V with the measured ionization rate R_I, we obtain $k_{15} = 2 \times 10^{-13}$ cm^3/sec; here we have used the values of k_{16} and k_{17} reported by Felder and Young.[52b] This value for k_{15} would appear to be reasonable in terms of previous estimates[54,55] of two-body associative chemiionization rate constants.

Additional support for the participation of $O(^1S)$ in chemiionization in the N–O system may be found in the observations of Fontijn, *et al.*,[31,56] that both $O(^1S)$ and chemiionization are substantially enhanced by the addi-

tion of carbon compounds, *e.g.*, C_2F_4, to N–O mixtures. Also, both $O(^1S)$[52a,57,58] and ion formation[30a] are strongly quenched by N_2O.

Evidence against mechanism 15–17 is given by the reported magnitudes[52] of the rate constants of two additional reactions that are thought to form $O(^1S)$ in this system

$$N(^4S) + O(^1P) + O(^3P) \longrightarrow NO + O(^1S) \quad (18)$$

and

$$N(^4S) + N(^4S) + O(^3P) \longrightarrow N_2 + O(^1S) \quad (19)$$

The occurrence of these reactions with the rate constants of ref 52b, under the assumption[52b] that (17) continues as the predominant quenching process for $O(^1S)$, would require that the combined rates of (18) and (19) become equal to the rate of (16) at less than 2% undertitration. The rate of ionization per [N] determined here increases no more than 20% in the same range, and does not double until 10% undertitration. However, examination of Figure 2 of ref 52a, upon which the relative values of k_{16}, k_{18}, and k_{19} are based, reveals that $[O(^1S)]$ increases more slowly as a function of undertitration than required by the values of the rate constants given in ref 52b, and in fact only doubles at 10% undertitration. These measurements were made under conditions very similar to those of the present experiment. Therefore it appears that reaction 15 need not be rejected as the source of the chemiionization observed in the present experiment near the equivalence point of (1). Indeed, the several means of populating $O(^1S)$ and the correlations between $[O(^1S)]$ and chemiionization noted above suggest that (15) may contribute to the chemiionization over a wider range of relative N–O concentrations than has been studied here. This possibility should be explored through a systematic examination of the concentration dependence, quenching, and enhancement of the $O(^1S)$ concentration and the chemiionization rate in the N–O system.

Acknowledgments. Acknowledgment is made to the Donors of the Petroleum Research Fund, administered by the American Chemical Society, and to the Research Foundation of SUNY for support of this research. We thank Rudy Schlott for fabrication of the electrode assembly and Ron Epstein for assistance with the measurements.

References and Notes

(1) M. L. Spealman and W. H. Rodebush, *J. Amer. Chem. Soc.*, **57**, 1474 (1935).
(2) F. Kaufman and J. R. Kelso, *J. Chem. Phys.*, **27**, 1209 (1957).
(3) R. A. Young and R. L. Sharpless, *Discuss. Faraday Soc.*, **33**, 228 (1962); *J. Chem. Phys.*, **39**, 1071 (1963).
(4) J. Kaplan, W. J. Schade, C. A. Barth, and A. F. Hildebrandt, *Can. J. Chem.*, **38**, 1688 (1960).
(5) A. A. Westenberg and N. DeHaas, *J. Chem. Phys.*, **40**, 3087 (1964).
(6) H. Von Weyssenhoff and M. Patapoff, *J. Phys. Chem.*, **69**, 1756 (1965).
(7) F. A. Morse and F. Kaufman, *J. Chem. Phys.*, **42**, 1785 (1965).
(8) G. B. Kistiakowski and G. G. Volpi, *J. Chem. Phys.*, **27**, 1141 (1957); J. T. Herron, *ibid.*, **35**, 1138 (1961).
(9) P. D. Goldan, A. L. Schmeltekopf, F. C. Fehsenfeld, H. I. Schiff, and E. E. Ferguson, *J. Chem. Phys.*, **44**, 4095 (1966); E. E. Ferguson, A. L. Schmeltekopf, and F. C. Fehsenfeld, unpublished, cited in E. W. McDaniel, V. Cermák, A. Dalgarno, E. E. Gerguson, and L. Friedman, "Ion-Molecule Reactions," Wiley-Interscience, New York, N. Y., 1970, p 46.
(10) L. Elias, *J. Chem. Phys.*, **44**, 3810 (1966).
(11) R. A. Back and J. Y. P. Mui, *J. Phys. Chem.*, **66**, 1362 (1962).
(12) P. Harteck, R. R. Reeves, and G. Manella, *J. Chem. Phys.*, **29**, 608 (1958).
(13) J. E. Morgan, L. Elias, and H. I. Schiff, *J. Chem. Phys.*, **33**, 930 (1960).
(14) A. N. Wright and C. A. Winkler, "Active Nitrogen," Academic Press, New York, N. Y., 1968; (a) p 75, (b) p 22, (c) p 120, (d) p 177, (e) p 84.
(15) R. Brown and C. A. Winkler, *Angew. Chem., Int. Ed. Engl.*, **9**, 181 (1970); B. Brocklehurst and K. R. Jennings, *Progr. React. Kinet.*, **4**, 1 (1967); O. K. Fomin, *Russ. Chem. Rev.*, **36**, 725 (1967).
(16) R. A. Young, *Can. J. Chem.*, **47**, 1927 (1969).
(17) W. Brennan and R. L. Brown, *J. Chem. Phys.*, **52**, 4910 (1970).
(18) K. H. Becker, E. H. Fink, W. Groth, W. Jud and D. Kley, *Discuss. Faraday Soc.*, **53**, 35 (1972).
(19) R. W. F. Gross and N. Cohen, *J. Chem. Phys.*, **48**, 2582 (1968).
(20) I. M. Campbell and B. A. Thrush, *Proc. Roy. Soc., Ser. A*, **296**, 201, 222 (1967).
(21) I. M. Campbell, S. B. Neal, M. F. Golde, and B. A. Thrush, *Chem. Phys. Lett.*, **8**, 612 (1971); I. M. Campbell and S. B. Neal, *Discuss. Faraday Soc.*, **53**, 72 (1972).
(22) K. H. Becker, W. Groth, and D. Thran, *Symp. (Int.) Combust., [Proc.], 14th, 1972*, 353 (1973).
(23) F. Kaufman, *Proc. Roy. Soc., Ser. A*, **247**, 123 (1958); M. A. A. Clyne and B. A. Thrush, *ibid.*, **269**, 404 (1962).
(24) (a) R. J. Strutt, *Proc. Roy. Soc., Ser. A*, **86**, 56 (1911); (b) *ibid.*, **87**, 179 (1912); (c) *ibid.*, **180**, 140 (1942).
(25) W. B. Kunkel and A. L. Gardner, *J. Chem. Phys.*, **37**, 1785 (1962).
(26) H. P. Broida and I. Tanaka, *J. Chem. Phys.*, **36**, 236 (1962).
(27) G. N. Spokes and B. E. Evans, *Symp. (Int.) Combust., [Proc.], 10th, 1964*, 639 (1965).
(28) D. K. Böhme and J. M. Goodings, *Rev. Sci. Instrum.*, **37**, 362 (1966); *J. Appl. Phys.*, **37**, 4261 (1966); W. H. Kasner, W. A. Rogers, and M. A. Biondi, *Phys. Rev. Lett.*, **7**, 321 (1961).
(29) A. Fontijn, *Progr. React. Kinet.*, **6**, 75 (1971).
(30) (a) C. R. Gatz, R. A. Young, and R. L. Sharpless, *J. Chem. Phys.*, **39**, 1234 (1963); (b) C. R. Gatz, F. T. Smith, and H. Wise, *ibid.*, **40**, 3743 (1964); (c) R. A. Young and G. St. John, *ibid.*, **45**, 4156 (1966).
(31) A. Fontijn and P. H. Vree, *J. Phys. Chem.*, **70**, 2071 (1966); *Symp. (Int.) Combust., [Proc.], 11th, 1966*, 343 (1967).
(32) M. F. Golde and B. A. Thrush, *Discuss. Faraday Soc.*, **53**, 233 (1972).
(33) F. C. Fehsenfeld, K. M. Evenson, and H. P. Broida, *Rev. Sci. Instrum.*, **36**, 294 (1965).
(34) H. Melville and B. G. Gowenlock, "Experimental Methods in Gas Reactions," Macmillan, London, 1964, p 109.
(35) E. O. Johnson and L. Malter, *Phys. Rev.*, **80**, 58 (1950).
(36) J. C. Ingraham in "Handbook of Physics," 2nd ed, E. U. Condon and H. Odishaw, Ed., McGraw-Hill, New York, N. Y., 1967, p 4-188; J. M. Somerville in "An Introduction to Discharge and Plasma Physics," S. C. Haydon, Ed., University of New England, Armidale, N.S.W., 1964, p 190.
(37) J. Lawton and F. J. Weinberg, *Proc. Roy. Soc., Ser. A*, **277**, 468 (1968); "Electrical Aspects of Combustion," Clarendon Press, Oxford, 1969, p 315 *ff*.
(38) E. W. McDaniel, "Collision Phenomena in Ionized Gases," Wiley, New York, N. Y., 1964; (a) p 536, (b) p 655.
(39) $k_1 = 3 \times 10^{-11}$ cm^3/sec. D. L. Baulch, D. D. Drysdale, and D. G. Horne, "Evaluated Kinetic Data for High Temperature Reactions," Butterworths, London, 1973, p 171.
(40) Lord Rayleigh, *Proc. Roy. Soc., Ser. A*, **176**, 16 (1940).
(41) L. Elias, E. A. Ogryzlo, and H. I. Schiff, *Can. J. Chem.*, **37**, 1680 (1959).
(42) J. C. Greaves and J. W. Linnett, *Trans. Faraday Soc.*, **54**, 1323 (1958).
(43) H. D. Hagstrum, *Phys. Rev.*, **123**, 758 (1961).
(44) N. Ionov, *Progr. Surface Sci.*, **1**, 237 (1972).
(45) E. M. Bulewicz, *Symp. (Int.) Combust., [Proc.], 12th, 1968*, 957 (1969).
(46) D. T. Stewart, *Proc. Phys. Soc., London, Sect. B*, **69**, 956 (1956).
(47) Y. Tanaka, F. J. LeBlanc, and A. S. Jursa, *J. Chem. Phys.*, **30**, 1624 (1959).
(48) C.-L. Lin and F. Kaufman, *J. Chem. Phys.*, **55**, 3760 (1971).
(49) S. N. Foner and R. L. Hudson, *J. Chem. Phys.*, **37**, 1662 (1962).
(50) (a) J. A. Meyer, D. W. Setser, and D. H. Stedman, *J. Phys. Chem.*, **74**, 2238 (1970); (b) J. A. Meyer, D. H. Stedman, and D. W. Setser, *Astrophys. J.*, **157**, 1023 (1969).
(51) B. A. Thrush, *J. Chem. Phys.*, **47**, 3691 (1967).
(52) (a) R. A. Young and G. Black, *J. Chem. Phys.*, **44**, 3741 (1966); (b) W. Felder and R. A. Young, *ibid.*, **56**, 6028 (1972). The latter authors report the values (4.8, 256, and 1300) $\times 10^{-33}$ cm^6/sec for k_{16}, k_{18}, and k_{19}, respectively.
(53) S. Chapman, *Proc. Roy. Soc., Ser. A*, **132**, 353 (1931).
(54) J. A. Green and T. M. Sugden, *Symp. (Int.) Combust., [Proc.], 9th, 1962*, 607 (1963).
(55) W. J. Miller, *Symp. (Int.) Combust., [Proc.], 14th, 1972*, 307 (1973).
(56) A. Fontijn and R. Ellison, *J. Phys. Chem.*, **72**, 3701 (1968).
(57) G. Black, T. G. Slanger, G. A. St.John, and R. A. Young, *Can. J. Chem.*, **47**, 1872 (1969); R. A. Young, G. Black, and T. G. Slanger, *J. Chem. Phys.*, **50**, 309 (1969).
(58) S. V. Filseth, F. Stuhl, and K. H. Welge, *J. Chem. Phys.*, **52**, 239 (1970); F. Stuhl and K. H. Welge, *Can. J. Chem.*, **47**, 1870 (1969).

Conformation of N-Acetyl-L-alanine-N'-methylamide in 1,2-Dichloroethane by Circular Dichroism and Optical Rotatory Dispersion

Gordon M. Crippen and Jen Tsi Yang*

Cardiovascular Research Institute and Department of Biochemistry and Biophysics, University of California, San Francisco, California 94143 *(Received October 23, 1974)*

Publication costs assisted by the National Institutes of Health

The conformations of *N*-acetyl-L-alanine-*N'*-methylamide in 1,2-dichloroethane have been studied by infrared spectroscopy, optical rotatory dispersion, and circular dichroism as a function of temperature. The results were analyzed in terms of an equilibrium mixture of two conformations: a high-temperature non-hydrogen-bonded form and a low-temperature *intra*molecularly hydrogen-bonded form. By examining the optical activity at a number of temperatures for a number of wavelengths, the ΔH° for the conformational transition from low T form to high T form was found to be 2570 ± 5 cal/mol and ΔS° = 6.56 ± 0.01 eu. Although it was experimentally impossible to shift the equilibrium to predominantly one form or the other, it was possible to calculate the approximate ORD and CD of each pure form.

Optical rotatory dispersion (ORD) and circular dichroism (CD) are regularly used methods for observing conformational change and estimating helix content in polypeptides and proteins. Unfortunately, these methods are also sensitive to changes in the solvent and to chemical modification, whether or not these alterations give rise to significant conformational changes. Thus it has been difficult to establish the ORD and CD of different known conformations of the *same* compound under *very similar* conditions in order to unambiguously determine the dependence of the optical activity on conformation alone. For this purpose, *N*-acetyl-L-alanine-*N'*-methylamide ($H_3CCONHCH(CH_3)CONHCH_3$; hereafter referred to as AANMA) was chosen as a very simple, yet optically active, model compound simulating to some extent the behavior of an alanyl residue located in the middle of a polypeptide chain. Similar compounds have been investigated in the past by means of proton magnetic resonance spectroscopy and infrared-absorption spectroscopy[1] and by theoretical energy calculations.[2] Both the experimental and theoretical work showed that in dilute solution with a nonpolar solvent, the favored conformation(s) are those having an *intra*-molecularly hydrogen-bonded seven-membered ring formed by a hydrogen bond in, *e.g.*, AANMA between the acetyl carbonyl and the methyl acetamide NH. In this paper we will first establish that in the case of AANMA in 1,2-dichloroethane (DCE) solution, a significant fraction of the molecules are in such an intra-molecularly hydrogen-bonded cyclic conformation, as was found by Bystrov, *et al.*,[1] for similar compounds in carbon tetrachloride and chloroform. We will then show by examining the infrared (ir) spectrum that the temperature dependence of the ir, ORD, and CD of this solution is due to shifting the equilibrium between the H-bonded form(s) and the non-H-bonded conformations, which are taken together to constitite a non-H-bonded "form." From the temperature dependence of the ORD, ΔH° and ΔS° for the conformational transition are determined by fitting a two-state equilibrium model to the experimental data. Furthermore, even though experimental conditions do not permit the equilibrium to be almost completely shifted to one or the other form, the ORD and CD spectra of each pure form can be calculated.

Experimental Section

Materials. Two preparations of AANMA were used: one synthesized in this laboratory and the other purchased as a custom synthesis order from Miles-Yeda Ltd. Since to our knowledge no method of synthesis of this compound has been published, we feel we should describe in some detail our route which is based on the synthesis of *N*-acetyl-L-valine-*N'*-methylamide by Mizushima, *et al.*[3] L-Alanine (Eastman) was converted to acetyl-L-alanine by dropwise addition of acetic anhydride to a constantly stirred solution of L-alanine in 2 *N* aqueous sodium hydroxide, which was kept below 5° at all times. With the temperature maintained between 0 and 5°, the reaction mixture was then acidified with HCl to a strong Congo Blue pH. The acidified solution was evaporated to dryness under vacuum at temperatures between 20 and 30°, and the resulting residue was twice extracted with ethanol by stirring and refluxing for 0.5 hr. Crude acetyl-L-alanine was crystallized from the ethanol solution by addition of a large excess of dry ether and refrigerating overnight. Acetyl-L-alanine is apparently hygroscopic. This was then converted to acetyl-L-alanine methyl ester by adding an ethereal solution of diazomethane dropwise with constant stirring to a *p*-dioxane solution of acetyl-L-alanine. The reaction was apparently complete at the end of the 2-hr addition period. After evaporation of the solvent the remaining yellow viscous oil was extracted with ether to yield the crude methyl ester as both crystals and an oil. All the methyl ester was dissolved in a minimum of methanol and was added to a methanol solution of methylamine. The reaction of the methyl ester to form the *N*-methylamide seemed to be complete after standing for 5 days at room temperature. The methanol was removed and an ethanol-insoluble fraction of the resulting oil was discarded. The oil was further purified by repeated trituration with ethyl acetate and finally dissolved in a 40% ethanol-60% ethylacetate mixture from which the AANMA precipitated suddenly during evaporation under vacuum at room temperature. Recrystallization in ethanol–ethylacetate mixtures gave small white crystals of AANMA, mp 176° (very sharp). The elemental analysis of these crystals for C, H, and N gave percentages that agreed with the calculated values to ±0.2%.

By way of comparison, the AANMA synthesized by Miles-Yeda had a melting range of 186–187°, and the elemental analysis agreed with calculated percentages to ±0.1%. Perhaps a different solvent was used for the final recrystallization of the Miles-Yeda AANMA, which might account for the difference in melting points. The Miles-Yeda batch $[\alpha]^{16}D = -57.0$ for 2% solution, while ours had $[\alpha]^{25}D = -51.2$ in water solution, which we take as evidence that the synthesis did not significantly racemize the L-alanine.

Most of the spectral work (on AANMA) was done with the one Miles-Yeda synthesized lot dissolved in DCE (spectroquality, Matheson Coleman and Bell) from the same bottle.

Methods. Infrared spectra were measured with a Beckman IR-9 spectrophotometer, ORD with a Cary 60 spectropolarimeter, and CD with a Durrum-Jasco J-10 spectropolarimeter. Since DCE tends to absorb a few per cent of water upon exposure to the atmosphere, all DCE to be used was first dried by letting it stand over P_2O_5 for a few days. However, because AANMA precipitates from DCE solutions in the presence of desiccant, such as silica gel or P_2O_5, the solutions were prepared with dried, filtered DCE, and then stored in a desiccator containing P_2O_5. It will be shown in the next section how crucial traces of water can be.

Infrared difference spectra were taken using a pair of 0.5-mm path length calcium fluoride cells, which are transparent in the region of interest. Optical activity measurements were made with 1- or 0.5-mm path length quartz cells. Temperature control was effected by circulating thermostatically controlled water baths surrounding the sample cells. For the ir measurements, the cell containing the AANMA solution was held at the desired temperature, but the cell in the reference beam containing pure DCE was always at the same temperature, about 30°.

Computations were performed using Fortran on the CDC 6400 computer at the University of California, Berkeley. Ir spectra were resolved into gaussian bands by means of an analog du Pont 310 curve resolver so that areas of overlapping bands could be compared.

Results

The ir spectrum of AANMA in DCE at a concentration of 4 g/l. with pure DCE as reference shows two partially overlapping peaks at 3400 and 3300 cm^{-1}. On the basis of the work of many other authors, *e.g.*, Bystrov, *et al.*,[1] these are assigned to the NH stretching mode, nonhydrogen bonded, and hydrogen bonded, respectively. The relative areas of the two peaks were unchanged by two-, four-, and eightfold dilutions, which was taken as proof that the hydrogen bonding was *intra*molecular, not intermolecular. Conformational calculations on AANMA[2] and experiments on similar compounds[1] show that intramolecular hydrogen bonding takes place only between the oxygen of the acetyl carbonyl group and the hydrogen of the NH of the methylamide group to form a seven-membered ring

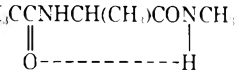

There are two conformations of AANMA in which this can take place, corresponding to different puckerings of the ring, but this study does not attempt to distinguish which (if either) is preferred.

The relative areas of the two ir bands are a function of temperature. The experimentally practical upper limit for temperature is 60° because DCE boils at 83°, and the lower limit for the 4 g/l. AANMA solution is 10° because the AANMA crystallizes out below that point. At 54°, the ratio of the area of the 3400-cm^{-1} peak to that of the 3300-cm^{-1} peak is 64:34, while at 9° it is 47:52. However, if the solution contains a few per cent water, as indicated by significant peaks at 3670 and 3580 cm^{-1} in the difference ir spectrum, then the ratio at 54° is 78:20, and at 9° it is 70:30. In other words, the ir of a wet solution is essentially independent of temperature, whereas in a dry solution the area of the 3400-cm^{-1} peak (non-H-bonded) increases with rising temperature at the expense of the 3300-cm^{-1} peak (H bonded). At no experimentally accessible temperature does one peak disappear, so the molar extinction coefficients of the H-bonded and non-H-bonded NH bands cannot be umambiguously determined. Consequently, it is impossible to determine anything quantitative about this conformational change from the ir evidence alone. However, a qualitative picture does emerge: namely, that of an equilibrium between a low-temperature "form" A of AANMA consisting of all intramolecularly hydrogen bonding conformations and a high-temperature "form" B consisting of an average over all other conformations. Thus at any temperature, T, we can consider the equilibrium

$$A \rightleftharpoons B \tag{1}$$

to have equilibrium constant K, where

$$K = [B]/[A] = e^{-\Delta G^\circ/RT} \tag{2}$$

where $\Delta G^\circ = \Delta H^\circ - T\Delta S^\circ$ is the Gibb's free energy for the reaction 1. Then

$$[A] = C/(1 + e^{-\Delta G^\circ/RT})$$

and

$$[B] = Ce^{-\Delta G^\circ/RT}/(1 + e^{-\Delta G^\circ/RT}) \tag{3}$$

where $C = [A] + [B]$ = total concentration of AANMA. We have assumed the activity coefficients to be unity, that the experimental situation is simply a two-state equilibrium, and that the ΔH° and ΔS° of the reaction are independent of temperature over the range being considered.

As might be expected, the ORD (Figure 1) and CD (Figure 2) spectra also vary with temperature for a dry solution. On the other hand, while the small pertubation of solvent entailed by the addition of a few per cent of water does not affect the ORD spectrum (±2%) at 50°, yet the temperature dependence of the ORD is completely eliminated (±1%). This is to say that the spectrum of a wet solution remains at all temperatures the same as the spectrum of a dry solution at high temperatures. Consequently, it is not necessary to correct the data for thermal expansion of the solvent. Neither is it likely that the dependence of ORD on temperature for the dry solution is due to solvation changes leading to perturbations of the chromophores.

In general, the ORD above 300 nm is monotonic, negative, and weak. Above 240 nm there is little temperature dependence, and below 214 nm the DCE solvent absorbs too strongly. For wavelengths λ between 214 and 240 nm, the optical rotation was noted at 2-nm intervals at T = 53, 43, 33, 23, and 14°.[4] For any λ and T, the optical rotation α was assumed to be the linear superposition of the rotations of the two forms α_A and α_B

$$\alpha(\lambda, T) = [A](T)\alpha_A(\lambda) + [B](T)\alpha_B(\lambda) \tag{4}$$

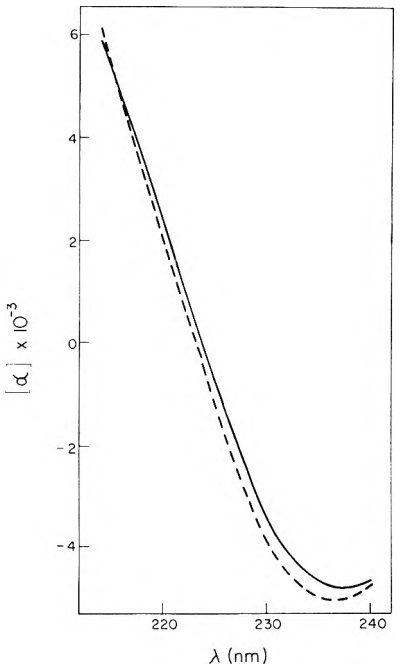

Figure 1. The specific rotation $[\alpha]$ of AANMA in DCE as a function of wavelength λ: 53° (——); 14° (- - - - -).

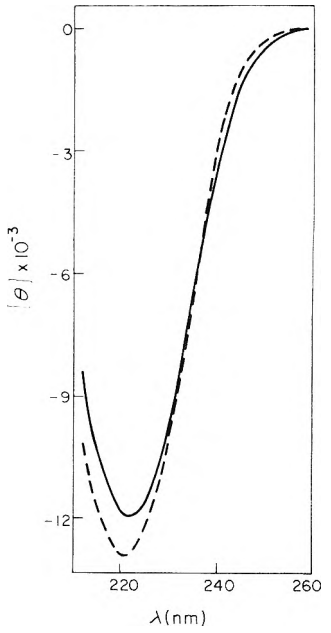

Figure 2. The molar ellipticity $[\theta]$ of AANMA in DCE as a function of wavelength λ: 51° (——); 14° (- - - - -).

where [A](T) and [B](T) are given by eq 3. Then the ORD data, $\alpha(\lambda T)$, for all wavelengths and temperatures were fit to the two-state model by adjusting $\Delta H°$, $\Delta S°$, $\alpha_A(\lambda_i)$, and $\alpha_B(\lambda_i)$ for all $214 \leq \lambda_i \leq 240$ nm by minimizing

$$F(\Delta H°, \Delta S°, \alpha_A, \alpha_B) = \sum_{j=1}^{n_T} \sum_{i=1}^{n_\lambda} \left| [\alpha(\lambda_i, T_1) - \alpha(\lambda_i, T_{n_T})] \times \left\{ \frac{[A]\alpha_A(\lambda_i) + [B]\alpha_B(\lambda_i) - \alpha(\lambda_i, T_j)}{|\alpha(\lambda_i, T_j)| + 0.00001} \right\} \right| \quad (5)$$

The expression in the curly brackets is the per cent deviation of the calculated spectrum from the experimental, while the expression in the square brackets weights the data for each wavelength according to how much the optical rotation changes at that wavelength over the whole temperature range (T_1 = lowest temperature, and T_{nT} = highest temperature). The constant 0.00001 in the denominator is merely to avoid dividing by zero even if $\alpha(\lambda_i, T_j) = 0$.

The function F was minimized with respect to $\Delta H°$, $\Delta S°$, $\alpha_A(\lambda_i)$, and $\alpha_B(\lambda_i)$, $i = 1, \ldots, n_\lambda$ by starting at some initial value for all variables and sequentially varying each individually in the stated order until F was minimized with respect to the one variable, and then proceeding on to the next variable. This whole procedure was iterated some 50 times until F was minimized simultaneously with respect to all variables. Changing one variable was done in discrete steps with an arbitrary but small step size chosen in advance. The final minimum in F was refined with smaller step sizes. The above minimization procedure is extremely crude and slow but also extremely reliable, even in this unstable case where some of the variables, such as $\Delta H°$ and $\Delta S°$, are in exponents. More elegant minimization algorithms might have been more time consuming in the long run.

The result of the fit was that $F = 0.02$ when $\Delta H° = 2570$ cal/mol (at step size of 5 cal/mol) and $\Delta S° = 6.56$ cal/mol deg (step size = 0.01). This value of F corresponds to roughly an average fractional deviation of the calculated α from the experimental α of 9%. The calculated values of $\alpha_A(\lambda)$ and especially $\alpha_B(\lambda)$ were reasonable but very sensitive to experimental error since, for example, [B] = 33% at T = 53° and [B] = 23% at T = 14°, while α(236 nm, T) changed about 4%. In other words, small shifts in the relative concentrations of the two forms were being called upon to explain shifts in ORD which were subject to substantial error. To summarize the calculated spectra, $[\alpha_A]_\lambda$ had a minimum value of −5320 at λ 235 nm and $[\alpha_B]_\lambda$ had a minimum of −4580 at 238 nm, whereas the experimental minimum specific rotation at 53° was −4830 at 237 nm. The "melting temperature," the temperature at which $\Delta G° = 0$, is 119°, which is considerably higher than the boiling point of the solvent.

Using the foregoing equations and the same $\Delta H°$ and $\Delta S°$, it is possible to calculate the CD of the two forms from the CD spectra at only two temperatures, 51.5 and 14°. Here the region of interest is from the absorption cutoff at 212 nm to the tail of the trough at 260 nm. At 51.5°, the molar ellipticity, $[\theta]$, has a single minimum of −12,000 at 222 nm, while for form A the minimum is −15,000 at 220 nm and for B it is −10,000 at 226 nm.

Discussion

The simple two-state model proposed here may well be an oversimplification, but the data from the ORD experiments are certainly not precise enough to justify a more complicated model, even though the experimental precision was better than 1%. The thermodynamic parameters calculated are of the same order as those found in similar studies (*e.g.*, $\Delta H°$ = 3100 cal/mol and $\Delta S°$ = 9.8 eu[1]), and the calculated specific rotations and molar ellipticities of the two forms are reasonable in that they have about the same magnitudes and shapes as the experimental curves (which are themselves typical for small peptides). In addition, the calculated curves are the same as the experimental ones at wavelengths where the optical activity is independent of temperature. As often occurs, the CD was more sensitive to the conformational change than the ORD. The temperature dependence of the ORD and CD

must be due strictly to a conformational change, first because of the shifts in area of the ir bands at 3300 and 3400 cm^{-1} with temperature, and second because the addition of a few per cent water gives a spectrum which is the same as that of the high temperature dry solution (±2%), yet the wet solution shows no temperature dependence. This at least clearly rules out the possibility of a spectrum change due directly to temperature. It also illustrates how important interaction with the solvent can be in determining the conformation. Apparently equimolar amounts of AANMA and water in DCE preferentially associate with each other in such a way as to make intramolecularly hydrogen-bonded conformations unfavorable. Considering the rather small differences in the ORD and CD spectra of the two forms, it would seem unlikely that one could detect such hydrogen-bonded rings in a protein or polypeptide when only a few per cent of the residues are in that conformation. Apparently, in general, optical rotatory methods are much more sensitive to the interaction of large numbers of peptide chromophores, as in the case of a helix-coil transition, than to the interaction of only two chromophores, as in this study.

Acknowledgments. We wish to thank Professor I. D. Kuntz for the use of the Beckman IR-9 and related infrared equipment and Dr. H. Yamamoto for his aid in the synthesis of AANMA. This work was supported by NIH Research Grant No. GM-10880 from the National Institute of General Medical Sciences and No. HL-06285 from the National Heart and Lung Institute.

Supplementary Material Available. A listing of $[\alpha]_\lambda$ at these wavelengths and temperatures will appear following these pages in the microfilm edition of this volume of the journal. Photocopies of the supplementary material from this paper only or microfiche (105 × 148 mm, 24× reduction, negatives) containing all of the supplementary material for the papers in this issue may be obtained from the Journals Department, American Chemical Society, 1155 16th St., N.W., Washington, D. C. 20036. Remit check or money order for $3.00 for photocopy of $2.00 for microfiche, referring to code number JPC-74-1127.

References and Notes

(1) V. F. Bystrov, S. L. Portnova, V. I. Tsetlin, V. T. Ivanov, and Yu. A. Ovchinnikov, *Tetrahedron*, **25**, 493 (1969).
(2) G. N. Crippen and H. A. Scheraga, *Proc. Nat. Acad. Sci. U. S.*, **64**, 42 (1969).
(3) S. Mizushima, M. Tsuboi, T. Simanouchi, T. Sugita, and T. Yashimoto, *J. Amer. Chem. Soc.*, **76**, 2479 (1954).
(4) See paragraph at end of text regarding supplementary material.

Flash Photolysis of Aqueous Solutions of Cysteine

Tzu-Lin Tung and John A. Stone*

Chemistry Department, Queen's University, Kingston, Ontario, Canada *(Received December 13, 1973)*

Publication costs assisted by the National Research Council of Canada

Cysteinyl radicals (CyS·) produced by flash photolysis of dilute aqueous solutions of cysteine at pH >6.5 form the cystine radical anion ($CySSCy^-$). At low concentrations ($<6 \times 10^{-7}$ *M*) this transient decays by a first-order reaction ($k = 2 \times 10^{-3}$ sec^{-1}) independent of pH and cysteine concentration and not involving dissociation to CyS· and CyS^-. At higher concentrations the transient decays by the well-studied second-order process which is pH and cysteine concentration dependent. The yield of $CySSCy^-$ is reduced by the addition of acrylic acid or allyl alcohol but the subsequent first-order decay is little affected. A new reaction between $CySSCy^-$ and cystine has been observed ($k = 3 \times 10^6$ M^{-1} sec^{-1}). Pulse radiolysis studies confirm these results.

Introduction

The pulse radiolysis of aqueous solutions of mercaptans and disulfides has been extensively studied since certain of these compounds behave as radiobiological protection agents. A focus for many of these studies has been the formation and decay of the transient disulfide radical anion ($RSSR^-$).[1-3] This species is generally formed either by the addition of a hydrated electron to a disulfide[4]

$$e_{aq}^- + RSSR \longrightarrow RSSR^- \quad (1)$$

or by the oxidation of a mercaptan (RSH) or its conjugate base (RS^-) yielding a thiyl radical which takes part in the equilibrium

$$RS\cdot + RS^- \rightleftharpoons RSSR^- \quad (2)$$

The decay kinetics for noncyclic $RSSR^-$ formed by reaction 1 in the absence of RS^- are always first order with rate constants of 10^5-10^6 sec^{-1} and can be related to the dissociation[4]

$$RSSR^- \longrightarrow RS\cdot + RS^- \quad (3)$$

However, when equilibrium 2 is set up the lifetime of the transient is increased and its decay has been found in pulse radiolysis experiments to be purely second order.[5] In apparent contradiction, Caspari and Granzow[6] found a first-order decay for $RSSR^-$ formed by flash photolysis of aqueous solutions of cysteine, cysteamine, and benzene-

thiol. Their reported rate constants of 10^3–10^4 sec^{-1} are about 10^2 times less than the pulse radiolysis results for reaction 3.

We have studied the flash photolysis of aqueous cysteine solutions with the aim of resolving the question of the order of the reaction in which $RSSR^-$ disappears in the presence of RS^-. A previously unreported reaction of the disulfide anion of cystine with disulfides has been observed.

Experimental Section

L-Cysteine (Schwarz/Mann), cystine (Aldrich), allyl alcohol (Fisher), and acrylic acid (Fisher) were used as received. Solutions were made up with triply distilled water, the pH being adjusted using sodium hydroxide or sulfuric acid. Freshly prepared solutions were immediately deoxygenated by bubbling with purified nitrogen for a least 40 min. Allyl alcohol if required was added afterward with a syringe.

Two xenon-filled flash tubes delivered from 100 to 5000 W, the corresponding flash duration (⅓ peak) being from 20 to 80 μsec. Most experiments were performed at 350 W (30-μsec flash duration). The cylindrical photolysis cell, 28 cm long and 1.9 cm diameter, was of Vycor with optically flat quartz windows at each end. The transients were monitored using a Heath EU-700 monochromator, an IP21 photomultiplier, and a Tektronix 564B storage oscilloscope.

All kinetic data were derived from the first flash delivered to a fresh solution. For a pure cysteine solution the maximum initial absorbance of the transient at 410 mμ and the decay rate were reproducible for several successive flashes. For solutions containing additional solutes this was not always the case although there was little difference between results from first and second flashes. All photolyses were carried out at 23 ± 2°.

The pulse radiolysis facilities have been described.[7]

Results and Discussion

The flash photolysis of aqueous cysteine solutions produces the cystine anion ($CySSCy^-$).[6] The spectrum of this transient and the variation of maximum absorbance with pH are shown in Figure 1. These results are in agreement with those of ref 6. The pH dependence of the yield can be understood in terms of the acid dissociation of cysteine.[8] The carboxyl group ionizes at such low pH values that in the range studied here it is always fully ionized. The acid dissociations of importance in this work are represented by the steps[8]

$$\begin{array}{ccc} HSCH_2CH(NH_3^+)COO^- & \xrightleftharpoons{pK_A = 8.53} & {}^-SCH_2CH(NH_3^+)COO^- \\ \Big\Updownarrow pK_B = 8.86 & & \Big\Updownarrow pK_C = 10.36 \\ HSCH_2CH(NH_2)COO^- & \xrightleftharpoons[pK_D = 10.03]{} & {}^-SCH_2(NH_2)COO^- \end{array}$$

with ionization of the sulfhydryl group becoming significant only above pH 6.

Light of wavelength greater than 230 nm is transmitted by the Vycor cell and although this wavelength provides sufficient energy to dissociate the S-H bond (bond strength ~88 kcal mol^{-1}),[9] little absorption occurs in this spectral region until the sulfhydryl group is ionized[8] when photoionization occurs.[10]

$$CyS^- + h\nu = CyS\cdot + e_{aq}^- \qquad (4)$$

CyS^- represents both forms containing the thiolate group.

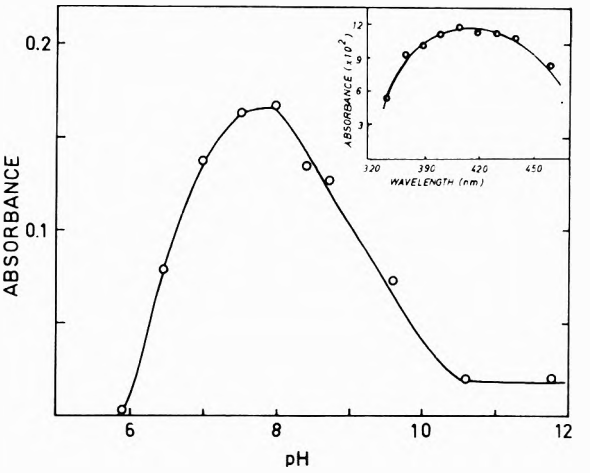

Figure 1. The variation in yield of the cystine radical anion with pH at constant flash intensity (350 W, 1.0×10^{-3} *M* cysteine). Inset shows the absorption spectrum of the cystine radical anion (1.0×10^{-3} *M* cysteine, pH 8.7).

e_{aq}^- reacts rapidly with cysteine ($k = 1.3 \times 10^{10}$ M^{-1} sec^{-1} at pH 5.8 falling to 2.0×10^8 M^{-1} sec^{-1} at pH 12.5 where the $-NH_3^+$ group has deprotonated),[3] the probable product from CySH being the alanyl radical (Cy·)[11]

$$CySH + e_{aq}^- \longrightarrow Cy\cdot + SH^- \qquad (5)$$

which abstracts from CySH

$$Cy\cdot + CySH \longrightarrow CyH + CyS\cdot \qquad (6)$$

The product of the reaction of CyS^- with e_{aq}^- is not known.

The two CyS· radicals produced per photon will enter into the equilibrium

$$CyS\cdot + CyS^- \underset{k_{-7}}{\overset{k_7}{\rightleftharpoons}} CySSCy^- \qquad (7)$$

The concentration of $CySSCy^-$ depends on (a) the concentration of CyS^- and (b) the equilibrium constant $K = k_7/k_{-7}$. At pH 7 only 2% of the sulfhydryl groups are ionized and little formation of CyS· by reaction 4 occurs. If photolysis of CySH should occur the low concentration of CyS^- would allow little formation of $CySSCy^-$. With increasing pH more CyS· is formed but the equilibrium constant K decreases since k_7 decreases[3] and k_{-7} increases[4] as the $-NH_3^+$ group deprotonates. A similar decrease in the equilibrium constant has been observed in irradiated penicillamine solutions.[12] The net result is that although the number of CyS· radicals produced for a given flash intensity is increasing with pH, the equilibrium constant is decreasing, so that there is a maximum concentration of $CySSCy^-$ at pH 8. Above pH 11 when ionization is complete the concentration assumes a constant value. At high pH reaction 5 cannot play a major role. If the product of the reaction of e_{aq}^- with CyS^- does not ultimately lead to CyS· formation then this change in mechanism will account for some of the decline in $CySSCy^-$ concentration.

Decay of $CySSCy^-$

With the 28-cm flash photolysis cell a second order decay is observed when the absorbance is above 0.20, between 0.20 and 0.15 there is mixed order kinetics, and below 0.15 there is a pure first-order decay. The pulse radiolysis and flash photolysis results are therefore reconciled. With the molar extinction coefficient of $CySSCy^-$

at 410 nm taken as $8.8 \times 10^3\ M^{-1}\ cm^{-1}$[4] first-order decay is observed only below $6 \times 10^{-7}\ M$. This is lower than the concentrations with which it is customary to work in pulse radiolysis when analyzing light paths are usually 0.5–2 cm. At the doses usually employed the concentrations of disulfide anion are around $5 \times 10^{-6}\ M$ and greater which places the kinetics in the second-order region. A mixed order decay has been observed in the pulse radiolysis of aqueous penicillamine solutions at low dose with a maximum absorption of 0.67% in a 2.0-cm cell; the pure first-order region was not attained.[12] We have observed a similar behavior in preliminary experiments on the pulse radiolysis of cysteine solutions (see later).

First-Order Decay of $CySSCy^-$

Figure 2 shows the first-order decay curve for a $1.0 \times 10^{-3}\ M$ cysteine solution at pH 8.7. The rate constant is $2.1 \times 10^3\ sec^{-1}$ in good agreement with the value of $2.7 \times 10^3\ sec^{-1}$ obtained by Caspari and Granzow at pH 8.1.[6] There appears to be a very slight effect of pH on this rate constant, the values being 2.2. 2.1, 1.8, and $1.8 \times 10^3\ sec^{-1}$ at pH 7, 8.7, 9.6, and 10.6, respectively. Figure 2 also shows the decay of $CySSCy^-$ formed by pulse radiolysis of a $2 \times 10^{-3}\ M$ N_2O saturated solution at pH 8.7 in a 2.0-cm cell. The later linear part of the decay curve when the concentration of $CySSCy^-$ is below $6 \times 10^{-7}\ M$ yields $k = 1.8 \times 10^3\ sec^{-1}$ in confirmation of the flash photolysis results.

The decay constant is independent of cysteine concentration over the range $0.5\text{–}2.0 \times 10^{-3}\ M$ at pH 7 so that a pseudo-first-order reaction with either CySH or CyS^- is ruled out. On these grounds the generalized reaction

$$CySSCy^- \rightleftharpoons CyS\cdot + CyS^- \longrightarrow \text{products} \qquad (8)$$

suggested by Caspari and Granzow[6] is eliminated.

This slow first-order decay is obviously not the first-order decomposition of $CySSCy^-$ obtained by reaction 1 which has a pH-dependent rate constant two orders of magnitude large.[4] The slow reaction cannot lead to the formation of another CyS· radical and therefore probably involves the breaking of the C–S bond as suggested for the penicillamine disulfide radical anion[12]

$$CySSCy^- + H_2O \longrightarrow CySS\cdot + CyH + OH^- \qquad (9)$$

There is no evidence that this reaction occurs in cysteine solutions, however, product analysis at pH >7 has not been reported. This slow first-order decay should be of importance in low dose-rate radiolysis but since it occurs with both cysteine, a radiation protector, and penicillamine, a radiation sensitizer, it is improbable that this reaction is of significance in radiobiological protection.

Second-Order Decay of $CySSCy^-$

Figure 3 shows the second-order plots of the initial parts of the decay of $CySSCy^-$ in 2, 3, and $5 \times 10^{-3}\ M$ cysteine at pH 7 which yield rate constants of 9.7, 5.2, and $3.7 \times 10^9\ M^{-1}\ sec^{-1}$, respectively. For constant pH and cysteine concentration there is no effect of flash intensity on the second-order rate constant. The decrease in the second-order rate constant, k_{obsd}, with increasing mercaptan concentration has been observed in the pulse radiolysis of aqueous solutions of cysteamine[5] and penicillamine.[12] $k[RS^-]$ is practically constant ($\sim 5.5 \times 10^5\ sec^{-1}$) in agreement with the conclusion of Barton and Packer[13] that the reaction

$$CyS\cdot + CySSCy^- \longrightarrow CySSCy + CyS^- \qquad (10)$$

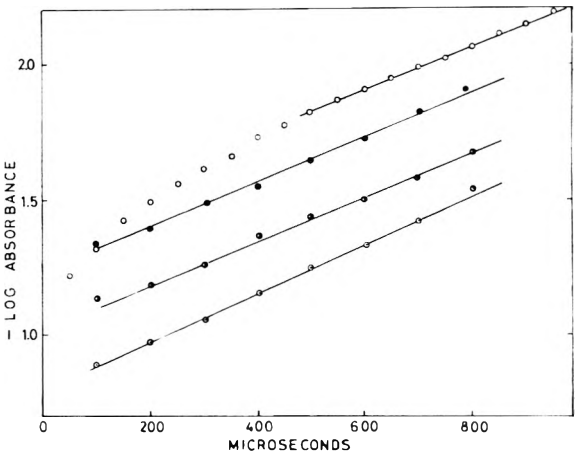

Figure 2. First-order decay of the cystine radical anion: — flash photolysis ($1.0 \times 10^{-3}\ M$ cysteine); ●, pH 10.6; ◑, pH 9.6; ⊙, pH 8.7; ○, pulse radiolysis ($2 \times 10^{-3}\ M$ cysteine, pH 8.7, N_2O saturated).

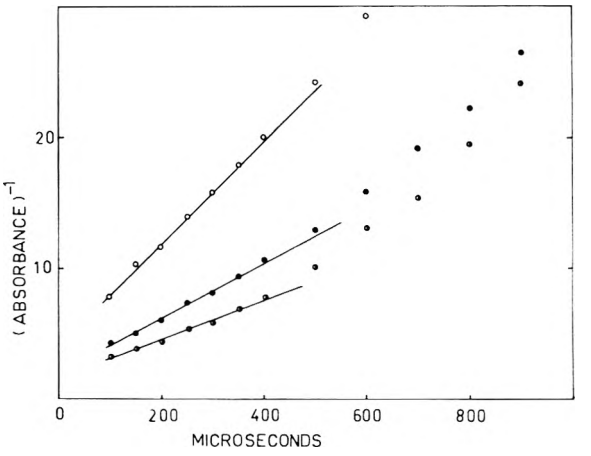

Figure 3. Second-order decay of the cystine radical anion at pH 7: cysteine concentrations ○, $2 \times 10^{-3}\ M$ ($k = 9.7 \times 10^9\ M^{-1}\ sec^{-1}$); ●, $3 \times 10^{-3}\ M$ ($k = 5.2 \times 10^9\ M^{-1}\ sec^{-1}$); ◑, $5 \times 10^{-3}\ M$ ($k = 3.7 \times 10^9\ M^{-1}\ sec^{-1}$).

is more important than that of the dimerization of radicals.

The rate constant decreases with increasing pH, being $5.1 \times 10^9\ M^{-1}\ sec^{-1}$ at pH 8.7 for $2 \times 10^{-3}\ M$ cysteine. This is expected since the reactants become more negatively charged as the degree of ionization increases with increasing pH.

Reaction of $CySSCy^-$ with Cystine

When cystine (CySSCy) is present in concentrations from 2.0 to $8.0 \times 10^{-4}\ M$ in a $1.0 \times 10^{-3}\ M$ cysteine solution at pH 7 there is no change in the initial, maximum absorbance of $CySSCy^-$. The cystine is therefore not photodissociating in the Vycor cell. It can capture electrons ($k = 1.3 \times 10^{10}\ M^{-1}\ sec^{-1}$ at pH 6.1[14]) in competition with CySH but the substitution of this reaction for reactions 5 and 6 does not change the yield of $CySSCy^-$.

The decay rate of $CySSCy^-$ in the first-order region increases in the presence of cystine and follows a pseudo-first-order expression

$$\frac{-d[CySSCy^-]}{dt} = k_{obsd}[CySSCy^-] = (k_{12}[CySSCy] - k_9)[CySSCy^-] \qquad (11)$$

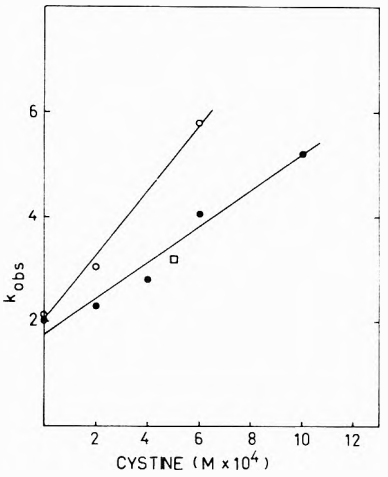

Figure 4. Pseudo-first order decay of the cystine radical anion in the presence of cystine: cysteine = 1.0×10^{-3} *M*; O, pH 8.7 ($k_{12} = 7.5 \pm 1 \times 10^6\ M^{-1}\ sec^{-1}$); ●, pH 7 ($k_{12} = 3.4 \pm 0.4 \times 10^6\ M^{-1}\ sec^{-1}$); □, pulse radiolysis, pH 7, N_2O saturated.

Where k_9 is the rate constant for reaction 9. The plot of k_{obsd} *vs.* concentration (Figure 4) yields $k_{12} = 3.4 \pm 0.4 \times 10^6\ M^{-1}\ sec^{-1}$ at pH 7 and $7.5 \pm 1.0 \times 10^6\ M^{-1}\ sec^{-1}$ at pH 8.7. The single result from a pulse radiolysis experiment is consistent with these results. The reaction

$$CySSCy + CySSCy^- \longrightarrow \text{products} \qquad (12)$$

is preferred over one involving the attack of CyS· on cystine since in this case with increasing pH a greater fraction of the radicals is tied up as $CySSCy^-$ which would lead to a lowering of the observed rate constant contrary to observation. The products of the reaction are not known but CyS· radicals cannot be among them.

The reaction of a disulfide radical anion with a disulfide has not previously been reported. It may play an important role in radiation protection by sulfur compounds especially if it leads to interchange of sulfhydryl groups. In preliminary experiments we find that the disulfide formed by the oxidation of glutathione, a radiation protector, also increases the rate of decay of $CySSCy^-$ but the disulfide of penicillamine, which has no protective properties, does not. Since electron transfer might occur in these solutions and since the equilibrium between CyS· and $CySSCy^-$ will be affected if mixed radical anions are formed these latter systems will be complex.

Photolysis of Cysteine in the Presence of Olefins

Allyl alcohol or acrylic acid decreases the yield of $CySSCy^-$ but at the same time the first-order decay rate is changed only slightly. Caspari and Granzow[6] noted the decrease in the intensity of the transient absorption with added allyl alcohol but in contradiction to the present work found that the decay was pseudo-first order, the second-order rate constant being $1.4 \times 10^5\ M^{-1}\ sec^{-1}$ at pH 8.1. Both the effects were ascribed to scavenging of CySSCy⁻. At pH 8 the first-order rate constant for disappearance of $CySSCy^-$ is 4.1 and $4.3 \times 10^3\ sec^{-1}$ in the presence of 0.77 and $1.55 \times 10^{-5}\ M$ allyl alcohol, respectively. At pH 8.7 acrylic acid decreases the rate constant to $9 \times 10^2\ sec^{-1}$ again practically independent of olefin concentration. A simple kinetic treatment of these results is not possible.

The decreases in the initial yields of $CySSCy^-$ are large, for example, at pH 8 with $1.0 \times 10^{-3}\ M$ cysteine, reductions of 30, 45, and 55% are observed for allyl alcohol concentrations of 0.77, 1.55, and $4.35 \times 10^{-5}\ M$, respectively. If these reductions are treated as due to competition between the olefin and CyS^- for CyS· radicals

$$CyS\cdot + HOCH_2CH{=}CH_2 \longrightarrow \text{radical product} \qquad (13)$$

$k_{13}/k_7 = 1.3$. Similarly for acrylic acid at pH 10 the rate constant ratio is 3.1. Since $k_7 \sim 10^9\ M^{-1}\ sec^{-1}$ [3] this implies that k_{13} has a value of the same order of magnitude, *i.e.*, 100 times greater than previously suggested values for the reaction of thiyl radicals with aliphatic olefins.[15] This appears unlikely. A possible explanation for the decrease in initial yield is that the added olefin quenches the excited state of RS^- which leads to e_{aq}^-.

Acknowledgment. The authors thank the Defense Research Board of Canada and the National Research Council of Canada for financial assistance. Pulse radiolysis studies were carried out at Chalk River Nuclear Laboratories with the assistance of Drs. W. A. Seddon and J. W. Fletcher.

References and Notes

(1) G. E. Adams, G. S. McNaughton, and B. D. Michael, *Trans. Faraday Soc.*, **64**, 902 (1968).
(2) W. Karmann, A. Granzow, G. Meissner, and A. Henglein, *Int. J. Radiat. Phys. Chem.*, **1**, 395 (1969).
(3) M. Z. Hoffman and E. Hayon, *J. Phys. Chem.*, **77**, 990 (1973).
(4) M. Z. Hoffman and E. Hayon, *J. Amer. Chem. Soc.*, **94**, 7950 (1972).
(5) G. E. Adams, G. S. McNaughton, and B. D. Michael, "The Chemistry of Ionization and Excitation," G. R. A. Johnson and G. Scholes, Ed., Taylor and Francis, London, 1967, p 281.
(6) G. Caspari and A. Granzow, *J. Phys. Chem.*, **74**, 836 (1970).
(7) W. A. Seddon, C. Willis, M. J. Young, and E. B. Selkirk, Atomic Energy of Canada, Ltd., Report No. AECL-3853 (1971).
(8) R. E. Benesch and R. Benesch, *J. Amer. Chem. Soc.*, **77**, 5877 (1955).
(9) H. Mackle, *Tetrahedron*, **19**, 1159 (1963).
(10) Manohar Lal, *Indian J. Chem.*, **9**, 1108 (1971).
(11) V. G. Wilkening, M. Lal, M. Arends, and D. A. Armstrong, *J. Phys. Chem.*, **72**, 185 (1968).
(12) J. W. Purdie, H. A. Gillis, and N. V. Klassen, *Can. J. Chem.*, **51**, 3132 (1973).
(13) J. P. Barton and J. E. Packer, *Int. J. Radiat. Phys. Chem.*, **2**, 159 (1970).
(14) R. Braams, *Radiat. Res.*, **27**, 319 (1966).
(15) W. A. Pryor, "Free Radicals," McGraw-Hill, New York, N. Y., 1966, p 221.

COMMUNICATIONS TO THE EDITOR

On the Existence of Associated Species in Lanthanum(III) Chloride–Potassium Chloride Melts[1]

Publication costs assisted by the Atomic Energy Commission and the National Science Foundation

Sir: Recently thermodynamic studies[2] of molten lanthanum(III) chloride–potassium chloride mixtures by calorimetric and electromotive-force methods indicated the presence of associated species involving lanthanum(III) ions and chloride ions. In accord with our continuing interest in the structure of binary charge-unsymmetrical fused-salt systems,[3,4] we have undertaken an investigation of the Raman spectra of a series of $LaCl_3$–KCl melts to establish the presence of complex species in these melts and, if possible, to characterize them from a structural viewpoint. The sources and methods of purification of the potassium chloride and lanthanum(III) chloride were the same as those described previously.[2] The apparatus and general technique used to obtain the Raman spectra have also been described elsewhere.[3-6]

Raman spectra of $LaCl_3$–KCl melts were recorded for seven compositions in the range from 10 to 65 mol % $LaCl_3$. Spectra recorded on the Stokes side of the exciting line contained an appreciably enhanced background in the region of the Raman scattering (50–300 cm^{-1}). This background scattering, which persisted to several thousand cm^{-1} beyond the exciting line, is presumably due to fluorescence from trace amounts of a rare earth impurity originally present in the LaO used for the preparation of $LaCl_3$. Spectra recorded on the anti-Stokes side of the exciting line contained less of this background; as a result, the region of the Raman scattering on the anti-Stokes side was less obscured than on the Stokes side.

Anti-Stokes Raman spectra recorded to 700° for samples containing 10 to 53.3 mol % $LaCl_3$ and just above the melting point (~730°) for a sample containing 65 mol % $LaCl_3$ are shown in Figure 1. The spectral changes that take place over the composition range investigated indicate the presence of a complex equilibrium, but the number of species involved cannot be determined reliably from a simple inspection of the data in Figure 1. Studies of the depolarization characteristics of these spectra show that the band which peaks near 250 cm^{-1} for the mixtures containing from 10 to 33.7 mol % $LaCl_3$ is strongly polarized; hence, the complex from which it originates must be highly symmetrical. Furthermore, this band appears to reach maximum intensity in the range from 20 to 25 mol % $LaCl_3$, in consonance with the observation of Papatheodorou and Ostvold[2] that the interaction parameter, λ^m [$\lambda^m = \Delta H^m/X_i(1 - X_i)$, ΔH^m = enthalpy of mixing and X_i = mole fraction of component i], determined from measurements of the enthalpy of mixing, reaches a minimum in the range from 15 to 25 mol % $LaCl_3$.

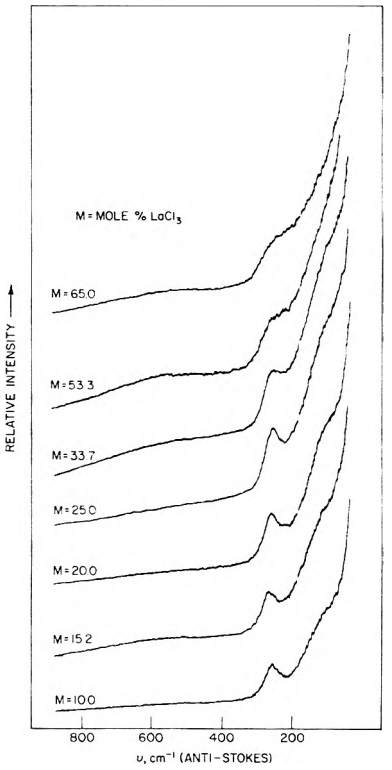

Figure 1. Raman spectra of $LaCl_3$–KCl melts recorded with the exciting radiation polarized perpendicular to the direction of observation. The curves for M = 10 through 53.3 were recorded at 700°. The curve for M = 65 was recorded just above its melting point (~730°): spectral slit width ~15 cm^{-1}, time constant = 3 sec, scan rate = 15 cm^{-1}/min.

An attempt was made to examine the Raman data recorded for these $LaCl_3$–KCl melts by curve-resolution techniques of the type used in our previous study[3] of $SnCl_2$–KCl melts; however, the present examination was complicated by the observed fluorescence, which created difficulties in the determination of a reliable baseline. Even the anti-Stokes data consistently showed a residual background extending almost to 2000 cm^{-1}. Compensation for this background was made difficult by an apparently large asymmetry of the fluorescence in the region of the exciting line. As a result, the curve-resolution data contained larger overall errors (by a factor of two or more) than were experienced in our previous study[3] of the $SnCl_2$–KCl system. For the most part, these errors arose because of poor fitting at the extremities of the extrapolated Raman curves, which in our experience is a characteristic consequence of baseline inaccuracies.

Although the results of the curve-resolution analyses contained appreciable uncertainties, several reasonably accurate observations could be made. The resolved spectra consistently showed a strongly polarized band at 250 ±

4 cm^{-1} and two bands of roughly equal integrated intensity in the range from 40 to 200 cm^{-1}. (The computed peak positions of the latter two bands were nominally 147 ± 15 and 90 ± 10 cm^{-1}.) There was some question regarding the states of polarization of the latter two bands, although in most of the calculated spectra both appeared to be totally depolarized.

Based on results obtained thus far in our studies of $LaCl_3$-containing melts, the following conclusions can be made. The spectral data clearly indicate the presence of at least one highly symmetrical, associated species in $LaCl_3$–KCl melts. The maximum concentration of this species appears to occur near 25 mol % $LaCl_3$, but in the absence of internal intensity standards, this observation is not firmly established. In general, these results confirm the contention of Papatheodorou and Ostvold[2] that discrete complex species exist in $LaCl_3$–KCl melts.

References and Notes

(1) Work performed under auspices of the U. S. Atomic Energy Commission.
(2) G. N. Papatheodorou and T. Ostvold, *J. Phys. Chem.*, **78**, 181 (1974).
(3) E. J. Hathaway and V. A. Maroni, *J. Phys. Chem.*, **75**, 2796 (1972).
(4) V. A. Maroni, E. J. Hathaway, and E. J. Cairns, *J. Phys. Chem.*, **75**, 155 (1971).
(5) V. A. Maroni and P. T. Cunningham, *Appl. Spectrosc.*, **27**, 428 (1973).
(6) V. A. Maroni and E. J. Cairns in "Molten Salts: Characterization and Analysis," G. Mamantov, Ed., Marcel Dekker, New York, N. Y., 1969, pp 256–263.

Chemical Engineering Division
Argonne National Laboratory
Argonne, Illinois 60439

Victor A. Maroni*
Ellen J. Hathaway

The James Franck Institute
University of Chicago
Chicago, Illinois 60637

G. N. Papatheodorou

Received February 4, 1974

Reversible Trap to Carbanion Electron Transfer in γ-Irradiated Hydrocarbon Glasses[1]

Publication costs assisted by the U. S. Atomic Energy Commission

Sir: γ-Irradiation of hydrocarbon glasses produces trapped electrons, radicals, and cations.[2] Experiments[3] in which the e_{tr}^- ir spectrum and photoconductivity[4] are regenerated by 375-nm light after complete bleaching by ir light imply formation and subsequent photoionization of carbanions (or, less probably, impurity anions) ($R\cdot + e^- \rightarrow R:^-$; $R:^- + h\nu \rightarrow R\cdot + e^-$). Thus, anion formation and the retrapping process compete with the cations for mobile electrons. We report here (Table I) experiments which show that this competition is maintained through at least seven ir-uv bleaching cycles, and does not change markedly over a 12-fold range of dose and radical concentration.

The probability for a trapped electron to escape neutralization in the *first* ir-uv cycle is not revealed by the data of Table I, because the yield of anions produced during γ-irradiation and present before the first ir illumination is not known. Attempts to determine this yield by measuring the growth of the esr singlet of e_{tr}^- during uv irradiation of a freshly γ-irradiated sample at various wavelengths from 320 to 375 nm have been unsuccessful. A decrease rather than an increase in the signal height always occurs, implying that the ir spectrum of e_{tr}^- has a tail extending into the uv (unless these wavelengths are able to activate cations to react with electrons; or photoinduced fluorescence from the Suprasil tube detraps electrons).

TABLE I: Yields of Reversible Transfer of Electrons from Trapped State to Carbanion State in γ-Irradiated 3MP and 3EP Glasses[a]

	Dose, eV $g^{-1} \times 10^{-19}$									
	2.7	2.7	1.6	4.8	4.8	3.2	3.2	11	20	20
Cycle	% of e_{tr}^- from γ-irradiation which remain following ir-uv bleaching cycles									
0	100	100	100	100	100	100	100	100	100	100
1	33	33	37	30	31	38	32	35	35	37
2	15	15		9	12	17	17	15		
3						12	11	8		
4						9	7	4		
5						7	5			
6						6	5			
7						5	5			

[a] Columns 2 and 3, 3MP at 72°K; all other columns for 3EP at 77°K. Uv illumination for columns 2, 3, and 4 was at 360 nm with high-intensity Bausch and Lomb monochromator with HBO 200-W mercury lamp and Corning 7-37 filter; other uv illuminations were filtered light (Corning 7-37) from an AH4 medium-pressure mercury lamp. Ir illuminations were made with a tungsten light and Corning 7-56 filter. Yields assumed proportional to height of the e_{tr}^- esr singlet at 4 μW. The 3MP and 3EP were purified by passage through silica gel degassing on the vacuum line and storage over a sodium mirror.

There is no effect of dose on the percentage yields of the ir-uv bleaching cycles from 1.6×10^{19} to 20×10^{19} eV g^{-1}, within the experimental accuracy (Table I). This is of particular interest since it is known[3,5] that the e_{tr}^- concentration rises to a maximum at *ca.* 1×10^{20} eV g^{-1} and then falls, approaching zero at *ca.* 3×10^{20} eV g^{-1}, while the concentration of radicals continues to increase. The constancy of the e_{tr}^- regeneration yields with dose implies that the ratio of the concentration of radicals to that of cations changes with dose in a way such that the fractional loss of electrons to trapping during the ir-uv cycles remains constant. Neither the concentration of cations ($[M^+] = [e_{tr}^-] + [R:^-]$) nor of carbanions can, at present, be measured directly, but the concentration of cations must be as large or larger than that of e_{tr}^-. The concentrations of e_{tr}^- at the maxima of the concentration *vs.* γ-dose curves are *ca.* 3×10^{-5} and 1×10^{-5} mole fraction in 3MP and 3EP, respectively, as estimated from earlier data,[3] assuming $G(e^-)$ initial in 3MP = 0.7.[2] The concentration of radicals is 4×10^{-4} mole fraction, assuming $G(R\cdot) = 3$.[6]

The regeneration of e_{tr}^- by photoionization of carbanions allows evaluation of the $R:^-$ decay rate. Samples of 3MP bleached with ir immediately after a γ dose of 2.7×10^{19} eV g^{-1} at 72°K were exposed at 72°K to a medium-pressure Hg arc with 7.4 mm of Corning 7-37 filter after 0, 30, 90, 240, and 2900 min of standing at 77°K. The yields of e_{tr}^- relative to the population before the first ir bleaching were 33, 27, 22, 17, and 16%, respectively. The decay of *ca.* 50% in the first 4 hr and only a few per cent in the next 44 hr is similar to that of 3-methylpentyl radicals under the same conditions,[6] implying that both intraspur and random diffusive combinations occur at about the

same rate for carbanion-cation and radical-radical reactions.

We have made a single test in which γ-irradiated 3MP was allowed to stand in the dark for 2 days at 77°K and then exposed to uv light. Fourteen per cent of the original e_{tr}^- population was regenerated, in close agreement with the yield from the ir bleached sample after 2 days of standing. This suggests that thermally detrapped and photochemically detrapped electrons have the same relative probability of reaction with radicals as compared to cations.

In analogy to the results of Table I, which imply scavenging of electrons by radicals at concentrations of 7×10^{-5} mole fraction or less and reversible transfer between physical traps and the carbanion state, early work has shown reversible electron transfer between biphenylide ion and physical trapping in 3MP[7] and methyltetrahydrofuran[8] glasses containing 6×10^{-5} and 2×10^{-4} mole fraction biphenyl. New evidence[9] on spectral shifts during exposure of e_{tr}^- in hydrocarbon glasses to ir light indicates a considerable probability for a mobilized electron to undergo multiple detrapping-retrapping steps before encountering (or tunnelling[10] to) a cation, a radical, or other scavenger.

References and Notes

(1) This work has been supported in part by the U. S. Atomic Energy Commission under Contract No. AT(11-1)-1715 and by the W. F. Vilas Trust of the University of Wisconsin.
(2) For reviews see (a) W. H. Hamill in "Radicals Ions," E. T. Kaiser and L. Kevan, Ed., Interscience, New York, N. Y., 1967, pp 321–416; (b) J. E. Willard in "Fundamental Processes in Radiation Chemistry," P. Ausloos, Ed., Interscience, New York, N. Y., 1968, pp 549–649; (c) A. Ekstrom, *Radiat. Res. Rev.*, **2**, 381 (1970); (d) J. E. Willard, *Science*, **180**, 553 (1973); (e) L. Kevan in "Advances in Radiation Chemistry," Vol. 4, M. Burton and J. L. Magee, Ed., Wiley-Interscience, New York, N. Y., 1973.
(3) A. Ekstrom, R. Suenram, and J. E. Willard, *J. Phys. Chem.*, **74**, 1883 (1970).
(4) (a) B. K. Dietrich, Ph.D. Thesis, University of Wisconsin, 1971; (b) J. E. Willard, *Int. J. Radiat. Phys. Chem.*, **4**, 405 (1972).
(5) M. Shirom and J. E. Willard, *J. Amer. Chem. Soc.*, **90**, 2184 (1968).
(6) M. A. Neiss and J. E. Willard, unpublished.
(7) J. B. Gallivan and W. H. Hamill, *J. Chem. Phys.*, **44**, 1279 (1966).
(8) P. J. Dyne and O. A. Miller, *Can. J. Chem.*, **43**, 2696 (1965).
(9) S. L. Hager and J. E. Willard, *Chem. Phys. Lett.*, **24**, 102 (1974).
(10) J. R. Miller, *J. Chem. Phys.*, **56**, 5173 (1972).

Department of Chemistry
University of Wisconsin
Madison, Wisconsin 53706

D. P. Lin
J. E. Willard*

Received March 7, 1974

You don't have to search the archives for data . . .

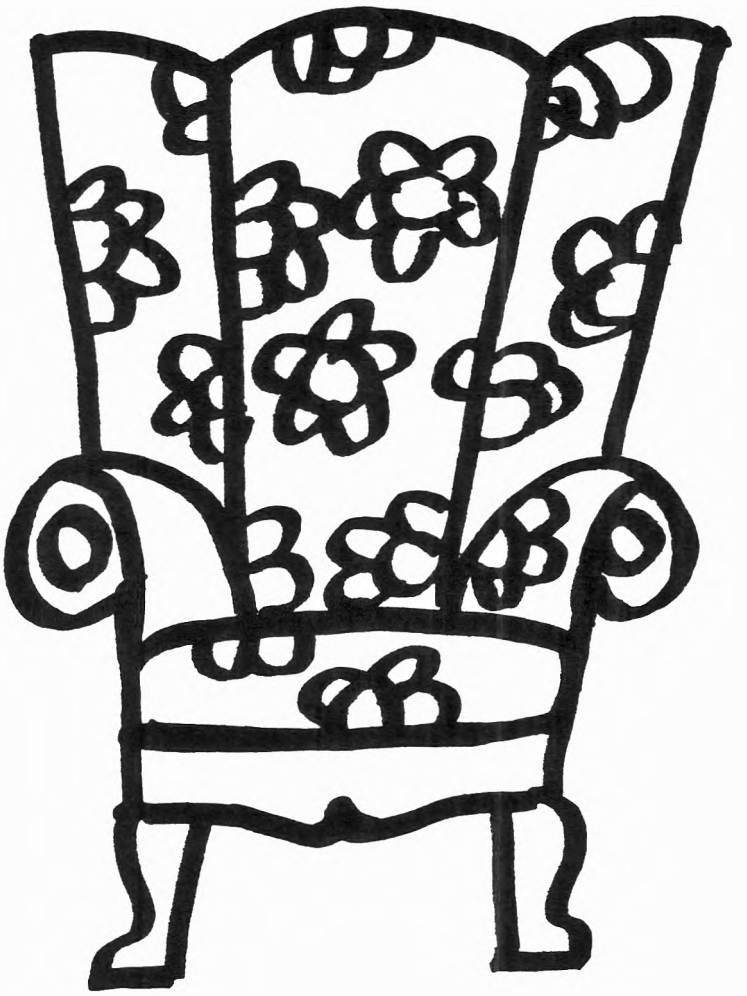

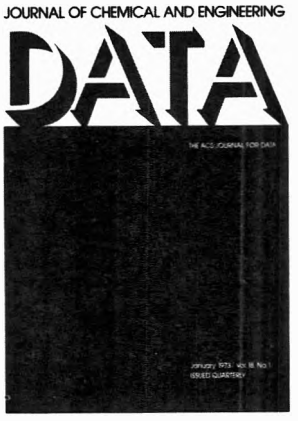

. . . because THE JOURNAL OF CHEMICAL AND ENGINEERING DATA will bring precise, reliable, useful technical information right to your fingertips quarterly! With a year's subscription, you'll receive a total of over 500 pages of valuable science and engineering data that are especially relevant now in light of today's new instrumentation. The information in JCED includes:

- experimental data relating to pure compounds or mixtures covering a range of states;
- manuscripts based on published experimental information which make tangible contributions through their presentation or which set forth a sound method of prediction of properties as a function of state;
- experimental data which aid in identifying or utilizing new organic or inorganic compounds; and
- papers relating primarily to newly developed or novel synthesis of organic compounds and their properties.

Start to benefit now from this "arm-chair" source of pertinent technical data—with your own personal subscription to JCED . . . just complete and return the form below . . . get your data without the dust.

. . . *another ACS service*

Journal of Chemical & Engineering Data

Journal of Chemical & Engineering Data
American Chemical Society
1155 Sixteenth Street, N.W.
Washington, D.C. 20036

1974

Yes, I would like to receive the JOURNAL OF CHEMICAL & ENGINEERING DATA at the one-year rate checked below:

	U.S.	*Canada***	*Latin America***	*Other Nations***
ACS Member One-Year Rate*	☐ $15.00	☐ $18.00	☐ $18.00	☐ $18.50
Nonmember	☐ $45.00	☐ $48.00	☐ $48.00	☐ $48.50

Bill me ☐ Bill company ☐ Payment enclosed ☐

Air freight rates available on request.

Name _____

Street _____ Home ☐ Business ☐

City _____ State _____ Zip _____

*NOTE: Subscriptions at ACS member rates are for personal use only. **Payment must be made in U.S. currency, by international money order, UNESCO coupons, U.S. bank draft, or order through your book dealer.

AMERICAN CHEMICAL SOCIETY PUBLICATIONS IN MICROFORM

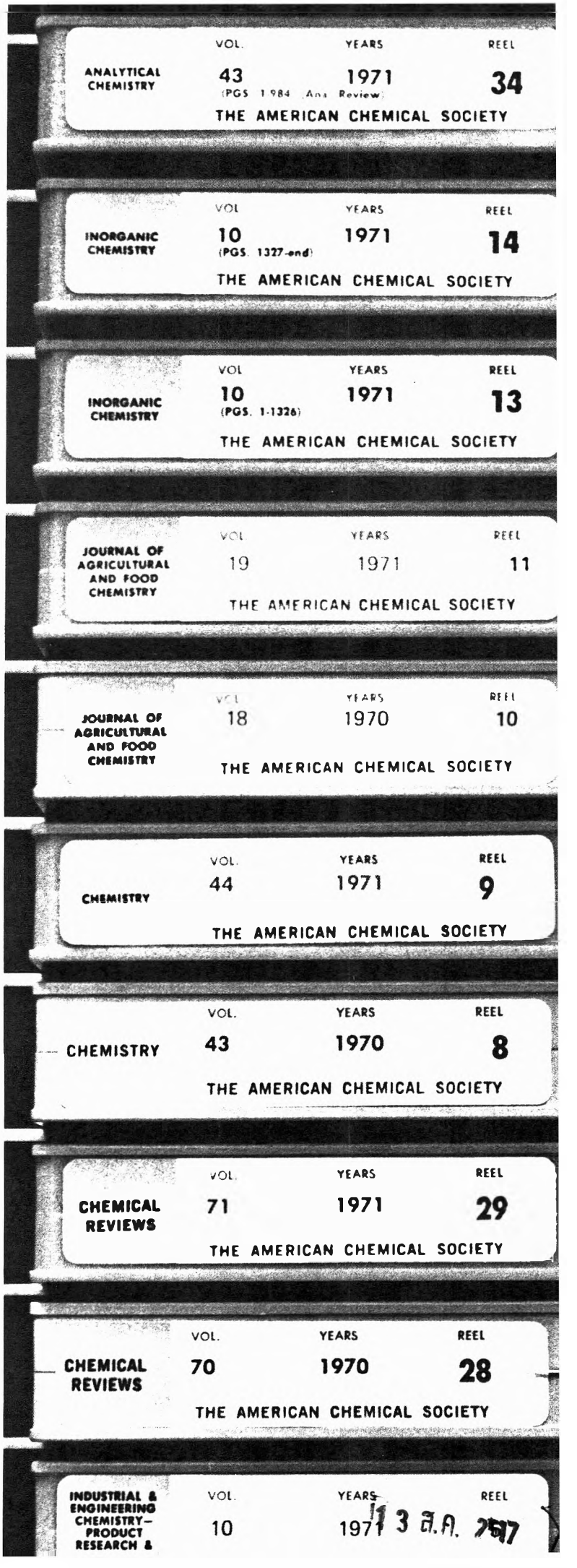

- Well over a million pages of chemistry's premier publications
- Back volumes and current subscriptions available in 35- or 16-mm microfilm and various cartridges
- Unlimited copying privileges built into microfilm subscriptions
- Current availability of nonprint materials in microfiche
- For full details of the ACS microform program, write or call:

  Mr. Kenneth Phillips
  Special Issues Sales
  American Chemical Society
  1155 16th St., N.W.
  Washington, D. C. 20036
  Tel: (202) 872-4364

  and ask for your free copy of the informative booklet on the "Information Implosion!"